University of Liverpool

School of Engineering

Non-smooth Dynamic Behaviour of Friction-induced Self-excited Vibration

Thesis submitted in accordance with the requirements of

the University of Liverpool for the Degree of Doctor in Philosophy

by

Zilin Li

September 2017

To my family

ABSTRACT

Friction is everywhere and important in our daily life as well as in industry. In general, dry friction acts as a resistance to the relative motion and dissipates energy of a system; however, under certain conditions, it can cause self-excited vibration of a system, which is known as friction-induced vibration. Friction-induced vibration can potentially cause problems like wear, fatigue failure, and noise, among which brake squeal is a typical engineering problem. As a comprehensive understanding of friction-induced vibration has not been achieved, friction-induced vibration is still a challenging research topic. The aim of this research is to carry out a theoretical study of the dynamic behaviour of nonlinear/non-smooth friction-induced vibration of phenomenological mechanical models. Discrete and continuous mechanical models with dry friction that involve nonlinear contact stiffness, stick-slip motion, or separation and reattachment at the contact interface are proposed, and numerical simulations of the transient dynamic behaviour of the non-smooth frictional systems are implemented. Their complex dynamic behaviour and the influences by various system parameters are predicted. In addition, a reduction strategy for the complicated frictional systems is presented and validated via theoretical and experimental results, which is a preliminary step in analysing complicated systems (real structures) with nonlinear/non-smooth friction behaviour in future research.

The main objectives of the research work reported in this thesis are:

1. To carry out the transient dynamic analysis of non-smooth friction-induced vibration. A varying time-step numerical algorithm, which combines Runge-Kutta method that is specifically for the second-order differential equation of motion and the bisection method, is proposed (Chapter 3). This algorithm ensures the accuracy of the results of the non-smooth vibration in which the motion states keep switching among distinct motion states of separation and reattachment, or stick and slip, which is testified by providing the same results of a classic non-smooth stick-slip vibration of a single-degree-of-freedom model.

2. In consideration of improving previous research on theoretical mechanical models with the assumptions that the contact stiffness is linear or separation is ignored, a nonlinear 2-degree-of-freedom slider-on-moving-belt model developed from Hoffmann's model and the theoretical formulations are proposed (Chapter 4), in which a cubic contact spring is included; loss of contact (separation) at the slider-belt interface is allowed and importantly reattachment of the slider to the belt after separation is also considered. The stability and dynamic behaviour of the system are investigated. Complex eigenvalue analysis (CEA) indicates that the roles of the preload and the nonlinear stiffness on the stability of the nonlinear system are not monotonous. Transient dynamic analysis (TDA) shows that separation and reattachment could happen. Ignoring separation between bodies in sliding frictional contact in vibration is unsafe as this may underestimate the vibration amplitude, and predicts incorrect effects of the key parameters on the vibration, thus considering separation is very important. Moreover, frequency domain results show the necessity of implementing both CEA and TDA in the study of nonlinear friction-induced vibration and the importance of considering separation from the frequency domain point of view. Finally, non-smooth Coulomb's law of friction is introduced in the nonlinear 2-degree-of-freedom (2-DoF) slider-belt model. Numerical results show that diverse dynamic behaviour of this 2-DoF system with nonlinearity/non-smoothness can be generated when both of the stick-slip and mode-coupling instability are involved.

3. Separation, reattachment and impact are considered in the study of friction-induced vibration of a system having an elastic disc, excited by the in-plane stick–slip vibration of a moving mass-damper-spring slider attached to a rigid wall that is dragged around on the disc surface at a constant rotating speed (Chapter 5). Theoretical formulations and the numerical procedure for the current non-smooth system are developed. Numerical results show that separation and reattachment could occur in a low speed range well below the critical disc speed in the context of a constant rotating load. Poincare maps of the system of the two distinct cases (considering separation and ignoring separation) are plotted which exhibit the diversity of nonlinear dynamic behaviour of the system and the importance of considering separation. Furthermore,

the roles of the key system parameters on the vibration are investigated. Time-frequency analysis reveals the time-varying properties of this system and the contributions of separation and in-plane stick-slip vibration to the system frequencies. One major finding is that ignoring separation, as is usually done, often leads to very different dynamic behaviour and possibly misleading results.

4. Based on the idea of mode synthesis method, a reduction strategy for complicated frictional systems is put forward, in which the natural contact interfaces and the tangential friction force are involved, and its applications and experimental validation are presented (Chapter 6). Firstly, its application to a theoretical multi-degree-of-freedom model with linear contact verifies the accuracy and feasibility of the strategy. The influence of the system parameter, and the mode number that is used in the reduced model on the stability of the reduced model are investigated. The reduced model is capable of preserving the key features (bifurcation of the eigenvalue and unstable frequencies) of the original model. Furthermore, a specific reduction strategy, for a real pad-on-disc test rig and its corresponding finite element model which involve direct contact of the interface, is proposed. The results of the reduced model with a small number of modes of the substructures correlate fairly well with theoretical results of the full model and the test results in terms of predicting mode-coupling instability and unstable frequencies, which validates this promising method for future work on friction-induced vibration of complicated frictional systems or real structures.

Key Words: Dry friction; Nonlinear vibration; Contact; Stick-slip vibration; Non-smooth dynamics

COLLABORATIONS

This research has been carried out in the framework of the University of Liverpool and Dalian University of Technology 'Dual PhD Program'. The essential target of this project is to theoretically study nonlinear friction-induced vibration. The work in the last chapter is a preliminary study and a preparation for future research, which is a collaboration with the Tribology Research Institute of Southwest Jiaotong University (SWJTU), China, and includes experimental tests on a laboratory rig based in SWJTU and theoretical validation via a detailed finite element model of the test rig.

ACKNOWLEDGEMENTS

I would like to express my gratitude to the Dual PhD program of University of Liverpool-Dalian University of Technology which has offered me a precious opportunity to study in two amazing universities and I have been also grateful to the financial support of the University of Liverpool-China Scholarship Council Scholarship during my study in the University of Liverpool.

I would like to express my sincerest thanks to my supervisors Professor Hujiang Ouyang and Professor Zhenqun Guan. I have been amazingly fortunate to have supervisors who always give supports and encourages. I am sincerely thankful to Professor Ouyang, who is a professional, mindful and responsible gentlemen with true integrity. His experienced guidance, suggestions and patience have encouraged me to take on challenges and brought my knowledge to the next level in the past four years. Also, I would like to thank Professor Zhenqun Guan, who are supportive and gave me the freedom to explore on my own.

I would like to thank my collaborators (Prof Jiliang Mo, Miss Xiaocui Wang and Mr Qi Zhang) in the Tribology Research Institute of Southwest Jiaotong University (SWJTU), China, who kindly gave the permission to include the collaboration work in my thesis.

I would like to thank my colleagues and academic members at the Dalian University of Technology and University of Liverpool for their kind suggestions and support.

Finally, I would like to express my special thanks to my parents, husband and sister. They have been supportive and encouraging during my PhD study.

LIST OF PUBLICATIONS

Journal Papers

1. **Zilin Li**, Huajiang Ouyang, Zhenqun Guan, Friction-induced vibration of an elastic disc and a moving slider with separation and reattachment, Nonlinear Dynamics (2016); DOI:10.1007/s11071-016-3097-2. (Corresponding to part of Chapter 4 of this thesis)

2. **Zilin Li**, Huajiang Ouyang, Zhenqun Guan, Nonlinear friction-induced vibration of a slider-belt system, ASME Journal of Vibration and Acoustics; DOI: 10.1115/1.4033256. (Corresponding to Chapter 5 of this thesis)

3. **Zilin Li**, Shengli Xu, Zhenqun Guan, Dynamic analysis of the axial vibration of the impeller in a reactor coolant pump induced by the radial leakage flow, Chinese Journal of Computation in Mechanics. (in Chinese) (accepted)

Conference

1. **Zilin Li**, Huajiang Ouyang, Zhenqun Guan, Friction induced vibration of a moving slider on an elastic disc with separation and reattachment, 10th International Conference on Advances in Experimental Mechanics, Edinburgh, UK, 2015 (Presenter)

2. **Zilin Li**, Huajiang Ouyang, Zhenqun Guan, Nonlinear fiction-induced vibration of a slider-belt system, 7th International Conference on Vibration Engineering, Shanghai, China, 2015 (Presenter)

CONTENTS

LIST OF FIGURES

LIST OF TABLES

NOMENCLATURE

Symbol	Name of Measure [Unit]
F_r	friction force [N]
F_n	normal force [N]
μ	coefficient of friction
μ_s	coefficient of static friction
μ_k	coefficient of kinetic friction
Ω	rotating speed (rad/s)
N	the initial load between the two contact bodies in Chapter 5
F	pre-compression force acting on the mass in Chapter 4
P	contact force [N]
$\mathbf{M}$	mass matrix of the system
$\mathbf{C}$	damping matrix of the system
$\mathbf{K}$	stiffness matrix of the system
$\mathbf{f}_{NL}$	Nonlinear force vector
f_r	friction force vector
$\mathbf{f}_{ex}$	external force vector
$\mathbf{K}_f$	asymmetrical matrix due to friction
$\mathbf{\Phi}$	mode shape matrix
$\boldsymbol{\varphi}_i$	mode shaper vector for the ith mode
$\mathbf{q}$	modal coordinate vector
$q^{(i)}$	modal coordinate corresponding to the ith mode
$\mathbf{J}$	Jacobian matrix
T	transformation matrix
λ	eigenvalue of the discrete system
k_{nl}	nonlinear stiffness [N/m^3]
ω	circular frequency
ω_i	the ith natural frequency/ imaginary part of the eigenvalue λ_i

α_i	real part of the eigenvalue λ_i
i	square root of -1
ρ	density of the annular plate [kg/m]
h	thickness of the annular plate [m]
D^*	Kelvin-type damping coefficient of the annular plate [N/(m/s)]
D	flexural rigidity of the annular plate
ξ	damping factor of the plate
w, w_0	transverse displacement of the disc and its initial value [m]
u, u_0	vertical displacement of the slider on the disc and its initial value [m]
E	Young's modulus of the disc material [MPa]
ν	Poisson ratio
r	radial coordinate in the cylindrical coordinate system
θ	circumferential coordinate in the cylindrical coordinate system
a	inner radius of the annular plate [m]
b	outer radius of the annular plate [m]
t	time [s]
Δt	time step
t_r	time for the reattachment
β	eigenvalue of the plate
q_{kl}	modal coordinate for k nodal circles and l nodal diameters
ω_{kl}	circular frequency corresponding to q_{kl}
Ψ_{kl}	mode function for the transverse vibration of the disc corresponding to q_{kl}
$J(\bullet)$	the first Bessel function
$Y(\bullet)$	the second Bessel function
$I(\bullet)$	the modified first Bessel function
$K(\bullet)$	the modified second Bessel function
$\delta(\bullet)$	Dirac delta function
r_0	radial position of the slider [m]

k_p	stiffness of the horizontal spring between the slider and the driving point [N/m]
c_p	damping of the horizontal damper between the slider and the driving point [N/(m/s)]
R_{kl}	combination of Bessel functions to represent the mode shape in the radial direction for k nodal circles and l nodal diameters
φ	absolute circumferential position of the slider on the disc [Rad]
φ_{stick}	Absolute circumferential position of the slider in stick motion [Rad]
ψ	circumferential position of the slider on the disc relative to the drive point [Rad]
subscript e	for equilibrium point
$\mathbf{x}_p$ / $\mathbf{x}_d$	physical displacement vector of the pad/disc
$\mathbf{q}_p$ / $\mathbf{q}_d$	Modal coordinate vector of the pad/disc
$\mathbf{\Phi}_p$ / $\mathbf{\Phi}_d$	mode shaper matrix of the pad/disc
$\mathbf{C}_c$	contact damping matrix
$\mathbf{K}_c$	contact stiffness matrix
$\widehat{\mathbf{C}}_p$	diagonal matrix of $2\xi_p\omega_p$
$\widehat{\mathbf{C}}_d$	diagonal matrix of $2\xi_d\omega_d$
$\widehat{\mathbf{K}}_p$	diagonal matrix of ω_p^2
$\widehat{\mathbf{K}}_d$	diagonal matrix of ω_d^2
$\mathbf{n}$	normal load vector
superscript *u*	tangential DoFs on the interface between the pad and the disc
superscript *w*	normal DoFs on the interface between the pad and the disc
superscript *o*	the OTHER degrees of freedom of the pad or the disc
subscript *p*	in Chapter 5 is for the horizontal direction, and in Chapter 6 is for the pad part
subscript d	in Chapter 6 is for the disc

1 Introduction

1.1 Problem overview

Dry friction results from the contact of solids (without lubricants) that are sliding relatively to each other or that have a tendency to do so. In general, it is supposed to dissipate the mechanical energy and acts as a resistance to the relative motion, which has been utilised in mechanical components like dampers and brakes. However, dry friction can induce self-excited vibration under certain conditions. Friction-induced vibration is a certain kind of oscillations that often occurs in engineering as well as in our daily life, and in most cases is undesirable. Waves within vibrating solids may lead to the radiation of sound, which appears frequently as noise and music. Two common examples of the sound in our daily life caused by friction are: (1) noise produced by a chalk being pushed across the blackboard, (2) music generated by a violin bow sliding across its strings. In engineering, examples include squealing railway wheels of a train on a sharp curved track, brake squeal of automobiles and aircraft, the drill string vibration, truck judder and data loss of the hard disc drive. Brake squeal is a common and annoying problem that happens in the brake system of an automobile, when braking action takes place between the rotor and brake pads. It is shown that brake noise was once among the top 10 noise problems in the early 1930s. Nowadays, brake noise is perceived as a lack of quality by customers, which leads to large warranty cost every year and effects the brand reputation as well. Numerous works concerning friction-induced vibration problems have been conducted during decades in terms of different applications and scales, which shed light on the nature of friction-induced vibration. While better understanding has been achieved, friction-induced vibration problem is still ongoing along with the development of the industry. There has been no single solution for friction-induced vibration problems. Moreover, nonlinearity aggravates the complexity of dynamic systems. In friction-induced vibration problems, non-smoothness is one of the important features of dry friction. Besides, non-smoothness due to the contact and the impact often appears during the vibration of frictional systems. The lack of comprehensive understanding of friction problems

especially the dynamic behaviour of nonlinear/non-smooth frictional systems is a major motivation of this research.

1.2 Aim and objectives

The Aim of this project is to study nonlinear/non-smooth friction-induced vibration problem of a general nature. The mechanisms of friction-induced vibration, the nonlinearity and parametric contributions are theoretically examined.

Objectives are:

1. To build up a low degree of freedom model and study the effects of friction and nonlinearities, including the contact status (slip, stick and separation) and the nonlinear contact stiffness, on the mode coupling instability.

2. To analyse the nonlinear friction-induced vibration of an elastic plate and moving slider system, in both time and frequency domains, considering in-plane and out-of-pane non-smoothness due to stick-slip and contact loss.

3. To propose a model reduction strategy applicable for frictional systems and apply it to a 9-degree-of-freedom system for theoretical validation as well as a real test rig with experimental validation.

1.3 Scope and description of contents

This PhD thesis summarises the progress made by the author in the understanding of nonlinear/non-smooth friction-induced vibration during the dual PhD program. Chapter 2 offers a literature review on the studies of friction-induced vibration which covers research in many aspects, in particular the instability mechanisms, dynamic behaviour, nonlinearities of friction problems, analysis approaches and model reduction of complex structures. Chapter 3 introduces the basic knowledge of the thesis and transient dynamic analysis algorithm for non-smooth vibration. Firstly, exhaustive introductions of the four main instability mechanisms for friction-induced vibration are offered through four examples. Then the fundamental dynamic theories

in terms of the multi-degree-of-freedom system and the elastic plate are described. Finally, a strategy for solving the non-smooth problem is proposed. Chapter 4 attempts to study the mechanisms and dynamic behaviour of a nonlinear 2-degree-of-freedom slider-belt model. The contact is described by a linear and a cubic nonlinear spring. Theoretical derivations of the system with considering the changes of the contact state (in contact and separation) are formulated. The effects of nonlinear stiffness and the preload on the stability and the vibration amplitude of the system are studied. Moreover, the roles of contact status (stick, slip and separation) on the vibration of the system are predicted. Chapter 5 presents the study of a non-smooth friction-induced vibration of a continuous model. The theoretical formulations of an elastic plate excited by a rotating slider system are presented on the base of friction dynamics and the moving load theory. Nonstationary dynamic behaviour of the system in time and frequency domain and the roles of key parameters of the system on the nonlinear friction-induced vibration are analysed numerically. Chapter 6 introduces a reduction strategy aiming to reduce the orders of complex frictional system. The feasible of this method is tested by reducing a multi-degree-of-freedom model as well as a real pad-on-disc system with theoretical and experimental supports. Chapter 7 summarises the interesting findings and important conclusions of the PhD project and gives the plans of future work.

2 Literature Review

2.1 Fiction in general

Friction is a very complex physical phenomenon. Dating back to ancient times, the importance of friction was recognised by human, such as utilising the friction force to generate fire, creating wheels, painting, etc. Scientific explorations on friction have been conducted for centuries. Nowadays, with the development of engineering, and the increasing demands of comfort and the cost reduction, the crucial role of friction in numerous industry applications, such as manufacturing industry, automotive and aerospace areas, are highlighted.

Friction is an important subject of tribology, which studies the interacting surfaces with relative motion and covers several disciplines in both science and technology. Additionally, tribology also comprises the study of lubrication (lubricants) and wear. Lubrication is an efficient way to reduce friction and wear. Common machinery components, like bearings, seals, gears, have lubricants. Wear is a younger topic than others which results in material loss or surface damages and even failure of the system. The study of the nature of the rubbing surfaces [1], such as the origins of friction [2], energy dissipation [3, 4], wear [5, 6], lubrication [7], and friction modelling [8], has achieved many remarkable findings which facilitate the development of tribology.

Dry friction refers to the friction occurring between two clean surfaces without lubricants. Ding [9] reviewed some recent works on the dynamics of mechanical systems with friction. Systems with friction exhibit diverse behaviour, especially when it comes to friction-induced vibration problems. Friction-induced vibration causes growing deformation or noise [10-13] which arouses large attention of researchers. The important role of the nonlinearity in friction-induced vibration has been recognised. The detailed descriptions of the nonlinearity/non-smoothness in frictional systems will be given in Section 2.4. Up to now, because of the elusive properties of friction itself, friction-induced vibration is still a challenging topic.

2.2 Mechanisms of Friction-induced vibration

Several disciplines of the study of friction-induced vibration have been developed during the century. A large amount of literature devoted to explore the reasons for the occurrence of friction-induced vibration, which is one important branch and gave important contributions to current research attempting to solve this problem. From the literature review [12], it has been known that the mechanisms of friction-induced vibration mainly fall into four categories, which are the negative friction-velocity slope, stick-slip, sprag-slip and mode-coupling instability. Several other mechanisms are also found as reasonable explanations for some friction-induced vibration problems.

2.2.1 Negative friction-velocity slope

In earlier researches, Mills[14], Fosberry and Holubecki [15], Sinclair and Manville[16] lead the idea that the decreasing feature of the friction with the increasing of the relative velocity accounted for the instability of a brake structure, which is known as the negative friction-velocity slope instability of the friction-induced vibration. In the same research line, the negative damping effects due to the negative friction-velocity slope were investigated by many researchers [17-20] and reviewed in Ref. [12]. Ouyang et al. [21] considered the effect of negative friction-velocity relationship on the parameter resonances of a disc model rotating in a high speed range. Yuan [18] predicted that although unstable vibration of the system can be caused by mode-coupling even when the slope of the friction-velocity relationship is positive under certain conditions, instability was more likely to happen with a negative slope which was the main reason for brake squeal of some brake systems.

On the other hand, Chen and Zhou [20] found that, in a laboratory test rig, unstable vibration sometimes occurred at the negative slope stage of the friction-velocity relation, but sometimes at the positive slope stage. The decrease of friction with respect to the velocity was not an essential reason for the brake squeal. As the negative slope theory can explain [22, 23] only a limited number of engineering problems, this kind of mechanism receives less attentions in recent years.

2.2.2 Stick-slip instability

The stick-slip phenomenon due to dry friction, that was early identified in the study of tribology [1, 16], has been observed in dynamics by many researchers. Two distinct motion states (stick and slip) are involved in the vibration process. The stick-slip instabilities are responsible for many problems in the mechanical engineering [24-27] and geodynamics [28, 29]. Macro slip-stick between two elastic materials at a very low moving velocity was observed in the experimental research [30]. Stick-slip happens when the friction at the interfaces follows particular friction laws with the different static and kinetic friction coefficients, such as the most general Coulomb's law friction, the friction law with a decreasing friction-velocity relationship [31, 32], and even the friction law in which the kinetic friction coefficient is greater than the static one [33, 34].

Various studies focus on the characteristics of stick-slip motion which are influenced by the system parameter values, laws of friction and operation conditions [34-39]. Berman et al. examined the different origins of stick-slip between the solid-solid surfaces in Ref. [40]. The periodical stick-slip motion of a classical mass-on-moving-belt model was studied analytically in Ref. [41]. The critical belt speed for the transition of pure slip motion to stick-sip motion was derived. In Ref. [42], three motion states in the vibration of an undamped spring-block system including the continuous sliding motion, the oscillatory sliding without sticking motion and the stick-slip motion were discussed and the analytical expression of the limit cycle amplitude of the oscillatory sliding motion was obtained. In Ref. [43], the stability around the equilibrium points and bifurcation behaviour of a classical mass-on-a-belt system with a decaying friction coefficient were investigated by the first order averaging method. Depending on the system parameters, two kinds of stability before reaching the stick-slip cycle were found: one was that the system only had an unstable fixed point, the other was that the system had a stable fixed-point with a stable limit cycle. Additionally, the oscillation patterns of the stick-slip motion of a coupled spring-mass system were studied in Ref. [44]. Pascal [45] explored the sticking and non-sticking orbits of a two-degree-of-freedom model under a harmonic excitation.

The bifurcation of systems with stick-slip and the unstable stick-slip behaviour were also explored by many researchers [46-49]. Popp and Stelter [46] explained the excitation mechanism of the violin string. Rich dynamic behaviour of the stick-slip motion of two discrete and two continuous models, including stable vibration, bifurcations, periodical and chaotic vibration, was clearly illustrated. Ref. [50] investigated the bifurcation and stability of systems with dry friction by the mapping approach, which gave insight into the unstable stick-slip phenomenon, and also provided an efficient and simple way to study bifurcation and stability of non-smooth problems. Diverse stick-slip motion and chaos were observed in a three-degree-of-freedom model with dry friction [51]. Li et al. [52] investigated the stability and bifurcations of a nonlinear single-degree-of-freedom slider-belt system, in which a cubic spring and damping are considered.

2.2.3 Mode-coupling instability

Mode-coupling [53] or mode locking [54, 55] instability essentially is a kind of geometry-induced instability, which are generally acknowledged as the main mechanism for squeal in brakes [12, 56] and has gained many attentions in the friction-induced vibration area [57-65].

North firstly reported that brake squeal was due to the friction force with a constant friction coefficient. A later model [53] illustrated the coalescence of two modes of a frictional system and the evolution of eigenvalues with varied system parameters. It was pointed out that the system turns to be unstable as the real part of the eigenvalues becomes positive after coalescing. The properties of the mode-coupling instability of a two-degree-of-freedom model with a sideling spring are studied [57, 58]. In Ref. [58], the inclined spring in the system coupled the horizontal and vertical vibration of the system. The friction force caused the asymmetry of the system, which leaded to a complex eigenvalue problem. The system became unstable, when the friction coefficient was beyond the critical value that resulted in a positive real part of the eigenvalues. The key point of the later paper [57] is that increasing damping was shown to destabilise the system within certain damping values, which was not a conventional role of damping. Hultén [66, 67] proposed a new kind of mode-coupling

mechanism. The coupling of the system is not due to the inclined spring but the friction forces in two orthogonal directions [66, 67]. Chen [59] investigated the eigenvalues of 8 car brakes through experimental and numerical analysis. The unstable frequencies of the in-plane and out-plane modes calculated from the complex eigenvalue analysis showed a good agreement with the brake squeal frequencies tested in experiments. It is predicted that the coupling of the in-plane and out-of-plane modes of the brake was the main reason for squeals above 3 kHz. Additionally, the distributions of the heterogeneities of the contact played an important role in mode lock-in instability. Uniformly distributed contact stiffness was more likely to produce mode-coupling instability, while the heterogeneous contact was a stabilising factor [68].

2.2.4 Sprag-slip instability

Sprag-slip instability was firstly studied by Spurr [69] to describe the brake squeal. Despite of the complexity of the friction model, this theory makes sense even when the friction coefficient is constant. Sprag-slip is due to the constrained interactions of the system in various degrees of freedom, in which the sprag angle of the structure is an important criterion for the occurrence of sprag-slip behaviour. Sinou et al. [70] proposed a nonlinear mass-belt model to study the truck judder problems. The influences of parameters on the sprag-slip stability are examined.

Another notable line of research, parallel to sprag-slip, is about the existence and uniqueness of the solutions of the frictional system [71-75]. The inconsistent solutions in a multi-degree-of-freedom system are called Painleve paradox. Following this theory, a friction impact oscillator was exemplified by Leine et al. [76]. The formulations in this work did not have an asymmetric stiffness matrix that was the cornerstone of the mathematical framework for brake squeal, which also result in unstable vibration depending on the values of a geometric character of an angle and the friction coefficient. Champneys and Varkonyi [77] showed the complexity in terms of inconsistency and indeterminacy that can arise when a system consisted of two unilateral frictional contact. Charles and Ballard [75] developed the strategy for studing Painleve paradox in the frictional system with finite numbers of contact points.

Hoffmann et al. [78, 79] examined the sprag-slip instability through a beam-on-belt model. The sufficient criterion for the occurrence of sprag-slip was the nonexistence of the steady-sliding state. Adding damping will not make significant contributions to the characteristics of sprag-slip vibration. Moreover, Ref. [80] addressed that the stiffness relations in the system were the essential condition for the absence of the steady-sliding state.

2.2.5 Other mechanisms

Besides the four broadly accepted mechanisms, friction-induced vibration can be explained by other reasons, such as the creep-slip [81], the follower force, the moving load, and the friction couple. In Refs. [53, 82-85], friction was also modelled as a follower force, whose direction is always at the tangential direction of the contact surface and changes with the surface deformation. Mottershead and co-works produced a series of works [86-88] to explore the effects of the follower force on disc brake squeal. Ouyang et al. [89] discovered that a moving load produced by friction were able to induce instability of a brake-disc system. The friction couple [60, 90, 91] was found as one factor accounting for the instability. In Ref. [91], a vibration model consisting of an elastic disc with two rotating oscillators acting on each side of the disc was developed. The instability of the disc due to the friction couple was studied.

Furthermore, Kinkaid et al. [92] proposed a four-degree-of-freedom model to describe the braking process. Interactions between the three in-plane degrees of freedom changed the direction of the friction force, which was recognised as a new reason for brake squeal. Chen et al. [93] suggested that the ploughing, asperity deformations and adhesion, that resulted in fluttering friction forces, were responsible for the squeal generation. Refs. [94, 95] analysed the instability of a simplified friction system caused by the time delay between the normal force and the friction force.

2.3 Mechanical models

2.3.1 Low-degree-of-freedom models

A fair amount of researchers devote to use simple models of a few degrees of freedom (DoFs) to study the fundamental causes of friction-induced vibration phenomenon. Although some features of the original structures are omitted, the studies of these simple models often offer insight into friction-induced unstable vibration, which are valuable from either a theoretical or a practical point of view. After the development of the lumped parameter models [53, 90, 96] by early researchers, other successful lumped parameter models for the study of brake squeal were developed, which involved more degrees of freedom, more distinct configurations or more complicate friction models. Some work was reported in Refs. [43, 46, 58, 61, 92, 97-104].

The slider-on-moving-belt systems are one kind of classic models used in the study of friction-induced vibration [46, 58]. Andreaus and Casini [98] studied the responses of a single-degree-of-freedom model with dry friction. The influences of the constant speed of the moving base, the driving force and the friction model on the dynamic behaviour of the system were investigated. In Ref. [100], stick-slip and impact motion of a single-degree-of-freedom oscillator excited by a frictional moving base and restricted by a unilateral rigid or deformable obstacle was studied. The slider-on-moving-belt model was also used for the study of stick-slip motion considering a statistic velocity [105] and stochastic friction coefficients[106].

Analytical work on the limit cycle and stability analysis of the classic slider-on-moving-belt has been reported in Ref. [43, 107-109]. Luo and co-workers [110-112] analysed the stick-slip motion through the analytical theory for non-smooth systems. Recently, Brunetti et al. [113] proposed a multi-degree-of-freedom lumped system, which gave insights into the vibration and contact behaviour during the braking process and can also be utilised in the study of joints. The analytical solution of a system with dry friction which included 2 stick-slip motion trajectories during one period were derived [109]. Li et al. [114] proposed a self-excited smooth and

discontinuous oscillator with dry friction. Bifurcation analysis of the system offered insights into friction-induced vibration with the geometric nonlinearity.

Jarvis and Mills [90] were the first to proposed a 3-DoF pin-disc model. Both the analytical study and the simplified experiments have had a considerable inspiration to later research. Earles and co-workers produced many articles on the investigations of the sprag-slip mechanism related to brake squeal. In some of their early papers, lumped parameter models containing one pin on one side of a disc were used [115]. In later work [116, 117], systems containing a pair of pins which located on each side of the disc were developed. Damping of the pin was found to make the system more unstable under certain conditions [117]. Furthermore, Tworzydlo et al. [118] built a pin-on-disc test rig to investigate the correlations between the instability predicted through analytical calculations and the test results. Emira [119] conducted the parametrical study of the vibration of a typical pin-on-disc model, in which the pin was rotating. A three-DoF mechanical model containing a rigid body, constrained by a horizontal spring, a vertical spring and a torsional spring in the centre of pin, is used.

Plenty of other interesting simple models have been proposed in literature [92, 103, 120-122]. Bengisu and Akay [123] analysed friction-induced vibration by using a 3-DoF model with a exponentially expressed friction model. Luo and Thapa [103] analysed the periodic motion and local instability of a simplified brake system analytically, which provided a good understanding of nonlinear and non-smooth vibration of brake systems. Shin et al. [99] modelled the disc and pad system as a model having two single-degree-of-freedom systems in friction contact. It was reported that either increasing the damping of the pad or the disc potentially reduced the stability of the system. Wagner et al. [121] reviewed a number of small models and developed a new 2-DoF system including a rigid rotating disc in point contact with two point pads. The stability of the wobbling disc motion was studied with various values of the key parameters (the normal pre-load, the rotating velocity and the friction coefficient), which gave a clear insight into the causes of the instability of the friction-induced disc vibration. Rusli and Okuma [124] proposed a 2-DoF model and a multi-

DoF model in which rough contact was involved. Low frequency squeal was more likely to occur at a rough surface with a low contact stiffness value.

A recent study [125] suggested that the number of degrees-of-freedom should not be too small. Moreover, an efficiency method was proposed which gave a guidance for the minimum mode shall be used in the reduction of complex systems.

2.3.2 Continuous models

The continuous components, like beams and plates, which have infinite numbers of DoFs, have been used in the study of friction-induced instability mechanism, or theoretical analysis of vibration characteristics. Flint and Hultén [60] proposed two continuous models to model the pad and disc system. The simpler one modelled the brake as a beam which was in contact with the pads that were modelled as elastic foundations. Additionally, an extended brake model assembled by a beam, rigid bodies and finite spring elements was developed. This paper showed a useful way of modelling complex systems as reduced number degrees of freedom models that were suitable for sensitivity analysis. Results showed that the mode coupling resulted from the deformations of the pad and the follower force were the key factor in the instability of the system. Meziane et al. [62] presented a comprehensive study on an analytical beam-on-beam model which showed a close correlation to the experimental results. Hochlenert et al. [126] proposed two theoretical models that one contained a beam component and another contained a plate, and verified that discretisation method could be used for the stability analysis of continuous systems. It concluded that the kinetics of the system in all of the three dimensions should be all considered in the study that the brake squeal mechanism is concerned.

Discs are key components in a wide range of mechanical applications such as turbine discs, brakes, clutches, computer drives, and saws. A series of works that used mechanical models, having an elastic disc subjected to a rotating slider system, to investigate the friction-induced vibration have been reported in Refs. [19, 127-130]. Mottershead [129] reviewed the vibration of both stationary and rotating discs under the friction force and other kinds of load. In Ref. [82], parametric resonances in a disc

with a rotating mass-spring-damper system were studied in the subcritical speed range, in which the friction force was treated as a follower force. Ouyang et al. [130] examined the transverse instability of an elastic disc under the action of a moving friction slider with stick-slip vibration. Interesting Poincare maps of the disc's transverse vibration and the slider's horizontal stick-slip vibration were shown with various parameter values of the system.

Other analytical disc-pad models were reported in Refs. [131-136]. Spelsberg-Korspeter et al. [133] proposed a new model that contained a rotating Kirchhoff plate in contact with an idealised elastic pad. In that paper, both of the stretching and bending vibration of the rotating plate due to distributed friction forces were investigated. In Ref. [135], the wave pattern and the limit cycle of the stick-slip motion of a simplified rotating disc brake system, which was in the frictional contact with a pad under the uniform pressure, were analysed.

2.3.3 Finite element models

The models with low degrees of freedom lumped systems or continuous components were usually used for the theoretical study of friction-induced vibration. In recent years, the finite element method (FEM) becomes a widely-used tool for dealing problems with more complex structures, loading process or boundary conditions, which has provided new insights into the brake squeal problem. Although different finite element models were employed in different research, most works focused on the dynamic side, rather than developing distinct finite element models.

One of the basic uses of FEM is to investigate the natural frequency and modes of complex systems. A series of research using the complex eigenvalue analysis have been put forward, which mainly have two directions: the stability analysis of the stationary discs [137-140] and the rotating brake systems [84, 141] . Liles [137] is one of the earliest researchers, who conducted the finite element analysis of a real brake and verified the results by comparing with experimental results. Dai and Lim [140] introduced the theoretical relationship between the friction and the contact force into a finite element (FE) model by building up distributed springs between the contact

surfaces and eventually proposed a combined finite element model. Kang [142] proposed a rotating pad and disc FE model in which the brake is modelled as hat shape. Results showed that the mode coupling and the negative slope of the friction-velocity relationship are the two reasons for brake squeal, and the latter one can explain brake squeal even when the mode coupling is absent. Wei et al. [143] investigated the influences of key parameters, such as the rotating speed, the friction coefficient and the braking pressure, on the instability of a brake model using Abaqus. Comparisons between experimental results and complex eigenvalue analysis (CEA) results verified the feasible of the numerical analysis and also showed that CEA may sometimes overestimate and sometimes underestimate the unstable frequency.

The investigation of squeal propensity is one of the popular topics [18, 144, 145]. Blaschke [144] examined the squeal propensity by a FE model, in which the contact between the pad and disc was not assumed as a 'imaginary' spring. A new approach, by which the contact force was directly calculated from the state of the system, was proposed. In recent years, the relation between the in-plain vibration of the rotor and squeal was recognised gradually [146, 147]. Kang [147] considered the damping shims which were modelled as the constrained-layer insulator in the FE model. One significant finding was that the in-plane torsion mode could easily lead to brake squeal, and this kind of squeal propensity could not be suppressed by the damping shim. In Ref. [63], the unstable dynamic behaviour of a system with an elastic torus, whose inner radius was in friction contact with another rotating torus, was studied numerically. The energy flow during transient vibration showed that more energy was added in the system and the energy dissipation at the friction surfaces decreased when friction-induced self-excited vibration occurred. Moreover, the energy dissipated by friction of the unstable system was much smaller than a stable one.

2.4 Nonlinearity in frictional systems

As it is known, most systems actually behave nonlinearly in reality and the nonlinearity plays an important role in the engineering applications such as mechanical systems, aerospace structures, etc [148]. In the research area of nonlinear systems, a number of

researchers focus on studying dynamics of nonlinear oscillators, such as Duffing oscillator [149], Van der Pol oscillator or SD (smooth and discontinuous) oscillator [150, 151], or developing methods to solve nonlinear problems, which offers useful results for the study of nonlinear dynamics of mechanical systems. In the frictional system, nonlinearity could possibly arise from the materials, the friction force, and the contact [152]. Research on the nonlinear friction-induced vibration has been carried out through experimental, analytical [52, 153] and numerical approaches [154-156]. In this subsection, related studies are reviewed.

2.4.1 Terminology of the non-smooth nonlinearity

Mechanical systems with non-smoothness have gained large attentions and the non-smooth dynamics has been an important research topic. The non-smoothness may be generated by clearance, constraints, dry friction, hysteresis and others [157].

When the term ’non-smooth’ or ‘discontinuous’ is used, it should be stated that which physical quantities of the system are considered to be ‘non-smooth’. The terminology of non-smooth dynamical systems can be classified as three types [158] which refer to the right hand side of the differential equations (shown in Table 2.1): (1) the system with a purely elastic one-sided support is a non-smooth continuous system, (2) the system with dry friction is a discontinuous system, (3) the system with impact is an impulsive kind of non-smooth system.

In terms of friction-induced vibration, as it is known, even for the simplest friction law, the direction change of the friction force results in the non-smooth characteristic of the dynamic system. Stick-slip is a typical non-smooth vibration in friction-induced vibration problem, and many studies on it have been reported in Section 2.2.2. On the other hand, as the frictional system is composed of components that are in contact rather than linked together as a whole system, thus separation or impact may occur during the vibration which indicates that the system itself is potentially non-smooth. Moreover, more than one non-smooth characteristics shown above can be involved in the dynamic system with friction. The change scenario of the motion state will be stated in specific problems.

Table 2.1 Non-smooth and discontinuous systems

Model	(1) Elastic support	(2) Dry friction	(3)Impact
	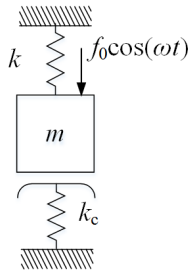	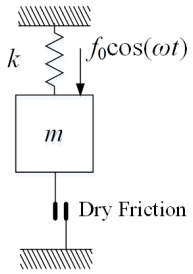	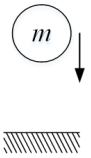
Right hand side of the differential equations	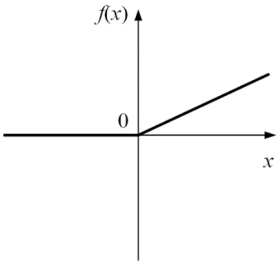	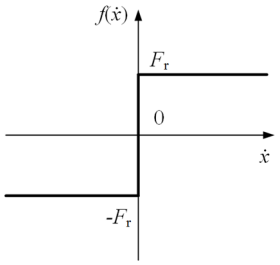	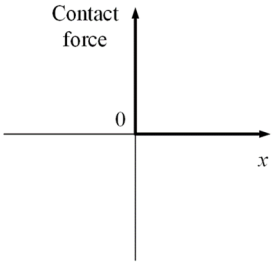
	Non-smooth continuous	Discontinuous	Impulsive

Some researchers study the non-smooth dynamics of structures like gears [159], joints [160] and rubbing rotors [161-166] with friction but self-excited friction-induced vibration is not the main concern. Cao et al. [160] reviewed the non-smooth models (the impact and frictional models) for space deployable mechanisms and studied the non-smooth dynamics of the system with joints and clearance. The dynamic behaviour of the systems with non-smooth characteristics can be very complex. Yuan et al. [161] investigated the bifurcations of the rotor under rubbing and impact. Jiang and Chen [166] reviewed the researches on nonlinear dynamics of rotor/stator rubbing in engines. There are many other works on non-smooth dynamics in which friction is not involved, for example the multibody system dynamics with impact [167, 168].

2.4.2 Nonlinear nature of friction

Friction itself at contact surfaces is a complicated nonlinear phenomenon [169]. Characterising the friction force has been a focused research topic for a long time [170,

171]. So far, friction is recognised to be related to many factors through tribology study, such as the properties of the material, the humidity, the temperature, the sliding speed, the acceleration and the compression force. The development of a quantitative perspective of the sliding friction relies on the contributions of a lot of researchers [49, 172-174], among which some early researchers are: Leonardo da Vinci, who was the first engineer who observed that friction force is proportional to the normal load at 1495; Guillaume Amontons, who rediscovered these results after 200 years and described the proportionality of the frictional force to the normal force, known as 'Amontons' laws; Leonard Euler, who introduced the concept of static and kinetic friction coefficients through analytical as well as experimental study; Charles Augustin Coulomb, who made outstanding contributions of the examination of dry friction including quantitatively confirming Amontons's results, substantiating the difference between static and kinetic friction and establishing the well-known Coulomb law of friction; Bowden and Tabor [175], who firstly claimed the importance of roughness of the contact surface and the real contact area in friction; and so on [176]. As tribology is not the main interest of this thesis, the readers of interest can refer to Refs. [175, 177].

2.4.2.1 *Basic laws of friction*

Friction modelling is a very large topic in terms of the applications of friction and the scale across macroscopic to microscopic, which progresses with the evolution of industry. Here, friction laws generally used in friction dynamics are introduced.

A large number of friction laws belong to the classic friction law which assumes that the friction force is proportional to the normal force and independent of the apparent contact area, and opposes the motion [178]. The first conventional law of friction discovered by Amontons is given by Eq. (2.1):

$$F_{\mathrm{r}} = \mu F_{\mathrm{n}} \operatorname{sgn}\left(\left|v_{\mathrm{r}}\right|\right) \tag{2.1}$$

where μ is the friction coefficient, F_{n} is the normal force, and v_{r} is the relative velocity.

Coulomb's law of friction, shown in Fig. 2.1, states that the kinetic friction coefficient is independent of the velocity.

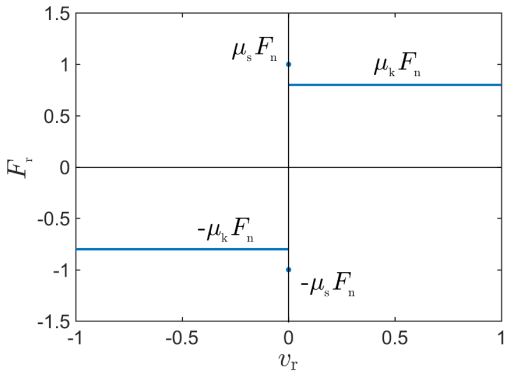

$$\mu(v_r)=\begin{cases}\mu_k & (v_r>0)\\ \pm\mu_s & (v_r=0)\\ -\mu_k & (v_r<0)\end{cases} \tag{2.2}$$

Fig. 2.1 The Coulomb's law of friction

in which μ_s and μ_k denote the static and kinetic friction coefficients respectively, and v_r is the relative speed between the surfaces in contact. The non-smooth characteristic of Coulomb's friction brings mathematical difficulties and extra programming work for dynamic study.

The velocity weakening characteristic of the friction coefficient with respect to the velocity at small values was observed by early researchers [38]. Among the various friction models, the velocity-dependent friction is universally used in different applications [8], which is also a general feature of friction. The simplest friction model with the decreasing feature is given by Eq. (2.3), and depicted in Fig. 2.2 (a).

$$\mu(v_r)=\mu_s-\mu_2|v_r| \tag{2.3}$$

in which μ_s and μ_2 are constants and μ_2 is the gradient coefficient of $\mu(v_r)$.

Fig. 2.2 (b) shows another friction model that illustrates the nonlinearly deceasing characteristic of the friction coefficient dependent on the velocity. This relation can be fitted by an exponential function, in the following form [43]:

$$\mu(v_r)=\mu_1+\Delta\mu e^{-a|v_r|} \tag{2.4}$$

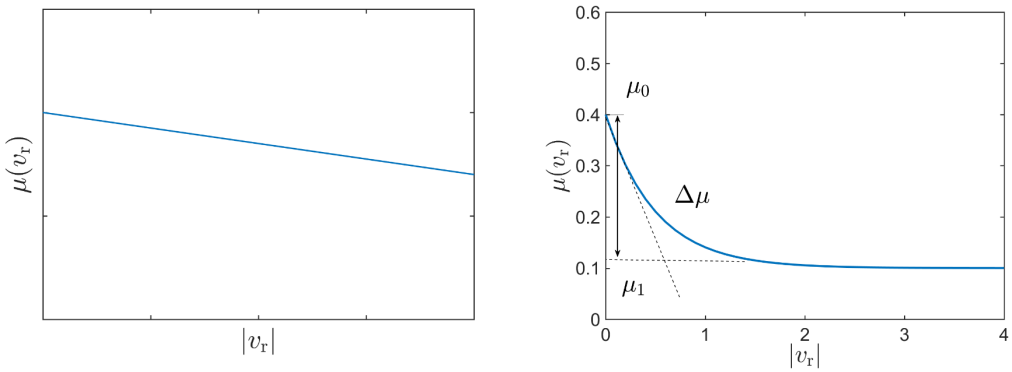

(a) (b)

Fig. 2.2 Velocity weakening friction laws: (a) the friction model with a negative slope (b) the friction model described by the exponential function

The Stribeck effect of friction in dependence of the velocity was originally discovered in the lubrication area, which has been a commonly seen friction model in the studies on dry friction [41, 46]. There are several formulations that can describe this phenomenon: the friction coefficient firstly decays and then increases with the relative velocity. Fig. 2.3 (a) shows one friction-velocity curve [41] which combines the Stribeck effect with Coulomb friction, expressed in Eq. (2.5):

$$\mu(v_r) = \mu_s \operatorname{sgn}(v_r) - \kappa_1 v_r + \kappa_3 v_r^3 \tag{2.5}$$

in which $\kappa_1 = \frac{3}{2}(\mu_s - \mu_m)/v_m, \kappa_3 = \frac{1}{2}(\mu_s - \mu_m)/v_m^3$, and μ_s, μ_m , v_m are constants.

Additionally, in order to reduce the tedious computation procedure for dealing with the discontinuity in the classic Coulomb's law of friction, and allow the analytical methods to be easily applied, several smooth friction using different functions (linear, exponential [123, 179], and trigonometric [50, 180]) were described. The smoothened friction model is an easily used model that allows standard numerical techniques to be directly applied. When Eq. (2.5) is smoothen by an arctangent function, one gets Eq. (2.6) and the friction-velocity curve is illustrated in Fig. 2.3 (b):

$$\mu(v_r) = \frac{2}{\pi}\arctan(c_1 v_r) * \mu_o(v_r) \tag{2.6}$$

in which $\mu_o(v_r)$ follows Eq. (2.5), c_1 is a parameter determined by the slope of the original friction law $\mu_o(v_r)$.

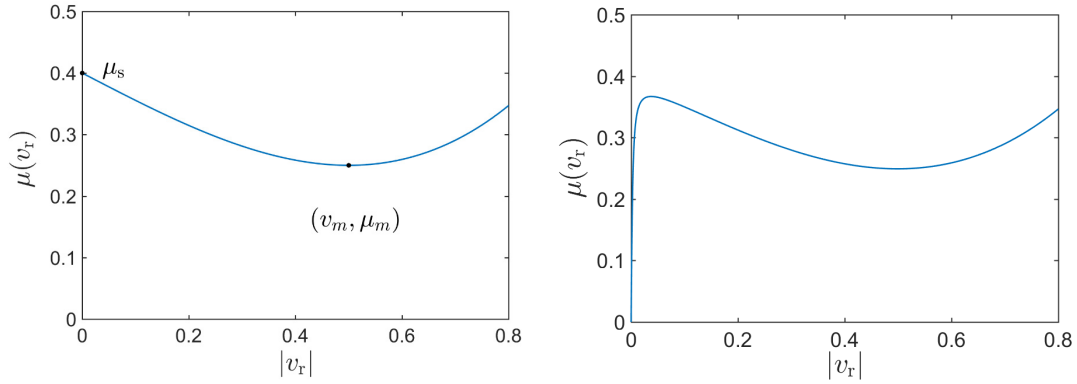

Fig. 2.3 Stribeck friction law: (a) Stribeck+Coulomb friction ($\mu_s = 0.4$, $\mu_m = 0.23$, $v_m = 0.5$) (b) Smoothed Stribeck friction ($c_1 = 400$)

Apparently, the above classic friction laws describe the intrinsic properties of friction. In more recent years, friction models that can describe more friction phenomena are proposed. The rate and state dependent friction laws, stemming from geodynamics [181-183], recently have been applied to other problems as well [184]. Eq. (2.7) shows the Dieterich-Ruina law, which has the best agreement with the experimental results of rock friction[185], formulated as:

$$\tau = \left[\mu_s + a \ln\left(\frac{v}{v_0}\right) + b \ln\left(\frac{v_0 \theta}{L}\right) \right] \bar{\sigma} \tag{2.7}$$

where τ is the shear stress, $\bar{\sigma}$ is the effective normal stress, v is the slip rate, v_0 is the reference velocity, μ_s is the static friction coefficient at $v = v_0$, constants a and b depend on material properties, L is the critical slip distance, and θ is the state variable.

For control purposes, the so-called dynamic friction models, such as LuGre model, Dahl's model [186], and Bristle model [187], are developed, which introduce parameters to describe the friction phenomenon including the Coulomb friction, Stribeck friction, viscous, pre-sliding friction, time-dependent sticking friction and frictional memory. Canudas de Wit et al. [188] presented a six-parameter model called

the LuGre model, which is able to capture the various friction behaviour, but the price paid for this is that six parameters need to be identified. Eqs. (2.8)- (2.10) show the formulations with six parameters σ_0, σ_1, σ_2, v_s, μ, and μ_s:

$$F_r = \left(\sigma_0 z + \sigma_1 \frac{\mathrm{d}z}{\mathrm{d}t} + \sigma_2 v_r \right) F_n \tag{2.8}$$

The friction interface is likened as contact between the bristles on two rigid bodes. The bristles on the lower part is assumed as rigid. The bristle deformation of the upper part is defined by

$$\frac{\mathrm{d}z}{\mathrm{d}t} = v_r - \frac{\sigma_0 | v_r |}{g(v_r)} z \tag{2.9}$$

in which $g(v_r)$ is a parameter-dependent function with the general form:

$$\sigma_0 g(v_r) = \mu + (\mu_s - \mu) \mathrm{e}^{-|v_r / v_s|^\alpha} \tag{2.10}$$

and σ_0 is the characteristic bristle stiffness, σ_1 is the damping parameter, σ_2 is the viscous damping coefficient, v_r is the relative velocity, z is the average of the bristle direction, F_n is the contact normal force, μ is the Coulomb friction coefficient, μ_s is the static friction coefficient, v_s is the Stribeck velocity, and α is a constant parameter. Some other dynamic friction models can be found in Refs. [178, 189, 190].

2.4.2.2 *Applications of nonlinear friction in dynamics*

Berger [8] reviewed a vast body of literature in various engineering areas and examined the implications of the use of different friction models. He pointed out that developing an appropriate and ultimately useful model including a dynamic model and a friction model was a challenging task.

Discontinuity of the friction model is one basic source of the nonlinearity in friction problems [11, 12]. Non-smoothness or discontinuity in dynamic systems may result in bifurcations of the system [191]. Some works on non-smooth stick-slip vibration have been reviewed in Section 2.2.2. Moreover, Shin et al. [192] used the negative

relationship between friction and velocity in the dynamic analysis of a system which consisted two single-degree-of-freedom systems in parallel. It is found that the conventional role of damping that was supposed to dissipate energies now had more complex effects on the vibration. Stable vibration, stable stick-slip motion and even chaotic vibration can occur depending on the damping value. Kim and Perkins [107] derived the analytical solution of the non-smooth stick-slip motion using the Harmonic/Galerkin method. Awrejcewicz [120] conducted the analysis of the stick-slip vibration of a rigid plate, which had both rolling and sliding motion on a moving belt, and the Stribeck friction was considered. Vielsack [193] examined the decelerate velocity effect on the friction-induced vibration using four different friction models. It showed that even for the positive slope friction-velocity relationship, stick-slip vibration could happen. The simulation results with four different friction models were similar, which indicated that it was the decaying velocity that played the fundamental role in the stick-slip motion of the system rather than the friction models. Heilig and Wauer [194] investigated the stability of a brake system using two kinds of contact models, in which friction was velocity-dependent, and found that the inner resonance accounted for the instability. Moreover, the contact model, which considered the direction change of the friction with the deformation of the brake, brought no additional effects, which leaded the conclusion that a general contact model was sufficient to describe the contact properties. In Ref. [195], the Wojewoda's hysteresis loop friction model was used to analyse the dynamics of the classic slider-belt system. It is noticed that the system can form multiple limit cycles of which the amplitude was affected by the velocity and the brake pressure.

Many works used the smooth friction laws in the study of friction-induced vibration [27, 196-199]. Van de Vrande et al. [198] used a smoothed friction law to simulate the dynamics of the drill spring, which predicted that non-smooth kind of nonlinearity could happen even for a problem with the continuous friction model. However, the smoothed friction causes stiff equations of motion, which largely increase the simulation time. Leine et al. [200] proposed a switch method for the non-smooth problem. Additionally, the advantage of this method was that it could directly work with general ODE solver in software such as Matlab and Maple with high accuracy.

Several other works used rate and state dependent friction laws for dynamic study. The importance of the varying normal load on the motion of sliding system subjected to rate/state dependent friction was examined in Refs. [37, 184]. In Ref. [201], the stability analysis of 2-Dof system with a velocity related dynamic friction model was carried out for the brake-induced vibration of trains. The analytical expression of the critical speed for the bifurcation was obtained through the Routh–Hurwitz criterion. Elmer [42] studied the nonlinear behaviour of a harmonic spring-block systems, in which friction was modelled as a sticking-time-dependent static friction force and a velocity-dependent kinetic friction force.

There are several researchers using LuGre model in their work on friction-induced vibration [202-204]. Jia and Li [204] carried out experimental and numerical study on the brake with the LuGre friction. Results showed that the tangential motion of the pad undergo pure sliding or stick-slip, and may become chaotic depending on the parameter values. Hoffmann [202] predicted that the influences of LuGre model on the mechanism of mode-coupling instability were rather small in most of the parameter ranges. Comparison to the pure velocity-dependent friction model, determination of the instability boundary of the sliding motion were more complicated with LuGre friction. Li and Ding [205] considered the LuGre model in the study of a self-excited 3-DoF model. With the decreasing of the velocity, the vibration changed from the pure sliding motion to combinations of pure sliding and stick-slip motion, finally to the stick-slip motion with oscillations. The viscous damping coefficient played an important role in the tangential and torsional vibration of the system, that could lead to chaotic vibration at very large values.

As the dynamic friction model itself is complicated, it is not surprised to find that classic friction laws have much wilder applications in the theoretical study of friction-induced vibration than the dynamic ones so far.

2.4.3 Nonlinear contact stiffness

Contact is one of the significant nonlinearity sources in friction-induced vibration. During the past decades, several contact force models have been developed for

different applications, such as the pure elastic Hertz's contact law [206], and the dissipative contact force models [207]. Experiments show that the deformation-loading relationship between the disc and pad was highly nonlinear [155]. The contact between the pad and the disc can be modelled as polynomial nonlinear contact springs which were easy to be treated by general nonlinear techniques [208-212].

Liu [213] considered the polynomial nonlinear contact in the study of an aircraft brake squeal. The nonlinear contact springs to fit the first and third order of the compression curve of the pad under loading were involved in the study of friction-induced vibration that produced new findings on disc brake squeal [214, 215]. In Ref. [216], a complex nonlinear modal analysis method was utilised which also showed its efficiency in terms of the limit cycle prediction. In [217], theoretical analysis of a friction-induced vibration system with a cubic nonlinear contact stiffness was carried out through new techniques developed from the classic methods.

The nonlinear properties in the structures were taken into account in the sprag-slip vibration [70]. Stability of the nonlinear system was investigated through eigenvalue analysis of the Jacobian matrix of the linearised system. The centre manifold approach turned out to be a much more efficient method for studying the amplitude of the nonlinear system than solving the time response. Sinou and Jézéquel [61] proposed a nonlinear 2-DoF model on the base of the linear one [66, 67]. The critical friction coefficient for mode-coupling was derived through Routh–Hurwitz criterion and the damping effects on mode-coupling instability and the vibration amplitude of the nonlinear model were analytically analysed.

2.4.4 Change of contact due to dynamics

As known, the tangential friction can result in oscillations in the normal direction, therefore the change of contact does not only affect the normal force but also the friction force either [17], which could potentially lead to separation between the friction interfaces [218]. The phenomenon of a pin separating from a disc was detected in both the numerical simulations and test results [118]. Elmaian et al. [219] performed an exploration on the motion configurations of a phenomenological model, which

facilitated the understanding of friction-induced vibration in the automobile. Three kinds of the main mechanisms (stick-slip, sprag-slip and mode-coupling) for friction-induced vibration as well as separation can be observed during the motion. The contact states were taken into account in the principle of classifying the noise categories. Nonlinear simulations by Chen et al. [95] showed that the time delay between the normal force and friction force can lead to squeal, and the encounter of separation between two sliding surfaces was a main nonlinear factor that gets squealing vibration bounded.

Besides being observed in experiments, contact and loss of contact phenomenon were considered in many finite element simulations of the brakes [63, 136, 220-222]. Massi et al. [222] studied the dynamics of a simplified finite element disc-pad model. Both of the complete separation and the local detachment between the surfaces of the pad and the disc were detected. In particular, the contact situations determined the strength of the brake squeal because they affected the final limit cycle of the vibration. Sinou [136] pointed out that the contact nonlinear springs as well as separation resulted in the appearance of harmonic components and combinations of the harmonic components of the unstable vibration.

In addition, Baillet and his co-workers [145, 220, 221, 223], and Adams [218] carried out the research on the local unstable behaviour of smooth contact surfaces of the deformable solids, in the form of the wave propagation. In Ref. [221], the local instability of a deformable pin/disc model, generated by the propagation of stick-slip, slip-separation and stick-slip-separation kind of waves at the interfaces were studied through an explicit dynamic finite element program (PLAST3). Due to the variation of the local contact state, the global friction coefficient, which was defined as the ratio of the friction force over the normal force, can be smaller than or equal to the local friction coefficient of the node, which is assumed as a constant. A later paper [223] showed that the occurrence of impacts at the interface generated by steady-self pulse corresponding to the periodic peaks of the structure vibration. Meziane et al. [145] investigated the instability of a pad-disc tribometer through a finite element software PLAST3 with experimental validation. It highlighted that stick-slip-separation and

stick-slip waves accounted for the different noises of squeal. Wang [224] studied the stability and nonstationary vibration of a 4-DoF pad and disc model with nonlinearities from the Stribeck friction model and contact loss. It showed that tangential stiffness of the system is important to the configuration of stick-slip vibration, on the other hand, the normal stiffness of the pad and disc, and the contact stiffness are key factors that influence the behaviour of separation.

2.5 Analysis methods

Friction-induced vibration has been investigated through various experimental [225-228] and theoretical methods. Theoretical study through analytical or numerical methods gives insights to friction-induced vibration problems and offers useful guidance to set up test-rigs. To carry out the simulation or analysis, complex eigenvalue analysis and dynamic transient analysis are two big categories. Ouyang [229] reviewed the relevant research on the numerical analysis of automotive disc brake squeal. The pros and cons of both methods were stated.

2.5.1 Complex eigenvalue analysis (CEA)

Complex eigenvalue analysis (CEA) is a useful tool for stability analysis and provide sufficient estimations for the onset of unstable motion. Besides, Routh–Hurwitz criterion is another useful method for stability analysis [61, 201, 230].

The preceding section has involved several works on the CEA of the linear system [58, 64, 101]. Generally, analytical expressions of eigenvalues can be obtained in linear problems. Kang [231] formulated the equation of motion of a system with a rigid pad and distributed springs, and derived the analytical expressions of the eigenvalue. The mode coupling between the rigid pad and contact springs was investigated.

For a nonlinear system, basically, its stability can be investigated through the complex nonlinear eigenvalue analysis of the corresponding linearised system [214, 229, 232]. Sinou et al. [214] built a nonlinear finite element brake model and studied the instability of the system with a stationary disc. The main steps of the nonlinear stability analysis are: (1) calculate the equilibriums of the nonlinear system; (2) linearise the

nonlinear system around its equilibrium point; (3) derive the Jabobian matrix of the linearised system; (4) calculate the eigenvalues of the Jabobian matrix; (4) simulate the evolution of the eigenvalues with the friction coefficient or other parameter values. That paper showed that even if the dominant vibration frequency of the transient response sometimes can be different from the unstable frequencies of CEA, this did not mean that new unstable frequencies arose during the vibration. The new frequencies could be harmonic components of the unstable frequencies or combinations of them.

Additionally, Bajer et al. [233] described a new complex eigensolver in Abaqus to simulate nonlinear CEA of a simplified brake model with velocity-dependent friction. Liu et al. [139] used Abaqus to implement the stability analysis of a simplified pad-disc system and found that the influences of hydraulic pressure and the rotating speed on the stability of the system are not significant. Moreover, the role of the viscoelastic damping on the instability of a brake system was examined [234] through the CEA of Abaqus. Adding the viscoelastic damping could stabilise some of the unstable modes, but resulted in new mode-coupling between other modes.

Ref. [136] concluded that although unstable frequencies predicted by CEA could be overestimate or underestimate the unstable vibration, it gave insights to the instability of the nonlinear system. Massi et al. [222] investigated the unstable dynamics of two numerical disc-pad models (linear and nonlinear model) and identified that CEA of the linear model was convenient to predict the onset of instability, and transient dynamics analysis of the nonlinear model was able to obtain the development of the instability with the nonlinearity during the braking process. Some unstable modes predicted by CEA were the same with the results of transient dynamic analysis in terms of the frequency values. But as CEA relies on the linearisation of the nonlinear systems around its static position, thus one of the main limitations of the CEA of linearised systems is that the results only accurate around its static state [229].

2.5.2 Transient dynamic analysis (TDA)

Unlike CEA, TDA of the nonlinear system is important for the observations of the true evolution of the motion when the vibration is far away from its static state, or the system is time varying [217, 229].

In the literature about TDA of complex structures, Ref. [156] introduced a nonlinear contact model in a simplified disc model. The loading process was highlighted as an important factor in the squeal propensity. Wang et al. [235] considered to cut grooves on the surface of the pad to eliminate the brake squeal of a laboratory rig. The transient responses with different grooves were calculated numerically. Results showed that the friction noise can be reduced largely when the angle of the grooves is at 45 or 90 degrees with respect to the rotating direction. In Ref. [62], both of a mechanical model and a test-rig of a beam-on-beam system were built up. Theoretical analysis of the transient response gave explanations of the unstable phenomenon observed in experiments, and showed that the contact states (stick, slip or separate) and the relative velocity played much more important roles in the vibration than the external normal force.

On the other hand, transient dynamic analysis also has limitations, such as the long computation time issue and the subsequent storage problem. Furthermore, Ref. [236] pointed out that for the analysis of high frequency vibration, results obtained through different numerical methods were not identical. The rule of choosing a suitable numerical method should refer to the specific application. AbuBakar and Ouyang [237] studied the correlation of the results between CEA and TDA. It addressed that although the unstable frequencies could be predicted by transient analysis, due to the limitations of the model and algorithms, frequencies obtained from the transient analysis could not cover all the unstable natural frequencies predicted by CEA.

2.6 Model reduction

As known, the excessive time cost is one major drawback of the dynamic transient analysis, which makes parametric study hard to be performed. On the other hand,

although stability study of the friction-induced vibration by solving the non-symmetrical eigenvalue problem of a large system with friction is feasible, it is also expensive from the computation cost point of view.

2.6.1 Techniques

Model reduction is a good solution to overcome the high computational cost of large/complicated structures, and at the same time can preserve the key features of the original high-order model. Besselink et al. [238] reviewed the model reduction techniques that usually applied in structural dynamics and control. Popular model reduction techniques in structural dynamic analysis are related to mode superposition for the full system and component mode synthesis (CMS) [239] for substructures. Balanced truncation is the most popular model reduction method in the area of systems and control, owing to its advantage at preserving the stability properties of the original high-order systems. In addition, Krylov subspace based method is widely applied in the reduction of large electronic circuits [238], but can be also used to give good approximations of the system's transfer function in structural dynamics. Furthermore, reduction techniques are often utilised in the study of uncertainties in dynamics [240, 241].

2.6.2 Applications in friction-induced vibration

In the study of friction-induced vibration, many reduced order models have been proposed these years in order to save the computational time [215, 242]. Do et al. [242] proposed a completely new strategy that coupled the control approach, the homotopy and CMS techniques to reanalysis the stability of friction-induced vibration problem . Brizard et al. [243] applied model reduction techniques in the investigation of the stability of a disc-pad system and gave enrichment suggestions for two popular model reduction methods. The classical CMS technique caused errors regarding to the frequencies, divergence rates and shapes. That paper suggested that the precision of the system reduced by CMS method can be improved by adding the tangential attachment modes. For the method using a reduced basis of the unstable coupling modes of the full model, better results will be achieved if the first-order approximated

static response to the friction force or the tangential attachment modes were included. In a later paper, Fazio et al. [244] proposed a reduction strategy aiming to reduce the number of contact points, by which improvements on the stability analysis of a real brake were gained.

Kappagantu and Feeny [245] pointed out that with proper orthogonal modes (POMs) built from experimental data, a reduction of a multi-degree-of-freedom system with the stick-slip kind of non-smooth vibration can reflect the dynamic characteristics of the original system, including the occurrence the bifurcation of the original full system. Another work [246] used proper orthogonal modes (PODs) from the chaotic vibration tested in experiments [247] to reduce a frictionally excited Euler–Bernoulli beam.

Loyer et al. [248] tested the performance of two kinds of model reduction bases in the study of the nonlinear behaviour of a friction destabilised elastic layer. One was the conventional modal truncation, and the other considered both of the fundamental frequencies and the harmonic components due to nonlinearity. It concluded that both reduction bases gave good accuracy. However, for the second method with harmonic bases, including more unstable modes was not necessary as the improvement of the accuracy is inconspicuous.

3 Basic Theories of Friction-induced Vibration and Transient Dynamic Analysis Algorithm for Non-smooth Vibration

3.1 Introduction

This chapter mainly introduces the basic knowledge related to the thesis and the transient dynamic analysis algorithm for non-smooth vibration. As is known, friction-induced vibration has been a long-term issue in various engineering applications. Constantly ongoing engineering problems arouse the attention to investigate the instability mechanisms of friction-induced vibration. As reviewed in Chapter 2, the mechanisms mainly fall into four categories: the negative friction-velocity slope, stick-slip instability, mode-coupling instability and sprag-slip instability. In Section 3.2, the fundamental dynamic characteristics of these four kinds of friction-induced instability are explained in detail through classical examples reported in the works of Hoffmann, Popp, Spurr, Ouyang et al.

Lumped mass systems and plates are very often used models for the study of friction-induced vibration. Fundamental theory of mechanical vibration, including the analytical formulations of discrete systems and elastic annular plates are presented in Section 3.3. Especially, the modal analysis method of multi-degree-of-freedom systems, and the derivation process of an annular plate are described in detail. For a comprehensive theory of mechanical vibration, readers may refer to books [249, 250].

Because of friction, complex properties such as nonlinearity, non-smoothness, discontinuity and asymmetry, can be involved in the dynamic system. Transient response is a very useful result to reveal the dynamic characteristics of the system. In Section 3.4, a numerical method as well as an algorithm for simulating transient dynamic response of the non-smooth systems are presented, which are very useful to the study of following chapters.

3.2 Mechanisms of friction-induced vibration

3.2.1 Negative friction-velocity slope

Various kinds of friction laws are developed during the past decades. Negative gradient of the friction coefficient with respect to the relative velocity is a common feature of most friction laws. In this part, a friction law that reflects this deceasing feature is used to give an insight to the idea of the instability caused by the negative slope of the friction law.

A one-degree-of-freedom mass-spring-belt model, shown in Fig. 3.1 is used. In Fig. 3.1, the slider is a point mass, referred to as m, x describes the horizontal displacement of m, k is the spring stiffness, c is the damping, F_n is the normal compression force, and v_0 is the velocity of the moving belt. There is friction contact between the mass and the moving belt. Although this model is simple, it involves friction in a smart way as friction is a primary factor affecting the dynamics of the system, which is very suitable for mechanism study. This system is a classic model that can be used for study of various friction-induced vibration problems.

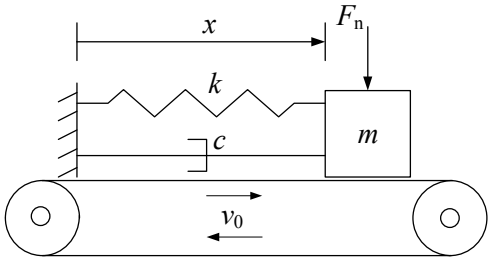

Fig. 3.1 The one-degree-of-freedom mass-spring-belt system

According to Newton's second law, the equation of motion of the system is expressed as:

$$m\ddot{x} + c\dot{x} + kx = F_r(v_r) \tag{3.1}$$

in which $F_r(v_r)$ is the friction force function of v_r, and v_r is the relative velocity between the mass and the belt, defined by Eq. (3.2):

$$v_r = \dot{x} - v_0 \tag{3.2}$$

Assuming the friction force F_r is proportional to F_n, with coefficient $\mu(v_r)$ known as the friction coefficient, the friction force is expressed as $\mu(v_r)F_n$. In the following, the relation $F_r = \mu(v_r)F_n$ is used, if there is no further clarification. Here, friction coefficient function $\mu(v_r)$ uses the expression given by Eq. (2.3), then the friction force is expressed as:

$$F_r = \mu(v_r)F_n = (\mu_s - \mu_2 \mid \dot{x} - v_0 \mid)F_n \tag{3.3}$$

in which μ_s and μ_2 are constants. μ_2 is the gradient coefficient of $\mu(v_r)$.

As the friction force changes direction when the relative velocity changes the sign, the friction force function is given by Eq. (3.4)

$$F_r(v_r) = -[\mu_s F_n - \mu_2 F_n \mid \dot{x} - v_0 \mid]\mathrm{sgn}(\dot{x} - v_0) \tag{3.4}$$

which also can be written as:

$$F_r(v_r) = \begin{cases} -\mu_s F_n + \mu_2 F_n (\dot{x} - v_0) & \dot{x} > v_0 \\ [-\mu_s F_n,\ \mu_s F_n] & \dot{x} = v_0 \\ \mu_s F_n + \mu_2 F_n (\dot{x} - v_0) & \dot{x} < v_0 \end{cases} \tag{3.5}$$

By substituting Eq. (3.4) into Eq.(3.1), the equation of motion is rewritten as Eq. (3.6) :

$$m\ddot{x} + (c - \mu_2 F_n)\dot{x} + kx = -\mu_s F_n \,\mathrm{sgn}(\dot{x} - v_0) + \mu_2 F_n v_0 \tag{3.6}$$

In Eq. (3.6), it can be found that, when $\mu_2 F_n > c$, the damping of the system becomes negative, which results in divergent vibration. Therefore, the negative slope of friction coefficient with respect to the relative velocity may cause negative damping in the system, which is recognised as one of the reasons for unstable friction-induced vibration.

3.2.2 Stick-slip vibration

In this part, the idea of friction-induced stick-slip vibration is illustrated. Various kinds of stick-slip vibration from periodic to chaotic vibration are illustrated.

3.2.2.1 *Stick-slip limit cycle*

The one-degree-of-freedom mass-spring-belt model shown in Fig. 3.2 is used to study the stick-slip vibration. This model differs slightly from the model shown in Fig. 3.1 as damping is not included. The same notations, which are defined in Section 3.2.1, are used. The friction at the interface follows the Coulomb's law of friction.

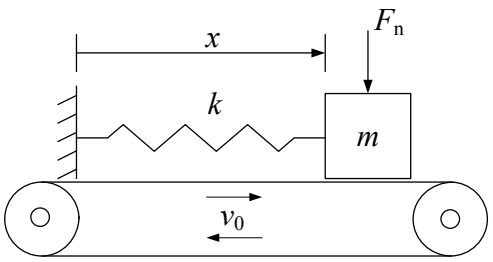

Fig. 3.2 One-degree-of-freedom mass-belt model

The mass experiences the following process: it sticks on the belt and moves with it, at the commencing stage. At the same time, the spring is stretched and the spring force keeps growing. The static friction force holds the mass to stick on the belt as long as the spring force is smaller than the friction capacity. However, once the spring force exceeds the friction capacity, the slider starts to slide. At the same instant, the friction regime suddenly changes from the static one to the kinetic one whose friction coefficient is smaller. Thus, the mass can slide further on the belt. As the spring force is larger than the kinetic friction force, the forward sliding (the slider slips at the same direction of the moving belt) velocity of the slider decreases, and at the reversal point of the velocity the sliding direction of the slider changes to the direction opposite to that of the moving belt (backward sliding). After a while, the spring is compressed and the backward sliding of the slider is resisted, which makes slider change its sliding direction to forward sliding. Then when it reaches the same speed with the moving belt and the spring force is smaller than static friction capacity, the mass sticks on the

moving belt again. The preceding stick-slip motion repeats during the vibration of the system. As motion states alternate, this is a non-smooth process.

The formulations of stick-slip vibration are presented below. For stick motion, the displacement and velocity of the mass are given by Eq. (3.7).

$$x = v_0 t\ , \quad \dot{x} = v_0 \tag{3.7}$$

For slip motion, friction force $F_r = \mu_k F_n$, and its direction is determined by the relative velocity between the mass and the moving belt. The equation of motion of the mass is given by Eq. (3.8):

$$m\ddot{x} + kx = -\mu_k F_n \operatorname{sgn}(v_r) \tag{3.8}$$

The condition for the switching from stick mode to slip mode is:

$$|kx| > \mu_s F_n \tag{3.9}$$

in which kx is the spring force, and $\mu_s F_n$ is the static friction capacity.

On the other hand, the conditions for switching from the slip to stick mode are:

$$\dot{x} = v_0 \quad \text{and} \quad |kx| < \mu_s F_n \tag{3.10}$$

Table 3.1 shows the parameter values for the numerical calculations below. The vibration results of the mass are visualised in the phase plane.

Table 3.1 Parameter values

m	k	F_n	v_0	μ_s	μ_k
1kg	1N/m	5kg	0.2m/s	0.4	0.2

Fig. 3.3 illustrates the phase portrait described by $\dot{x}$ against x of the mass, and the time history of the friction force. In Fig. 3.3 (a), the horizontal straight line, represents the stick motion as its corresponding velocity is 0.2 (v_0); and the curve represents the slip motion. The stick and slip motion in phase plane form a closed trajectory, which is referred to as the stick-slip limit cycle. Furthermore, Fig. 3.3 (b) shows that the

friction force jumps at the transition points at stick to slip or slip to stick, which results in the non-smoothness of the vibration.

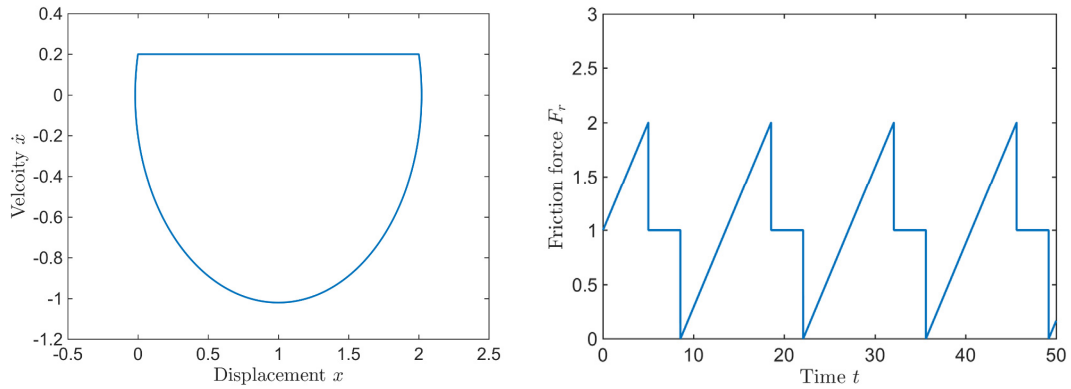

(a) (b)

Fig. 3.3 Time response of the system. (a) Phase portrait of the slider (b) Time history of the friction force

3.2.2.2 *Chaotic stick-slip vibration*

In the preceding subsection, the self-excited one-degree-of-freedom stick-slip vibration is introduced which generates a stable stick-slip limit cycle. However, stick-slip vibration can be very complex and crucially depends on the system parameters. In the current part, unstable stick-slip vibration is predicted.

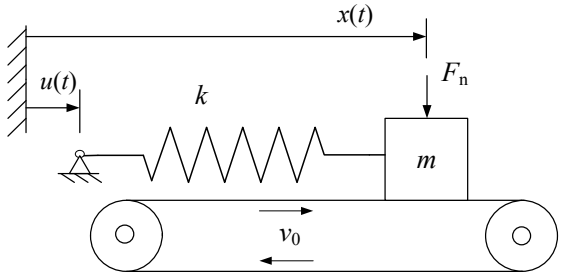

Fig. 3.4 The one-degree-of-freedom mass-belt model with a base excitation

Fig. 3.4 illustrates a model that was studied in Ref. [46], which is similar to Fig. 3.2, but with an external excitation. The same notation defined in Section 3.2.1 is used. Dry friction occurs between the slider and the moving belt, and the friction force is $F_r(v_r)$. $u(t)$ is a displacement excitation, in the following form:

$$u(t) = u_0 \cos(\Omega t) \tag{3.11}$$

in which Ω is the excitation frequency, and u_0 is the amplitude.

The equation of motion of the system, in the non-dimensional form is given by Eq. (3.12):

$$\ddot{x}_1 + x_1 = F_r(v_r)/k + u_0 \cos(\eta\tau) - x_s \tag{3.12}$$

The variables and parameters in Eq.(3.12) are non-dimensionalised by

$$\omega_0^2 = \frac{k}{m},\quad \eta = \frac{\Omega}{\omega_0},\quad x_s = \frac{F_r(-v_r)}{k},\quad x_1 = x - x_s,\quad \tau = \omega_0 t$$

The friction force $F_r(v_r)$ is expressed as:

$$F_r(v_r) = -\mu(v_r) F_n \operatorname{sgn}(v_r) \tag{3.13}$$

in which $\mu(v_r)$ is a friction model following Eq. (3.14) and depicted in Fig. 3.5:

$$\mu(v_r) = (\mu_0 - \mu_1)/(1 + \lambda |v_r|) + \mu_1 + \alpha v_r^2 \tag{3.14}$$

in which all the parameters are constant: μ_0 =0.4, μ_1 =0.2, λ =1.42 sm^{-1}, α = 0.01 s^2m^{-2}.

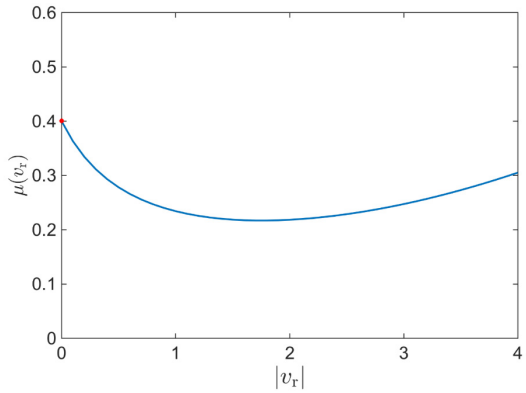

Fig. 3.5 The friction model used in Eq. (3.14)

Numerical calculations are performed with parameter values: ω_0=1, F_n/k=10, u_0=0.5, and v_0=1. Stick-slip vibration of the system under the external excitation of different η

is calculated. Results are given by Fig. 3.6 (a)-(e). Different types of vibration can be seen: single periodic vibration, double periodic vibration, multi-periodic vibration, and even chaotic vibration.

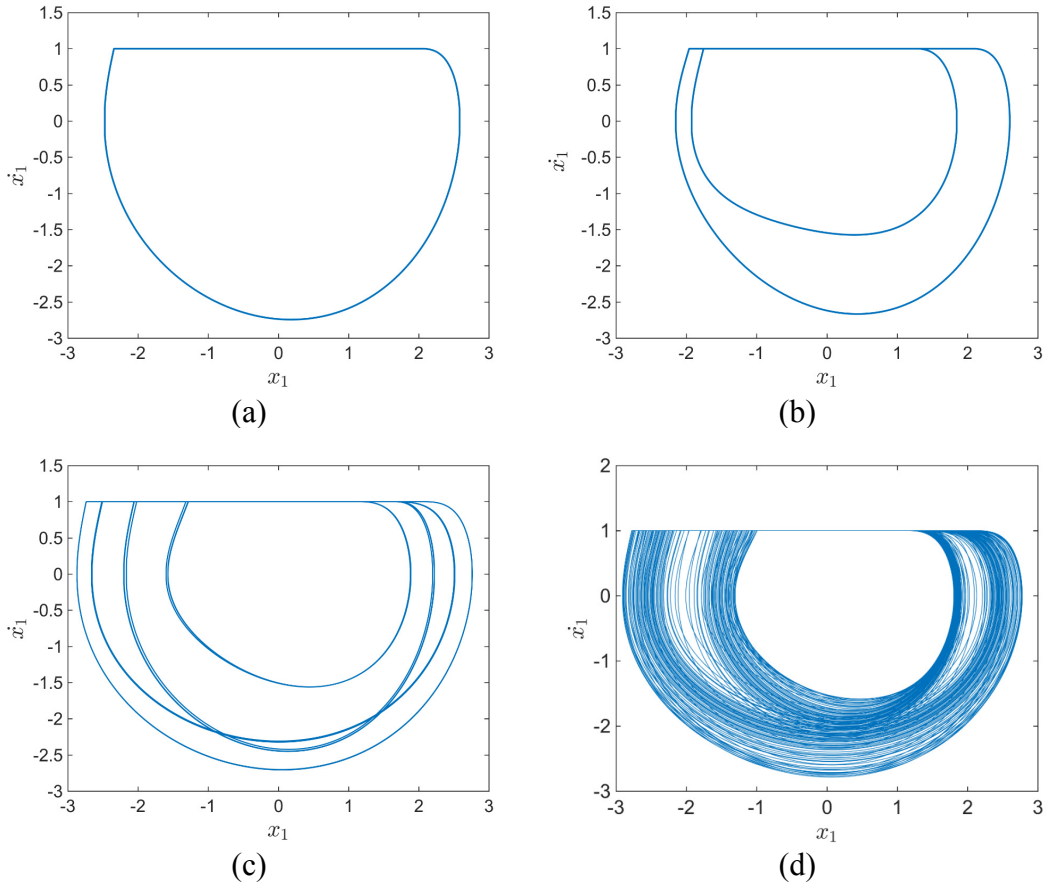

Fig. 3.6 Phase portraits. (a) $\eta = 1.5$; (b) $\eta = 1.98$; (c) $\eta = 1.3$ (d) $\eta = 1.2$

when the degrees of freedom of the system is more than two, richer dynamic behaviour of the unstable self-excited stick-slip vibration may happen, for example the two mass model in Ref. [46]. Work on stick-slip instability has been reviewed in Chapter 2.

3.2.3 Mode-coupling instability

Mode-coupling instability has been accepted as the most general mechanism for brake squeal. Instead of relying on the friction laws to cause friction-induced vibration, this mechanism focuses on the contribution of the structure's geometry on system

dynamics with friction, which facilitates the friction-induced vibration study from a different point of view.

In this part, one model put forward and studied by Hoffmann [58] that illustrates the essential idea of the model-coupling instability is exhibited. The mechanical model is shown in Fig. 3.7. In this model, k_1, k_2 and k_3 are linear springs. The bottom end of spring k_3 is linked to a massless slider, which has frictional contact with the underneath belt moving at constant velocity v_0. The friction force is denoted by F_r, with a constant friction coefficient μ.

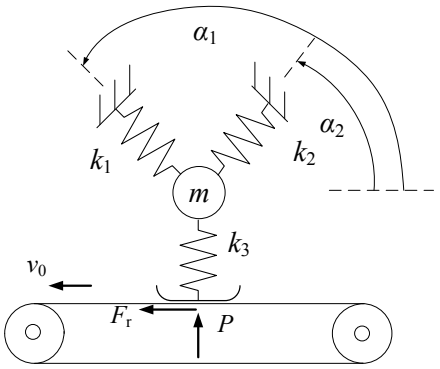

Fig. 3.7 The two-degree-of-freedom model

The contact force between the slider and the belt is spring force $k_3 y$, thus the friction force is implied as:

$$F_r = \mu k_3 y \tag{3.15}$$

The equations of motion can be expressed as Eq. (3.16):

$$\begin{bmatrix} m & 0 \\ 0 & m \end{bmatrix} \begin{pmatrix} \ddot{x} \\ \ddot{y} \end{pmatrix} + \begin{bmatrix} k_{11} & k_{12} - \mu k_3 \\ k_{21} & k_{22} \end{bmatrix} \begin{pmatrix} x \\ y \end{pmatrix} = \begin{pmatrix} 0 \\ 0 \end{pmatrix} \tag{3.16}$$

in which

$$\begin{cases} k_{11} = k_1 \cos^2 \alpha_1 + k_2 \cos^2 \alpha_2 \\ k_{12} = k_{21} = k_1 \sin \alpha_1 \cos \alpha_1 + k_2 \sin \alpha_2 \cos \alpha_2 \\ k_{22} = k_1 \sin^2 \alpha_1 + k_2 \sin^2 \alpha_2 + k_3 \end{cases} \tag{3.17}$$

It can be seen that the stiffness matrix becomes asymmetric due to the friction force term $\mu k_3 y$. Then the eigenvalues λ can be solved through the eigenvalue analysis. The analytical solutions of the eigenvalues for parameter values m=1, $\alpha_1 = 150^\circ$, $\alpha_2 = 30^\circ$, $k_1 = 2(2-\sqrt{3})/3$ $k_2 = 2(2+\sqrt{3})/3$, $k_3 = 4/3$, are given by Eq. (3.18):

$$\lambda = \pm\left[-2 \pm \sqrt{1-\mu k_3}\right]^{\frac{1}{2}} \tag{3.18}$$

It is noticed that friction related term μk_3 is involved in the eigenvalues. More importantly, if $\mu k_3 > 1$, λ may be complex numbers with a positive real part. By setting μ as a control parameter, the changes of the eigenvalues are illustrated in Fig. 3.8 (a) shows that with the increase of the friction coefficient, one real part of the eigenvalues becomes positive, which means that the system becomes unstable. Additionally, Fig. 3.8 (b) shows that the frequencies of two modes merge together when the real part become positive. The friction coefficient at the coalescence point is refer to as the critical friction coefficient.

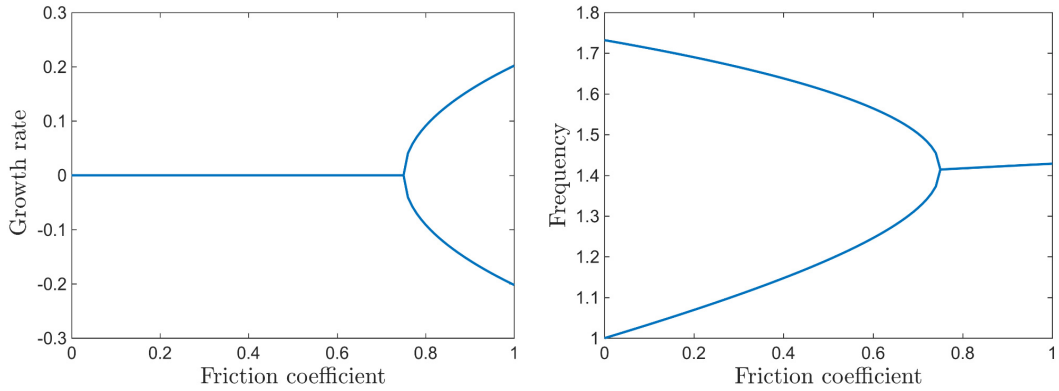

(a) (b)

Fig. 3.8 Real and imaginary parts of the eigenvalues. (a) real part; (b) imaginary part

Time histories of the vibration with different μ are shown in Fig. 3.9. The important role of friction in the stability of the system can be observed. When μk_3 is smaller than one, the real part of the eigenvalues is zero, vibration does not grow, shown in Fig. 3.9 (a); when the real part of the system is zero but at the bifurcation point, Fig. 3.9 (b) shows that the vertical motion of the mass grows and horizontal vibration is

stable; However, when μk_3 is larger than one, with the real part of the eigenvalue becoming positive, both of the horizontal and vertical vibration grow unbound, shown in Fig. 3.12 (c).

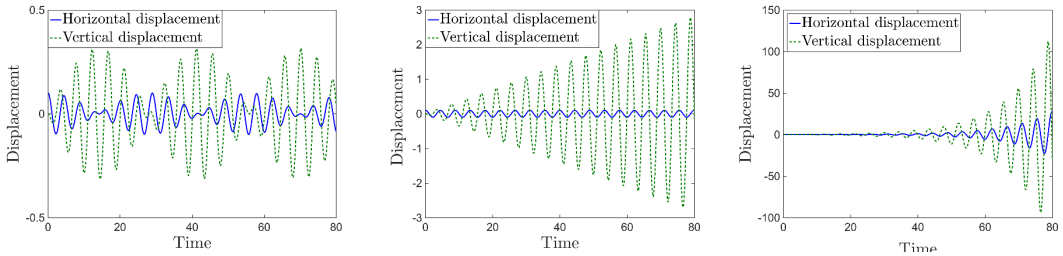

Fig. 3.9 Time history of the vibration. (a) $\mu k_3 = 0.9$; (b) $\mu k_3 = 1$; (c) $\mu k_3 = 1.05$

The preceding analysis shows that, self-excited unstable vibration can happen even in a system having only two degrees of freedom with sliding friction, because of the mode-coupling instability.

3.2.4 Sprag-slip instability

Sprag-slip is a phrase firstly created by Spurr [69] to describe the vibration which he assumed should happen when a brake squeals. In this theory, the friction coefficient is assumed to be a constant value μ independent of the relative speed, and the constraint-induced instability is revealed. In this part, an introduction of the sprag-slip mechanism described in Spurr's work is presented. Because sprag-slip is not involved in the current work, other insights relating to sprag-slip are not reported here and interested reader can refer to the papers cited in Chapter 2.

To describe the sprag-slip vibration, a perfectly rigid model is used in Ref. [69], shown in Fig. 3.10. In this model, a rigid rod inclines to a moving belt at one end with an angle θ, and is pivoted at the other end. F_{n} is a normal force compressing the rod on the belt. As a consequence, a friction resistance acts between the two relatively moving components.

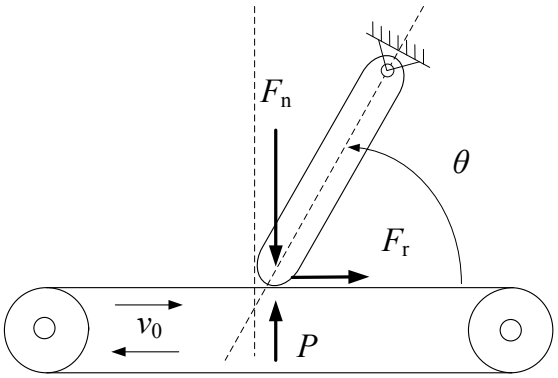

Fig. 3.10 The rigid bar with a moving belt model

According to the equilibrium condition of the momentums at the pivoted point, the constrained relationship between the contact force P and F_r is obtained:

$$P = F_n + F_r \tan\theta \tag{3.19}$$

With the assumption $F_r = \mu P$, the friction force and the contact force are derived as:

$$F_r = \frac{\mu F_n}{1-\mu\tan\theta} \quad , \quad P = \frac{F_n}{1-\mu\tan\theta} \tag{3.20}$$

Eq. (3.20) shows that, the friction force can become infinitely large, when $1-\mu\tan\theta$ is approaching to zero. Thus, this state is recognised as the rod is 'spragged' on the belt.

On the other hand, if the rod is an elastic component, it will bend with spragging, followed by the increase of θ. While bending, the value of $1-\mu\tan\theta$ becomes non-zero and increases with the increase of θ. As a consequence, the value of F_r drops. At the same time, elastic energy of the elastic component increases while bending. At this moment, the elastic force overcomes the spragging friction force, that makes the elastic rod release and go back to its original position, and θ becomes smaller again. Subsequently, the motion of the rod repeats this sprag-slip loop. In this theory, sideling angle θ of the structure is pointed out as a key factor in the vibration of the system.

3.3 Fundamental theory of the discrete system and the elastic plate

3.3.1 Vibration of discrete systems with dry friction

For many engineering systems, the components are continuous which have an infinite number of degrees of freedom. The properties of the continuous structures bring difficulties to dynamic analysis, for example, it is hard to obtain the solutions of the partial differential equations of continuous systems. Therefore, continuous systems are usually discretised for dynamic analysis, especially in complex problems with nonlinearity. In the following, the process of vibration analysis of the multi-degree-of-freedom systems with dry friction is presented.

3.3.1.1 *The theme of complex eigenvalue analysis with friction*

To theoretically carry out dynamic analysis, complex eigenvalue analysis (CEA) in frequency domain and the transient dynamic analysis (TDA) in time domain are two mainstream approaches. Each approach has advantages and disadvantages. Ouyang [229] reviewed the research on friction-induced vibration carried out by these two approaches. Vibration and noise problems caused by friction, like brake squeal, are usually associated with instability of a system. Complex eigenvalue analysis has been widely used by researchers as it provides a convenient way to identify the natural frequencies, modes and the stability of a system, which offers useful supports for quenching the unstable vibration.

The motion of a system can be expressed as the equation of motion derived on the base of the Newton's second law, or Lagrange's equations in terms of generalised coordinates. The differential equations of motion, derived by Newton's law, of an *n*-degree-of-freedom system subjected to friction, in matrix form, generally are expressed as:

$$\mathbf{M}\ddot{\mathbf{x}} + \mathbf{C}\dot{\mathbf{x}} + \mathbf{K}\mathbf{x} = \mathbf{f}_r \tag{3.21}$$

in which $\mathbf{M}$, $\mathbf{C}$ and $\mathbf{K}$ are respectively the mass, damping and stiffness matrices, and $\mathbf{f}_r$ is the friction force vector.

The analysis methods for solving general vibration of multi-degree-of-freedom systems are quite mature and can be found in many vibration text books [250, 251].

In terms of the systems with friction, there are many ways to incorporate friction into a system. It is notable that the dry friction force may relate the degree of freedom in the normal direction to the degree of freedom in tangential direction, e.g. friction-loaded springs [252]. This allows friction force to be expressed by the degree of freedom in the normal direction, given by Eq. (3.22):

$$\mathbf{f}_{\mathrm{f}} = \mu \mathbf{K}_{\mathrm{f}} \mathbf{x} \tag{3.22}$$

in which $\mathbf{K}_{\mathrm{f}}$ represents an asymmetric matrix generated at the friction contact, and μ is the corresponding friction coefficient.

The newly formed equations of motion of the system is given by Eq. (3.23)

$$\mathbf{M}\ddot{\mathbf{x}} + \mathbf{C}\dot{\mathbf{x}} + \left(\mathbf{K} - \mu \mathbf{K}_{\mathrm{f}}\right)\mathbf{x} = \mathbf{0} \tag{3.23}$$

A distinct feature of the stiffness matrix $\mathbf{K} - \mu \mathbf{K}_{\mathrm{f}}$ is that it is asymmetric.

According to the theory of the multi-degree-of-freedom system, the solutions of Eq. (3.23) are in the form of Eq. (3.24):

$$\mathbf{x}(t) = \boldsymbol{\varphi} \mathrm{e}^{\lambda t} \tag{3.24}$$

By substituting Eq. (3.24) into Eq. (3.23), a quadratic eigenvalue equation can be derived:

$$\left(\lambda^2 \mathbf{M} + \lambda \mathbf{C} + \mathbf{K} - \mu \mathbf{K}_{\mathrm{f}}\right)\boldsymbol{\varphi} = \mathbf{0} \tag{3.25}$$

Then the eigenvalue λ and the eigenvector $\boldsymbol{\varphi}$ can be solved, which may be complex numbers. λ is expressed as:

$$\lambda_i = \alpha_i \pm \mathrm{i}\omega_i \tag{3.26}$$

in which α_i is the real part, and ω_i is the imaginary part that is the natural frequency of the system; i is square root of -1. Apparently, there are three kinds of vibration depending on the sign of α_i :

1. when all α_i are negative, the system is stable as $\mathbf{x}(t) = \boldsymbol{\varphi} e^{\lambda t}$ decreases.

2. when one $\alpha_i = 0$ and all other real parts are negative, the system is neutrally stable. The stability of the nonlinear system cannot be predicted by the complex eigenvalue analysis and further transient analysis are required.

3. when one of the α_i is positive, the system is unstable as $\mathbf{x}(t) = \boldsymbol{\varphi} e^{\lambda t}$ increases.

3.3.1.2 *Complex eigenvalue analysis with nonlinearity*

For a nonlinear dynamic system with friction, one kind of unstable vibration is implied by the growth of motion of the system at the steady-sliding equilibrium point. Generally, stability analysis is carried out by the complex eigenvalue analysis on its linearised system at the equilibrium point. Assuming the equation of motion of the nonlinear system is in the following form:

$$\mathbf{M}\ddot{\mathbf{x}} + \mathbf{C}\dot{\mathbf{x}} + \mathbf{K}\mathbf{x} = \mathbf{f}_{\mathrm{NL}}(\mathbf{x}) \tag{3.27}$$

where $\mathbf{M}$, $\mathbf{C}$ and $\mathbf{K}$ are respectively the mass, damping and stiffness matrices, and $\mathbf{x}$ is the displacement vector. $\mathbf{f}_{\mathrm{NL}}(\mathbf{x})$ is the nonlinear force vector that contains all the nonlinear forces including the nonlinear contact forces and friction forces and they are functions of $\mathbf{x}$ and $\dot{\mathbf{x}}$. The equilibrium point $\mathbf{x}_{\mathrm{e}}$ is defined by Eq. (3.28), corresponding to a static nonlinear problem:

$$\mathbf{K}\mathbf{x}_{\mathrm{e}} = \mathbf{f}_{\mathrm{NL}}(\mathbf{x}_{\mathrm{e}}) \tag{3.28}$$

By defining a perturbation $\tilde{\mathbf{x}}$ around the equilibrium in the form $\tilde{\mathbf{x}} = \mathbf{x} - \mathbf{x}_{\mathrm{e}}$, then one gets $\dot{\tilde{\mathbf{x}}} = \dot{\mathbf{x}}$ and $\ddot{\tilde{\mathbf{x}}} = \ddot{\mathbf{x}}$. The governing equation of the linearised system is given by Eq. (3.29):

$$\mathbf{M}\ddot{\tilde{\mathbf{x}}} + \mathbf{C}\dot{\tilde{\mathbf{x}}} + \mathbf{K}\tilde{\mathbf{x}} = \mathbf{J}\big|_{\mathbf{x}_{\mathrm{e}}}\,\tilde{\mathbf{x}} \tag{3.29}$$

in which $\mathbf{J}\big|_{\mathbf{x}_e}$ refers to the approximation of the nonlinear vector at the equilibrium point, which can be obtained by Eq. (3.30):

$$\mathbf{J}\big|_{\mathbf{x}_e} = \left.\frac{\partial \mathbf{F}_{\mathrm{NL}}(\tilde{\mathbf{x}})}{\partial \tilde{\mathbf{x}}}\right|_{\mathbf{x}_e} \tag{3.30}$$

According to Section 3.3.1.1, the complex eigenvalue problem of the linearised system is Eq. (3.31):

$$\left[\lambda^2\mathbf{M} + \lambda\mathbf{C} + \left(\mathbf{K} + \mathbf{J}\big|_{\mathbf{x}_e}\right)\right]\boldsymbol{\varphi} = \mathbf{0} \tag{3.31}$$

in which λ and $\boldsymbol{\varphi}$ are the complex eigenvalues and eigenvectors of the linearised system. Complex eigenvalue analysis provides the local stability information around the equilibrium point. How the stability implied by the real part of λ has been stressed in Section 3.3.1.1.

3.3.1.3 *Modal analysis of an undamped system with friction*

In general, there are two strategies to solve the differential equations of motion of dynamic systems. One is the direct integration method. The mode superposition method is another popular strategy to facilitate the vibration analysis of multi-degree-of-freedom systems, by decoupling the differential equations of motion in physical coordinates to independent equations with respect to generalised coordinates. The principle of mode superposition method is presented in this part.

For an undamped *n*-degree-of-freedom system subjected to excitation forces, the equations of motion are expressed as:

$$\mathbf{M}\ddot{\mathbf{x}}(t) + \mathbf{K}\mathbf{x}(t) = \mathbf{f}_{\mathrm{r}}(t) + \mathbf{f}_{\mathrm{ex}}(t) \tag{3.32}$$

in which $\mathbf{f}_{\mathrm{r}}$ is the friction force vector, and $\mathbf{f}_{\mathrm{ex}}$ is the external excitation vector.

According to the expansion theorem, the transformation of the physical coordinates to generalised coordinates is given by Eq. (3.33):

$$\mathbf{x}(t) = \boldsymbol{\varphi}_1 q^{(1)}(t) + \boldsymbol{\varphi}_2 q^{(2)}(t) + \ldots + \boldsymbol{\varphi}_i q^{(i)}(t),\ i = 1,\ 2,\ \ldots,\ n \tag{3.33}$$

in which $\boldsymbol{\varphi}_i$ is the *i*th mode vector, $q^{(1)}(t)$, $q^{(2)}(t)$, …, $q^{(i)}(t)$ are the time-dependent generalised coordinates. By defining a modal matrix $\boldsymbol{\Phi}$, whose *i*th column is the mode vector $\boldsymbol{\varphi}_i$.

$$\boldsymbol{\Phi} = \left[\boldsymbol{\varphi}_1, \boldsymbol{\varphi}_2, \ldots, \boldsymbol{\varphi}_i\right] \tag{3.34}$$

and then Eq. (3.33) can be rewritten as:

$$\mathbf{x}(t) = \boldsymbol{\Phi}\mathbf{q}(t) \tag{3.35}$$

in which $\mathbf{q} = \left[q^{(1)};\ q^{(2)};\ \ldots;\ q^{(i)}\right]$ is a vector of the generalised coordinates.

On the base of the orthogonal properties of the normal mode vector $\boldsymbol{\varphi}_i$, one can get:

$$\boldsymbol{\Phi}^{\mathrm{T}}\mathbf{M}\boldsymbol{\Phi} = \mathbf{I}, \text{ and } \boldsymbol{\Phi}^{\mathrm{T}}\mathbf{K}\boldsymbol{\Phi} = \mathrm{diag}\left(\omega^2\right) \tag{3.36}$$

in which $\boldsymbol{\Phi}^{\mathrm{T}}$ is the transpose of $\boldsymbol{\Phi}$, and ω_i is the *i*th natural frequency of the structure. $\boldsymbol{\Phi}$ in Eq. (3.34) is mass-normalised.

By substituting Eq. (3.35) into Eq. (3.32), a new set of equations of motion in terms of $\mathbf{q}(t)$ is obtained:

$$\mathbf{M}\boldsymbol{\Phi}\ddot{\mathbf{q}}(t) + \mathbf{K}\boldsymbol{\Phi}\mathbf{q}(t) = \mathbf{f}_{\mathrm{r}}(t) + \mathbf{f}_{\mathrm{ex}}(t) \tag{3.37}$$

By premultiplying $\boldsymbol{\Phi}^{\mathrm{T}}$ on both side of Eq. (3.37), and according to Eq. (3.36), the equations of motion of the *n*-degree-of-freedom system is decoupled to *m* number of independent equations, written as Eq. (3.38), with respect to $q^{(i)}(t)$ (*i*=1, 2, …, *m*):

$$\ddot{\mathbf{q}}(t) + \mathrm{diag}\left(\omega^2\right)\mathbf{q}(t) = \boldsymbol{\Phi}^{\mathrm{T}}\mathbf{F}_{\mathrm{r}}(t) + \boldsymbol{\Phi}^{\mathrm{T}}\mathbf{F}_{\mathrm{ex}}(t)$$

or

$$\ddot{q}^{(i)}(t) + \omega_i^2 q^{(i)}(t) = \sum_{j=1}^{n} \Phi_i^{(j)} f^{r}{}_j(t) + \sum_{j=1}^{n} \Phi_i^{(j)} f^{\mathrm{ex}}{}_j(t) \tag{3.38}$$

in which $f^{r}{}_j(t)$ and $f^{\mathrm{ex}}{}_j(t)$ are the jth element of force vector $\mathbf{f}_{\mathrm{r}}(t)$ and $\mathbf{f}_{\mathrm{ex}}(t)$, respectively. $m \le n$. For large systems, usually *m* is chosen to be much smaller than *n*.

As friction force can be written as Eq. (3.22), then Eq. (3.38) is rewritten as:

$$\ddot{\mathbf{q}}(t)+\left(\mathrm{diag}\left(\omega^2\right)+\mu\boldsymbol{\Phi}^{\mathrm{T}}\mathbf{K}_{\mathrm{f}}\boldsymbol{\Phi}\right)\mathbf{q}(t)=\boldsymbol{\Phi}^{\mathrm{T}}\mathbf{f}_{\mathrm{ex}}(t)$$

or

$$\ddot{q}^{(i)}(t)+\left(\omega_i^2+\mu\sum_{i=1}^{n}\sum_{j=1}^{n}\Phi_i^{(j)}K^{\mathrm{f}}{}_{ij}\Phi_i^{(j)}\right)q^{(i)}(t)=\sum\nolimits_{j=1}^{n}\Phi_i^{(j)}f^{\mathrm{ex}}{}_j(t) \tag{3.39}$$

in which $K^{\mathrm{f}}{}_{ij}$ is the element of stiffness matrix $\mathbf{K}_{\mathrm{f}}$ generated from the friction contact.

The solution of Eq. (3.39) $q^{(i)}(t)$ can be obtained through a general process of the forced vibration problem of a single degree of freedom system. Then the solution of $\mathbf{x}(t)$ with respect to physical coordinates can be obtained by Eq. (3.35).

3.3.2 Fundamental theory of an elastic annular plate

3.3.2.1 *The equation of motion of the annular plate*

On the base of the linear bending theory of a plate [253], the equation of motion for forced transverse vibration of an annular plate in polar coordinates is given by Eq. (3.40) [249].

$$\rho h\frac{\partial^2 w}{\partial t^2}+D^*\nabla^4\dot{w}+D\nabla^4 w=f \tag{3.40}$$

where w is the transverse displacement, ρ the density of the plate, h the thickness of the plate and D^* is the Kelvin-type damping coefficient of the plate, D represents the flexural rigidity of the plate:

$$D=\frac{Eh^3}{12(1-v^2)} \tag{3.41}$$

where v is the Poisson ratio, and

$$\nabla^2 = \frac{\partial^2}{\partial r^2} + \frac{1}{r}\frac{\partial}{\partial r} + \frac{1}{r^2}\frac{\partial^2}{\partial \theta^2} \tag{3.42}$$

$$\nabla^4 w = \nabla^2\left(\nabla^2 w\right) \tag{3.43}$$

For the free vibration of the plate, the external load f equals to zero. By using the method of separation of variables, the transverse displacement of the plate can be represented as:

$$w(r,\theta,t) = W(r,\theta)T(t) \tag{3.44}$$

After separation of variables, the governing equation of $T(t)$ and $W(r, \theta)$ are given by Eqs. (3.45) and (3.46):

$$\frac{\mathrm{d}^2}{\mathrm{d}t^2}T(t) + \frac{D^*}{D}\omega^2\frac{\mathrm{d}}{\mathrm{d}t}T(t) + \omega^2 T(t) = 0 \tag{3.45}$$

$$\nabla^4 W(r,\theta) - \beta^4 W(r,\theta) = 0 \tag{3.46}$$

in which $\beta^4 = \dfrac{\rho h\omega^2}{D}$.

The general solution of Eq. (3.46) can be obtained:

$$\begin{aligned} W(r,\theta) = \big[& C_s^1 J_s(\beta r) + C_s^2 Y_s(\beta r) + C_s^3 I_s(\beta r) \\ & + C_s^4 K_s(\beta r)\big]\left(A_s \exp(\mathrm{i}s\theta) + B_s \exp(-\mathrm{i}s\theta)\right), \quad s = 1,2,3,\cdots,n \end{aligned} \tag{3.47}$$

where the constants C_s^1, C_s^2, C_s^3, C_s^4, A_s, B_s and β must be found from the boundary conditions of the plate.

3.3.2.2 *The natural frequencies and mode shapes of the annular plate with free outside edge and clamped inside edge*

When the boundary conditions for an annular plate are clamped at the inside radius and free at the outside radius, the deflection and slope must be zero at the inside radius a; and both of the bending moment and shear force resultants must be zero, at the free outside radius b. Thus, the boundary conditions become:

$$W(a,\theta)=0,\ \ \frac{\partial W(a,\theta)}{\partial r}=0 \tag{3.48}$$

$$M_r\,|_{r=b}=0,\ \ \left(Q_r+\frac{1}{r}\frac{\partial M_{r\theta}}{\partial \theta}\right)\Bigg|_{r=b}=0 \tag{3.49}$$

in which M_r is the radial moment, Q_r represents the transverse shear force, and $M_{r\theta}$ is the twisting moment. The moment resultant-transverse displacement relations are defined as Eqs. (3.50)-(3.52):

$$M_r=-D\left[\frac{\partial^2 W}{\partial r^2}+\frac{v}{r}\frac{\partial W}{\partial r}+\frac{v}{r^2}\frac{\partial^2 W}{\partial \theta^2}\right] \tag{3.50}$$

$$M_{r\theta}=-(1-v)D\frac{\partial}{\partial r}\left(\frac{1}{r}\frac{\partial W}{\partial \theta}\right) \tag{3.51}$$

$$Q_r=-D\frac{\partial}{\partial r}\left(\nabla^2 W\right)=-D\frac{\partial}{\partial r}\left(\frac{\partial^2 W}{\partial r^2}+\frac{v}{r}\frac{\partial W}{\partial r}+\frac{v}{r^2}\frac{\partial^2 W}{\partial \theta^2}\right) \tag{3.52}$$

Substituting the expression of W (Eq. (3.47)) into Eqs. (3.48)-(3.49) and using the relationships of the first, second, modified first and modified second Bessel functions and their derivatives [254], the boundary conditions give Eq. (3.53):

$$\begin{bmatrix} H_{11} & H_{12} & H_{13} & H_{14} \\ H_{21} & H_{22} & H_{23} & H_{24} \\ H_{31} & H_{32} & H_{33} & H_{34} \\ H_{41} & H_{42} & H_{43} & H_{44} \end{bmatrix} \begin{Bmatrix} C_s^1 \\ C_s^2 \\ C_s^3 \\ C_4^1 \end{Bmatrix} = 0 \tag{3.53}$$

The characteristic equation can be obtained through Eq. (3.54):

$$\begin{vmatrix} H_{11} & H_{12} & H_{13} & H_{14} \\ H_{21} & H_{22} & H_{23} & H_{24} \\ H_{31} & H_{32} & H_{33} & H_{34} \\ H_{41} & H_{42} & H_{43} & H_{44} \end{vmatrix} = 0 \tag{3.54}$$

in which the elements are given below:

$H_{11}=J_s(\beta a)$ $\qquad\qquad$ $H_{12}=Y_s(\beta a)$

$$H_{13} = I_s(\beta a) \qquad H_{14} = K_s(\beta a)$$

$$H_{21} = \frac{s}{a} J_s(\beta a) - \lambda J_{s+1}(\beta a) \qquad H_{22} = \frac{s}{a} Y_s(\beta a) - \beta Y_{s+1}(\beta a)$$

$$H_{23} = \frac{s}{a} I_s(\beta a) + \beta I_{s+1}(\beta a) \qquad H_{24} = \frac{s}{a} K_s(\beta a) - \beta K_{s+1}(\beta a)$$

$$H_{31} = \left(\frac{s(s-1)(1-\nu)}{b^2} - \beta^2 \right) J_s(\beta b) + \beta \frac{(1-\nu)}{b} J_{s+1}(\beta b)$$

$$H_{32} = \left(\frac{s(s-1)(1-\nu)}{b^2} - \beta^2 \right) Y_s(\beta b) + \beta \frac{(1-\nu)}{b} Y_{s+1}(\beta b)$$

$$H_{33} = \left(\frac{s(s-1)(1-\nu)}{b^2} + \beta^2 \right) I_s(\beta b) - \beta \frac{(1-\nu)}{b} I_{s+1}(\beta b)$$

$$H_{34} = \left(\frac{s(s-1)(1-\nu)}{b^2} + \beta^2 \right) K_s(\beta b) + \beta \frac{(1-\nu)}{b} K_{s+1}(\beta b)$$

$$H_{41} = \left(\frac{-s\beta^2 b^2 + (1-s)(1-\nu)s^2}{b^3} \right) J_s(\beta b) + \left(\frac{\beta^3 b^3 + \beta b(1-\nu)s^2}{b^3} \right) J_{s+1}(\beta b)$$

$$H_{42} = \left(\frac{-s\beta^2 b^2 + (1-s)(1-\nu)s^2}{b^3} \right) Y_s(\beta b) + \left(\frac{\beta^3 b^3 + \beta b(1-\nu)s^2}{b^3} \right) Y_{s+1}(\beta b)$$

$$H_{43} = \left(\frac{s\beta^2 b^2 + (1-s)(1-\nu)s^2}{b^3} \right) I_s(\beta b) + \left(\frac{\beta^3 b^3 - \beta b(1-\nu)s^2}{b^3} \right) I_{s+1}(\beta b)$$

$$H_{44} = \left(\frac{s\beta^2 b^2 + (1-s)(1-\nu)s^2}{b^3} \right) K_s(\beta b) + \left(\frac{-\beta^3 b^3 + \beta b(1-\nu)s^2}{b^3} \right) K_{s+1}(\beta b)$$

For a given value of order s, the eigenvalues of Eq. (3.54) can be solved which is denoted by β_{rs}. Subscript s is the nodal diameter of plate, and subscript r is the nodal circle of plate. Then the nature frequencies can be obtained by Eq. (3.55):

$$\omega_{rs} = \beta_{rs}^2 \left(\frac{D}{\rho h} \right)^{1/2} \tag{3.55}$$

After getting the eigenvalues of the plate, then substitute the roots into H_{nn} (n=1,2,3,4). The relations among C_{rs}^1, C_{rs}^2, C_{rs}^3 and C_{rs}^4 can be determined by Eq. (3.53).

For the annular plate, each natural frequency ω_{rs}, there are two mode shapes (except $s=0$, there is only one mode). The two mode shapes (except s=0) are given by Eq. (3.56):

$$W_{r,\pm s}(r,\theta) = \left(C_{rs}^1 J_s(\beta_{rs} r) + C_{rs}^2 Y_s(\beta_{rs} r) + C_{rs}^3 I_s(\beta_{rs} r) + C_{rs}^4 K_s(\beta_{rs} r) \right) \exp(\pm \mathrm{i} s\theta) \tag{3.56}$$

Therefore, the solution of free vibration of the annular plate in given by Eq. (3.57):

$$w(r,\theta,t) = \sum_{r=0}^{+\infty} \sum_{s=-\infty}^{+\infty} \left[\left(C_{rs}^1 J_s(\beta_{rs} r) + C_{rs}^2 Y_s(\beta_{rs} r) + C_{rs}^3 I_s(\beta_{rs} r) + C_{rs}^4 K_s(\beta_{rs} r) \right) \exp(\mathrm{i} s\theta) \right] T_{rs}(t) \tag{3.57}$$

$T_{rs}(t)$ is the solution of Eq.(3.45), which can be solved by following the idea of damped vibration of the single-degree-of-freedom system.

3.4 Transient dynamic analysis method for non-smooth vibration

3.4.1 Runge-Kutta method for a second order differential equation

In dynamics, the equations of motion of a system are differential equations, of which analytical solutions do not exist or are hard to be obtained in some cases, for example in nonlinear dynamics. Numerical methods provide the possibility to obtain the solutions and offer the efficiency for dynamic analysis. Discretisation methods, such

as Runge-Kutta method, Newmark β method, and other finite difference methods, are often used in dynamic simulations, and each has its own advantages at certain problems.

The forth order Runge-Kutta method is often used in non-stiff problems because it is easy to implement, and has high accuracy and good stability. The general iteration process is for the first order differential equations. However, numerical solutions can be also found directly from the second order differential equations [255] with no need of converting the second order differential equations into the first order ones. In this part, the formulas of this method [255] are given below.

The second order differential equation is denoted as $\ddot{y} = f(t, y, \dot{y})$ and the initial conditions are $y(t_0) = y_0$ and $\dot{y}(t_0) = \dot{y}_0$. If a small time increment Δt is used, the expressions of y and $\dot{y}$ at time $t = t_0 + \Delta t$ are given by Eq. (3.58), and the solutions at each step can be obtained following these iteration equations.

$$\begin{aligned} y(t_0 + \Delta t) &= y(t_0) + \frac{1}{6}(v_1 + 2v_2 + 2v_3 + v_4) \\ \dot{y}(t_0 + \Delta t) &= \dot{y}(t_0) + \frac{1}{6}(w_1 + 2w_2 + 2w_3 + w_4) \end{aligned} \tag{3.58}$$

where

$$v_1 = \dot{y}_0 \Delta t\,, \quad v_2 = \left(\dot{y}_0 + \frac{1}{2} w_1\right)\Delta t\,, \quad v_3 = \left(\dot{y}_0 + \frac{1}{2} w_2\right)\Delta t\,, \quad v_4 = \left(\dot{y}_0 + \frac{1}{2} w_3\right)\Delta t\,,$$

$$w_1 = f(t_0, y_0, \dot{y}_0)\Delta t\,, \; w_2 = f\left(t_0 + \frac{1}{2}\Delta t, y_0 + \frac{1}{2} v_1, \dot{y}_0 + \frac{1}{2} w_1\right)\Delta t$$

$$w_3 = f\left(t_0 + \frac{1}{2}\Delta t, y_0 + \frac{1}{2} v_2, \dot{y}_0 + \frac{1}{2} w_2\right)\Delta t\,, \text{ and } \; w_4 = f(t_0 + \Delta t, y_0 + v_3, \dot{y}_0 + w_3)\Delta t$$

The validation of the accuracy of this method is implemented in Section 5.4, through comparing its numerical results with the analytical solution of the free vibration of a plate.

3.4.2 Numerical iteration process for non-smooth problems

As it has been known, mechanical systems with dry friction are one kind of non-smooth problems. Although non-smooth friction laws sometimes can be smoothed by a smoothing tangent function, there are some shortcomings of the smoothed friction law, such as high computational cost and loss of certain properties during smoothing. Additionally, loss of contact and the subsequent impact, that usually occur, result in discontinuity of the vibration, which also is a non-smooth problem. Several states may exist during vibration, which are governed by different sets of equations of motion. Thus, at the time instant of state-switching, the governing equations change to another set. Many numerical methods [48], such as the smooth method, the switch mode method, event-driven iteration method, the time-stepping method [256], and other useful methods [257, 258] and techniques [259, 260] are developed to deal with non-smooth dynamic problems in different research background.

In this thesis, dynamic response of the non-smooth systems in a very long time duration need to be obtained, thus finding the accurate transition point is a key step, otherwise the small error of the initial condition of each state can result in a completely different result from what it is supposed to be, after numbers of the state transition. In this part, a simple iteration strategy, that can be easily applied to following study which contains both the dry friction and separation (loss of contact), is described. The specific iteration process is illustrated through a flow chart (Fig. 3.11) of an example with stick-slip, and separation and reattachment. There are three states during the vibration, which are stick, slip and separation, respectively. Rather than using very small time steps to capture the state transition point, which is computationally expensive and may introduce additional numerical errors, this iteration procedure can guarantee the accuracy by using a reasonable length of time step and only shortening the time step to find the accurate transition point when the corresponding command in the code is activated.

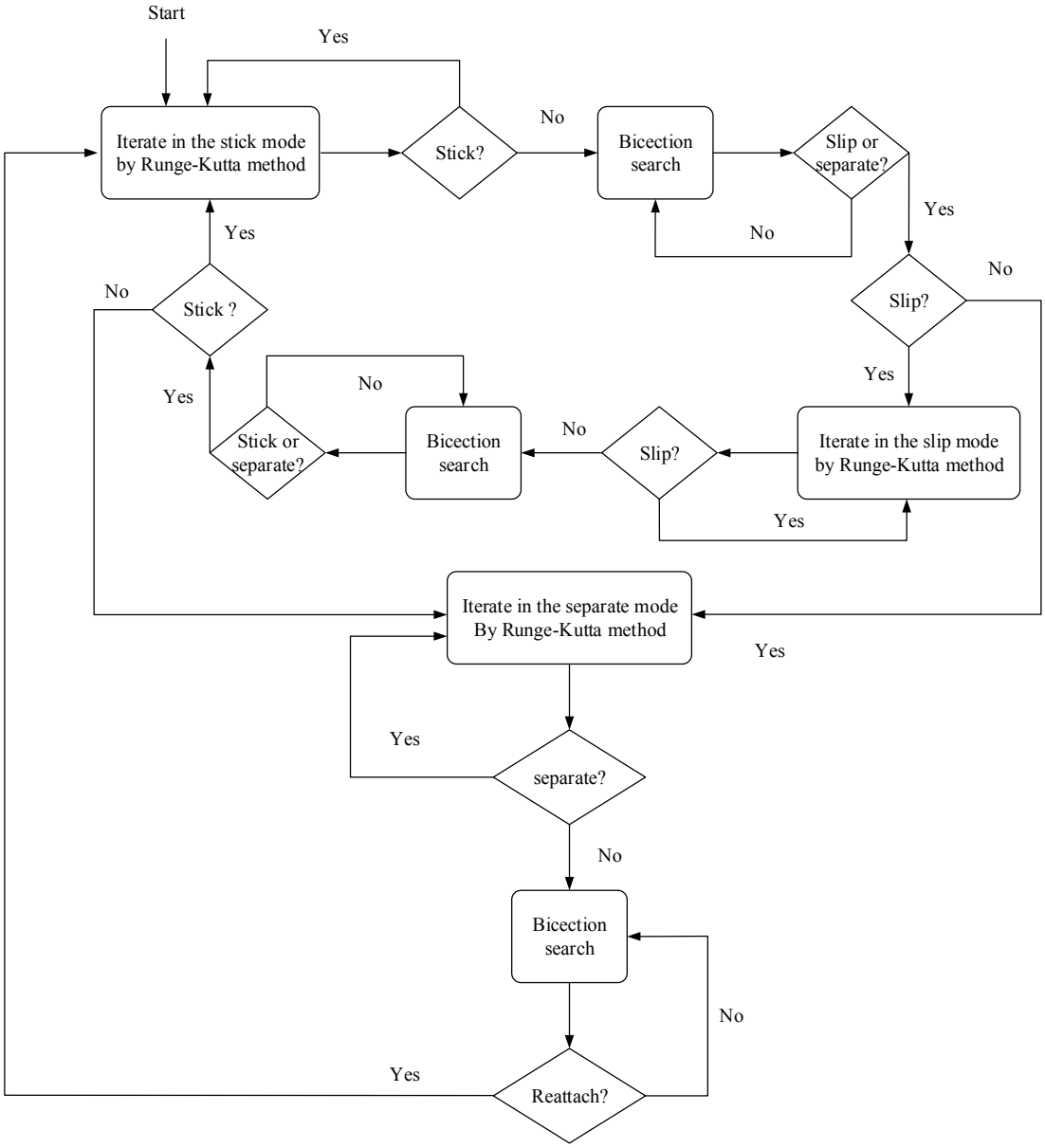

Fig. 3.11 The flow chart of the computational procedure for stick-slip vibration with separation and reattachment

During calculation, the time iteration strategy is shown in Fig. 3.12. In Fig. 3.12, blue dots on the time axis are the discretised time instants at the corresponding step, and the red dot is the time for the transition point. The iteration equation of the time at the non-transition point (blue dots) is expressed as:

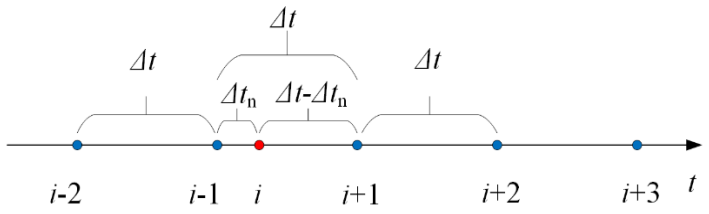

Fig. 3.12 The time iteration strategy

$$t(i+1)=(i-1-n)\Delta t-\Delta t_{\mathrm{n}} \tag{3.59}$$

in which i is the step number, Δt is a constant time step, n is the number of the transient point, and Δt_{n} is the time step between the transition step and its previous step. Initially n is zero and $\Delta t_{\mathrm{n}}=0$, during bisection searching loop, Δt_{n} keeps being renewed (after finishing each bisection searching, n and Δt_{n} are renewed). Then, after finishing the calculation at $t(i+1)$ (the time step after the transient point), Δt_{n} is 0 again, until the next transition happens. On the other hand, during the bisection loop, one has $t(i)=t(i-1)+\Delta t_{\mathrm{n}}$, where i denotes the step of the transition point.

The advantage of this iteration relationship is that after calculation, by scanning the saved results, the results at a regular time step can be obtained, which can then be used for further FFT analysis. For example, the data at $t(i-2)$, $t(i-1)$, $t(i+1)$ and $t(i+2)$ (all blue dots in Fig. 3.12) can be used for the FFT analysis.

The essential idea of the proposed algorithm is searching for accurate transition points between two motion states, such as stick and slip, and separation and reattachment. It is used to calculate the stick-slip vibration of the classic single-degree-of-freedom mass-on-moving-belt model (Popp's model) in Ref. [46], and the results are identical to the ones in that reference, detailed results have been given in Section 3.2.2.2. Besides, the comparison between the results of Leine's switch model [200] for the dynamic simulation of non-smooth system and the algorithm proposed in this thesis is implemented. Two methods show the identical stick-slip limit cycle of the example used in Leine's book[158], which is not shown here for the sake of simplicity. These works identify the correction of this algorithm.

3.5 Conclusions

This chapter presents the basic knowledge and the essential algorithm for the following PhD study on nonlinear friction-induced vibration. The simulations of mechanisms of friction-induced instability clearly show the fundamental phenomenon of the friction-induced vibration. The theories of the discrete system and the classic continuous plate are the base of the entire thesis. The numerical method and the corresponding algorithm for transient dynamic analysis of non-smooth problems provided are very useful to the following study.

4 Nonlinear Friction-induced Vibration of a Slider-belt Model

4.1 Introduction

As it is known, friction-induced vibration is one kind of self-excited vibration that can generate the flutter-type vibration and noise in machines and structures. Undesirable vibration of a system can reduce the service life of the components and largely raise the potential risk; in addition, friction noise is one of the major sources of noise pollution and also causes discomfort. Typical examples of friction-induced vibration include squeal of the automotive brakes and flutter of the computer hard disc drive. To reveal the fundamental reasons and dynamics of friction-induced vibration has been a challenging research topic.

In the research field of friction-induced vibration, one important research line is to carry out theoretical or experimental studies using simple models. Some studies involve simple test-rigs to develop new friction laws, and some present mechanical models to investigate the instability mechanisms and diverse dynamic behaviour of friction-induced vibration. The phenomenological mechanical models are idealised simple models of a few degrees of freedom which preserve the essential features of the original structures and omit some less important features. The studies of these simple models often offer insight into friction-induced unstable vibration, which are valuable from either a theoretical or a practical point of view.

For theoretical study, a mass-spring-damper slider excited into vibration by a moving rigid belt through friction is a major paradigm. This paradigm has two aspects that can be improved: (1) the contact stiffness at the slider-belt interface is often assumed to be linear; (2) the contact is usually assumed to be maintained during vibration (even when the vibration becomes unbounded at certain conditions).

In current work, a cubic contact spring is included; loss of contact (separation) at the slider-belt interface is allowed and importantly reattachment of the slider to the belt

after separation is also considered. These two features make a more realistic model of friction-induced vibration and are shown to lead to very rich dynamic behaviour even though a simple Coulomb friction law with a constant friction coefficient is used. Furthermore, when a Coulomb's law of friction with distinct kinetic and static friction coefficient is applied, non-smooth stick-slip vibration of the nonlinear coupling system results in a greater of vibration.

In this chapter, firstly a nonlinear two-degree-of-freedom model with a pre-compression force is introduced in Sections 4.2. The stability analysis of this mass-spring system when there is contact and during separation is carried out in Sections 4.3 and 4.4, respectively. In Section 4.3, complex eigenvalue analysis of the Jacobian matrix of the linearised system are calculated and the effects of nonlinear stiffness as well as the pre-load (pre-compression force) on the stability of the model are analysed. Subsequently, the natural frequencies of the mass-spring system during separation are calculated in Sections 4.4. In Section 4.5, separation and reattachment during vibration are numerically investigated through transient dynamic analysis. In particular the changes of vibration amplitudes at various loading and nonlinear stiffness values are compared between two cases when separation is considered and ignored. Study of the vibration in the frequency domain is carried out in Section 4.6. Additionally, dynamic behaviour of the system with stick-slip is investigated in Section 4.7. Finally, conclusions are drawn in Section 4.8.

4.2 Theoretical formulations

4.2.1 The mechanical model

The nonlinear two-degree-of-freedom model illustrated in Fig. 4.1 is developed from a classic linear coupled two-degree-of-freedom model put forward by Hoffmann [58]. The current model contains a point mass m which is compressed by a vertical compression force F to bring a rigid massless slider against a rigid belt moving at a constant speed. The contact between the mass and the belt is unilateral and a linear spring k_2 and a nonlinear spring k_{nl} together represent contact stiffness. From a realistic point of view, vertical separation may happen between the contacting surfaces. The

mass is constrained by a spring k_1 and a damper c_1 in the horizontal direction and by a grounded damper c_2 in the vertical direction. Moreover, a grounded spring k_3 is linked to the mass at a 135° angle relative to the horizontal direction, which couples vibration in both directions. The coordinate system defined in this chapter comprises a horizontal axis denoted by x and a vertical axis denoted by y, and the zero point of the coordinate system defined in the chapter is the position when the pre-compression force F (also called pre-load, and it is positive when acting in the downward direction) has not yet been applied and the horizontal spring has not deformed yet. Firstly, the belt starts to move at a constant speed. And then the static position of the mass after the pre-compression force F is applied is referred to as the original static state.

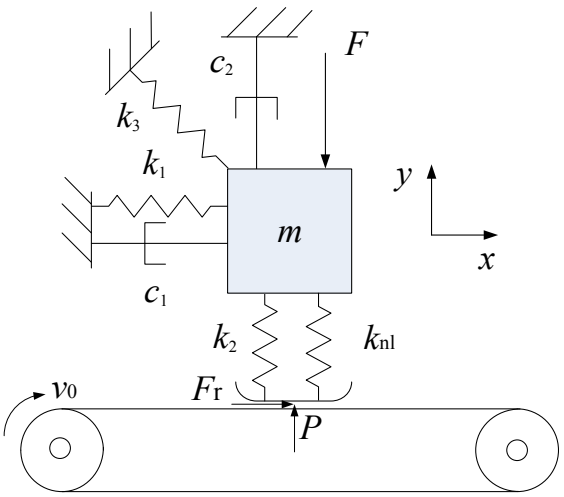

Fig. 4.1 A two-degree-of-freedom model with nonlinear stiffness

4.2.2 Equation of motion in friction contact

During vibration, if the mass and belt are in contact, then contact force P acting on the slider (positive when P is a compressive force) is expressed as:

$$P = -k_2 y(t) - k_{\mathrm{nl}} y(t)^3 \tag{4.1}$$

Since the focus of this chapter is on the influences of the nonlinear stiffness and separation on the instability, rather than the effects of friction characteristics, firstly a constant friction coefficient μ at contact point is assumed. Friction force F_{r} in Fig.

4.1 is assumed to be proportional to the contact force P, which is expressed as $F_r = \mu P$. According to Eq. (4.1), friction force is rewritten as Eq. (4.2) :

$$F_r(t) = -\mu\left(k_2 y(t) + k_{nl} y(t)^3\right) \tag{4.2}$$

The equations of motion of this system can be formed as:

$$\begin{bmatrix} m & 0 \\ 0 & m \end{bmatrix}\begin{bmatrix} \ddot{x} \\ \ddot{y} \end{bmatrix} + \begin{bmatrix} c_1 & 0 \\ 0 & c_2 \end{bmatrix}\begin{bmatrix} \dot{x} \\ \dot{y} \end{bmatrix} + \begin{bmatrix} k_1 + \frac{k_3}{2} & -\frac{k_3}{2} + \mu k_2 \\ -\frac{k_3}{2} & k_2 + \frac{k_3}{2} \end{bmatrix}\begin{bmatrix} x \\ y \end{bmatrix} + \begin{bmatrix} 0 & \mu k_{nl} \\ 0 & k_{nl} \end{bmatrix}\begin{bmatrix} x^3 \\ y^3 \end{bmatrix} = \begin{bmatrix} 0 \\ -F \end{bmatrix} \tag{4.3}$$

The basic parameters of this system are taken as constants, shown in Table 4.1.

Table 4.1 Parameter values of the linear part of the system

m	k_1	k_2	k_3	c_1	c_2
5 kg	100 N/m	50 N/m	60 N/m	0.32	0.32

It should be stressed that the above equations of motion Eq. (4.3) are valid only if the following condition is satisfied:

$$P(t) > 0 \tag{4.4}$$

If the value of the contact force drops below zero during vibration, loss of contact is identified to happen, and then the system is governed by another set of equations of motion, to be discussed in the following section.

4.2.3 Separation and reattachment

Loss of contact happens when contact force drops to zero. When loss of contact occurs, except for the friction force F_r, contact stiffness k_2 and k_{nl} no longer make contributions to the system. The mechanical model of the mass-spring-damper system during separation is shown in Fig. 4.2.

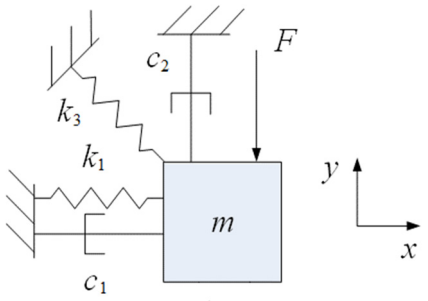

Fig. 4.2 The mechanical model during separation

The equations of motion of the mass-spring-damper system during separation are given by Eq. (4.5):

$$\begin{bmatrix} m & 0 \\ 0 & m \end{bmatrix}\begin{bmatrix} \ddot{x} \\ \ddot{y} \end{bmatrix}+\begin{bmatrix} c_1 & 0 \\ 0 & c_2 \end{bmatrix}\begin{bmatrix} \dot{x} \\ \dot{y} \end{bmatrix}+\begin{bmatrix} k_1+\frac{k_3}{2} & -\frac{k_3}{2} \\ -\frac{k_3}{2} & \frac{k_3}{2} \end{bmatrix}\begin{bmatrix} x \\ y \end{bmatrix}=\begin{bmatrix} 0 \\ -F \end{bmatrix} \tag{4.5}$$

As the contact surface of the belt is assumed to be rigid in this model, the condition for staying in separation only depends on the vertical motion of the vibrating mass m, which is given by Eq. (4.6):

$$y(t) > 0 \tag{4.6}$$

When y becomes negative, the mass is identified as getting reattached with the moving belt again. Then the system follows the equation of motion Eq. (4.3) until separation happens again. The switching between the two states (in contact and loss of contact) repeats during the vibration. Therefore, other than the nonlinearity from the nonlinear polynomial contact, the non-smooth vibration due to separation is another kind of nonlinear problem.

The initial conditions for Eq. (4.5) are calculated from Eq. (4.3) at the last moment in contact. Also, the state of the mass before reattachment is the initial condition for the equation of motion in contact (Eq. (4.3)).

4.3 Complex eigenvalue analysis of the whole system in friction contact

In this section, a classical stability analysis of the nonlinear system in friction contact is performed. Firstly, the equilibrium points of the system are determined by solving the nonlinear equations in the static condition. Then the local linear approximation about the equilibrium points is used to obtain the Jacobian matrix of the linearised system which also preserves the distinct stability behaviour of the original nonlinear system [261, 262]. Finally, the eigenvalues of the Jacobian matrix of this system are calculated in order to study the local instability of the system at the equilibrium points for various values of parameters.

4.3.1 Equilibrium points

The equilibrium points (fixed points) are the static states of the mass, as their velocity and acceleration are zero when the system is static. The equilibrium points denoted by (x_e, y_e) are the solutions of the algebraic Eq. (4.7). As Eq. (4.7) here is a set of non-homogeneous equations due to the pre-load term, equilibrium points are usually determined numerically. The equilibrium position in vertical direction are given in Table 4.2.

$$\begin{bmatrix} k_1+\frac{k_3}{2} & -\frac{k_3}{2}+\mu k_2 \\ -\frac{k_3}{2} & k_2+\frac{k_3}{2} \end{bmatrix}\begin{bmatrix} x_e \\ y_e \end{bmatrix}+\begin{bmatrix} 0 & \mu k_{nl} \\ 0 & k_{nl} \end{bmatrix}\begin{bmatrix} x_e^3 \\ y_e^3 \end{bmatrix}=\begin{bmatrix} 0 \\ -F \end{bmatrix} \tag{4.7}$$

When k_1=100 N/m, k_2=50 N/m, k_3=60 N/m, F=20N, k_{nl}=200N/m^3, the roots of y_e are given below, and corresponding x_e can also be calculated by substituting y_e into Eq. (4.7):

Table 4.2 Equilibriums in y direction

Friction coefficient	Root 1	Root 2	Root 3
μ =0	0.1186 + 0.6384i	0.1186 - 0.6384i	-0.2372

μ =0.2	0.1155 + 0.6327i	0.1155 - 0.6327i	-0.2311
μ = 0.4	0.1126 + 0.6275i	0.1126 - 0.6275i	-0.2253
μ =0.6	0.1099 + 0.6226i	0.1099 - 0.6226i	-0.2198
μ =0.8	0.1073 + 0.618i	0.1073 - 0.618i	-0.2146

Table 4.2 shows that although there are three roots of y_e, only one root has the physical meaning because the other two are a pair of complex conjugates. Moreover, the coordinates of equilibrium point of this problem are not only determined by the parameters of the linear system but also affected by the friction coefficient, the normal pre-compression force and the nonlinear contact stiffness.

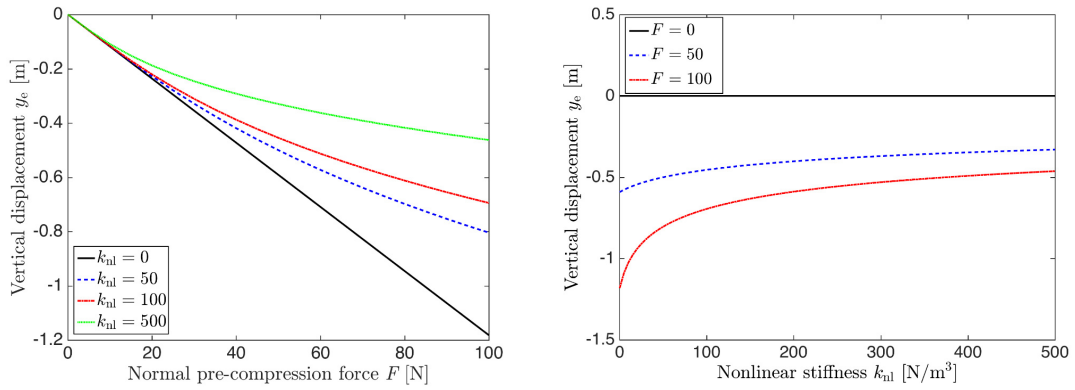

(a) (b)

Fig. 4.3 Vertical displacements of equilibrium points versus normal pre-compression force F (a) and nonlinear stiffness k_{nl} (b)

The change of the static vertical position of the mass with respect to the normal pre-compression force F and nonlinear stiffness k_{nl} are presented in Fig. 4.3 (a)-(b). Fig. 4.3 (a) shows that the vertical positions of the equilibrium points decrease with the increasing pre-compression force, and a larger nonlinear stiffness value offers more resistance to the vertical displacement shown in Fig. 4.3 (b). On the other hand, Fig. 4.3 (b) shows that if there is no pre-compression force, the nonlinear stiffness would not affect the equilibrium position. This means that the pre-compression force not only contributes to the system dynamics independently but also makes the nonlinear stiffness affect the equilibrium points of the nonlinear system. Thus the normal pre-

compression force is an important factor for the equilibrium points of the original nonlinear system.

4.3.2 Eigenvalue analysis of the system at the equilibrium point

One of the classical ways to perform the stability analysis of a nonlinear system is using the linear approximate method to analyse the stability of the linearised system around its equilibrium. In order to use this method, the equations of motion of the nonlinear system is converted into a set of first-order differential equations. The transformation relationships are designated as: $z_1=x$, $z_2=\dot{x}$, $z_3=y$, $z_4=\dot{y}$, thus Eq. (4.3) is transformed into Eq. (4.8):

$$\begin{bmatrix} \dot{z}_1 \\ \dot{z}_2 \\ \dot{z}_3 \\ \dot{z}_4 \end{bmatrix} = \begin{bmatrix} 0 & 1 & 0 & 0 \\ -\dfrac{k_1+\dfrac{k_3}{2}}{m} & -\dfrac{c_1}{m} & -\dfrac{-\dfrac{k_3}{2}+\mu k_2}{m} & 0 \\ 0 & 0 & 0 & 1 \\ \dfrac{k_3}{2m} & 0 & -\dfrac{k_2+\dfrac{k_3}{2}}{m} & -\dfrac{c_2}{m} \end{bmatrix} \begin{bmatrix} z_1 \\ z_2 \\ z_3 \\ z_4 \end{bmatrix} + \begin{bmatrix} 0 & 0 & 0 & 0 \\ 0 & 0 & -\dfrac{\mu k_{\mathrm{nl}}}{m} & 0 \\ 0 & 0 & 0 & 0 \\ 0 & 0 & -\dfrac{k_{\mathrm{nl}}}{m} & 0 \end{bmatrix} \begin{bmatrix} z_1^3 \\ z_2^3 \\ z_3^3 \\ z_4^3 \end{bmatrix} + \begin{bmatrix} 0 \\ 0 \\ 0 \\ -\dfrac{F}{m} \end{bmatrix} \tag{4.8}$$

By expanding the nonlinear equations in a first order truncated Taylor series at the equilibrium point [261, 262], the Jacobian matrix is given by Eq. (4.9):

$$J = \begin{bmatrix} 0 & 1 & 0 & 0 \\ -\dfrac{k_1+\dfrac{k_3}{2}}{m} & -\dfrac{c_1}{m} & -\dfrac{-\dfrac{k_3}{2}+\mu k_2}{m} - 3\dfrac{\mu k_{\mathrm{nl}}}{m} y_{\mathrm{e}}^2 & 0 \\ 0 & 0 & 0 & 1 \\ \dfrac{k_3}{2m} & 0 & -\dfrac{k_2+\dfrac{k_3}{2}}{m} - 3\dfrac{k_{\mathrm{nl}}}{m} y_{\mathrm{e}}^2 & -\dfrac{c_2}{m} \end{bmatrix} \tag{4.9}$$

The stability is manifested by the real parts of the eigenvalues λ of the Jacobian matrix. These eigenvalues reflect the features of the local stability around the equilibrium point $(x_{\mathrm{e}}, y_{\mathrm{e}})$. If all the real parts of the eigenvalues are negative, the system is stable;

otherwise, as long as the real part of any eigenvalues is positive, the equilibrium point is unstable.

It can be noted that, because y_e takes non-zero values, the nonlinear stiffness terms appear in Eq. (4.9), unlike in other similar systems, for example, in Ref [61]. For those systems whose equilibrium points are zero, the nonlinear terms do not make contributions to the Jacobian matrix of the linearised system.

By setting the friction coefficient μ as a control parameter, the changes of the bifurcation points of this system are studied for various values of the normal pre-compression force and the nonlinear stiffness. Here, the friction coefficient satisfying the following condition Eq. (4.10) for bifurcation is called the critical friction coefficient μ_c.

$$\mathrm{Max}\left(\mathrm{Re}(\lambda)\big|_{\mu=\mu_c}\right)=0 \tag{4.10}$$

Bifurcation behaviour is illustrated in Figs. 4.4-4.7. Figs. 4.4 and 4.5 show the results of eigenvalue analysis with proportional damping (c_1=c_2=0.32), in which the frequency and the growth rate are the imaginary part and real part of the eigenvalue respectively. Friction coefficient μ is the control parameter. There are two distinct imaginary parts and modes, and the real parts are negative when μ <μ_c. With the increase of μ, the two imaginary parts and modes merge together at μ_c, and at the same time one of the real parts becomes zero. After the bifurcation point, one of the real parts becomes positive, as shown in Figs. 4.4 and 4.5. Thus these results indicate that the system is stable when μ< μ_c, and is unstable when μ> μ_c. The scenario depicted in Figs. 4.4 and 4.5 illustrates the well-known mode-coupling mechanism of unstable friction-induced vibration.

As shown in Figs. 4.4 and 4.5, μ_c changes with the nonlinear stiffness. Moreover, the evolution of μ_c with the nonlinear stiffness is found to be non-uniform for different values of the pre-compression force if one compares the results.

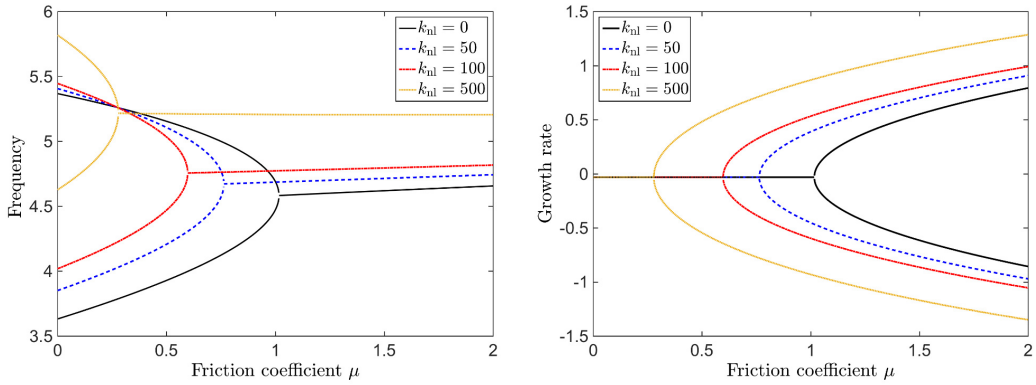

Fig. 4.4. The real (right) and imaginary part (left) of the eigenvalues versus the friction coefficient μ for various nonlinear stiffness. The imaginary parts are the frequencies and real parts are growth rates ($F = 20\text{N}$)

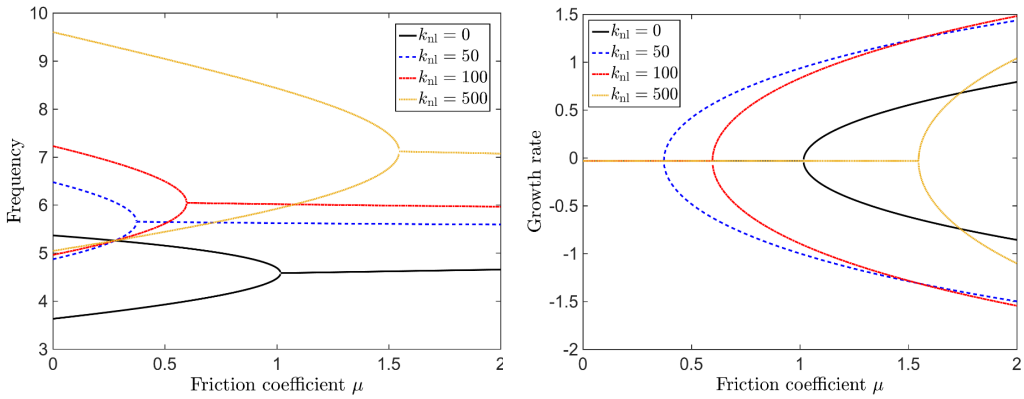

Fig. 4.5. The real (right) and imaginary part (left) of the eigenvalues versus the friction coefficient μ for various nonlinear stiffness. The imaginary parts are the frequencies and real parts are growth rates ($F = 100\text{N}$)

In Fig. 4.4 (F=20 N), the critical friction coefficient μ_c becomes smaller with the increasing nonlinear stiffness, and μ_c (coloured non-solid lines) are smaller than those of the linear system (black solid line). However, when the normal force is greater (F=100 N), as shown in Fig. 4.5, for the nonlinear system μ_c increases with the increasing nonlinear stiffness (k_{nl}=50, 100, 500 N/m^3), while the stability level of the nonlinear system (coloured non-solid lines) with respect to the linear system (black solid line) is complicated. For the case of k_{nl}=500 N/m^3, μ_c of the nonlinear system is

greater than μ_c of the linear system, but μ_c of the nonlinear system in other cases (k_{nl}=50, 100 N/m^3) are smaller than μ_c of the linear system.

In the case with non-proportional damping ($c_1 \neq c_2$), the results of the stability analysis of the example c_1=0.8 and c_2=0.32 are shown in Figs. 4.6 and 4.7, and other non-proportional damping values show the same phenomenon, which is not shown here for the sake of simplicity. It can be found that there are two distinct imaginary parts and modes when $\mu<\mu_c$, and the real parts are negative, which shows the same features as the proportional damping case. With the increase of μ, one of the real parts becomes zero at μ_c, while the two imaginary parts and modes get closer but do not coalesce. Similarly to the proportional damping case, one of the real parts becomes positive after the bifurcation point, as shown in Fig. 4.6. Moreover, whether the damping coefficient is proportional or non-proportional, it does not influence the trend of μ_c with F and k_{nl}, by comparisons between Figs. 4.4 and 4.6, and Figs. 4.5 and 4.7.

To further examine the evolution of the critical friction coefficient in relation to the pre-compression force F, eigenvalue analysis for various values of F is carried out. The results below are calculated by using proportional damping (c_1=c_2=0.32) because the results of non-proportional damping case give the same trend. Fig. 4.8 shows the changes of the critical friction coefficient with the pre-compression force F in four contact stiffness cases, including one linear system and three nonlinear systems with k_{nl}=50, 200, 500 N/m^3. The results shown by the solid black line indicate that the normal pre-compression force does not influence the stability of the linear system, as the values of the critical friction coefficient stay the same. However, when the system is nonlinear (k_{nl}=50, 200, 500 N/m^3) shown by the coloured non-solid lines, both nonlinear stiffness and pre-compression force influence the stability of this system. With the increasing normal pre-compression force, the nonlinear system (coloured non-solid lines) firstly is more unstable compared with its corresponding linear system since the critical friction coefficient of the nonlinear system is smaller; then at a certain value of the normal pre-compression force (which depends on the value of the nonlinear stiffness), μ_c starts to increase with the increasing normal pre-compression force. Moreover, in the case of a large nonlinear stiffness value of k_{nl}=500 N/m^3 (the

yellow dotted line), within the observation range of the normal pre-compression force, its μ_c finally becomes larger than the critical friction coefficient of the linear system (black solid line), which means that the nonlinear system under theses parameter values can become more stable than its corresponding linear system.

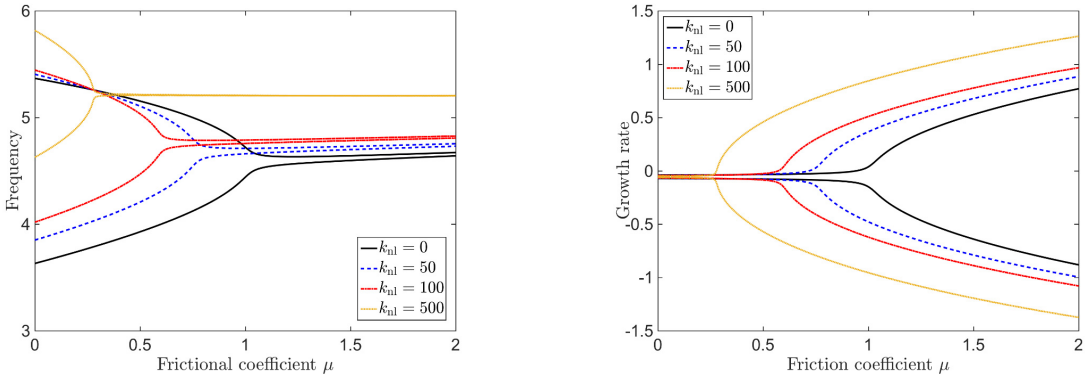

Fig. 4.6 The real (right) and imaginary part (left) of the eigenvalues versus the friction coefficient μ for various nonlinear stiffness with non-proportional damping. The imaginary parts are the frequencies and real parts are growth rates ($c_1 = 0.8$, $c_2 = 0.32$, $F = 20\text{N}$)

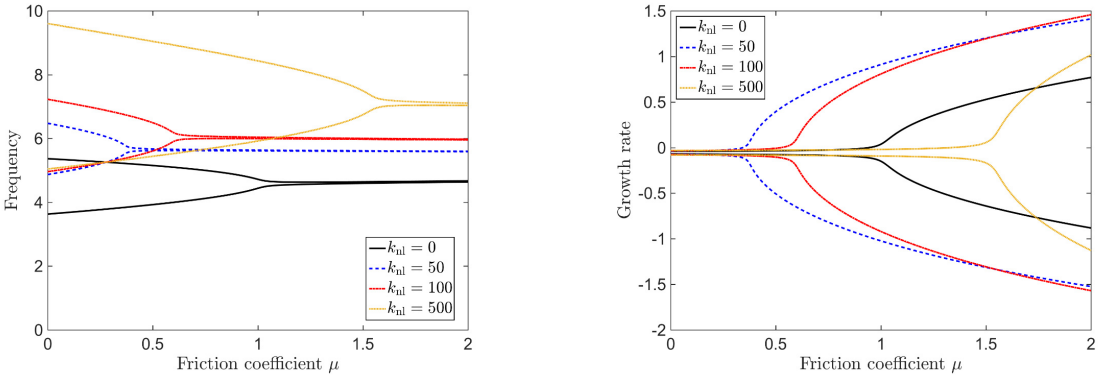

Fig. 4.7 The real (right) and imaginary part (left) of the eigenvalues versus the friction coefficient μ for various nonlinear stiffness with non-proportional damping. The imaginary parts are the frequencies and real parts are growth rates ($c_1 = 0.8$, $c_2 = 0.32$, $F = 100\text{N}$)

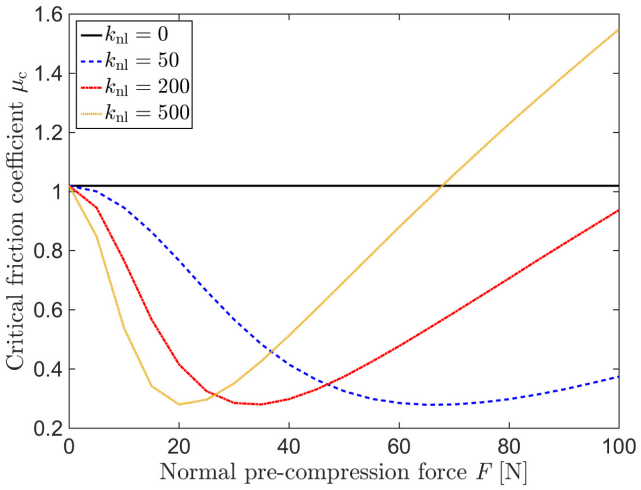

Fig. 4.8 Evolution of the critical friction coefficient against the pre-compression force

For a better understanding of the effects of nonlinear stiffness on the stability of this system, the evolution of μ_c against the nonlinear stiffness is studied. The numerical results are illustrated in Fig. 4.9. It is observed that when there is no normal pre-compression force in the system (shown by the solid black line), the nonlinear stiffness makes no contributions to the stability of the system. In the other cases with pre-load (F =5, 50,100 N) shown by coloured non-solid lines, by setting their friction coefficient μ as the same as the linear system (shown by the solid black line), the nonlinear system firstly becomes more unstable as its μ_c decreases with the nonlinear stiffness; In the case of a large pre-load (F =100 N) shown by the yellow dotted line, the nonlinear system becomes more stable than the linear system when the nonlinearity is strong. However, when the pre-load is small (F=5 N) shown by the blue dashed line in Fig. 4.9, the nonlinear system is less stable than its linear system. For example, when μ equals to 1.2, the linear system is unstable as its μ_c is smaller than 1.2; however, the nonlinear system can be stabilised when the pre-load is increased to 100 N while the nonlinear stiffness k_{nl} equals 300 N/m^3 is introduced.

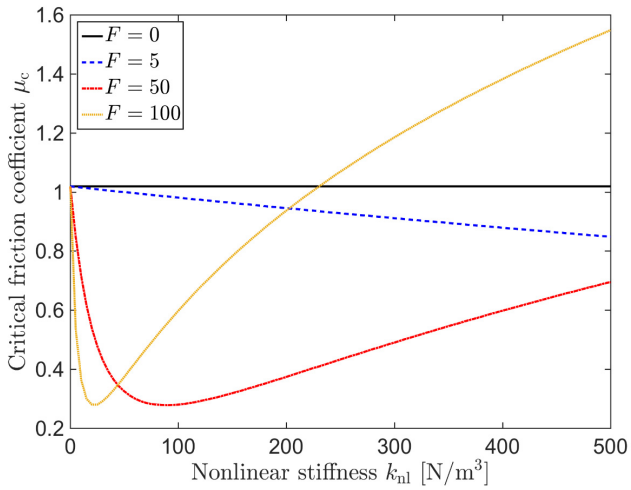

Fig. 4.9 Evolution of the critical friction coefficient against the nonlinear stiffness

The stability results from the above eigenvalue analysis match the time-history results shown in Figs. 4.10 and 4.11. In these cases for comparison, k_{nl} is 100 N/m and F is 50 N. The initial conditions for these two nonlinear examples are (x_e, 0, y_e+0.01, 0). The critical friction coefficient μ_c calculated from the eigenvalue analysis is 0.28. In Fig. 4.10, the vibration is stable when μ is 0.279; but it grows when μ is 0.28, as illustrated by Fig. 4.11. This indicates the agreement on the stability between time-domain response results of the nonlinear system and eigenvalue analysis results of the linearised system.

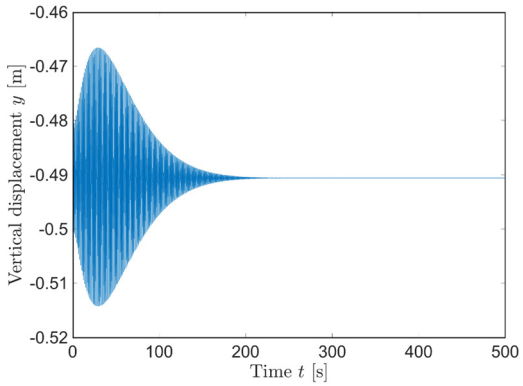

Fig. 4.10 Transient results of vertical displacement (μ =0.279)

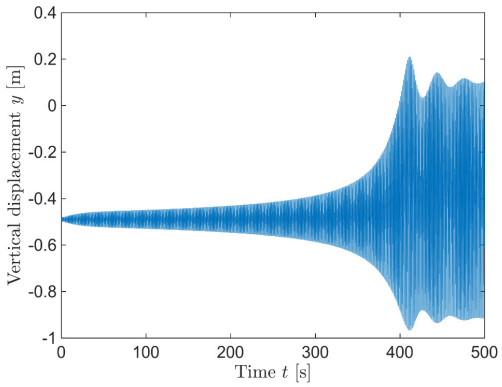

Fig. 4.11 Transient results of vertical displacement (μ =0.28)

On the other hand, if the horizontal linear stiffness takes sufficiently smaller values than the values of vertical linear stiffness, for example, k_1 =50 N/m and k_2 =100 N/m, the changes of the critical friction coefficient with the values of the normal pre-compression force and nonlinear stiffness, in Figs. 4.12 and 4.13, show different behaviour from the results when k_1=100 N/ m and k_2=50 N/ m. Basically, when k_1 =50 N/m and k_2 =100 N/ m, the nonlinear system is always more stable than its corresponding linear part. Moreover, with the increase of F and the k_{nl}, the stability of the nonlinear system is enhanced in a monotonic trend.

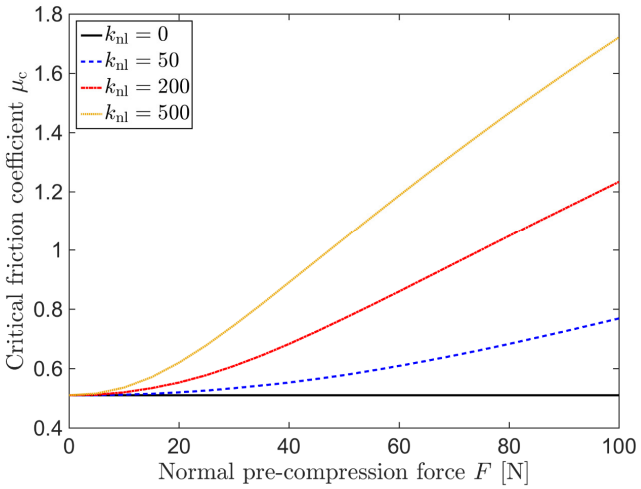

Fig. 4.12 Evolution of the critical friction coefficient against the pre-compression force

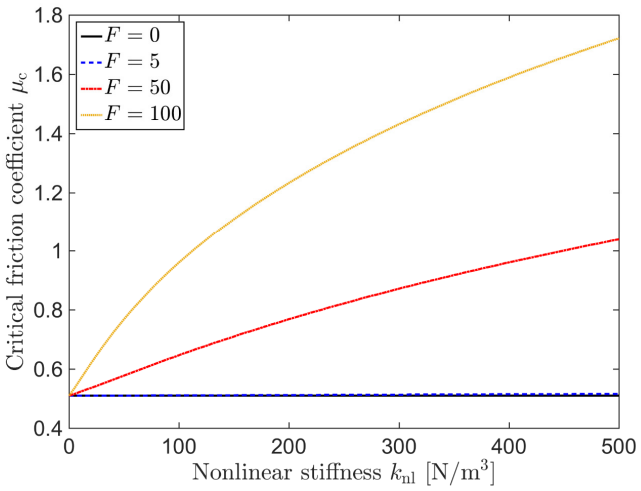

Fig. 4.13 Evolution of the critical friction coefficient against the nonlinear stiffness

To summarise, the stability of the nonlinear coupled system with sliding friction is much more complex than the corresponding linear system. Parametric studies show that the nonlinear stiffness as well as the pre-compression force play important roles in the stabilisation of the system. When the nonlinear stiffness and pre-compression force are introduced into the system, they firstly make the system unstable, which is not an intuitive conclusion; however, in the cases with a strong nonlinearity or a large normal compression force, certain combinations of the nonlinear stiffness and the normal pre-compression force stabilise the original unstable system. These phenomena can be exploited for controlling friction-induced vibration. On the other hand, the values of the linear stiffness of a nonlinear system are also important as they can influent how the nonlinear stiffness and the normal pre-compression force affect the stability of this nonlinear system.

4.4 Modal analysis of the system during separation

This section is to calculate the natural frequencies of the individual slider system during separation. The equations of motion of the mass-spring-damper system during separation, as introduced in Section 4.2.3, are shown again for the sake of convenience.

$$\begin{bmatrix} m & 0 \\ 0 & m \end{bmatrix}\begin{bmatrix} \ddot{x} \\ \ddot{y} \end{bmatrix}+\begin{bmatrix} c_1 & 0 \\ 0 & c_2 \end{bmatrix}\begin{bmatrix} \dot{x} \\ \dot{y} \end{bmatrix}+\begin{bmatrix} k_1+\frac{k_3}{2} & -\frac{k_3}{2} \\ -\frac{k_3}{2} & \frac{k_3}{2} \end{bmatrix}\begin{bmatrix} x \\ y \end{bmatrix}=\begin{bmatrix} 0 \\ -F \end{bmatrix} \tag{4.11}$$

The eigenvalue analysis of Eq. (4.11) is a general eigenvalue problem of a linear 2-degree-of-freedom system. Eq. (4.12) is obtained through the complex eigenvalue analysis process introduced in Section 3.3.2.

$$\left|\begin{bmatrix} m & 0 \\ 0 & m \end{bmatrix}\lambda^2+\begin{bmatrix} c_1 & 0 \\ 0 & c_2 \end{bmatrix}\lambda+\begin{bmatrix} k_1+\frac{k_3}{2} & -\frac{k_3}{2} \\ -\frac{k_3}{2} & \frac{k_3}{2} \end{bmatrix}\right|=0 \tag{4.12}$$

in which λ is the eigenvalue.

By using the parameters given in Table 4.1, the natural frequencies can be calculated through Eq. (4.12), whose value are 2.08 and 5.26 rad/s.

4.5 Transient dynamic analysis (TDA)

In order to find out the influence of separation on the dynamic behaviour of the nonlinear system, time domain responses are calculated numerically with various values of the key parameters. Firstly, the numerical process of current non-smooth simulation is introduced. Then one example is given to show the dynamic behaviour of the system when it is stable. Subsequently, as this section mainly focuses on the vibration of the unstable system considering separation, the occurrence of separation when the system is unstable is illustrated; then the influences of nonlinear stiffness and normal pre-compression force on the friction-induced vibration considering separation are investigated; finally, the role of separation on the vibration amplitude is analysed through the comparisons between the results of two cases: (1) separation is considered; (2) separation is ignored.

4.5.1 Procedure of the numerical simulation

In this work, the fourth-order Runge-Kutta method, is used to calculate the transient responses of the nonlinear system numerically. As the state of the system switches between separation and slip phases, the dynamic behaviour of the system needs to be obtained by solving two different sets of governing equations, which brings about some difficulties in the numerical computation, such as determining the motion state and searching for the transition point for the two distinct states. The process of the numerical computation is as follows: The equations of motion are given by Eq. (4.3). The contact force is checked at the end of every single time step during numerical computation. If during the in-contact phase the contact force $P(t)$ drops below zero at the end of a time step, the bisection method is used to find the critical contact force satisfying the error tolerance defined in the algorithm and the associated time instant and motion states (displacement, velocity and acceleration). Then separation is considered to take place.

During separation, the contact force is zero, and sliding friction force vanishes, so the states of the mass are calculated by a new set of equations of motion of the mass, Eq. (4.5). After separation, the condition for maintaining separation, Eq. (4.6), is checked in order to find out the exact moment for reattachment. Specifically, the vertical displacement $y(t)$ of the mass is monitored at the end of each time step. If $y(t) > 0$, separation is maintained; but if $y(t)$ becomes negative, which means that the mass is vibrating downward back to the original static position. Then the bisection method is used to find the critical point, at which $y(t)$ is very near zero satisfying the defined tolerance in the Matlab codes. At this critical point, the vibration is recognised to switch from separation phase to reattachment phase, and the slider is just touching the moving belt without any contact force. After reattachment, the equations of motion of this system switch to Eq. (4.3) until the condition of separation is satisfied again and the initial conditions are calculated from Eq. (4.5) at the last step before reattachment. This scenario of switching between contact and separation can be repeated.

4.5.2 Vibration of the stable system

Whether a nonlinear system becomes stable or unstable crucially depends on the values of the system parameters, which has been discussed in Section 4.3. It is found that separation does not occur for a stable system in most situations; and even if separation happens under some conditions, the vibration of the system still gradually decreases and eventually gets back to the equilibrium point. In the following, one numerical example is run to illustrate this point. In this example, the parameters of the linear part of the system are the same with previous examples, besides μ=1, F = 2N and k_{nl}= 100 N/m. The initial condition is (x_e, 0, y_e-0.1, 0). The time history of the contact force in Fig. 4.14 (a) shows that the contact force becomes zero occasionally at the early stage of the vibration, which means separation occurs. Fig. 4.14 (b) and (c) show the vibration of the system is stable as vibration decreases. Apparently, separation does not change the instability of the system and make significant contributions to the vibration of a stable system. Thus, stable vibration is not the interest of this work. The following study is devoted to explore the unstable friction-induced vibration with separation.

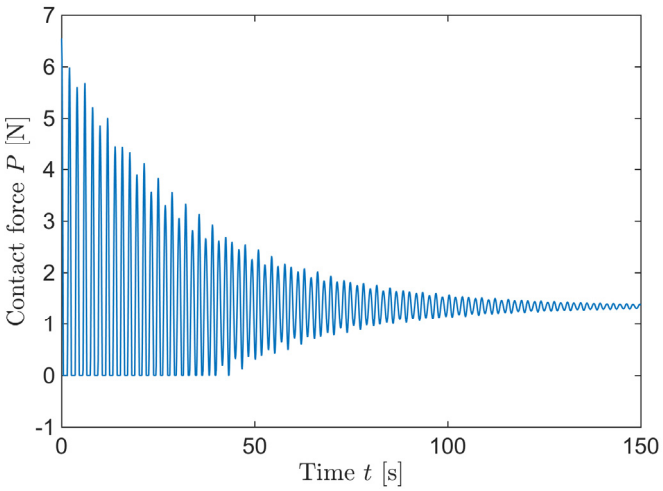

(a)

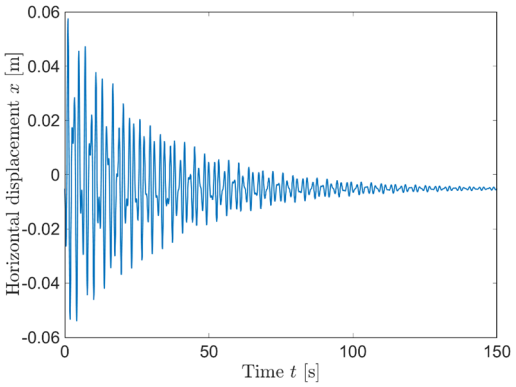

(b)

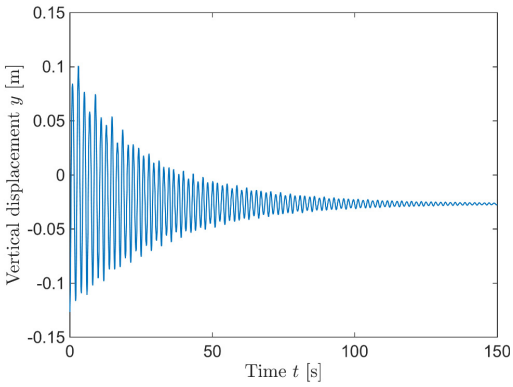

(c)

Fig. 4.14 Transient response of the system. (a) Contact force; (b) Horizontal displacement; (c) Vertical displacement.

4.5.3 Separation during vibration

The parameter values in this numerical example are: k_1 =100; k_2 =50; k_3=60; F=80; k_{nl}=100; μ=0.7. The critical friction coefficient μ_c for bifurcation with theses parameters is 0.28. Numerical results are given in Figs. 4.15-4.17.

Fig. 4.15 shows the fluctuation ranges of the contact force during vibration of the two cases: separation is ignored and is considered. It can be noticed that the contact force (shown by the blue solid line) gradually grows and becomes negative when separation is ignored. This means that the results of the ignoring separation case are not realistic as the contact force should always be non-negative. For the case when separation is

considered (shown by the green dashed line), multi-separation events can be observed as the values of contact force repeat the following process during the vibration: drop to zero (transition from in-contact state to separation state), remain zero (during separation), become positive (in-contact) and drop to zero again. Furthermore, the fluctuating contact force is asymmetric about the original static state when loss of contact is considered.

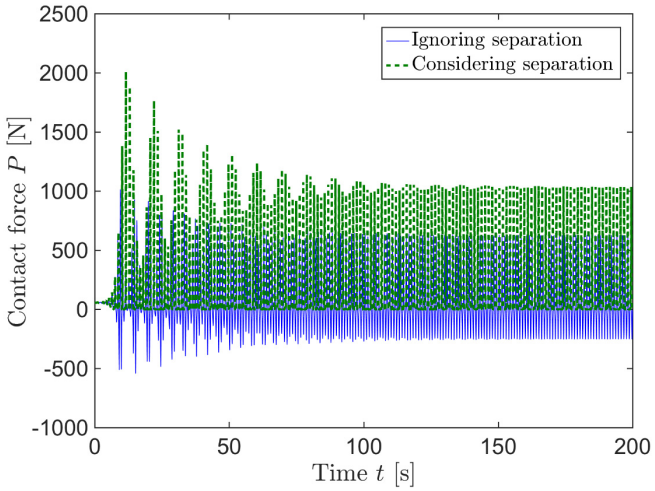

Fig. 4.15 Time-domain results of the contact force during the time period [0-200s]

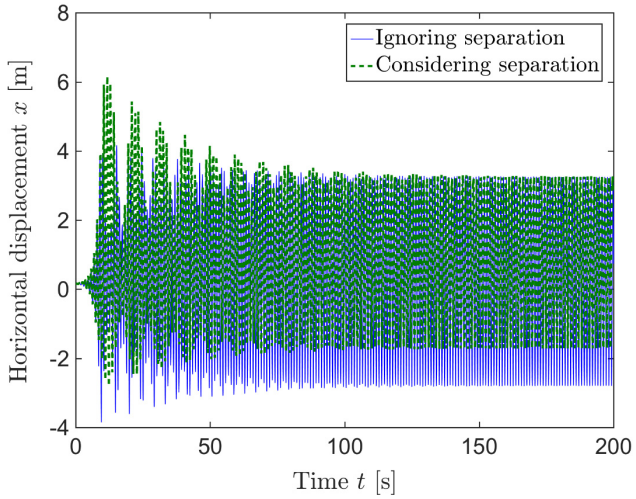

Fig. 4.16 Time response of the horizontal displacement during the time period [0-200s]

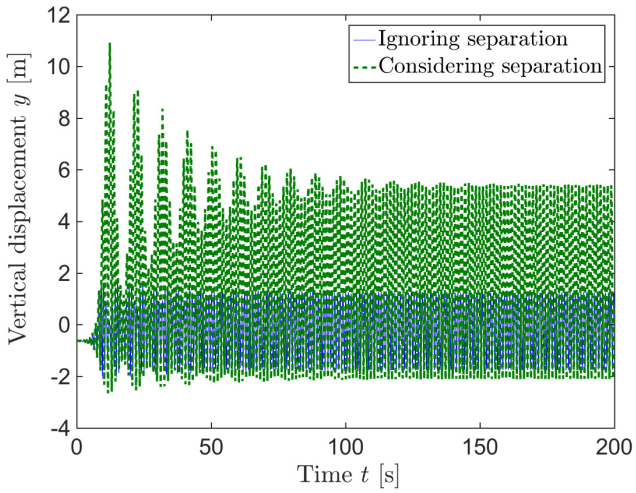

Fig. 4.17 Time response of the vertical displacement during the time period [0-200s]

Figs. 4.16 and 4.17 show that separation makes both the horizontal and vertical motion different from their counterparts when separation is ignored. Meanwhile the vibration is asymmetric about the original static state when loss of contact is considered. In conclusion, even in the presence of the normal pre-compression force as a pre-load, separation still can take place during vibration, and reattachment naturally occurs with separation.

4.5.4 Effects of separation on the amplitudes

To assess the influences of separation on the maximum vibration amplitude of the nonlinear friction-induced vibration, comparisons between cases of separation being considered (Case 1) and ignored (Case 2) are made through a parametric study for various values of nonlinear stiffness and normal pre-compression force.

Firstly, the changes in the maximum amplitudes of the vertical vibration of the mass are obtained by varying the values of the normal pre-compression force while keeping the nonlinear stuffiness as a constant. The results are shown in Figs. 4.18 (k_{nl}=20 N/m^3 and μ=0.5) and 4.19 (k_{nl}=100 N/m^3 and μ=0.7). These values are chosen based on the results of the eigenvalue analysis in Section 4.3.2, under which typical unstable motion of the mass can be obtained. The blue solid line represents the case when loss of contact

is ignored; the green dashed line is for the case when separation and reattachment are considered.

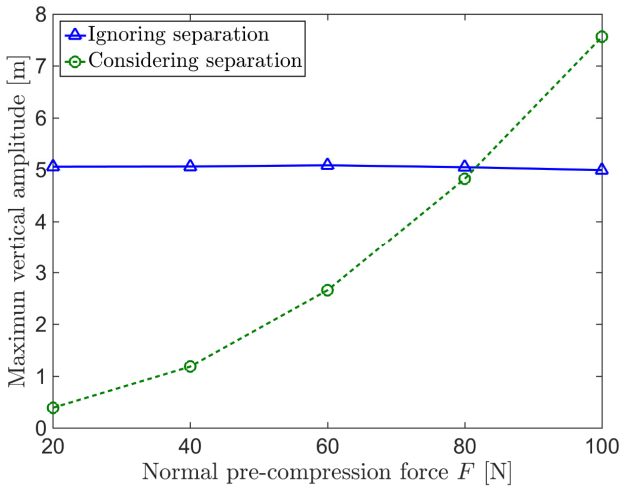

Fig. 4.18 Maximum vertical amplitudes against normal pre-compression forces ($k_{\mathrm{nl}} = 20\mathrm{N/m}^3$)

As shown in Fig. 4.18, a significant difference in the roles of the normal pre-compression force on the vibration amplitude can be observed between Case 1 and Case 2. When separation is ignored (blue solid line) in Fig. 4.18, the normal pre-load barely affects the maximum amplitude of the nonlinear vibration. In contrast, for the more realistic case when separation is considered (the green dashed line) in Fig. 4.18, the maximum vibration amplitude of the mass becomes larger with the increasing normal pre-compression force, which is not an intuitive expectation that increasing the normal pre-compression force leads to greater vibration. Moreover, at the initial increase of the normal pre-load, the maximum amplitudes are smaller than those in Case 2 (separation ignored). However, at a larger pre-compression force, the situation is reversed.

For the nonlinear system with a stronger nonlinear contact spring shown in Fig. 4.19, a similar trend of the maximum amplitudes to that of Fig. 4.18 is found, and the maximum amplitudes in Case 1 exceed those of Case 2 at a much lower value of the normal compression force. This means that ignoring separation during the vibration underestimates the vibration, which is unsafe for the system.

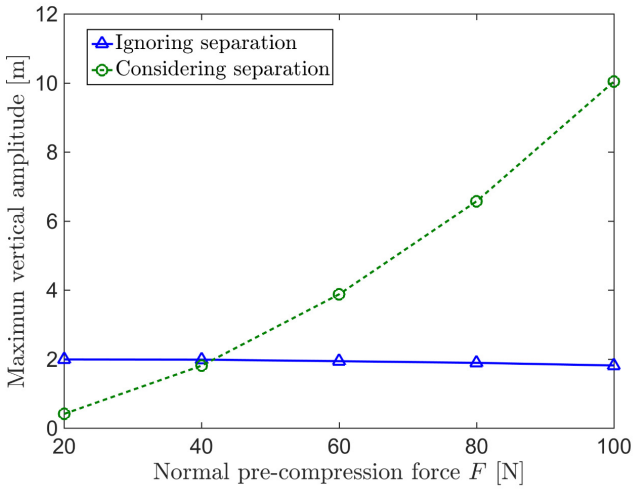

Fig. 4.19 Maximum vertical amplitudes against normal pre-compression forces ($k_{nl} = 100\text{N/m}^3$)

Then Figs. 4.20 and 4.21 show the changes of maximum vibration amplitude with respect to the nonlinear contact stiffness in two pre-load cases. Normal compression forces in Figs.4.20 and 4.21 are 40 N and 60 N, and μ is 0.7 and 1 respectively. The results clearly show that, if separation is not considered (blue solid line), the nonlinear contact stiffness appears stabilising. As separation does happen during the vibration, in fact the results with separation considered indicate that larger contact stiffness induces greater vibration, as shown in Figs. 4.20 and 4.21. Moreover, in Fig. 4.20, the maximum amplitudes in Case 1 (separation considered) initially are smaller than in Case 2 (separation ignored) at the same nonlinear stiffness value, but they tend to become larger than in Case 2 when the nonlinear stiffness is increased. In addition, the maximum amplitudes depend on the normal compression force, as shown in Fig. 4.21 (F=60 N), where even at a small value of nonlinear contact stiffness, the maximum amplitudes in Case 1 are greater.

The above apparently puzzling dynamic behaviour can be explained as follows. If separation is ignored, after the contact force becomes negative, the contact spring gets stretched and it still offers the resistance force hindering the mass from moving upward further, meanwhile the friction force still makes contributions to the horizontal vibration. However, when separation is allowed, the vertical contact stiffness is lost

during separation which does not offer the same amount of resistance force to the vertical vibration; at the same time, the horizontal friction force disappears which will not make any contribution to the horizontal vibration. Also because the horizontal and vertical vibration is coupled, the vibration of this system when separation is considered is actually more complex. These are very interesting findings and can be exploited in control of friction-induced vibration.

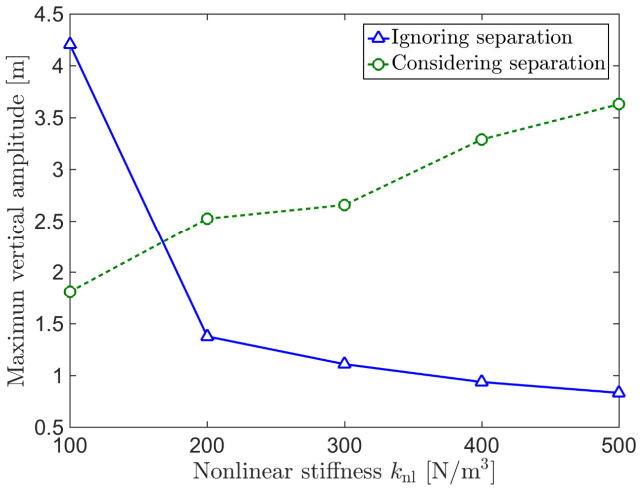

Fig. 4.20 Maximum vertical amplitudes for various nonlinear stiffness values ($F = 40\mathrm{N}$)

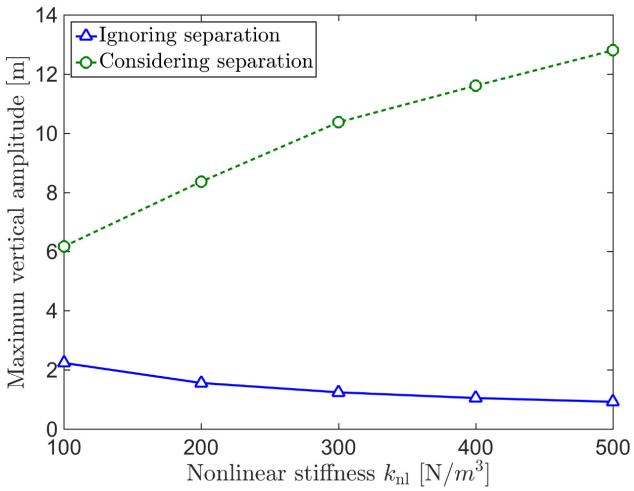

Fig. 4.21 Maximum vertical amplitudes for various nonlinear stiffness values ($F = 60\mathrm{N}$)

Finally, results of the case, when k_1=100 N/m and k_2=50 N/m which are different from the linear stiffness values of preceding examples (k_1=50 N/ m and k_2=100 N/m) are calculated, as shown in Fig. 4.22. The same tendency, in both of the ignoring separation and considering separation cases, of the maximum vertical amplitude with the nonlinear stiffness and the normal force with previous results can be seen. This means that the relations between the linear stiffness of the horizontal and vertical spring like whether the horizontal stiffness is smaller or larger do not change the roles of separation, the nonlinear stiffness as well as the normal force, although the linear parameter values of the system influent how the nonlinear stiffness and the normal pre-compression force affect the stability of this nonlinear system shown in Section 4.3.2.

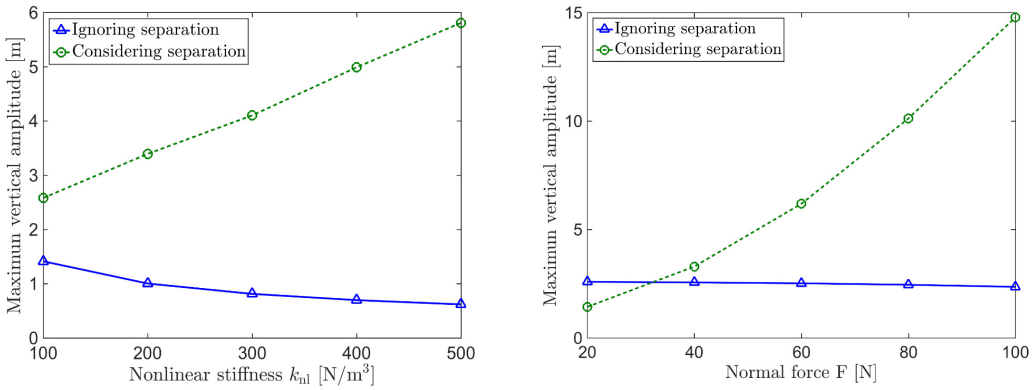

(a) (b)

Fig. 4.22 Maximum vertical amplitudes when $k_1 = 100\text{N/m}$ and $k_2 = 50\text{N/m}$. (a) change with the nonlinear stiffness ($F = 20\text{N}$); (b) change with the normal force ($k_{nl} = 20\text{N/m}^3$)

Consequently, when the loss of contact is considered, the effects of the nonlinear stiffness and normal pre-compression force on the evolution of vibration amplitude are not the same as the results when separation is ignored. Given the very important contributions of separation found in this work, it should be taken into account in models of friction-induced vibration. Flexibility of the moving belt and impact at reattachment after separation are other important factors to be considered in future, as the dynamic behaviour of the flexible moving belt is very complex [263]. The flexibility of the base as well as impact are involved in another model in Chapter 5.

4.6 Comparisons of vibration frequencies of TDA and CEA

The aim of this section is to illustrate the deficiency of CEA, and the necessity of TDA in the study of the unstable nonlinear friction-induced vibration problem. The comparisons between vibration frequencies solved through both methods (CEA and TDA) are carried out. Results show that stability analysis at the equilibrium point gives a clear indicator for the stability of the system, while the unstable frequencies from CEA are not the actual vibration frequencies of the nonlinear friction-induced vibration system. Therefore, TDA in the frequency domain needs to be performed as well to give the accurate unstable vibration frequencies.

A few examples are run and they all gives a similar phenomenon. So only some typical results with F=40 and k_{nl}=180 are illustrated in the following paragraphs. The critical friction coefficient μ_c for the bifurcation of the system is 0.29.

4.6.1 Frequencies of the stable vibration

Firstly, the dynamic transient responses with μ=0.2 are calculated. Fig. 4.23 illustrates the vertical vibration of the mass. The vibration is stable which also matches what is expected from CEA, as $\mu<\mu_c$. In this case, no separation happens during the vibration.

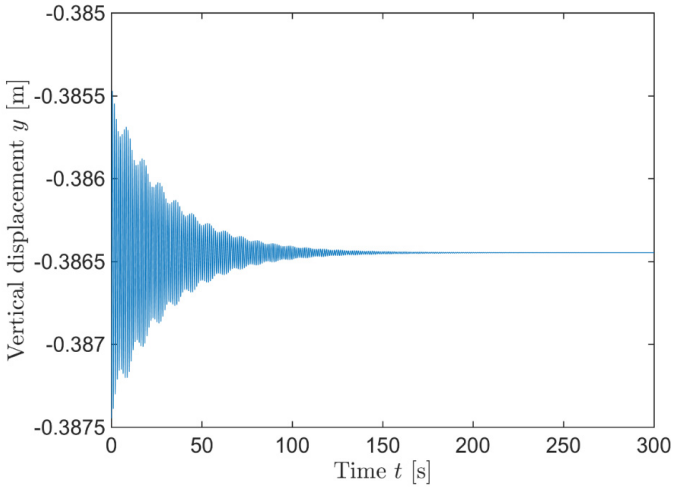

Fig. 4.23 Time response of the vertical displacement

Then vibration frequencies which are calculated through the fast Fourier transform of the transient vibration, and natural frequencies by CEA are given by Table 4.3.

Table 4.3 Frequencies of the stable system (rad/s)

Friction coefficient	CEA		FFT of TDA	
	ω_1	ω_2	ω_1	ω_2
μ=0.2	5.03	5.72	5.03	5.71

From Table 4.3, it can be seen that frequencies calculated through two different approaches only have a slight difference. This means that when the system is stable, even if CEA are based on the linearised system, its results are nearly the same as the FFT results of TDA.

4.6.2 Frequencies of the unstable vibration

Furthermore, the comparisons between frequencies of the unstable vibration calculated by CAE (case 1), FFT of TDA ignoring separation (case 2) and FFT of TDA considering separation (case 3), are carried out. The time responses of case 2 and case 3 are shown in Figs. 4.24 and 4.25 respectively.

FFT of the time responses of the vertical vibration during two time durations Δt_1 (the displacement within Δt_1 is smaller than 1) and Δt_2, which represent the motion in transient state and steady state respectively, are carried out. Results are shown in Table 4.4.

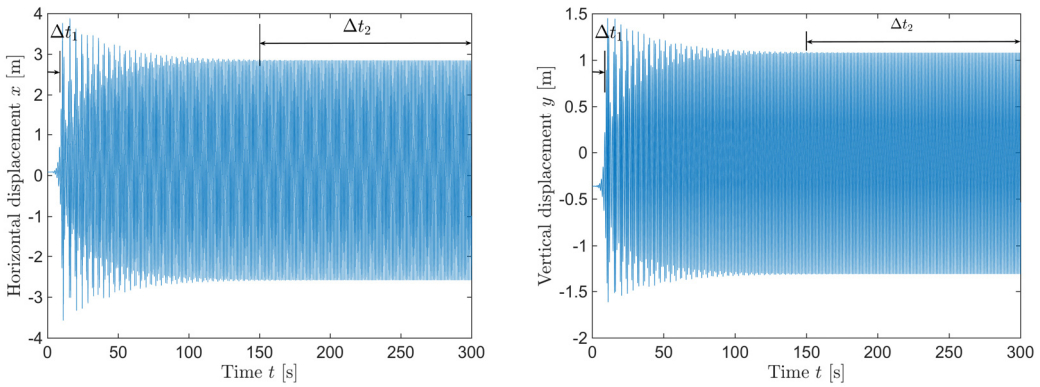

(a)

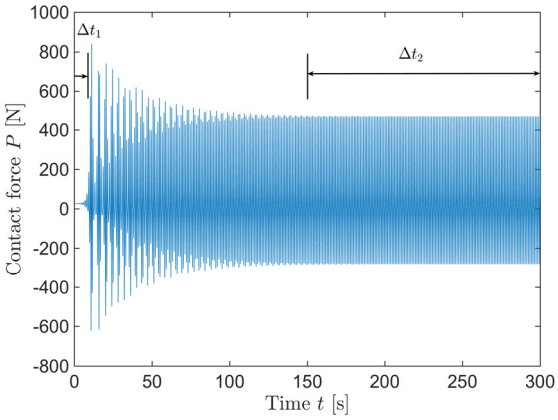

(b)

Fig. 4.24 Time responses of the ignoring separation case ($\mu = 0.8$). (a) Horizontal and vertical vibration; (b) Contact force.

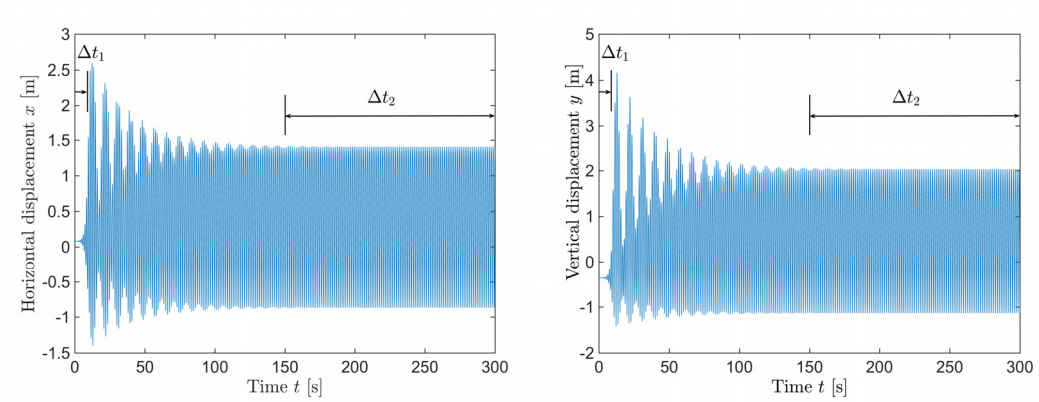

(a)

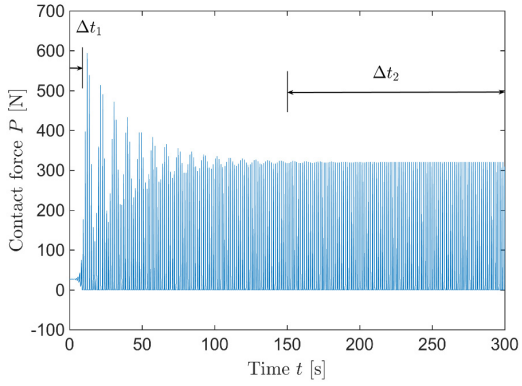

(b)

Fig. 4.25 Time responses of the considering separation case ($\mu = 0.8$). (a) Horizontal and vertical vibration; (b) Contact force.

Table 4.4 Frequencies of the unstable system (rad/s)

Friction coefficient	CEA (case 1)	FFT of TDA ignoring separation (case2)		FFT of TDA considering separation (case3)	
	Unstable frequency	Transient frequency	Steady state frequency (dominant)	Transient frequency	Steady state frequency (dominant)
μ=0.8	5.36	5.37	6.33	5.37	4.7

Because the system is unstable with two modes coupling together, the frequencies of the two modes of system are the same. This is also illustrated clearly in the frequency spectrums of case 2 and case 3 (Fig. 4.26 (a)-(d)). So Table 4.4 shows only one of the frequencies. For the steady state, when separation is ignored, although the contribution is tiny, the second harmonic component can be observed in Fig. 4.26 (b). On the other hand, when separation is considered, the contribution of the second harmonic components becomes larger and high-order harmonic component appears, as shown in Fig. 4.26 (d).

Additionally, from Table 4.4, it can be seen that if separation is ignored, the vibration frequency during transient vibration (Δt_1) is very close to the unstable frequency calculated by eigenvalue analysis at the equilibrium point. However, when the vibration settle down, its vibration frequency is 6.33 rad/s which is larger than unstable frequency 5.36 rad/s of CEA. On the other hand, when separation is considered, the frequency during Δt_1 (transient vibration) is also close to the unstable frequency of CEA; however, during steady state (Δt_2), the dominant vibration frequency (4.7 rad/s) is actually smaller than unstable frequency of CEA (5.36 rad/s). Therefore, ignoring separation in the nonlinear friction-induced vibration overestimates the vibration frequency of the system.

The phenomenon reflected from Table 4.4 can be explained. Because complex eigenvalue analysis only relies on the linear term without the higher order terms in the Taylor expansion of the nonlinear term, two consequences can happen: (1) when the vibration is near the equilibrium point, eigenvalue analysis of the linearised system

gives approximate eigenvalues, for example the frequency of case 2 and 3 during Δt_1 is close to the result of CEA; (2) when the vibration is far off the equilibrium point, especially, when the amplitude of the vibration is larger than 1, effects of the higher order terms of the Taylor expansion of the original nonlinear term become significant, so the eigenvalues of the linearised system which loses the contributions of the higher term, unlike the FFT of the TDA, are not accurate. Hence, the CEA of the linearised system are trustful when the vibration is small, otherwise FFT of the DTA needs to be carried out.

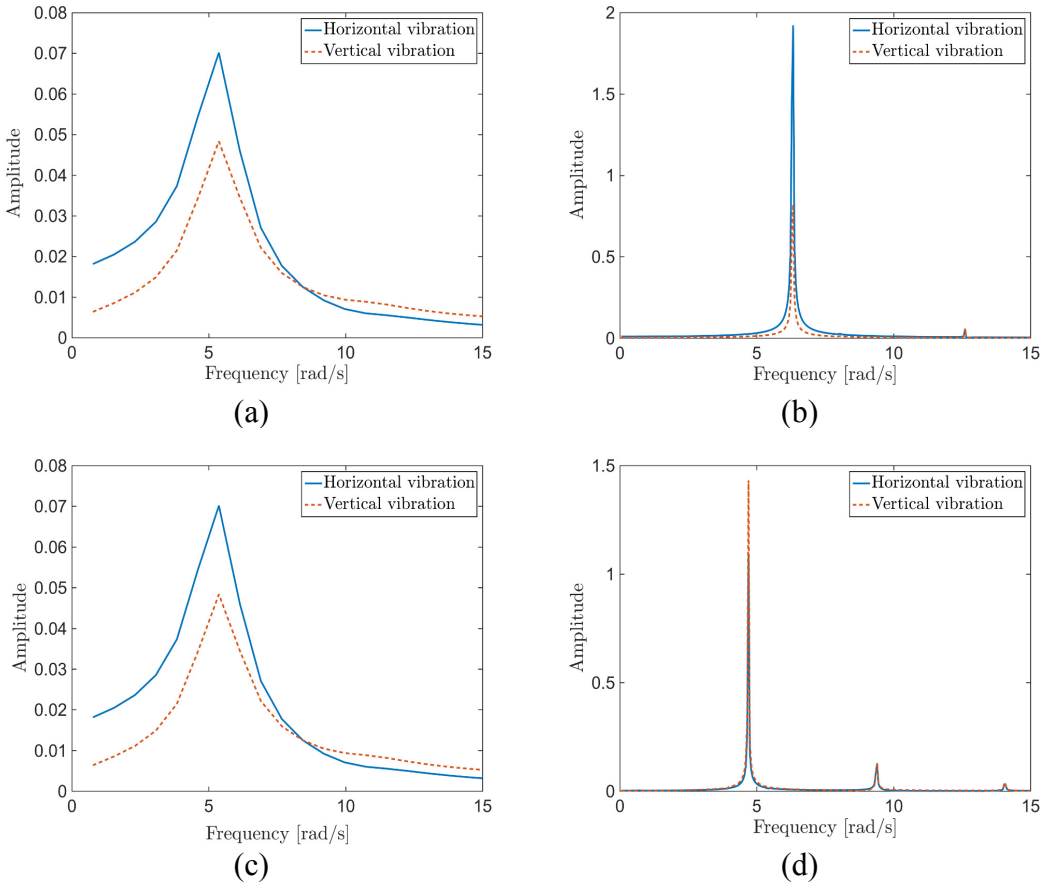

Fig. 4.26 FFT spectrums. (a) spectrum during Δt_1 of case 2; (b) spectrum during Δt_2 of case 2; (c) spectrum during Δt_1 of case 3; (d) spectrum during Δt_2 of case 3

For the vibration considering separation (case 3) shown in Fig. 4.25, initially, when the system vibrates around its equilibrium point (vibration amplitude is smaller than

1), according to previous explanations, it makes sense that the frequency given by CEA equals to the frequency through TDA. However, in the steady state, not only vibration is larger than 1, shown in Fig. 4.25 (a), but also the effects of separation are involved. Separation makes the system switch between two states (separate and in-contact), which have their own vibration frequencies. The effects of these two aspects are excluded in the stability analysis at equilibrium points (CEA), which results in its frequency results being not as accurate as the FFT of TDA with considering separation. Additionally, the results of case 2, which ignores the effects of separation, are not accurate either.

To sum up, the analysis of this part illustrates the importance of considering separation from the frequency point of view, and the necessity of stability analysis of the linearised system, as it is efficient and can give a clear indication for bifurcation; The most important finding is that, in nonlinear friction-induced vibration, FFT of DTA are necessary for the determination of unstable frequencies.

4.7 Nonlinear vibration involving Coulomb's law of friction

In this section, stick-slip vibration is considered at the contact interface. Coulomb friction is used, with a constant kinetic friction coefficient and a smaller constant static friction coefficient. As separation is also considered, the vibration of the nonlinear system becomes both discontinuous and non-smooth. The procedure of the numerical calculation may refer to the flow chart in Fig. 3.11 in Section 3.4.

In the following, some new dynamic behaviour of the system due to stick-slip vibration is illustrated through several examples. Parameter values of the linear part of the system are given by Table 4.1. The nonlinear stiffness k_{nl} takes 100 N/m^3, compression force F is 20 N, and the constant speed of the belt is 0.1 m/s.

Firstly, eigenvalue analysis of the nonlinear system, using the friction coefficient as a control parameter, is carried out, shown in Fig. 4.27. The critical friction coefficient μ_{c} for bifurcation is 0.6.

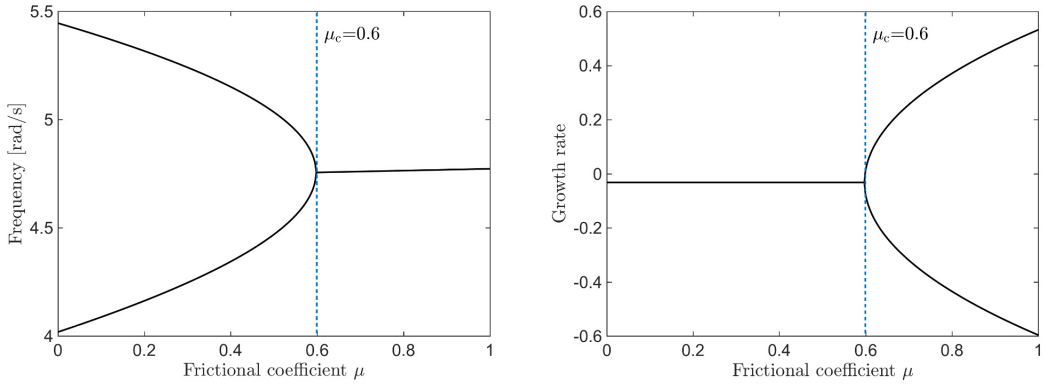

Fig. 4.27 The imaginary part (left) and real (right) of the eigenvalues versus the friction coefficient μ. The imaginary parts are the frequencies and real parts are growth rates ($F = 20\text{N}$, $k_{\text{nl}} = 100\text{N/m}^3$)

According to the value of μ_c, the dynamic behaviour with kinetic and static friction coefficients, denoted by μ_k and μ_s, located within three ranges ($\mu_k < \mu_s < \mu_c$; $\mu_k < \mu_c < \mu_s$; $\mu_c < \mu_k < \mu_s$) are examined.

4.7.1 Case 1: $\mu_k < \mu_s < \mu_c$

Case 1 corresponds to the situation that the system is stable at both the stick and slip state. Transient responses under two sets of friction coefficients are calculated. When the initial condition is (x_e, 0.1, y_e, 0), with the horizontal velocity of the mass equalling the speed of the belt, which means that the system starts from the stick phase. The results, using μ_k= 0.2, μ_s=0.4, are shown in Figs. 4.28 and 4.29; The results, using μ_k= 0.2, μ_s=0.5, are shown in Figs. 4.30 and 4.31. The time histories of the contact force, in Figs. 4.28 and 4.29, show that no separation occurs in either examples.

For the example, μ_k= 0.2, μ_s=0.4, shown in Fig. 4.29, the horizontal stick-slip limit cycle can be observed and the vertical vibration also settles down to a limit cycle. Thus, the horizontal and vertical vibration are periodic.

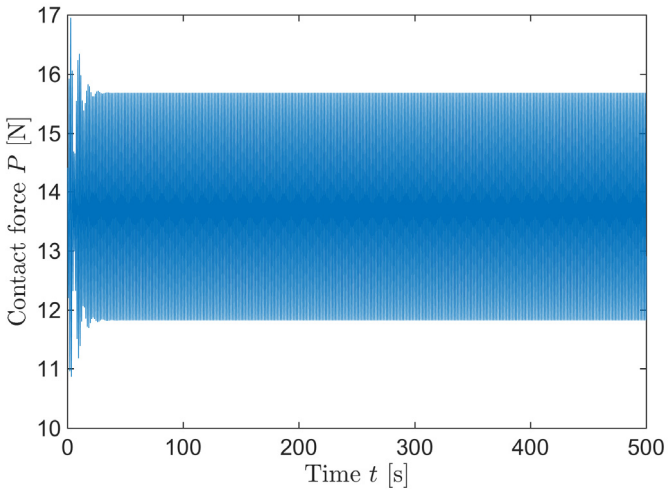

Fig. 4.28 Time history of the contact force ($\mu_k = 0.2$, $\mu_s = 0.4$)

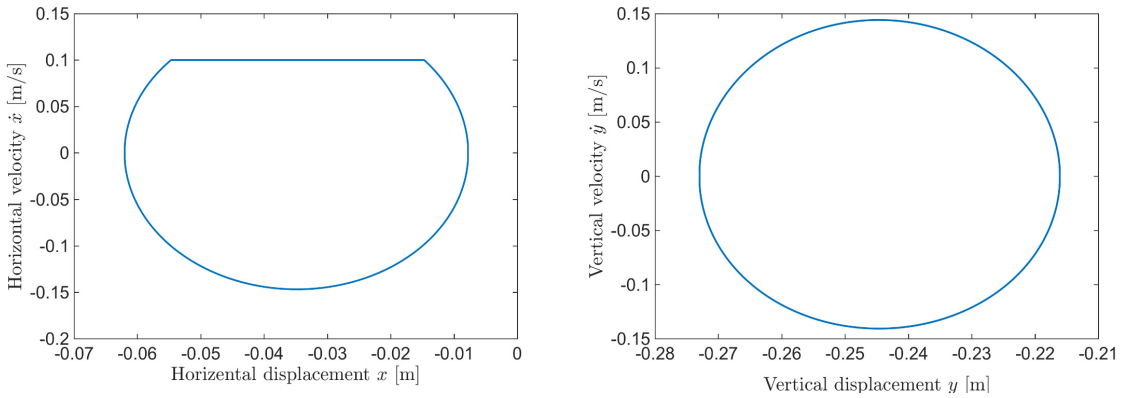

Fig. 4.29 Phase portraits of the horizontal and vertical motion ($\mu_k = 0.2$, $\mu_s = 0.4$)

However, when μ_s takes 0.5, which is closer to the critical friction coefficient μ_s, multiple limit cycles can be seen in Fig. 4.31. The horizontal stick-slip dynamic behaviour becomes diverse, and the slider's speed even can exceed the speed of the belt during the vibration. Furthermore, the FFT results in Fig. 4.22 show that although several frequencies take part in the vibration, fundamental frequency and its super harmonic component make the major contributions to the horizontal stick-slip vibration. The vertical vibration does not have super harmonics.

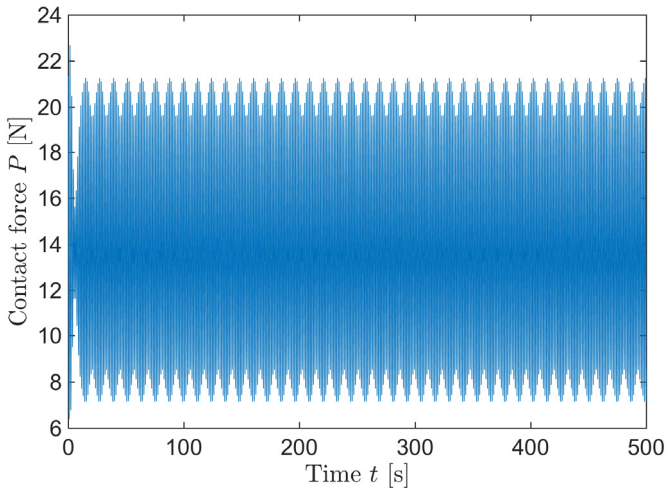

Fig. 4.30 Time history of the contact force ($\mu_k = 0.2$, $\mu_s = 0.5$)

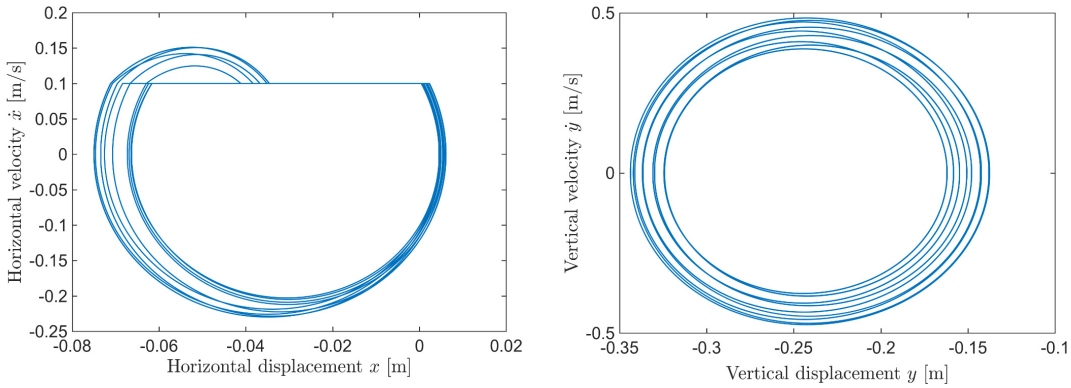

Fig. 4.31 Phase portraits of the horizontal and vertical motion ($\mu_k = 0.2$, $\mu_s = 0.5$)

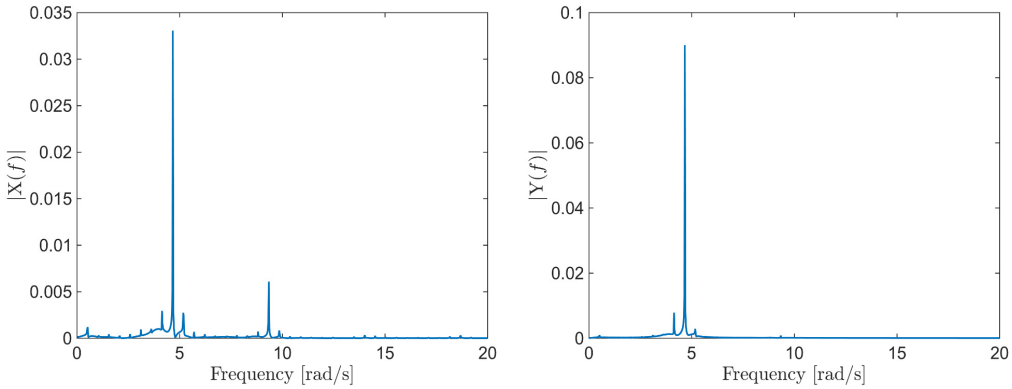

Fig. 4.32 FFT results of the horizontal (left) and vertical vibration (right). ($\mu_k = 0.2$, $\mu_s = 0.5$)

Additionally, it is found that whether the system commences from the slip motion or the stick motion does not influence the dynamic behaviour of the system. Fig. 4.33 shows the results with the same friction condition (μ_k= 0.2, μ_s=0.4) of Fig. 4.29, but initially the system starts from (-0.02,0,0,0), which leads to identical results in Fig. 4.29. However, when the system starts from a position not far away from the system's equilibrium point, stick-slip motion does not show up during the vibration, while the system gradually settles down to its equilibrium point, shown in Fig. 4.34, whose initial condition is (-0.01, 0, -0.2, 0).

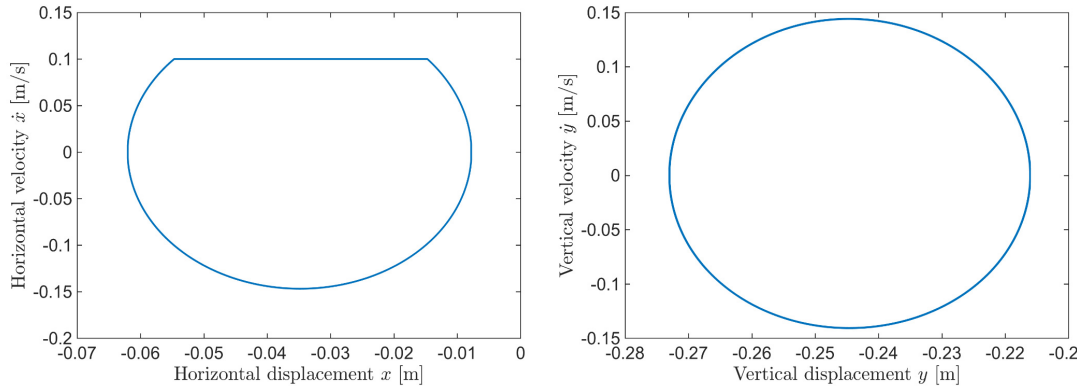

Fig. 4.33 Phase portraits of the horizontal and vertical motion ($\mu_k = 0.2$, $\mu_s = 0.4$)

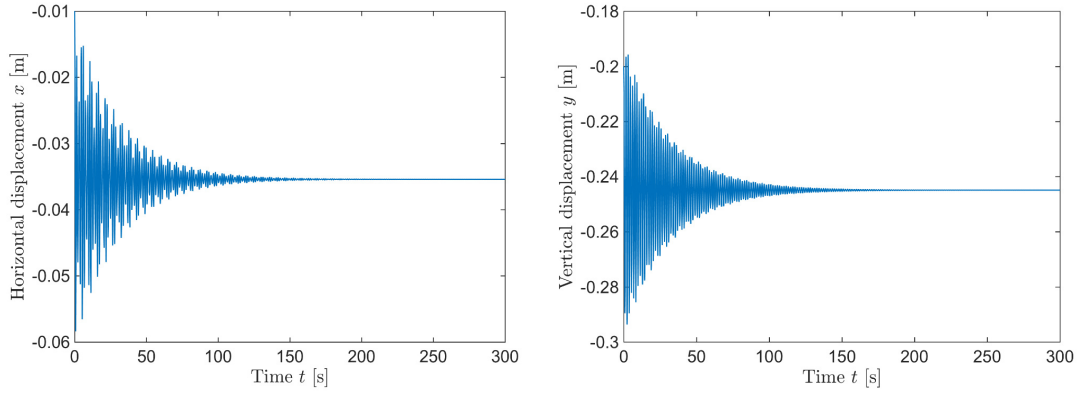

Fig. 4.34 Time history of the horizontal and vertical motion ($\mu_k = 0.2$, $\mu_s = 0.5$)

4.7.2 Case 2: $\mu_k < \mu_c < \mu_s$

A system with friction coefficients with the relationship $\mu_k<\mu_c<\mu_s$, is stable in slip motion and unstable in stick motion. Numerical results with μ_k =0.4, μ_s= 0.7, and initial condition (x_e, 0.1, y_e, 0) are shown in Figs. 4.35 and 4.36. Fig. 4.35 shows that separation and reattachment happen during the vibration as the contact force is zero occasionally. The phase plots of the vibration, shown in Fig. 4.36, are very unconventional: several limit cycles appear and repeat themselves; despite the commonly seen stick-slip limit cycle, the slider can slide on the belt with its speed passing through the speed of the belt without stick motion, called as slip1-slip2 motion; in addition, slip1-slip2-stick can be observed.

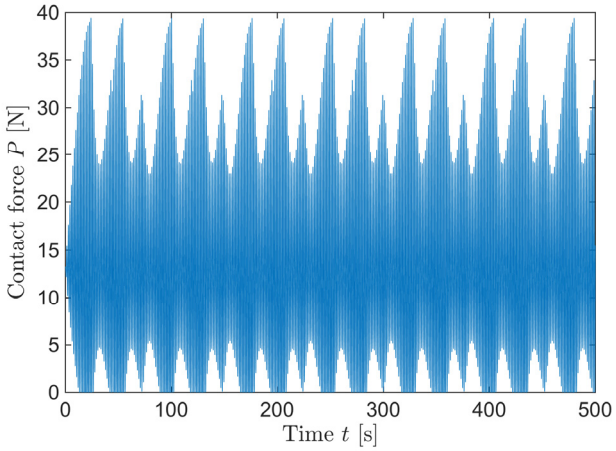

Fig. 4.35 Time history of the contact force ($\mu_k = 0.4$, $\mu_s = 0.7$)

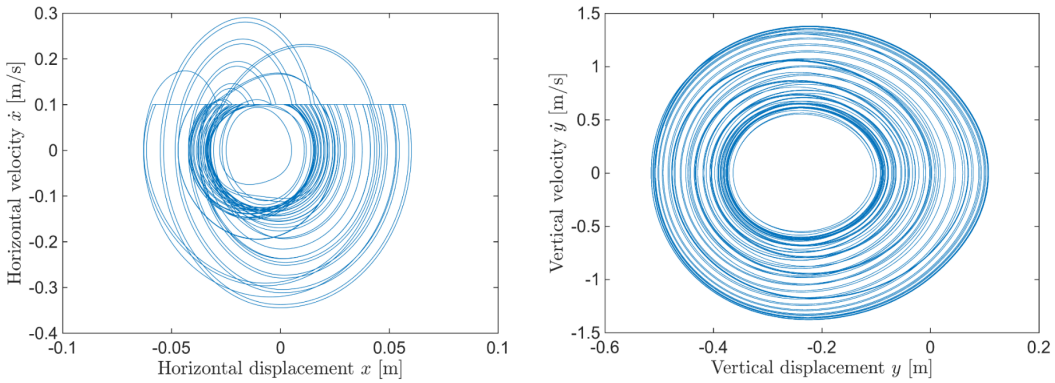

Fig. 4.36 Phase portraits of horizontal (left) and vertical motion (right) ($\mu_k = 0.4$, $\mu_s = 0.7$)

Then, through the FFT analysis, the frequency domain results are calculated, shown in Fig. 4.37. Apparently, when the system with friction coefficients in the relationship $\mu_k<\mu_c<\mu_s$, many frequency components contribute to the vibration, and the vibration is quasiperiodic.

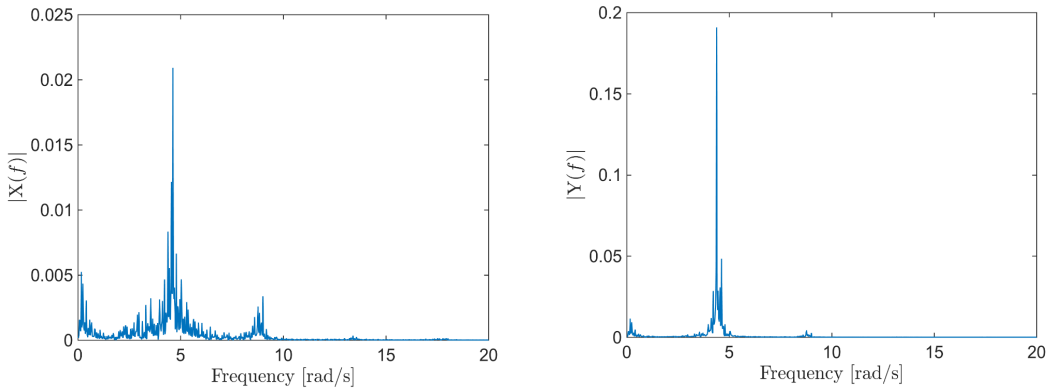

Fig. 4.37 FFT results ($\mu_k = 0.4$, $\mu_s = 0.7$)

The above results are calculated when the system starts from stick motion. Also when the system starts from slip motion with the initial position far away from the equilibrium position, vibration of the mass is identical to the stick-commencing case. However, Fig. 4.38 shows the vibration using the same friction condition (μ_k=0.4, μ_s=0.7), with the initial condition (0,0,0,0) which is near the equilibrium point. It can be seen that the vibration gradually decreases and eventually settles down to its static state.

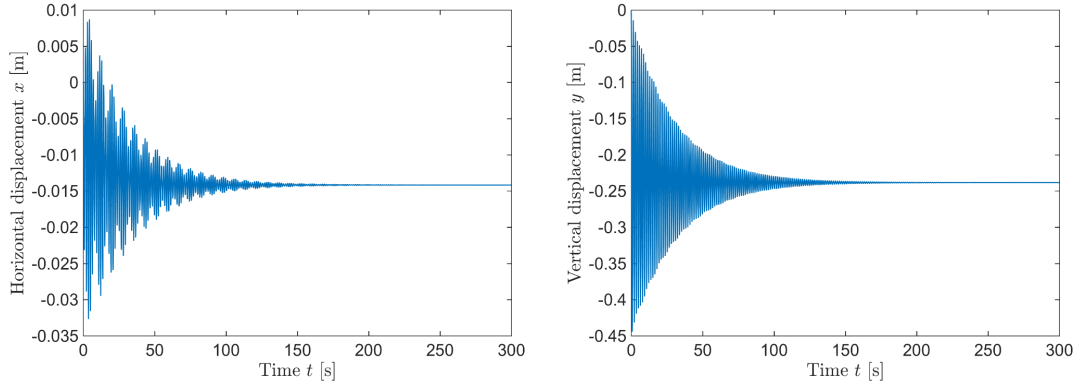

Fig. 4.38 Phase portraits of horizontal and vertical motion ($\mu_k = 0.4$, $\mu_s = 0.7$)

4.7.3 Case 3: $\mu_c < \mu_k < \mu_s$

Case 3 represents the situation in which the system is unstable in both slip and stick states. Responses under two initial conditions are calculated, but it is found that whether the system commences from the slip motion, stick motion, or even the initial condition which is very close to the equilibrium point, does not influence the eventual vibration of the system. Thus, only the results with initial condition (x_e, 0, y_e-0.01, 0) near the equilibrium position are shown in Figs. 4.39 and 4.40. The time history of the contact force illustrates that the procedure of separation and reattachment occurs repeatedly. Fig. 4.40 illustrates that stick-slip vibration occurs, and forms an interesting stick-slip limit cycle.

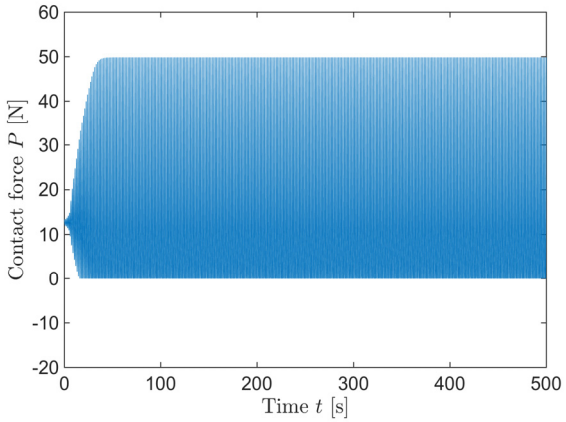

Fig. 4.39 Time history of the contact force ($\mu_k = 0.7$, $\mu_s = 1$)

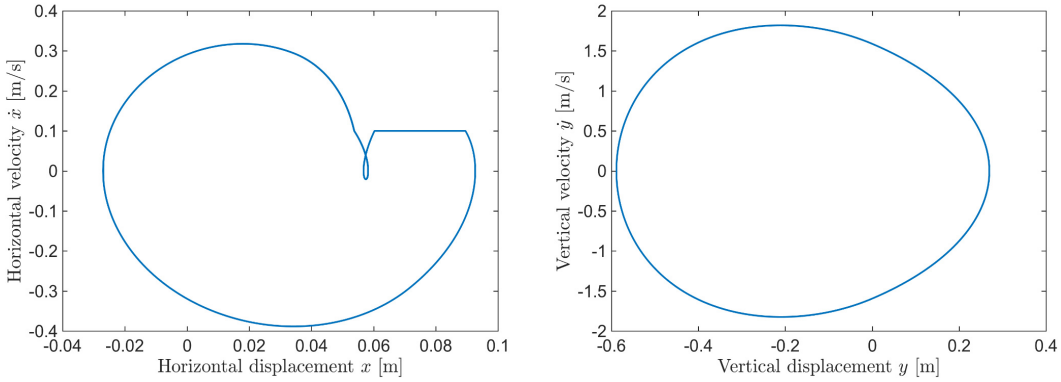

Fig. 4.40 Phase portraits of the horizontal and vertical motion ($\mu_k = 0.7$, $\mu_s = 1$)

To sum up, when stick-slip motion happens in a system with mode-coupling instability, its dynamic behaviour becomes richer, and crucially depends on the relationship between the friction coefficients and critical friction coefficient for mode-coupling.

As has been known, bifurcation of the equilibrium point only happens when the friction law is at least quadratically dependent on the state variables [43]. In this part, as Coulomb's law of friction is used, case 1 ($\mu_k<\mu_s<\mu_c$) and case 2 ($\mu_k <\mu_c<\mu_s$) show that the system is stable when it is disturbed from its equilibrium point; while the horizontal and vertical motion never settle down to its static state when it is disturbed far from its equilibrium point. However, when $\mu_c<\mu_k<\mu_s$ (case 3), the equilibrium point is not stable due to mode coupling, and horizontal stick-slip always happens. Moreover, the vibration of the system becomes quasi-periodic.

4.8 Conclusions

In this chapter, the vibration induced by the sliding friction in a nonlinear two-degree-of-freedom mass-belt model, in which a cubic nonlinear contact stiffness is introduced at the contact point between the slider and the belt, is studied.

1. The effects of nonlinear contact stiffness as well as the normal pre-load on the local stability near the equilibrium point are studied by the eigenvalue analysis. The results of both proportional damping and non-proportional damping cases show that, the roles of nonlinear stiffness and the pre-load on the stability of the system are complicated. Initially, increasing the nonlinear stiffness or the pre-load tends to make the nonlinear system more unstable than the linear system; but at certain higher values, they start to stabilise the system; at some even higher values, the nonlinear system is more stable than its corresponding linear system with the same friction coefficient. These properties can be taken advantage of in controlling friction-induced vibration. Additionally, the influence of the nonlinear stiffness and the pre-load in this nonlinear system can be different, depending on the values of the linear stiffness.

2. Through numerical studies, the process of contact loss and reattachment of the slider during vibration is demonstrated. It is found that separation can happen even under a

large pre-load. Moreover, when separation is considered, not only the change of vibration amplitudes against some system parameter values is opposite to the trend when separation is ignored, but also the values of the amplitudes are larger in certain conditions. Therefore, ignoring separation, as usually occurs in simple models for friction-induced vibration, is likely to under-predict vibration magnitude and thus is unsafe.

3. The study in frequency domain predicts that, for the nonlinear system with friction, besides complex eigenvalue analysis, transient dynamic analysis needs to be taken into account for predicting the actual unstable frequencies. Ignoring separation overestimates the vibration frequencies.

4. When stick-slip vibration is involved in the coupled system, the motion of the system is diverse and separation happens as well, which crucially depends on the relations between the friction coefficients and the critical friction coefficient for bifurcation. Quasi-periodic vibration can appear in the nonlinear 2-degree-of-freedom system.

Therefore, a major conclusion is that separation at the contact interface should be taken into account in nonlinear friction-induced vibration problems.

5 Friction-induced Vibration of an Elastic Disc and a Moving Slider with Separation and Reattachment

5.1 Introduction

Elastic discs are key components in a wide range of mechanical applications such as rotors and stators in some engines, brakes and clutches, computer hard disc drives, and saws. During the operation of these mechanical devices, dry friction plays an important role on the dynamic behaviour. Researchers proposed various theoretical disc models based on the engineering background, which are reviewed in Chapter 2.3.2. Mechanical models of the disc have been one kind of classic models in the theoretical study of friction-induced vibration.

The main purpose of the current work is to investigate the friction-induced nonstationary transverse vibration of a disc subjected to a rotating slider undergoing vertical vibration and in-plane stick-slip vibration with separation and reattachment. A model containing an elastic disc in friction contact with a rotating oscillator is developed. Stick-slip motion of the slider takes place on the disc surface due to friction governed by the non-smooth Coulomb's law of friction, which leads to the coupling between the transverse vibration of the disc and the horizontal (in-plane) vibration of the rotating slider. On the other hand, loss of contact at the friction interface of the disc, which is often neglected in most of the studies, is involved. Especially, the specific roles of separation and its importance to the friction-induced vibration are investigated. Moreover, impact at the instant of the reattachment is considered. Therefore, the current work contains both the continuous non-smoothness and the discontinuity in the state which increase the challenge of implementing the specific analysis.

The structure of this chapter is: firstly, the mechanical model is introduced in Section 5.2, followed by the theoretical development of the system including the derivations of the equations of motion of the system in stick, slip and separation states, the discussion of conditions for staying in individual motion states, and formulations of impact at the instant of reattachment. Then, in Section 5.3, modal analysis of the

annular disc and the whole system are carried out. In Section 5.4, the accuracy of the numerical method on simulating the vibration of the plate is verified. In Section 5.5, dynamic behaviour of the model is analysed and numerical results show that separation can happen during unstable vibration at a low rotating speed level. Moreover, comparisons between the dynamic behaviour of the disc considering and ignoring separation indicate the importance of considering separation. Then, the effects of key system parameters on the friction-induced vibration of the system are examined via a numerical parametric analysis. In Section 5.6, the evolutions of the frequencies of the system with time are studied through the short time Fourier transform, which reveals the time varying nature of the whole system due to the transverse separation-reattachment and in-plane stick-slip events. Finally, conclusions are given in Section 5.7.

5.2 Disc model and theoretical development

Fig. 5.1 presents the mechanical model studied in this chapter. The system contains an elastic annular disc, which is clamped at its inner radius a and free at its outer radius b, and a slider system in friction contact with the disc. In this model, a cylindrical coordinate system is defined, in which z is the vertical coordinate, and θ is the circumferential coordinate and r is the radial coordinate. The original position of z axis is recognised as at the location of the plate when it is not deformed. The annular disc is a Kirchhoff plate which exhibits only transverse motion. The mass (slider) has a vertical branch and a horizontal (in-plane) branch, each having a spring and a damper in parallel. A vertical displacement Δ is applied on the top of the vertical branch and is kept constant throughout the subsequent vibration, so that a vertical pre-load is generated and is always present. The horizontal branch is connected with a drive point that moves around on the surface of the elastic annular plate at a constant rotating speed Ω. In this work, the Coulomb's law of friction is used with a static friction coefficient μ_s and kinetic friction coefficient μ_k. The slider is capable of stick-slip oscillation in the horizontal direction. Such a system was studied in Ref. [130] in which loss of contact and subsequent reattachment were excluded.

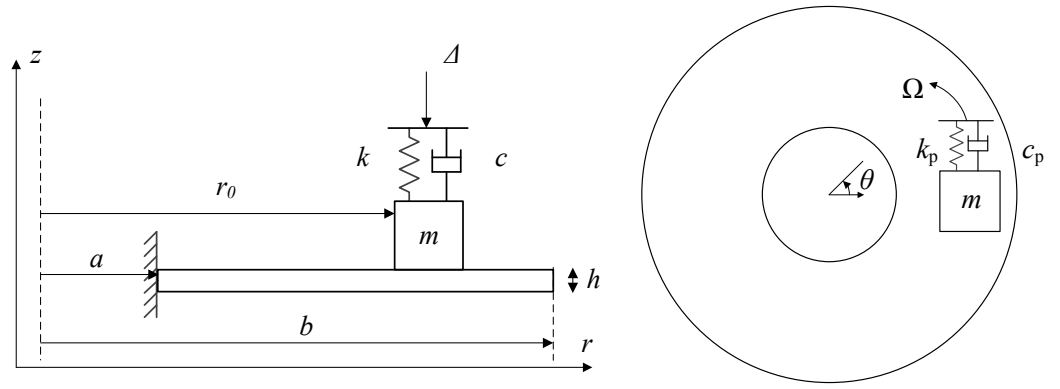

Fig. 5.1 The annular plate and slider system in the cylindrical coordinate system (left: view from the side; right: view from the top)

5.2.1 In-plane stick-slip motion of the slider

As the friction coefficient μ_s is assumed to be greater than μ_k in this work, the slider can undergo stick-slip oscillation in the horizontal direction. According to the Newton's second law of friction, when the slider is sliding, its in-plane equation of motion is expressed in Eq. (5.1):

$$r_0\left[m\ddot{\varphi}+c_p\left(\Omega-\dot{\varphi}\right)+k_p\left(\Omega t-\varphi\right)\right]=-\mu_k\,\mathrm{sgn}\left(\dot{\varphi}\right)P \tag{5.1}$$

in which φ describes the absolute circumferential angular position of the slider. r_0 is the radial position of the slider; c_p is the in-plane damping coefficient of the slider, k_p is the in-plane stiffness of the slider, and P is the (total) contact force between the disc and the slider.

If ψ is defined as the circumferential angular position of the slider relative to the drive point, expressed as:

$$\psi=\Omega t-\varphi \tag{5.2}$$

in which t is time, then the velocity and acceleration relation between the relative motion represented by ψ and absolute motion φ are:

$$\dot{\psi}=\Omega-\dot{\varphi},\ \ \ddot{\psi}=-\ddot{\varphi} \tag{5.3}$$

The equation of motion with respect to absolute motion φ in Eq. (5.1) can be reformed as Eq. (5.4), which is with respect to the relative motion ψ :

$$r_0\left(m\ddot{\psi}+c_{\mathrm{p}}\dot{\psi}+k_{\mathrm{p}}\psi\right)=\mu_{\mathrm{k}}\,\mathrm{sgn}\left(\dot{\varphi}\right)P \tag{5.4}$$

The sliding motion can be maintained if the following conditions are satisfied:

$$r_0\left|c_{\mathrm{p}}\dot{\psi}+k_{\mathrm{p}}\psi\right|\geq\mu_{\mathrm{s}}P \tag{5.5}$$

or

$$\dot{\psi}\neq\Omega \tag{5.6}$$

Otherwise, the slider sticks to the plate. In this motion phase, the slider's absolute circumferential velocity $\dot{\varphi}$ and its acceleration $\ddot{\varphi}$ equal to zero, and its circumferential position is referred to as φ_{stick}. The relative motion of the slider is given by Eq. (5.7)

$$\psi=\Omega t-\varphi_{\mathrm{stick}} \tag{5.7}$$

The condition for the slider staying in the stick phase is:

$$r_0\left|c_{\mathrm{p}}\dot{\psi}+k_{\mathrm{p}}\psi\right|<\mu_{\mathrm{s}}P \tag{5.8}$$

5.2.2 Transverse vibration of the disc

The equation of transverse motion of the disc under the action of the moving slider is given by Eq. (5.9):

$$\rho h\frac{\partial^2 w}{\partial t^2}+D^*\nabla^4\dot{w}+D\nabla^4 w=-\frac{1}{r}\delta\left(r-r_0\right)\delta\left(\theta-\varphi\right)P \tag{5.9}$$

where w denotes the transverse displacement of the plate, r and θ are the radial and circumferential coordinates in the cylindrical coordinate system respectively; D^* is the damping coefficient of the disc, ρ is the mass-density of the disc, D is the flexural rigidity of the disc; and $\delta(\bullet)$ is the Dirac delta function.

P can be obtained from the equation of vertical motion of slider m:

$$P = N + m\ddot{u} + c\dot{u} + k\left(u - u_0\right) \tag{5.10}$$

where u and $\dot{u}$ are the vertical motion and vertical velocity of the slider, u_0 is the initial vertical displacement of the slider, c is the damping coefficient and k is the stiffness of the vertical branch of the slider, N is the pre-load as a result of the vertical displacement Δ applied.

The initial displacement of the slider u_0 equals to the static position w_0 of the plate where the slider locates at. When the system is at static state, w_0 can be calculated through Eq. (5.11), as the contact force is N:

$$D\nabla^4 w = -N \tag{5.11}$$

Here contact force P is defined as positive when there is contact (so that P is a compressive force). Thus the condition for maintaining contact is:

$$P > 0 \tag{5.12}$$

If there is contact between the slider and the plate, the relationship between the transverse displacement w of the plate and the vertical displacement u of the slider is [264]:

$$u(t) = w\left(r_0, \varphi(t), t\right) \tag{5.13}$$

and therefore

$$\dot{u} = \dot{\varphi}\frac{\partial w}{\partial \theta} + \frac{\partial w}{\partial t} \tag{5.14}$$

$$\ddot{u} = \ddot{\varphi}\frac{\partial w}{\partial \theta} + \dot{\varphi}^2\frac{\partial^2 w}{\partial \theta^2} + 2\dot{\varphi}\frac{\partial^2 w}{\partial \theta \partial t} + \frac{\partial^2 w}{\partial t^2} \tag{5.15}$$

By substituting Eqs. (5.13), and (5.14) - (5.15) into Eq. (5.9), the equation of transverse motion of the disc can be derived as:

$$\rho h\frac{\partial^2 w}{\partial t^2}+D^*\nabla^4\dot{w}+D\nabla^4 w=-\frac{1}{r}\delta\left(r-r_0\right)\delta\left(\theta-\varphi\right)\left[N+m\left(\ddot{\varphi}\frac{\partial w}{\partial\theta}+\dot{\varphi}^2\frac{\partial^2 w}{\partial\theta^2}+2\dot{\varphi}\frac{\partial^2 w}{\partial\theta\partial t}+\frac{\partial^2 w}{\partial t^2}\right)+c\left(\dot{\varphi}\frac{\partial w}{\partial\theta}+\frac{\partial w}{\partial t}\right)+k\left(w-w_0\right)\right] \tag{5.16}$$

where w_0 is initial transverse displacement of the disc as a result of applying Δ to the vertical branch of the slider.

Although Eq. (5.16) is applicable to both stick and slip motion states, as $\dot{\varphi}$ and $\ddot{\varphi}$ are zero in the stick phase, Eq. (5.16) is simplified to Eq. (5.17) which represents the equation of motion when the slider sticks to the disc.

$$\rho h\frac{\partial^2 w}{\partial t^2}+D^*\nabla^4\dot{w}+D\nabla^4 w=-\frac{1}{r}\delta\left(r-r_0\right)\delta\left(\theta-\varphi\right)\left[N+m\frac{\partial^2 w}{\partial t^2}+c\frac{\partial w}{\partial t}+k\left(w-w_0\right)\right] \tag{5.17}$$

5.2.3 Coupled equations of motion of the whole system in modal coordinates

The transverse displacement of the disc can be expressed as an infinite series of modal coordinates:

$$w\left(r,\theta,t\right)=\sum_{k=0}^{\infty}\sum_{l=-\infty}^{\infty}\Psi_{kl}\left(r,\theta\right)q_{kl}\left(t\right) \tag{5.18}$$

where $\Psi_{kl}\left(r,\theta\right)$ is the mode shape of the plate given by Eq. (5.19):

$$\Psi_{kl}\left(r,\theta\right)=\frac{1}{\sqrt{\rho hb^2}}R_{kl}\left(r\right)e^{\mathrm{i}l\theta} \tag{5.19}$$

in which $R_{kl}\left(r\right)$ is a combination of the Bessel functions and the modified Bessel functions. Subscript k denotes the number of nodal circles and l denotes the number of nodal diameters; $\mathrm{i}=\sqrt{-1}$.

The ortho-normality conditions of modal functions are:

$$\int_a^b\int_0^{2\pi}\rho h\bar{\Psi}_{kl}\Psi_{rs}rdrd\theta=\delta_{kr}\delta_{ls},\ \int_a^b\int_0^{2\pi}\rho h\bar{\Psi}_{kl}\nabla^4\Psi_{rs}rdrd\theta=\omega_{kl}{}^2\delta_{kr}\delta_{ls} \tag{5.20}$$

in which $\bar{\Psi}_{kl}$ is the complex conjugate of Ψ_{kl}.

Then by multiplying Ψ_{kl} on both sides of Eqs. (5.16) and (5.17), then integrating them over the whole disc surface, and by using the ortho-normality conditions shown in Eq. (5.20), Eqs. (5.16) and (5.17) are rewritten in terms of modal coordinates $q_{kl}(t)$ shown below.

In the stick phase, the equation of transverse motion of the disc in terms of modal coordinates is expressed as:

$$\ddot{q}_{kl} + 2\xi\omega_{kl}\dot{q}_{kl} + {\omega_{kl}}^2 q_{kl} = -\frac{N-kw_0}{\sqrt{\rho hb^2}} R_{kl}(r_0)\exp(-\mathrm{i}l\varphi) - \frac{1}{\rho hb^2}\sum_{r=0}^{\infty}\sum_{s=-\infty}^{\infty} R_{rs}(r_0)R_{kl}(r_0)\exp(\mathrm{i}(s-l)\varphi)(m\ddot{q}_{rs} + c\dot{q}_{rs} + kq_{rs}) \tag{5.21}$$

in which

$$\varphi = \varphi_{\text{stick}} \tag{5.22}$$

and the relative motion of the slider in the stick phase has been given by Eq. (5.7).

The conditions for remaining in stick phase given by Eqs. (5.8) is transformed into Eq. (5.23):

$$r_0\left|c_{\mathrm{p}}\dot{\psi} + k_{\mathrm{p}}\psi\right| < \mu_{\mathrm{s}}\left[N - kw_0 + \frac{1}{\sqrt{\rho hb^2}}\sum_{r=0}^{\infty}\sum_{s=-\infty}^{\infty} R_{rs}(r_0)\exp(\mathrm{i}s\varphi)(m\ddot{q}_{rs} + c\dot{q}_{rs} + kq_{rs})\right] \tag{5.23}$$

During the sliding motion, the equations of transverse motion of the disc and the equation of horizontal motion of the slider are given by Eqs. (5.24) and (5.25):

$$\ddot{q}_{kl} + 2\xi\omega_{kl}\dot{q}_{kl} + {\omega_{kl}}^2 q_{kl} = -\frac{N-kw_0}{\sqrt{\rho hb^2}} R_{kl}(r_0)\exp(-\mathrm{i}l\varphi) - \frac{1}{\rho hb^2}\sum_{r=0}^{\infty}\sum_{s=-\infty}^{\infty} R_{rs}(r_0)R_{kl}(r_0)\exp(\mathrm{i}(s-l)\varphi) \left\{m\left[\ddot{q}_{rs} + \mathrm{i}2s\dot{\varphi}\dot{q}_{rs} + (\mathrm{i}s\ddot{\varphi} - s^2\dot{\varphi}^2)q_{rs}\right] + c(\dot{q}_{rs} + \mathrm{i}s\dot{\varphi}q_{rs}) + kq_{rs}\right\} \tag{5.24}$$

and

$$r_0\left(m\ddot{\varphi}+c_{\mathrm{p}}\dot{\varphi}+k_{\mathrm{p}}\varphi\right)=r_0\left(c_{\mathrm{p}}\Omega+k_{\mathrm{p}}\Omega t\right)$$
$$-\mu_{\mathrm{k}}\,\mathrm{sgn}\left(\dot{\varphi}\right)\left\{N-kw_0+\frac{1}{\sqrt{\rho hb^2}}\sum_{r=0}^{\infty}\sum_{s=-\infty}^{\infty}R_{rs}\left(r_0\right)\exp\left(\mathrm{i}s\varphi\right)\right.$$
$$\left.\left\{m\left[\ddot{q}_{rs}+\mathrm{i}2s\dot{\varphi}\dot{q}_{rs}+\left(\mathrm{i}s\ddot{\varphi}-s^2\dot{\varphi}^2\right)q_{rs}\right]+c\left(\dot{q}_{rs}+\mathrm{i}s\dot{\varphi}q_{rs}\right)+kq_{rs}\right\}\right\} \tag{5.25}$$

And because of the axial symmetry of the annular disc, the relationships in Eq. (5.26) are satisfied [82]:

$$R_{r,s}\left(r\right)=R_{r,-s}\left(r\right),\ \omega_{r,s}\left(r\right)=\omega_{r,-s}\left(r\right),\ q_{r,s}\left(t\right)=\overline{q}_{r,-s}\left(t\right) \tag{5.26}$$

One of the conditions for staying in the slip phase (Eqs. (5.5)) can be expressed in modal coordinates as:

$$r_0\left|c_{\mathrm{p}}\dot{\psi}+k_{\mathrm{p}}\psi\right|\geq\mu_{\mathrm{s}}\left\{N-kw_0+\frac{1}{\sqrt{\rho hb^2}}\sum_{r=0}^{\infty}\sum_{s=-\infty}^{\infty}R_{rs}\left(r_0\right)\exp\left(\mathrm{i}s\varphi\right)\right.$$
$$\left.\left\{m\left[\ddot{q}_{rs}+\mathrm{i}2s\dot{\varphi}\dot{q}_{rs}+\left(\mathrm{i}s\ddot{\varphi}-s^2\dot{\varphi}^2\right)q_{rs}\right]+c\left(\dot{q}_{rs}+\mathrm{i}s\dot{\varphi}q_{rs}\right)+kq_{rs}\right\}\right\} \tag{5.27}$$

5.2.4 Separation and reattachment

As it is known, separation takes place when contact force $P(t)$ drops to zero. During the numerical calculations, it is important to monitor $P(t)$ at each time step, because if separation happens, a new set of equations of motion of the slider and disc needs to be used. When $P(t)$ becomes negative, the bisection method is used to find the critical point at which $P(t)$ satisfying $|P(t)| \leq \varepsilon$, in which ε is a small tolerance defined in the Matlab codes. During separation, the contact force is zero and the sliding friction force vanishes.

The transverse motion of the disc and the vertical motion of the slider during separation are governed by Eqs. (5.28) and (5.29) respectively:

$$\rho h\frac{\partial^2 w}{\partial t^2}+D^*\nabla^4\dot{w}+D\nabla^4 w=0 \tag{5.28}$$

$$m\ddot{u}+c\dot{u}+k\left(u-u_0\right)+N=0 \tag{5.29}$$

The new equation of horizontal motion of the slider is expressed in Eq. (5.30):

$$m\ddot{\psi} + c_{\mathrm{p}}\dot{\psi} + k_{\mathrm{p}}\psi = 0 \tag{5.30}$$

Separation can be maintained when Eq. (5.31) is satisfied:

$$u > w \tag{5.31}$$

After separation, the slider may get into contact with the disc again. Reattachment takes place when the displacement of the slider u equals to the displacement w of a point on the disc having the same coordinate as the slider. During the very short time interval of reattachment, denoted by $(t_{\mathrm{r}}^{-},\ t_{\mathrm{r}}^{+})$, impact may happen. t_{r}^{-} and t_{r}^{+} are the starting and the ending time moments of the impact. The states of the disc and the slider at time t_{r}^{+} are determined based on the momentum theory. The procedure for determining the dynamic states immediately after reattachment, which was presented in Ref. [265] for a moving-mass-on-beam problem, is derived for the present problems below.

For simplification, a simple perfectly plastic impact is assumed. The slider sticks onto the disc after the impact and the transverse displacement is continuous and in-plane motion of the slider does not change by the vertical impact, so one can get:

$$q_{kl}\left(t_{\mathrm{r}}^{+}\right) = q_{kl}\left(t_{\mathrm{r}}\right) = q_{kl}\left(t_{\mathrm{r}}^{-}\right),\ \varphi\left(t_{\mathrm{r}}^{+}\right) = \varphi\left(t_{\mathrm{r}}\right),\ \dot{\varphi}\left(t_{\mathrm{r}}^{+}\right) = \dot{\varphi}\left(t_{\mathrm{r}}\right) \tag{5.32}$$

Suppose the impulse at t_{r} is p, the equation of motion of the disc is:

$$\rho h\frac{\partial^2 w}{\partial t^2} + D^{*}\nabla^4\dot{w} + D\nabla^4 w = -\frac{p}{r}\delta\left(r - r_0\right)\delta\left(\theta - \varphi\right)\delta\left(t - t_{\mathrm{r}}\right) \tag{5.33}$$

By using the same modal expansion process described in Section 3.3.2, Eq. (5.33) can be converted to Eq. (5.34) in modal coordinates:

$$\ddot{q}_{kl} + 2\xi\omega_{kl}\dot{q}_{kl} + {\omega_{kl}}^2 q_{kl} = -p\overline{\Psi}_{kl}\left(r_0,\ \varphi\left(t_{\mathrm{r}}\right)\right)\delta\left(t - t_{\mathrm{r}}\right) \tag{5.34}$$

The velocity jump as a result of the impact can be obtained from Eq. (5.34) and given by Eq. (5.35):

$$\dot{q}_{kl}\left(t_{\mathrm{r}}^{+}\right)-\dot{q}_{kl}\left(t_{\mathrm{r}}^{-}\right)=-\frac{p}{\sqrt{\rho h b^{2}}}R_{kl}\left(r_{0}\right)\exp\left(-\mathrm{i}l\varphi\left(t_{\mathrm{r}}\right)\right) \tag{5.35}$$

Similarly, the velocity jump of the slider can be obtained:

$$\dot{u}\left(t_{\mathrm{r}}^{+}\right)-\dot{u}\left(t_{\mathrm{r}}^{-}\right)=\frac{p}{m} \tag{5.36}$$

The combination of Eqs. (5.35) and (5.36) gives:

$$\dot{q}_{kl}\left(t_{\mathrm{r}}^{+}\right)-\dot{q}_{kl}\left(t_{\mathrm{r}}^{-}\right)=-m\left(\dot{u}\left(t_{\mathrm{r}}^{+}\right)-\dot{u}\left(t_{\mathrm{r}}^{-}\right)\right)\bar{\Psi}_{kl}\left(r_{0},\ \varphi\left(t_{\mathrm{r}}\right)\right) \tag{5.37}$$

For perfectly plastic impact, the slider takes the displacement and the velocity of the disc at time t_{r}^{+}. $\dot{u}\left(t_{\mathrm{r}}^{+}\right)$ can be expressed as Eq. (5.38):

$$\begin{aligned}&\dot{u}\left(t_{\mathrm{r}}^{+}\right)=\dot{\varphi}\frac{\partial w}{\partial\theta}+\frac{\partial w}{\partial t}\bigg|_{\theta=\varphi\left(t_{\mathrm{r}}^{+}\right)}=\\&\sum_{k=0}^{\infty}\sum_{l=-\infty}^{\infty}\left[\Psi_{kl}\left(r_{0},\ \varphi\left(t_{\mathrm{r}}^{+}\right)\right)\dot{q}_{kl}\left(t_{\mathrm{r}}^{+}\right)+\dot{\varphi}\left(t_{\mathrm{r}}^{+}\right)\frac{\partial\Psi_{kl}\left(r_{0},\ \varphi\left(t_{\mathrm{r}}^{+}\right)\right)}{\partial\theta}q_{kl}\left(t_{\mathrm{r}}^{+}\right)\right]\end{aligned} \tag{5.38}$$

By substituting Eq. (5.38) into (5.37), and combining (5.38), then modal velocity $\dot{q}_{kl}$ and vertical velocity $\dot{u}$ time t_{r}^{+} are derived as:

$$\dot{u}\left(t_{\mathrm{r}}^{+}\right)=\frac{\sum_{k=0}^{\infty}\sum_{l=-\infty}^{\infty}\left(m\dot{u}\left(t_{\mathrm{r}}^{-}\right)\Psi_{kl}\left(r_{0},\ \varphi\left(t_{\mathrm{r}}^{+}\right)\right)\bar{\Psi}_{kl}\left(r_{0},\ \varphi\left(t_{\mathrm{r}}\right)\right)+\Psi_{kl}\left(r_{0},\ \varphi\left(t_{\mathrm{r}}^{+}\right)\right)q_{kl}\left(t_{\mathrm{r}}^{-}\right)+S_{1}\right)}{S_{2}} \tag{5.39}$$

$$\dot{q}_{kl}\left(t_{\mathrm{r}}^{+}\right)=\dot{q}_{kl}\left(t_{\mathrm{r}}^{-}\right)-m\left[\frac{\sum_{k=0}^{\infty}\sum_{l=-\infty}^{\infty}\left(\Psi_{kl}\left(r_{0},\ \varphi\left(t_{\mathrm{r}}^{+}\right)\right)\dot{q}_{kl}\left(t_{\mathrm{r}}^{-}\right)+S_{1}\right)-\dot{u}\left(t_{\mathrm{r}}^{-}\right)}{S_{2}}\right]\bar{\Psi}_{kl}\left(r_{0},\ \varphi\left(t_{\mathrm{r}}\right)\right) \tag{5.40}$$

in which

$$\begin{cases}S_{1}=\dot{\varphi}\left(t_{\mathrm{r}}^{+}\right)\dfrac{\partial\Psi_{kl}\left(r_{0},\ \varphi\left(t_{\mathrm{r}}^{+}\right)\right)}{\partial\theta}q_{kl}\left(t_{\mathrm{r}}^{+}\right)\\S_{2}=1+m\sum_{k=0}^{\infty}\sum_{l=-\infty}^{\infty}\left(\Psi_{kl}\left(r_{0},\ \varphi\left(t_{\mathrm{r}}^{+}\right)\right)\bar{\Psi}_{kl}\left(r_{0},\ \varphi\left(t_{\mathrm{r}}\right)\right)\right)\end{cases} \tag{5.41}$$

5.3 Modal analysis

5.3.1 Natural frequencies of the plate

There are infinite numbers of natural frequencies of the plate. Actually, only several modes play dominant role in the vibration. In most analysis, to avoid expensive computations, truncated modal series of the disc's displacement is utilised. The basic parameter values used in the following examples of this chapter are listed in Table 5.1.

Table 5.1 The values of system parameters

a	b	r_0	h	E	v	D^*	
0.044 m	0.12 m	0.1 m	0.002 m	150 GPa	0.211	10^{-5} N/(m/s)	
μ_s	μ_k	k	k_p	m	ρ	c	c_p
0.4	0.24	5×10^4 N/m	2×10^4 N/m	0.1 kg	7200 kg/m^3	0	0

The natural frequencies of the plate can be calculated by MATLAB on the base of the theory of the plate [249], which has been introduced in Chapter 3. The first five distinguish frequencies are showed in Table 5.2, in which k denotes the number of nodal circles and l denotes the number of nodal diameters. According to the results, all of them correspond to the zero nodal circle. In order to verify the accuracy for results from MATLAB codes, finite element analysis by ANSYS is carried out as well. The FE mesh has 800 shell elements in total with 80 nodes in the circumferential direction and 10 nodes in the radial direction. All the nodes on the inner boundary are fixed. The first five frequencies are also given in Table 5.2:

Table 5.2 The first five distinct frequencies of the plate (rad/s)

	ω_0 (k=0, l=0)	ω_1 (k=0, l=1)	ω_2 (k=0, l=2)	ω_3 (k=0, l=3)	ω_4 (k=0, l=4)
EFM results	1491.00	1514.75	1818.98	2765.54	4368.64
Numerical results	1491.92	1516.76	1823.88	2774.19	4383.04

From the table given above, it can be seen that the numerical results are very close to the EFM results, which confirms the accuracy of numerical results.

5.3.2 Natural frequencies of the whole system

Due to the attachment of the mass-spring-damper system (slider system) on the plate, apparently the natural frequencies of the whole system are different from the natural frequencies of the plate. Moreover, the identical frequencies of the doublet modes of the symmetrical plate are split due to the attached slider. In the following, natural frequencies of the whole system when the slider stays stationary are derived. The equation of motion of this model is given in Eq. (5.9). However, in the case (the slider system does not rotate), the relationship between the vertical motion of the mass *u* and the transverse motion of the plate *w* is:

$$u = w(r_0,\ \varphi_0,\ t),\ \dot{u} = \dot{w}(r_0,\ \varphi_0,\ t),\ \ddot{u} = \ddot{w}(r_0,\ \varphi_0,\ t) \tag{5.42}$$

By substituting Eq. (5.42) into Eq. (5.9), then the equation of motion of this system can be written as:

$$\rho h\frac{\partial^2 w}{\partial t^2} + D^*\nabla^4\dot{w} + D\nabla^4 w = -\frac{1}{r}\delta(r-r_0)\delta(\theta-\varphi_0)\left[N + m\frac{\partial^2 w}{\partial t^2} + c\frac{\partial w}{\partial t} + k(w-w_0)\right] \tag{5.43}$$

By using the same modal expansion process described in Section 5.2.2, Eq. (5.43) can be converted into the equations of motion in modal coordinates, which is expressed as Eq. (5.44):

$$\begin{aligned}\ddot{q}_{kl} + 2\xi\omega_{kl}\dot{q}_{kl} + {\omega_{kl}}^2 q_{kl} &= -\frac{N-kw_0}{\sqrt{\rho h b^2}}R_{kl}(r_0)\exp(-\mathrm{i}l\varphi_0) - \\ &\frac{1}{\rho h b^2}\sum_{r=0}^{\infty}\sum_{s=-\infty}^{\infty}R_{rs}(r_0)R_{kl}(r_0)\exp(\mathrm{i}(s-l)\varphi_0)(m\ddot{q}_{rs} + c\dot{q}_{rs} + kq_{rs})\end{aligned} \tag{5.44}$$

By moving the right-hand side of Eq. (5.44) to the left-hand side of the equation and reforming the equation, the equations of motion of the whole system in the matrix form, when the first 9 modes of the disc are involved in the calculation, is given by Eq. (5.45):

$$\left(\mathbf{I}+\mathbf{M}_{\mathrm{m}}\right)\ddot{\mathbf{q}}+\left(\mathbf{C}_{\mathrm{d}}+\mathbf{C}_{\mathrm{m}}\right)\dot{\mathbf{q}}+\left(\mathbf{K}_{\mathrm{d}}+\mathbf{K}_{\mathrm{m}}\right)\mathbf{q}=\mathbf{F} \tag{5.45}$$

where $\mathbf{I}$ is an identity matrix, $\mathbf{M}_{\mathrm{m}}$, $\mathbf{C}_{\mathrm{d}}$, $\mathbf{C}_{\mathrm{m}}$, $\mathbf{K}_{\mathrm{d}}$, and $\mathbf{K}_{\mathrm{m}}$ are the square matrices, shown below:

$$\begin{cases}\mathbf{M}_{\mathrm{m}}=\dfrac{m}{\rho hb^{2}}\mathbf{v}_{l}\mathbf{v}_{s}{}^{\mathrm{T}}\\ \mathbf{C}_{\mathrm{d}}=2\xi\,\mathrm{diag}\left(\omega_{0},\ \omega_{1},\ \omega_{2},\ \omega_{3},\ \omega_{4},\ \omega_{1},\ \omega_{2},\ \omega_{3},\ \omega_{4}\right)\\ \mathbf{C}_{\mathrm{m}}=\dfrac{c}{\rho hb^{2}}\mathbf{v}_{l}\mathbf{v}_{s}{}^{\mathrm{T}}\\ \mathbf{K}_{\mathrm{d}}=\mathrm{diag}\left(\omega_{0}{}^{2},\ \omega_{1}{}^{2},\ \omega_{2}{}^{2},\ \omega_{3}{}^{2},\ \omega_{4}{}^{2},\ \omega_{1}{}^{2},\ \omega_{2}{}^{2},\ \omega_{3}{}^{2},\ \omega_{4}{}^{2}\right)\\ \mathbf{K}_{\mathrm{m}}=\dfrac{k}{\rho hb^{2}}\mathbf{v}_{l}\mathbf{v}_{s}{}^{\mathrm{T}}\end{cases} \tag{5.46}$$

in which

$$\mathbf{v}_{l}=\begin{bmatrix}R_{0}\\ R_{1}\exp\left(-\mathrm{i}\varphi\right)\\ R_{2}\exp\left(-\mathrm{i}2\varphi\right)\\ R_{3}\exp\left(-\mathrm{i}3\varphi\right)\\ R_{4}\exp\left(-\mathrm{i}4\varphi\right)\\ R_{1}\exp\left(\mathrm{i}\varphi\right)\\ R_{2}\exp\left(\mathrm{i}2\varphi\right)\\ R_{3}\exp\left(\mathrm{i}3\varphi\right)\\ R_{4}\exp\left(\mathrm{i}4\varphi\right)\end{bmatrix},\quad \mathbf{v}_{s}=\begin{bmatrix}R_{0}\\ R_{1}\exp\left(\mathrm{i}\varphi\right)\\ R_{2}\exp\left(\mathrm{i}2\varphi\right)\\ R_{3}\exp\left(\mathrm{i}3\varphi\right)\\ R_{4}\exp\left(\mathrm{i}4\varphi\right)\\ R_{1}\exp\left(\text{-}\mathrm{i}\varphi\right)\\ R_{2}\exp\left(\text{-}\mathrm{i}2\varphi\right)\\ R_{3}\exp\left(\text{-}\mathrm{i}3\varphi\right)\\ R_{4}\exp\left(\text{-}\mathrm{i}4\varphi\right)\end{bmatrix} \tag{5.47}$$

Natural frequencies of the plate ω_0, ω_1, ω_2, ω_3, and ω_4 have been obtained in the proceeding part. As all the above matrix are known, the natural frequencies of this system (Eq. (5.45)) can be calculated through the CEA analysis process in Chapter 3.3.1, which are 850.86, 1492.55, 1516.76, 1814.90, 1823.88, 2758.02, 2774.19, 4360.49, and 4383.04 rad/s, which are 135.42, 237.55, 241.40, 288.85, 290.28, 441.53, 438.95, 693.99, and 697.58 in Hz respectively. Apparently, if 9 modes are used in the simulation, this disc-slider system, when the slider is not rotating, has 9 distinct natural frequencies.

5.4 Validation of the numerical method

The numerical calculations in current study use Runge-Kutta method considering its advantage in accuracy, which is verified through comparing its results of the free vibration of an annular plate with the results obtained through the Newmark method and the analytical solution. The analytical solution is expressed in Eq. (3.57). The comparison results are shown in Fig. 5.2, with parameter values given by Table 5.1.

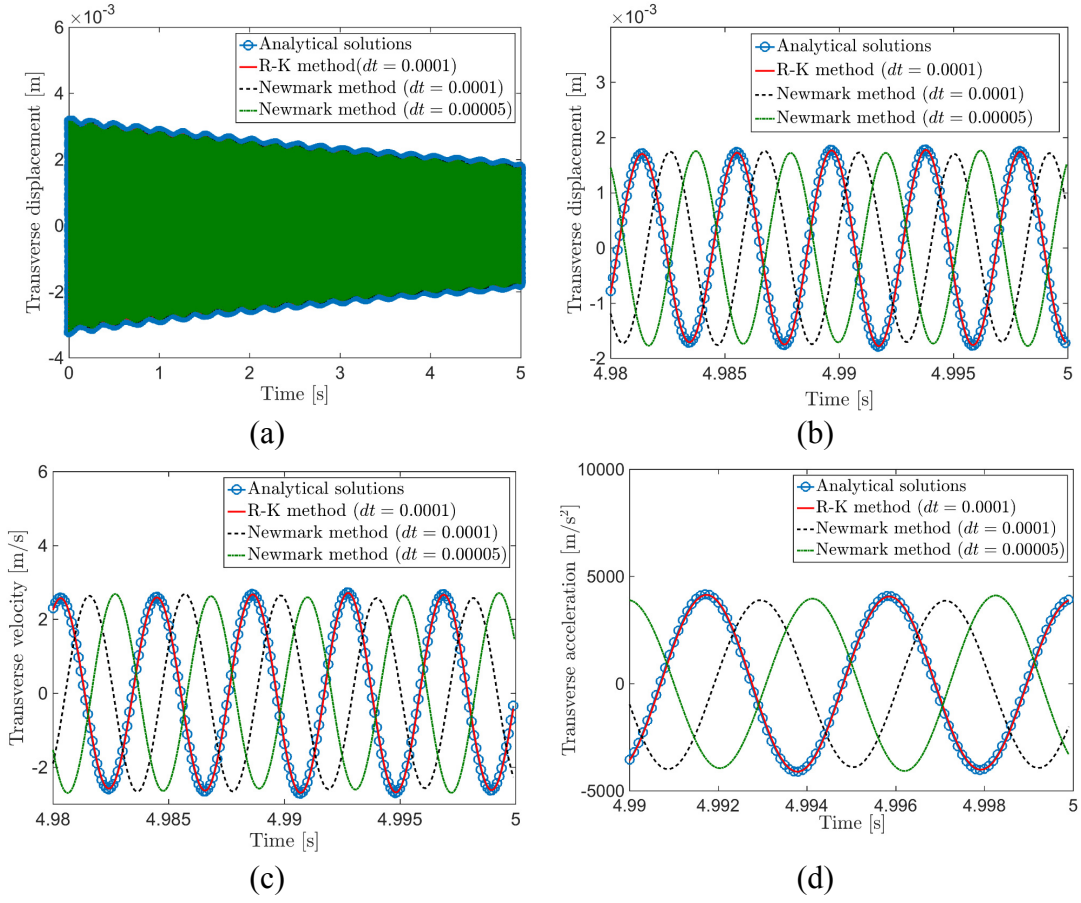

Fig. 5.2 Comparisons between the time response of the annular plate by three methods. (a) the displacement results; (b) the zoom-in displacement results; (c) the zoom-in velocity results; (d) the zoom-in acceleration results.

Fig. 5.2 shows the comparison results of the displacement, the velocity and the acceleration. Apparently, the results of Runge-Katta method are nearly identical to the analytical results, in terms of the vibration amplitude and phase angle. In contrast, the

results of Newmark method with the same time step size or even smaller (black dashed line) are not as accurate as the Runge-Katta method. Therefore, in the consideration of the accuracy, which is especially important in the calculations of long-term vibration histories and complicated problems with friction, Runge-Katta method is used in the following work.

5.5 Numerical study

5.5.1 Numerical procedure

As the state of the system switches between stick and slip phases, and between separation and contact phases, the dynamic behaviour of the system needs to be obtained by solving three different sets of governing equations, which brings about some difficulties in the numerical computations. The states of the disc and the slider during vibration, including the contact force, the absolute circumferential speed of the slider and the force in the horizontal spring and damper, are monitored at each time step. If the results at the end of a time step do not satisfy the conditions for the system to stay in the same motion phase as at the start of the time step, then the bisection method is used to find the critical point where the dynamics switches from one phase to another phase. After getting the critical point, the current set of equations of motion changes to another set. Rich dynamic behaviour, some of which has not been seen in the literature, is found. 9 mode shapes are involved in this simulation, because it is found that 9 disc modes are good enough since more modes do not lead to noticeable change in vibration behaviour. The numerical procedure is shown in Fig. 5.3.

5.5.2 Separation during vibration

The occurrence of separation is illustrated by a numerical example. The time response of the contact force and transverse vibration of the disc are shown in Figs. 5.4-5.5. In this example, the rotating speed of the driving point is Ω=20 rad/s, and the pre-load is N=200N. A long time calculation is run.

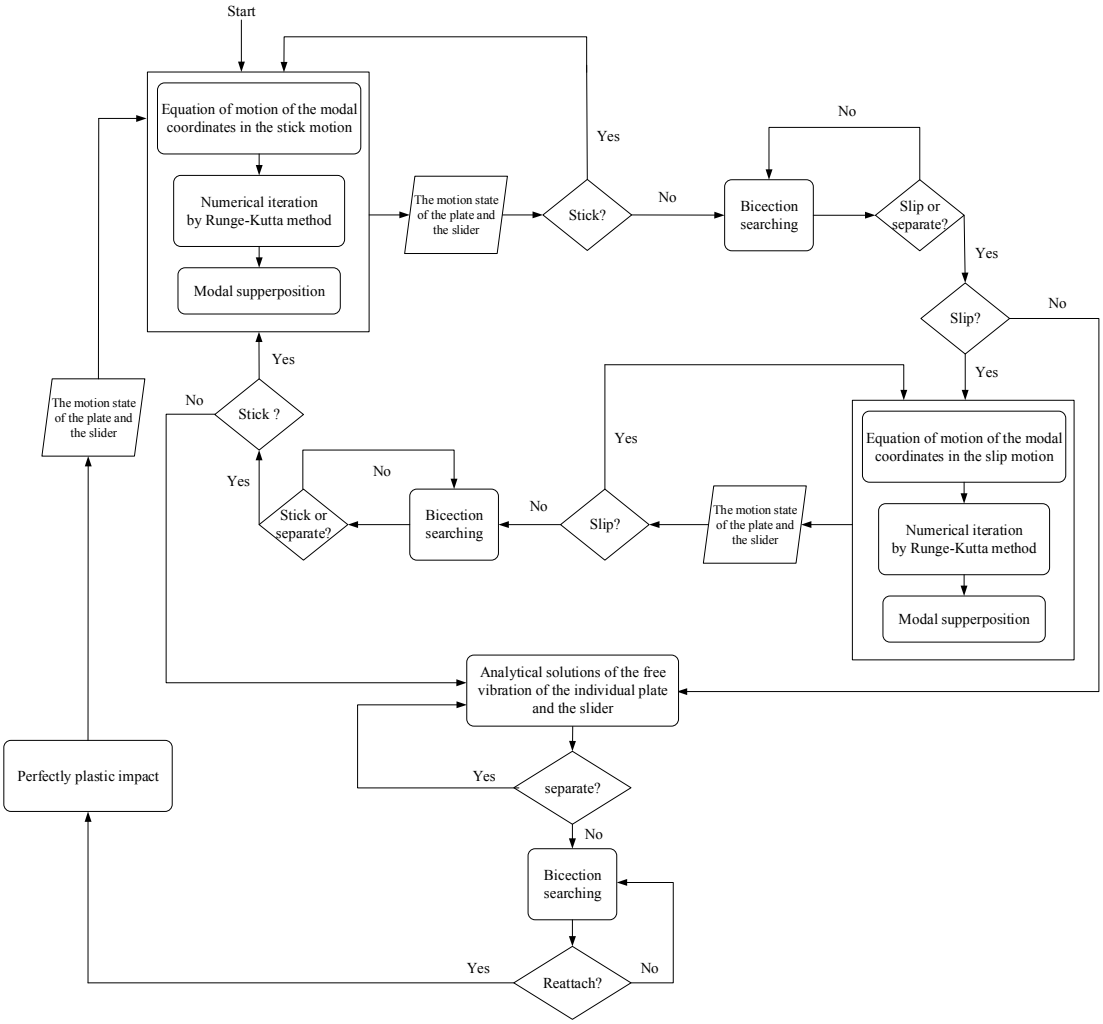

Fig. 5.3 The flow chart of the numerical simulation for non-smooth vibration

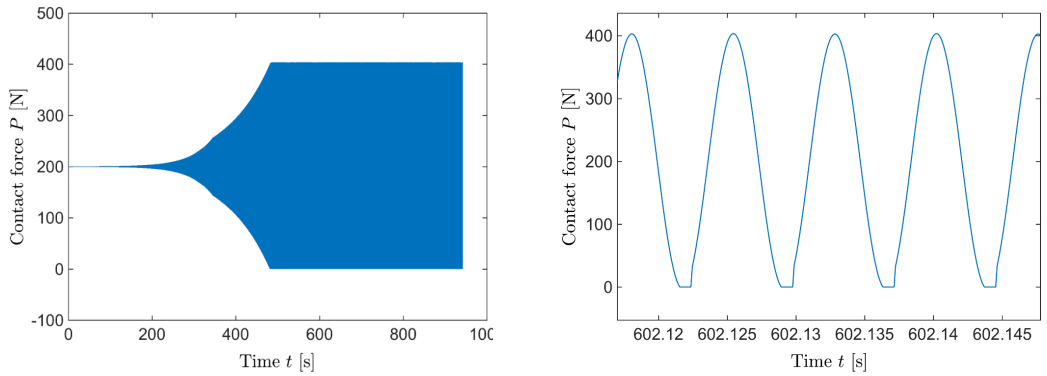

(a) (b)

Fig. 5.4 Time response of the contact force when $N = 200\text{N}$ and $\Omega = 20\text{rad/s}$. (a) In the entire time duration; (b) Its zoom-in plot during t=[602.115, 602.15] s

Fig. 5.4 (a) shows the time response of the contact force during the entire calculation time. Although details of the vibration cannot be observed easily from Fig. 5.4 (a), it can be observed that the oscillating range of the contact force grows, and the contact force can drop to zero, which means that separation can occur during the vibration. Then for a clearer observation, the zoom-in view of Fig. 5.4 (a) within a short time interval is given in Fig. 5.4 (b). It shows that when the contact force decreases to zero, separation takes place, then contact force remains zero during separation. Moreover, multiple separation events can happen.

The results of transverse vibration of the disc and the vertical vibration of the slider during one full event of the separation and reattachment process are shown in Fig. 5.5. As shown in Fig. 5.5, separation happens while the disc moves upward, therefore the growing vibration of the disc is bounded due to loss of contact. It shows that the duration of the separation is very short, which can be explained as follows: the pre-load acts on the slider all the time even during separation, so the slider quickly gets into contact with the disc again under these parameter values.

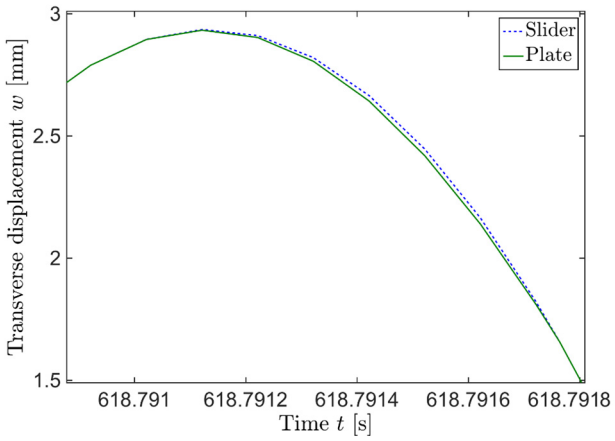

Fig. 5.5 The enlarged time response of the transverse displacement of the disc and the vertical displacement of the slider ($N = 200\text{N}$ and $\Omega = 20\text{rad/s}$)

It is found that separation may occur at different places during the vibration with a very high rotating speed. In the example, when N=350 N and Ω=500 rad/s, separation occasionally occurs, and the zoom-in results are shown in Fig. 5.6. Separation always

occurs at two place: the plate is going up or going down. In this example, separation durations are also very short.

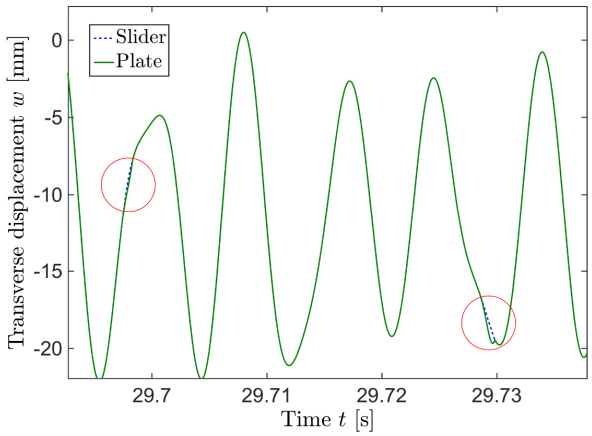

Fig. 5.6 The enlarged time response of the transverse displacement of the disc and the vertical displacement of the slider ($N = 350\text{N}$ and $\Omega = 500\text{rad/s}$)

5.5.3 The critical speed for separation

Firstly, two numerical examples are shown to give a brief description of the critical rotating speed Ω_c for separation. Figs. 5.7-5.10 illustrate the dynamic responses of the system in cases with different but close driving rotating speeds: Ω=15 rad/s and Ω=15.1 rad/s.

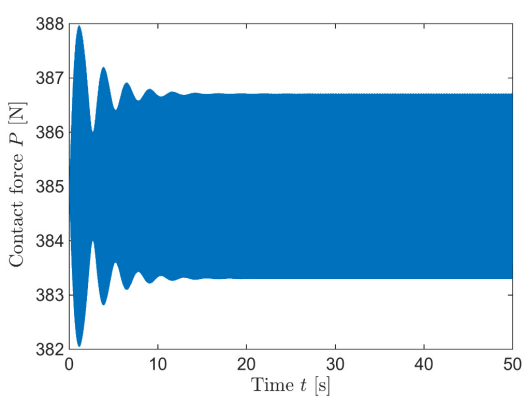

(a) Time history of the contact force

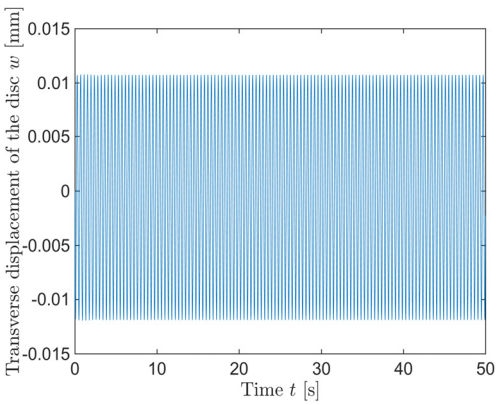

(b)Time history of the disc's transverse vibration

Fig. 5.7 Transient responses ($N = 385\text{N}$ and $\Omega = 15\text{rad/s}$)

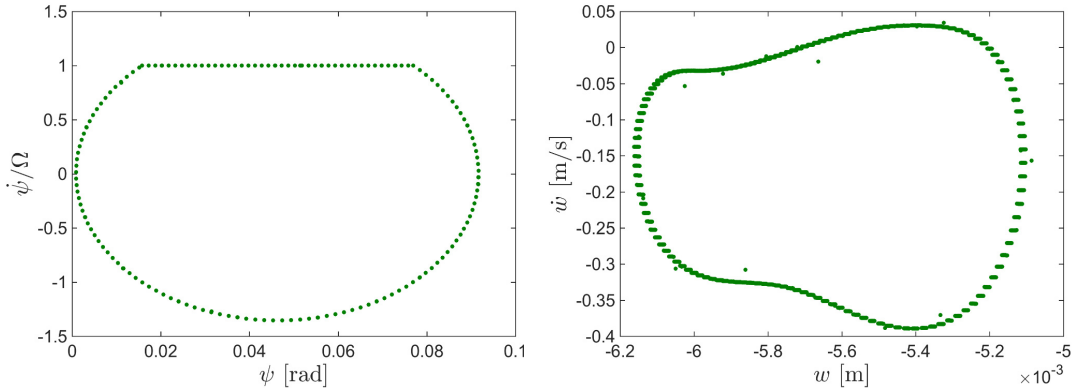

Fig. 5.8 Poincare maps of the relative horizontal motion of the slider (left) and the transverse motion of the disc (right) ($N = 385\text{N}$ and $\Omega = 15\text{rad/s}$)

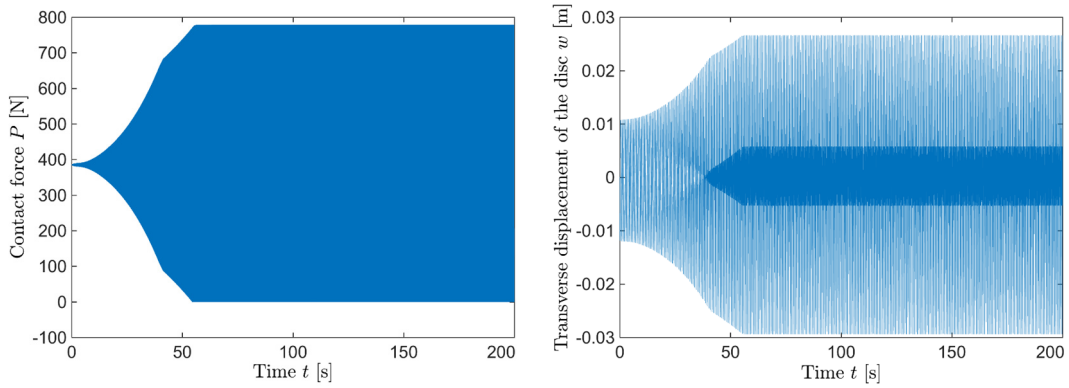

(a) Time history of the contact force

(b)Time history of the disc's transverse vibration

Fig. 5.9 Transient responses ($N = 385\text{N}$ and $\Omega = 15.1$ rad/s)

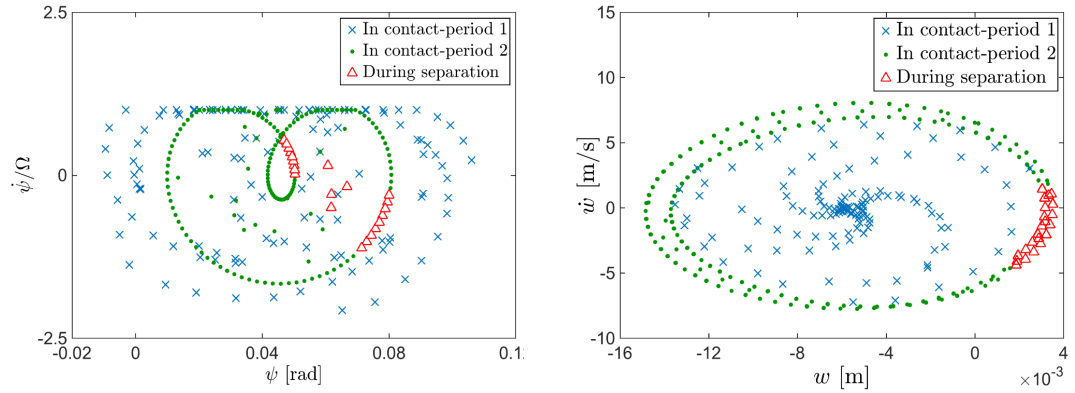

Fig. 5.10 Poincare maps of the relative horizontal motion of the slider (left) and the transverse motion of the disc (right) ($N = 385\text{N}$ and $\Omega = 15.1$ rad/s)

Fig. 5.7 (b) clearly indicates that separation does not happen at Ω=15 rad/s, and the disc vibration does not grow and only oscillates in a small constant range. However, at a slightly higher rotating speed of Ω=15.1 rad/s, the oscillation range of the contact force grows, as shown in Fig. 5.9 (a), and then several separation events take place. In this case, the disc vibrates in a larger range in Fig. 5.9 (b). The Poincare maps of these two cases shown in Figs. 5.8 and 5.10 indicate that the dynamic behaviour of the system can be very different when the system becomes unstable. This rotating speed is referred to as the critical speed for separation.

In order to study the critical speed range of this system, numerical calculations for various values of initial pre-load and rotating speed are carried out. Fig. 5.11 shows the changes of critical rotating speed Ω_c for the occurrence of separation with pre-load N. When the rotating speed is smaller than the critical speed, the contact is always maintained during vibration. Otherwise, when the rotating speed is greater than Ω_c, the slider can lose contact with the disc along with growing vibration. It can be seen that the critical speed for the loss of contact of this system can be low, which is much lower than the conventional critical speed (defined as the speed value of a rotating constant load which causes the resonance of the disc). Moreover, with the initial increase of pre-load N, the system becomes unstable and separation occurs at a lower rotating speed; from a certain value of N, with further increase of N, the system becomes unstable and separation takes place at a higher rotating speed.

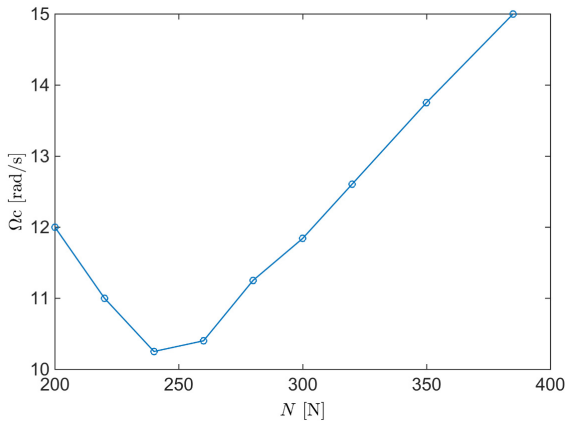

Fig. 5.11 The critical speed for separation

5.5.4 Influences of separation

The influences of the separation on the in-plane vibration of the slider and the transverse vibration of the disc are studied by comparing the results of the system with considering and ignoring separation. The transverse vibration of the disc is observed at a fixed point on the disc at $r=r_0$ and $\varphi=1$. Two sets of examples, at different values of pre-load N and driving speed Ω, are illustrated through Poincare maps in Figs. 5.12-5.15 in order to reveal the dynamic behaviour. The sampling rate of the Poincare maps is the driving point's speed.

For clear observation, the results of the entire simulated time duration are divided and shown in several stages. As to the results of ignoring separation, shown in Figs. 5.12 and 5.14, the entire time interval is divided into two stages. Blue crosses denote the motion of the first half of the total computing time, and the green dots denote the motions of the next half. In the results with separation, shown in Figs. 5.13 and 5.15, blue crosses denote the motion before the first separation which is called 'In contact-period1'; green dots denote the motion that occurs when contact reoccurs and is maintained after the first separation, which is called 'In contact-period2'; and red triangles denote the motion during separation.

In these comparison cases shown in Figs. 5.12 and 5.13, and Figs. 5.14 and 5.15, it can be observed that ignoring and considering separation result in different dynamic behaviour. In the Poincare maps of the in-plane motion of the slider, the dots or crosses forming the horizontal straight line represent motion in the stick phase and those dots and crosses away from this line represent motion in the slip phase. In all the cases when the contact is assumed to be maintained during vibration, shown in Figs. 5.12 and 5.14, the trajectories of horizontal stick-slip motion exhibit transient behaviour initially, but finally settle down to a steady state of stick and slip motion (given by the green dots). The stick and slip motion can be always maintained during the steady state, which are not affected by the values of the pre-load and the rotating speed.

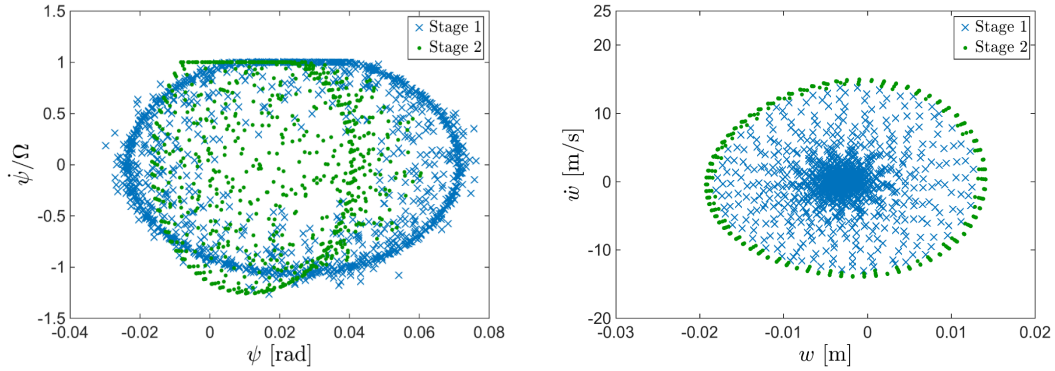

Fig. 5.12 Poincare maps of the relative horizontal motion of the slider (left) and the transverse motion of the disc (right) when separation is ignored ($N = 200\text{N}$, $\Omega = 20\text{rad/s}$)

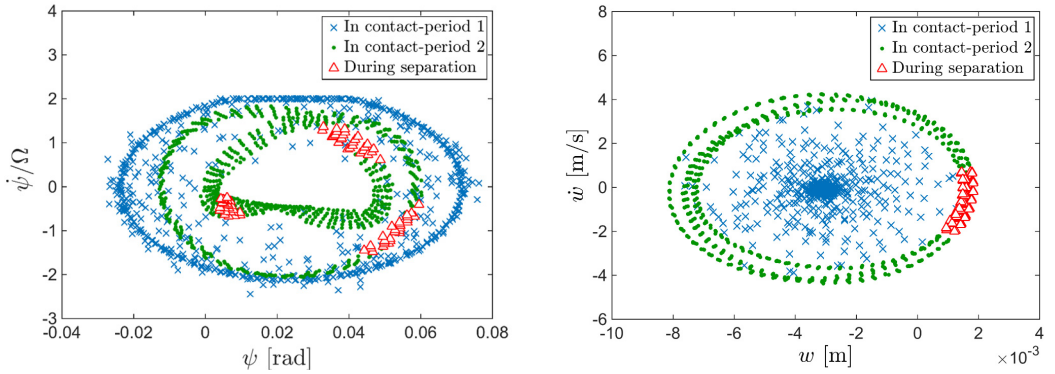

Fig. 5.13 Poincare maps of the relative horizontal motion of the slider (left) and the transverse motion of the disc (right) when separation is considered ($N = 200\text{N}$, $\Omega = 20\text{rad/s}$)

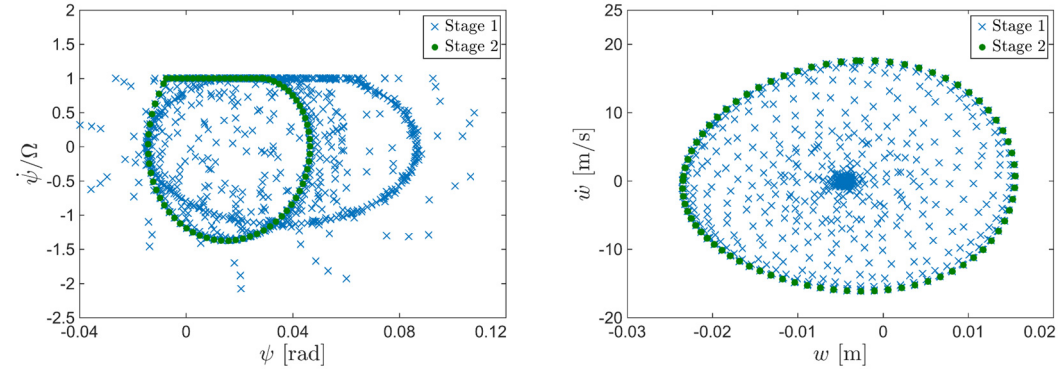

Fig. 5.14 Poincare maps of the relative horizontal motion of the slider (left) and the transverse motion of the disc (right) when separation is ignored ($N = 300\text{N}$, $\Omega = 20\text{rad/s}$)

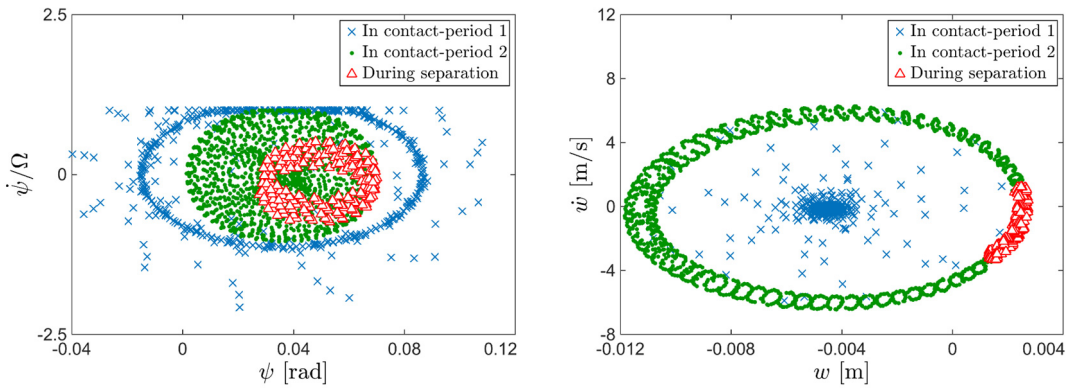

Fig. 5.15 Poincare maps of the relative horizontal motion of the slider (left) and the transverse motion of the disc (right) when separation is considered ($N = 300\text{N}$, $\Omega = 20\text{rad/s}$)

However, when separation is considered, shown in Figs. 5.13 and 5.15, separation changes the patterns of the trajectories formed by the Poincare points, which indicates that a variety of complex dynamic behaviour of the system can be produced, depending on system parameters like the pre-load and the rotating speed. In terms of the transverse vibration of the disc, more frequencies actually join in during the steady state when separation is considered, as there are more points on the Poincare plane in Figs. 5.13 and 5.15 (considering separation) compared with Figs. 5.12 and 5.14 (ignoring separation). As to the horizontal vibration of the slider, it is periodic at the steady state (in stage 2) when separation is ignored (Figs. 5.12 and 5.14), as confirmed by their phase portraits. In contrast, it is quasi-periodic at steady state (in contact-period 2 and during separation) in Figs. 5.13 and 5.15, as the collections of Poincare points are quite fuzzy. Further investigations on the vibration frequencies of the system are carried out in Section 5.6.

As supplements to the preceding discussion on the results presented in Figs. 5.14 and 5.15. Fig. 5.16 shows the phase portraits of the relative horizontal motion of the slider under the same operation conditions when separation is ignored and considered respectively. Fig. 5.16 (a) shows that the horizontal motion of the slider lies on a regular stick-slip limit cycle, during the steady state, when separation is ignored, which is periodic vibration. However, for the actual horizontal vibration when separation is

considered, the regular stick-slip limit cycle breaks out, instead an intricate phase portrait is presented in Fig. 5.16 (b).

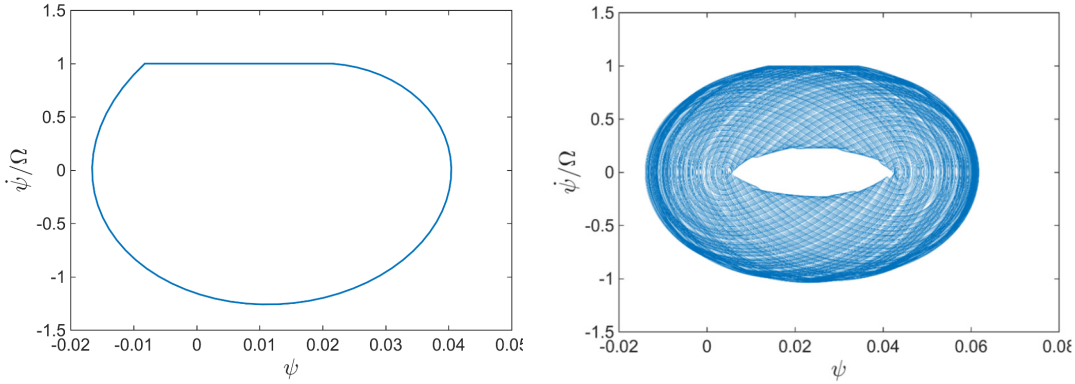

(a) (b)

Fig. 5.16 The phase portrait of the relative horizontal motion of the slider. (a) separation is ignored; (b) separation is considered ($N = 200\text{N}$, $\Omega = 20\text{rad/s}$)

Additionally, the vibration ranges of the disc when considering separation are much smaller than those when ignoring separation, shown by Fig. 5.17. The reason for this can be explained. Because of separation, the disc cannot get further excitation from the slider (note that the rotating slider is the source of excitation), unlike the cases when contact is assumed to be always maintained even though the contact force has dropped to a negative value. Therefore, separation serves to maintain the vibration in a smaller range of magnitude.

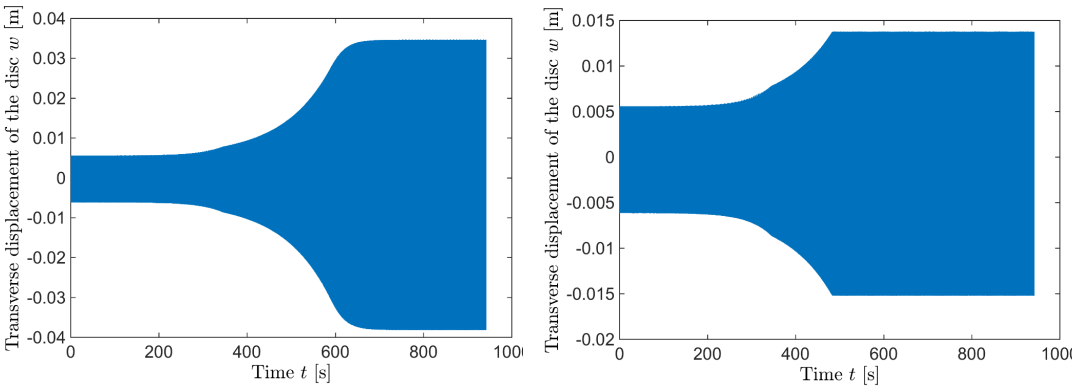

(a) (b)

Fig. 5.17 The time history of the transverse vibration of the disc ($N = 200\text{N}$, $\Omega = 20\text{rad/s}$). (a)Separation is ignored; (b)Separation is considered

Consequently, the necessity of considering separation in friction-induced vibration of this system is obvious. As this paper focuses on the dynamic behaviour of friction-induced vibration with separation, more numerical results with separation for various parameter values are provided in the following subsection.

5.5.5 Influences of significant parameters

To reveal the various dynamic behaviour of the system when separation is considered, parametric studies are carried out. In this section, the effects of the pre-load N are examined firstly. The Poincare map of three pre-load cases (N=385, 50 and 200N) are illustrated in Figs. 5.6, 5.18-5.20 respectively. The rotating speed in these examples is fixed at 15 rad/s.

When the initial pre-load is small (N=50 N), there are finite points on the Poincare plane, shown in Fig. 5.18, which mean that the in-plane vibration is periodic; the disc also vibrates periodically as there are finite number of points and they are quite close to each other. The Poincare points of the vertical vibration are very close to each other and look like a dot if the same order of the axis scale of the unstable vibration, eg. Fig. 5.20, is used. Additionally, the time history of the contact force, in Fig. 5.19, shows no separation happens during the vibration.

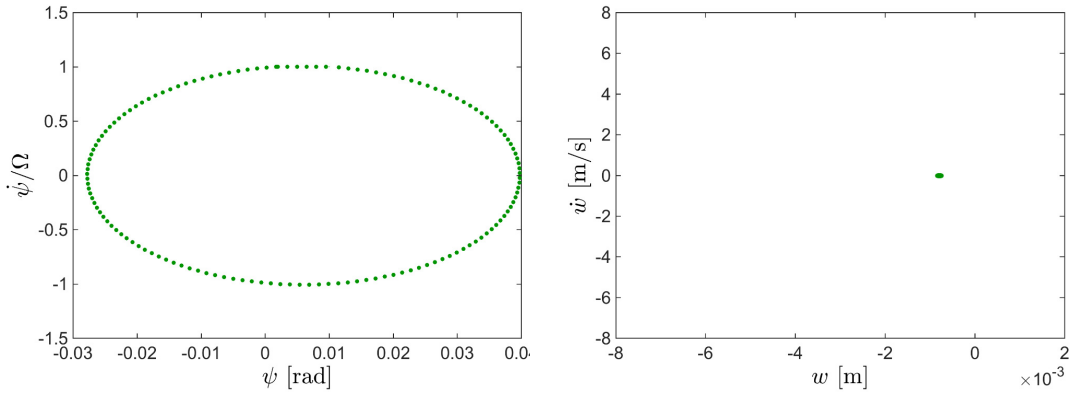

Fig. 5.18 Poincare maps of the relative horizontal motion of the slider (left) and the transverse motion of the disc (right) ($N = 50\text{N}$, $\Omega = 15\text{rad/s}$)

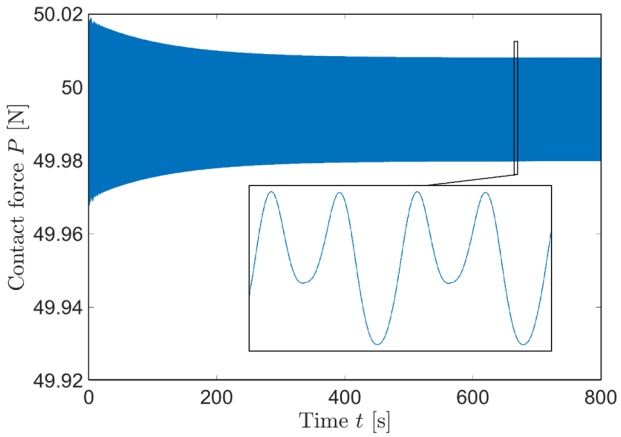

Fig. 5.19 Time response of the contact force ($N = 50\text{N}$, $\Omega = 15\text{rad/s}$)

At a larger pre-load (N =200 N), both of the slider's in-plane vibration and disc's transverse vibration become unstable and separation occurs, as shown in Fig. 5.20. As to the in-plane motion of the slider, the stick phase gets longer because of the larger pre-load, but then due to separation, the stick-slip vibration becomes very complicated. However, with further increase of the normal force (N=385 N), the vibration of the system becomes stable again and no separation occurs, as shown in Fig. 5.8 in Section 5.5.3. Therefore, pre-load N plays a complex role in the stability of this system and does not have a monotonous effect on the friction-induced disc vibration. Initial increase of N destabilises the system, while further increase of N leads to a stable system.

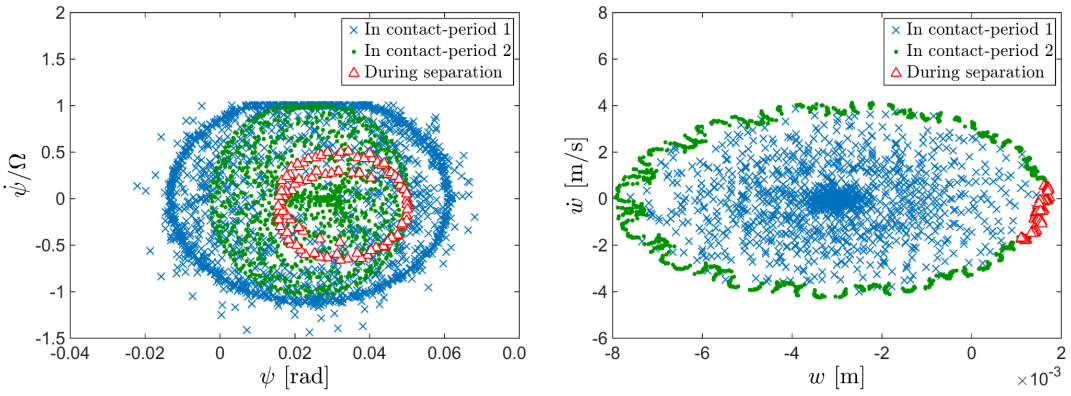

Fig. 5.20 Poincare maps of the relative horizontal motion of the slider (left) and the transverse motion of the disc (right) ($N = 200\text{N}$, $\Omega = 15\text{rad/s}$)

Although the specific reasons for its complex role in this model is difficult to identify because of coupling of non-smooth in-plane vibration of the slider with out-of-plane vibration of the slider, two extreme situations can shed some light onto this matter. One extreme situation is: when N is zero, there is no friction force, and thus the slider undergoes pure sliding motion in the horizontal direction; as the running speed in this case (Ω =15 rad/s) is far below the critical speed (Ω =911 rad/s) for the unstable vibration of the disc in the moving load problem, the system is stable when the normal force is zero at low rotating speed. The other extreme situation is: when N is extremely large, the slider can hardly move, which means that the slider sticks to the disc within the time duration of observation and the system is also stable. Between the two extreme situations, horizontal stick-slip motion appears and is affected by the value of the normal force N; as the horizontal motion of the slider is coupled with the vertical motion of the slider and the transverse motion of the disc, the whole system dynamics is affected by the normal force in a complicated way.

Secondly, the effects of damping, including the disc's damping, damping of the horizontal and vertical dampers, are examined. When there is no disc damping (D^*=0), the vibration of the system becomes unstable and separation occurs at a low rotating speed. Fig. 5.21 shows the Poincare maps when Ω=10 rad/s and N=200 N. The orbit of the in-plane Poincare map of the slider changes after the first separation, which is shown by the green dots in the left Poincare map of Fig. 5.21. When the disc's damping D^* is 1×10^{-5}, critical rotating speed Ω_c for separation and unstable vibration is at 12.6 rad/s, which is a little bit higher than the no damping case. Furthermore, when D^* is at 2×10^{-5}, both the horizontal vibration of the slider and the transverse vibration of the disc become stable.

The influences of the in-plane damping on the transverse vibration of the disc are more complicated. The in-plane damping can destabilise the system when the pre-load is large, otherwise it acts as a stabilising factor. When the in-plane damping is zero, shown in Fig. 5.8, the system is stable at c_p=0, N=385 N and Ω =15 rad/s. However, when there is in-plane damping (c_p=0.5), the vibration of the disc increases and it becomes unstable, and loss of contact happens as a consequence of the increase of

vibration. From the Poincare map in Fig. 5.22, after separation both of the slider's in-plane stick-slip motion and disc's transverse vibration are unstable periodic motion.

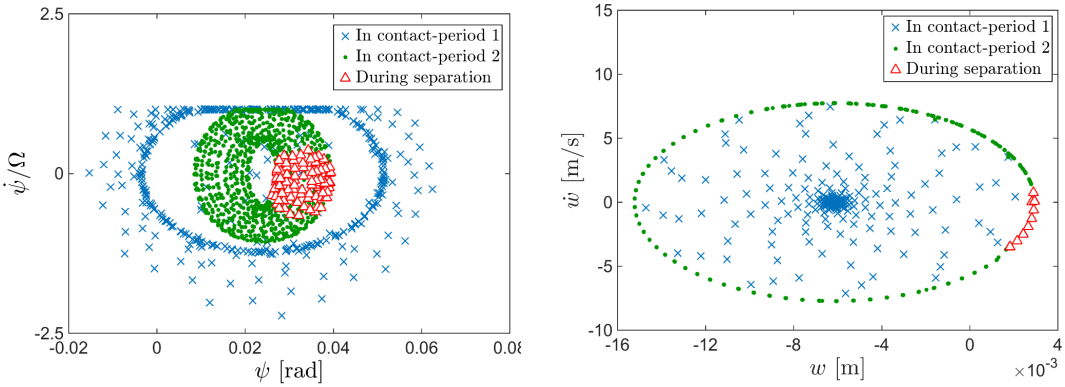

Fig. 5.21 Poincare maps of the relative horizontal motion of the slider (left) and the transverse motion of the disc (right) ($D^* = 0$, $N = 200\text{N}$, $\Omega = 10\text{rad/s}$)

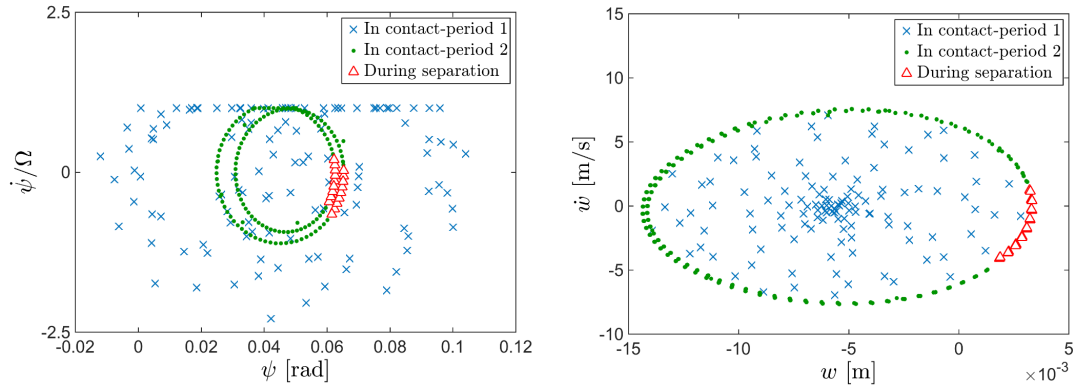

Fig. 5.22 Poincare maps of the relative horizontal motion of the slider (left) and the transverse motion of the disc (right) ($c_{\text{p}} = 0.5$, $N = 385\text{N}$, $\Omega = 15\text{rad/s}$)

The influences of the vertical damping coefficient are also studied. In contrast to the unstable vibration, shown in Fig. 5.13 (vertical damping is zero), the case with vertical damping is investigated. As shown in Fig. 5.23, the slider's in-plane motion is a periodic stable stick-slip motion; and the vibration of the disc is also stable and it oscillates within a small range around its static equilibrium position and looks like a dot if the same order of the axis scale of Fig. 5.23 is used. Therefore, vertical damping coefficient appears as a stabilising factor to the system.

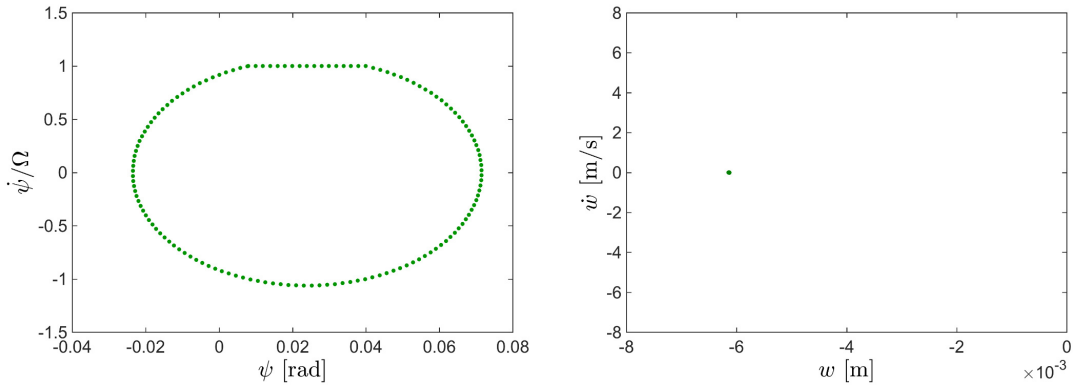

Fig. 5.23 Poincare maps of the relative horizontal motion of the slider (left) and the transverse motion of the disc (right) ($c = 0.5$, $N = 200\text{N}$, $\Omega = 20\text{rad/s}$)

Then the effects of the stiffness of the disc, and the stiffness of the vertical and horizontal springs on the vibration of the system when separation is considered are studied. Increasing the elasticity of the disc and the stiffness of the vertical spring stabilises the unstable transverse vibration of the disc. On the other hand, decreasing the value of the elasticity and the vertical stiffness makes the vibration more unstable. At sufficiently small value of *E*, separation does not happen in the unstable vibration. The transverse vibration of the disc seems quasi-periodic with fuzzy collections of points on the Poincare plane, shown in Fig. 5.24 (*E*=100GPa, *Ω*=11 rad/s) in which blue crosses denote the motions of the first half of the total computing time (stage 1), and the green dots denote the motions of the last half (stage 2).

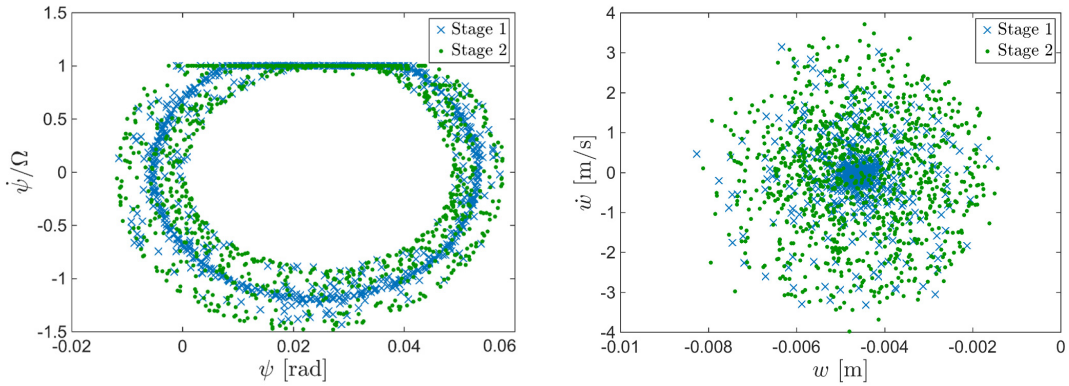

Fig. 5.24 Poincare maps of the relative horizontal motion of the slider (left) and the transverse motion of the disc (right) ($E = 100\text{GP}a$ and $\Omega = 11\text{rad/s}$)

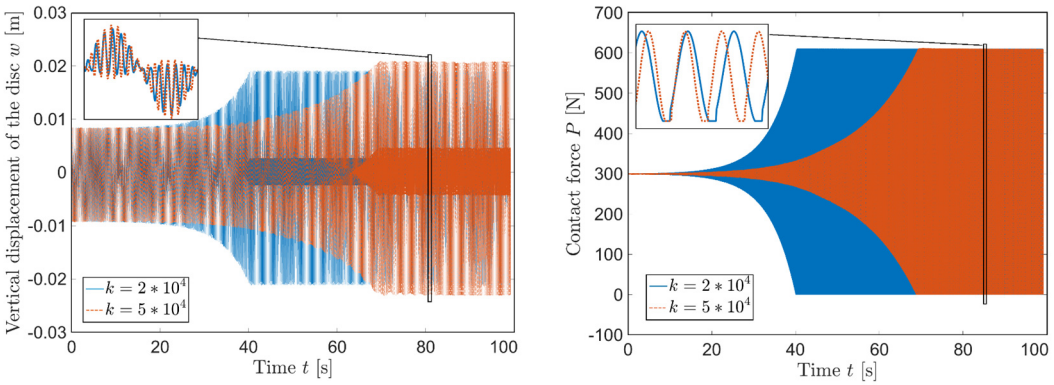

Fig. 5.25 Comparisons of the settling down time (left) and the starting time of separation(right). ($N = 300\text{N}$ and $\Omega = 50\text{rad/s}$)

When vertical stiffness k increase, it takes longer time for unstable vibration of the system to settle down to its steady state and for separation to take place. Fig. 5.25 shows the comparisons between the contact force and vertical vibration of the disc of two cases (k=2×10^4 N/m and k=5×10^4 N/m). The system becomes stable when k is large enough (i.e. k=2×10^5 N/m).

The role of the in-plane stiffness of the slider on the vibration of the system is complex. When k_p=2×10^3 N/m, the vibration of the disc initially vibrates quasi-periodically. However, after separation occurs, the points, shown by green dots, on the Poincare section of the disc wander within a certain range and become unpredictable, shown in Fig. 5.26. When k_p=2×10^4 N/m, the unstable vibration grows faster and separation takes place earlier. However, a large enough k_p (2×10^5 N/m) then appears to stabilise the system. One extreme case is when k_p=2×10^7 N/m, shown by Fig. 5.27, the slider undergoes pure slip motion and the slipping velocity tends to be the same with the speed of the driving point, and the vertical vibration is periodic.

Finally, the value of the slider's mass is found to influent the separation location in the vertical direction. In all the results, at low rotating range, shown above, separation happens while the disc is moving upward. However, the position of separation is changed if the mass is small (m=0.01). In this example, the zoom in results, shown in Fig. 5.28, illustrates that separation happens when the mass reaches its lowest vertical position.

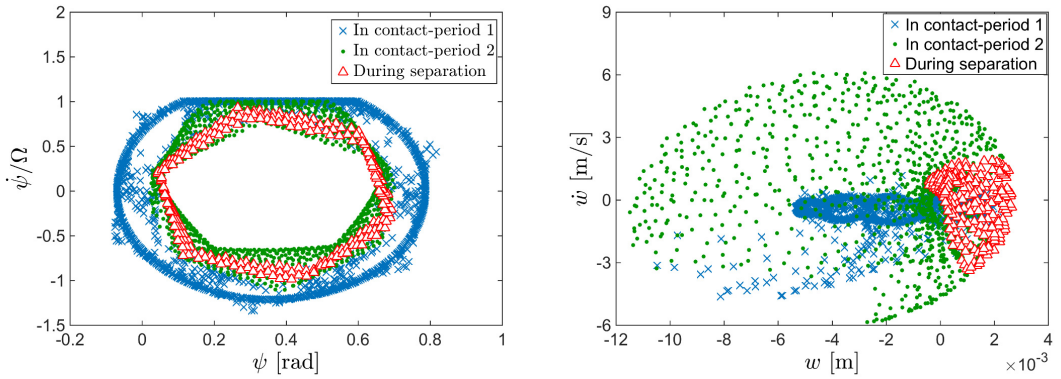

Fig. 5.26 Poincare maps of the relative horizontal motion of the slider (left) and the transverse motion of the disc (right) ($k_{\mathrm{p}} = 2\times10^{3}$, $N = 300\mathrm{N}$, $\Omega = 50\mathrm{rad/s}$)

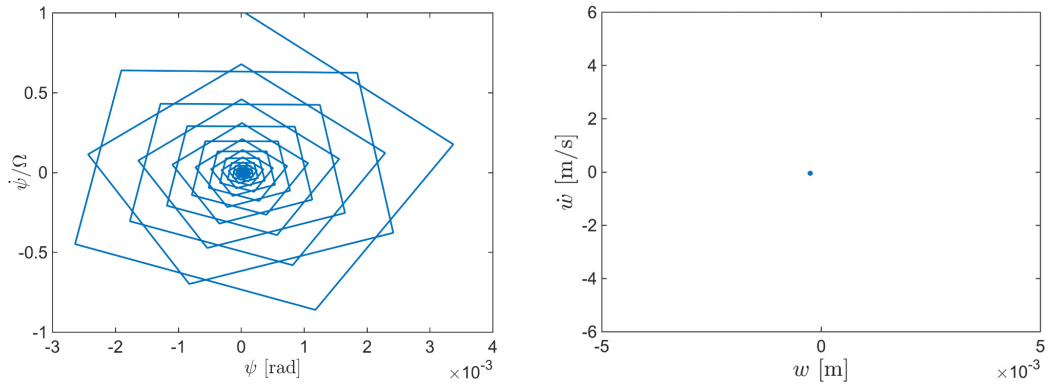

Fig. 5.27. Phase portraits of the relative horizontal motion of the slider (left) and the Poincare map of the transverse motion of the disc (right) ($k_{\mathrm{p}} = 2\times10^{7}$, $N = 300\mathrm{N}$, $\Omega = 50\mathrm{rad/s}$)

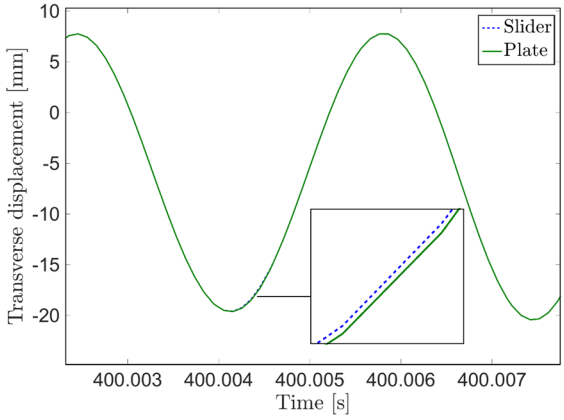

Fig. 5.28 The enlarged time response of the transverse displacement of the disc ($m = 0.01$, $N = 200\mathrm{N}$, $\Omega = 20\mathrm{rad/s}$)

Therefore, the vibration of the disc induced by the frictional moving slider is quite complex. Unstable vibration of the disc happens in a low speed range, and separation takes place along with the growing vibration of the disc. After separation, the transverse vibration of the disc becomes bounded; the horizontal slider exhibits pure slip vibration and the stick phase disappears under some parameter values. The different dynamic behaviour between the situations when separation is considered and when separation is ignored can be seen. Numerical results through a parametric analysis reveal the roles of key system parameters on the vibration of the system. It is notable that small and large values of the pre-load appear as stabilising factors to the system, but the intermediate values are destabilising. However, when the normal pre-load is large enough, the in-plane damping then appears as a destabilising factor to the system.

5.6 Nonstationary dynamic behaviour

As the system actually experiences distinct motion states during vibration, the vibration frequencies in these motion states can be different, and thus the system is nonstationary and FFT analysis is no longer suitable. In this sub-section, time-frequency analysis through the short time Fourier transform is carried out to explore evolution of the vibration frequency of the system studied in this paper.

In the following, the time-frequency analysis of three examples is carried out. The results of the first example are shown in Figs. 5.29-5.31. The time history of the contact force, shown in Fig. 5.9 in Section 5.5.3 , indicates that separation starts to take place at 54.5s, followed by events of repeated reattachment and separation. Fig. 5.29 shows that there are roughly three kinds of behaviour during transverse vibration of the disc. Its vibration frequency during four time segments, marked as (a), (b), (c), and (d) in Fig. 5.30, are calculated, and the corresponding time-frequency results are shown in Fig. 5.30 (a), (b), (c), and (d) respectively.

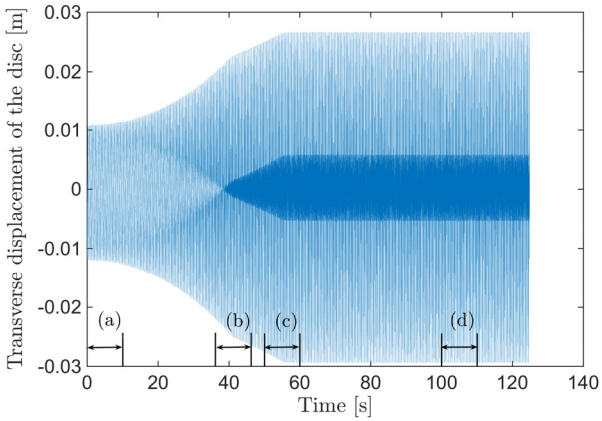

Fig. 5.29 The time history of the transverse displacement of the disc ($E=150\text{GPa}$, $N=385\text{N}$, $\Omega=15.1\text{rad/s}$)

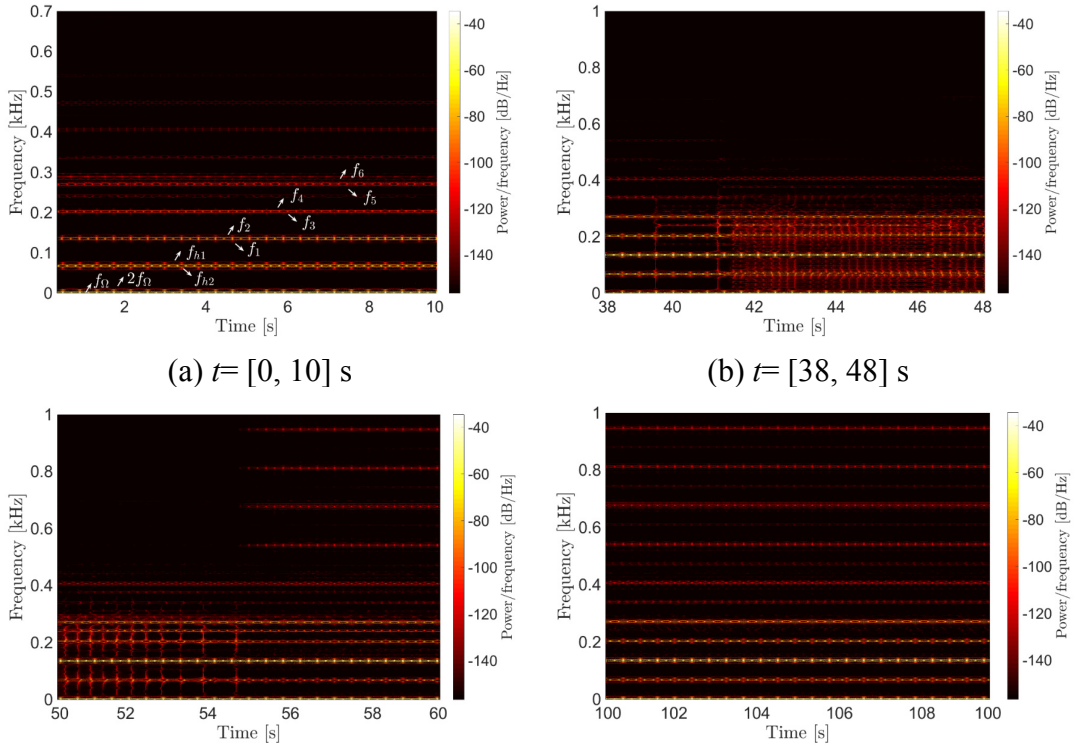

(a) t= [0, 10] s (b) t= [38, 48] s

(c) t =[50, 60] s (d) t =[100, 110] s

Fig. 5.30 Time-frequency spectrum of the transverse vibration of the disc ($E=150\text{GPa}$, $N=385\text{N}$, $\Omega=15.1\text{rad/s}$)

Firstly, in the starting stage of the transient vibration, the vibration amplitude grows, and the main frequencies of the unstable modes are indicated in Fig. 5.30 (a). It can be

seen that there are several frequencies involved in the vibration. The values of the main frequencies, shown in the time-frequency power spectrum, making significant contributions to the vibration during t = [0, 10] s are listed in Table 5.3.

Table 5.3 Significant frequencies (Hz) found through the time-frequency analysis

f_Ω	f_{h1}	f_{h2}	f_1	f_2	f_3	f_4	f_5	f_6
2.4	65.5	70	133	138	200	206	269	273

Among these frequencies, f_Ω is the predominant frequency, which comes from the rotating driving point, and its superharmonic components $2f_\Omega$ and $3f_\Omega$ also take part in the vibration. Additionally, frequencies f_{h1} and f_{h2} are associated with the in-plane vibration of the slider whose frequency is 70Hz and splits into the two frequencies due to the rotation of the slider.

The main frequencies for the transverse vibration of the disc when the slider and the driving point are not rotating are calculated in Section 5.3.2. The natural frequencies of the first nine modes are 135.42, 237.55, 241.40, 288.85, 290.28, 441.53, 438.95, 693.99, and 697.58 in Hz respectively. It is notable that any pair of natural frequencies corresponding to modes of the same number of nodal diameters of this disc with a stationary slider are not at the same values as the natural frequencies of the corresponding modes of the symmetrical disc given in Table 5.2.

f_1 to f_6 in Fig. 5.30 and in Table 5.3 are close to but not the same as some natural frequencies of the static system (135.42, 237.55 and 288.85 Hz). This is due to the effect of the in-plane rotation of the slider.

Fig. 5.30 (b) indicates that, in addition to the main frequencies (f_Ω, f_{h1}, f_{h2}, and f_1 to f_6), new vibration frequencies emerge during the transient vibration of the system due to unstable horizontal vibration of the slider, which are shifted from the main frequencies (f_Ω, f_{h1}, f_{h2}, and f_1 to f_6). Fig. 5.30 (c) shows that, when separation takes place at 54.5s, the frequency spectrum has a sudden change. Higher frequencies show up after separation. At the same time, the fuzzy frequencies (in Fig. 5.30 (b) and (c)) in the

midst of the main frequencies disappear from Fig. 5.30 (d), which can be explained by the horizontal responses of the slider shown in Fig. 5.31. Fig. 5.31 (a) is the time history of ψ which is very complex as the switching between stick and slip motion relies on not only the difference between the static and kinetic friction coefficients but also the oscillating contact force.

Fig. 5.31 (b) gives the frequency spectrum during t = [50, 60] s which shows that the obviously irregular shifting between the horizontal vibration frequency of the slider f_h and its superharmonics (nf_h, n=1, 2, 3...) disappear after separation, and the horizontal stick-slip motion becomes periodic which can be also seen from the Poincare map shown in Fig. 5.10 in Section 5.5.3. When the transverse disc vibration becomes steady long after the first separation event, it possesses constant values of frequencies (including the fundamental frequency and higher frequencies) due to separation, as shown in Fig. 5.30 (d).

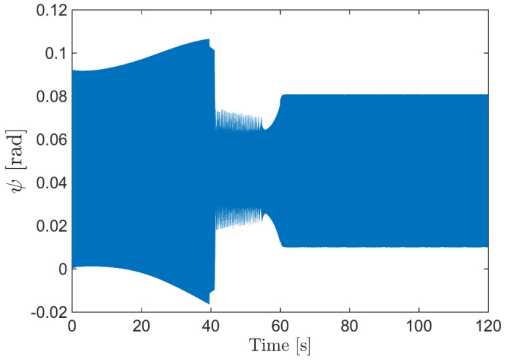

(a) The time history of ψ

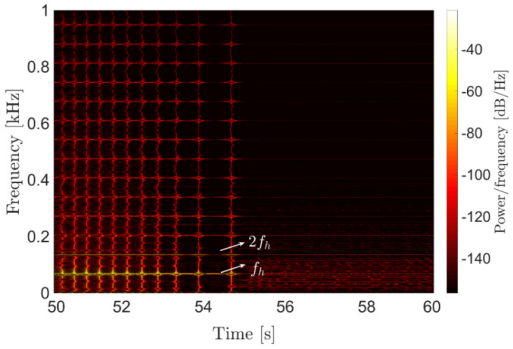

(b) Its time-frequency spectrum for t= [50, 60] s

Fig. 5.31 The horizontal response of the slider (E = 150GPa , N = 385N , Ω = 15.1rad/s)

The second example is computed using the following parameter values: E=150 GPa, N=300 N, Ω=20 rad/s. Fig. 5.32 (a) illustrates the time history of the transverse displacement of the disc. Firstly, the vibration grows gradually, then increases sharply for a while before the growth rate drops, and finally becomes bounded due to separation which firstly occurs around 149.5s. A time-frequency analysis is conducted within the time interval of t = [143, 153] s, since this time interval is very special which

covers different stages of the vibration (transient vibration, transition to separation and steady-state vibration after separation). Fig. 5.32 (b) shows that the vibration of the disc is mainly governed by its natural frequencies, meanwhile a number of fuzzy frequencies (shown by the dense red lines between the main system frequencies) start to make contributions to unstable transient vibration. After the transition point to separation, higher disc frequencies arise. On the other hand, the fuzzy frequencies maintain their contributions to the vibration, in contrast they disappear in the first example, which can be explained by the in-plane time-frequency results of the slider shown in Fig. 5.33 (b).

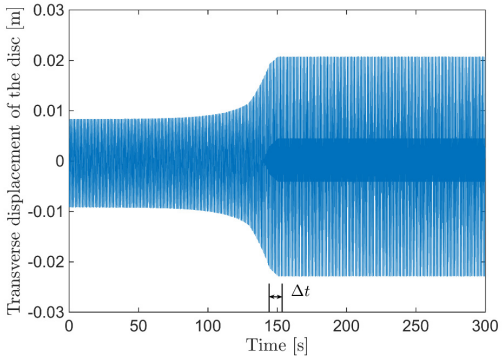

(a) The time history of the transverse displacement

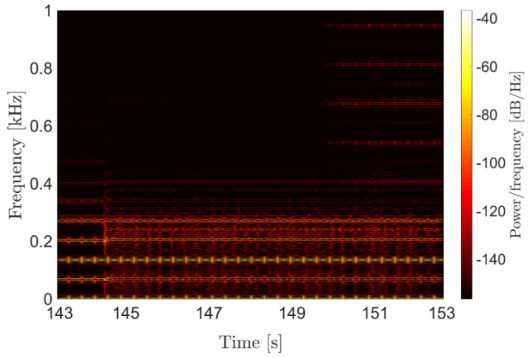

(b) Its time-frequency spectrum for t= [143, 153] s

Fig. 5.32 The transient response of the disc ($E = 150\text{GPa}$, $N = 300\text{N}$, $\Omega = 20\text{rad/s}$)

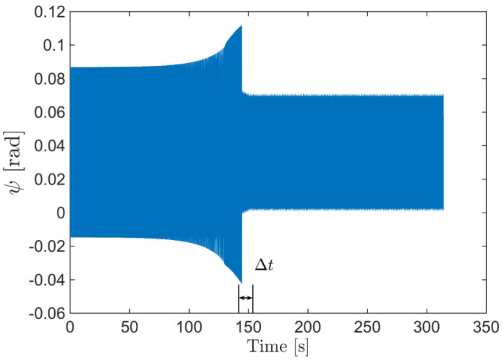

(a) The time history of ψ

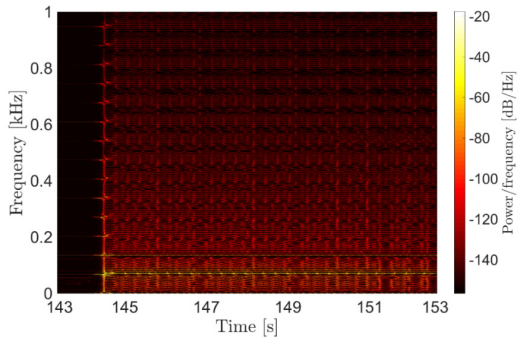

(b) Its time-frequency spectrum for t= [143, 153] s

Fig. 5.33 The horizontal response of the slider ($E = 150\text{GPa}$, $N = 300\text{N}$, $\Omega = 20\text{rad/s}$)

Fig. 5.33 (b) is obtained during the same time interval t = [143, 153] s, and the time history of ψ is illustrated in Fig. 5.33 (a). From the time-frequency results, it can be seen, in Fig. 5.33 (b), that the in-plane stick-slip vibration of the slider in steady state is quasi-periodic.

The dynamic response of the third example is shown in Fig. 5.34. Parameter values used are: E=100 GPa, N=200 N, Ω=11 rad/s. In this case, there is no separation during the vibration which has been illustrated in Fig. 5.24. Although the vibration magnitude of the disc, in Fig. 5.34 (a), is bounded due to the nonlinearity of the in-plane stick-slip vibration, how the limit cycle of the vibration evolving to is different from those cases in which the transverse disc vibration is non-smooth because of repeated events of separation and reattachment. Consequently, the time-frequency response in this case does not show any high frequency arising above the maximum natural frequency (4383.04 rad/s) of the system with slider being stationary, during steady-state vibration, after the transient phase of vibration (marked by t in Fig. 5.34 (a)). The vibration of the disc in this case is quite erratic as its frequency spectrum shows several prominent incommensurate frequencies and many low-amplitude frequencies emerge, vanish or shift with time.

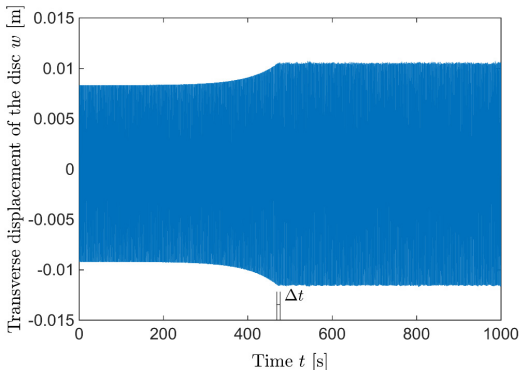

(a) The time history of the transverse displacement

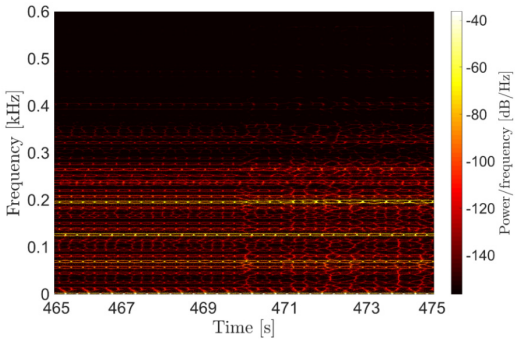

(b) Its time-frequency spectrum for t= [465, 475] s

Fig. 5.34 Transient responses of the disc ($E = 100\text{GPa}$, $N = 200\text{N}$, $\Omega = 11\text{rad/s}$)

In conclusion, the time-frequency analysis of all three examples reveals that the frequencies of the non-smooth self-excited friction-induced vibration problem vary with time in a complicated manner. The power spectrum of system frequencies is

nonstationary and other frequencies arise and shift between the main system frequencies. Higher frequencies can arise due to separation. It also shows the importance of considering separation from the point of view of evolution of the frequency with time. Moreover, the unstable in-plane stick-slip vibration of the slider which couples with the vertical vibration of the slider can make significant contributions to the frequencies of the disc's transverse vibration.

5.7 Conclusions

In this chapter, the dynamic behaviour of a disc modelled as a thin elastic annular plate excited by a rotating oscillator which has a vertical branch normal to the disc and a horizontal branch in the plane of the disc is studied. Because of the non-smooth nature of friction between the slider and the disc, the slider undergoes stick-slip vibration in the circumferential direction on the disc. The variable in-plane location of the slider leads to a varying contact force at the interface between the disc and the slider, which affects the transverse vibration of the disc, and makes the in-plane stick-slip vibration and vertical vibration of the slider system coupled and complicated. During vibration the slider can lose contact (separation) with the disc and then reattach to the disc again.

The equations of motion of this discrete-continuous system at three motion states (stick motion, slip motion and separation) are derived. The conditions for staying in each state are established, and impact at the moment of the reattachment is formulated. Then, a numerical study is carried out at various values of the key parameters. The following conclusions can be drawn:

1. Separation can happen during the unstable vibration of the system caused by friction. The time duration of separation is very short. Reattachment naturally occurs following separation.

2. The system becomes unstable and separation occurs in a low speed range of the driving point, which is much smaller than the critical speed of the disc in the corresponding moving load problem.

3. When separation is considered, the disc's transverse vibration becomes bounded within a smaller range; and the in-plane motion of the slider may change to a trajectory which is totally different from its trajectory before separation, and the stick phase disappears under certain parameter values. On the other hand, if contact is assumed to be maintained during vibration (in cases of ignoring separation), both the in-plane stick-slip vibration of the slider and transverse vibration of the disc can be very different from those cases of considering separation.

4. More interesting dynamic behaviour of the disc and the slider when separation is considered is revealed through a parametric analysis. The relationship between the stability of the system, and the pre-load, in-pane damping and in-plane stiffness is not monotonous. A pre-load appears as a destabilising factor within a certain range but becomes a stabilising factor within another range. Disc damping and vertical damping of the slider stabilise the friction-induced disc vibration, while the in-plane damping of the slider destabilises the vibration at some large pre-load values. Within the range of the stiffness values of the vertical spring of the slider considered in this paper, the vertical stiffness stabilises the system when it is large enough. Larger in-plane stiffness makes the vibration grow faster and separation occurs earlier, but it becomes a stabilising factor when it reaches a large enough value. Additionally, separation may not happen when the disc is soft enough. Where separation occurs during disc vibration can be affected by the mass of the slider.

5. The variation of the frequencies of the system over time is illustrated through a time-frequency analysis. The frequency of the rotating speed, the natural frequencies of the disc and the horizontal and vertical branches of the slider all make contributions to the frequencies of the whole system. Frequencies higher than the main frequencies of the disc arise due to separation. The in-plane stick-slip vibration results in complex evolution of the frequencies of the transverse disc vibration.

The most important conclusion of this paper is that separation should be taken into account in many friction-induced vibration problems.

6 Model Reduction of a Multi-degree-of-freedom System with Experimental Validation

6.1 Introduction

For complex large structures with dry friction, like brakes, finite element software are a broadly used tool for eigenvalue analysis and transient dynamic analysis. However, because of the large number of degrees of freedom and complex friction characteristics at the contact surfaces of real structures, expensive computation cost is a big issue. Chapters 4 and 5 indicate that the nonlinearity/non-smoothness has significant influences on the friction-induced vibration. As we know considering realistic factors, such as nonlinearity, complex law of friction or changes of contact states, in the simplified mechanical systems makes the problem more difficult, but it is still a realisable task. However, as to the real structures, it is a challenge to implement complicated properties of friction such as stick-slip, separation or other nonlinearities in the friction-induced vibration of a complicated frictional system.

Frictional systems are composed of substructures that are in contact rather than linked together, thus the system has natural interfaces. The frictional interface is the key part of the system and contains the key characteristics (the complex friction force, contact states) of the system. Generally, systems having substructures and connections can be analysed through substructuring techniques, which are a feasible and efficient method for both practical and theoretical studies.

The aim of this chapter is to study the friction-induced vibration of a complicated system which is different from the theoretical models studied in previous chapters. The work of this chapter reports the preliminary study of this new topic, and is a result of collaboration with some colleagues in the Tribology Research Institute of Southwest Jiaotong University (SWJTU), China. As it has been known, frictional systems have some distinct dynamic properties, for example, their stability can change with the friction coefficient. Thus, for the reduction of the frictional systems, a big concern is

whether the reduced system still can preserve these important properties of the original system.

In this chapter, a reduction strategy for systems with friction is proposed, which is described in Section 6.2. In Section 6.3 the accuracy of the method on predicting the natural frequencies of the system and mode-coupling instability is verified by comparing the results of a full 9-degree-of-freedom model and the reduced models with those results calculated by the general method for eigenvalue analysis. Then the feasibility of the reduction method for the frictional system that has rigid-body motion in the substructure is testified in Section 6.4. Finally, in Section 6.5, this reduction strategy is applied to the reduction of a complicated finite element model of a real test structure, followed by the validation via test results.

6.2 Theoretical formulations of the reduction strategy

Friction systems, like a brake system, can be modelled as two separate multi-degree-of-freedom systems which share friction contact at the interface. Fig. 6.1 shows the diagram of a discrete model with a pad on the surface of a disc. The contact between the pad and disc is modelled as linear springs.

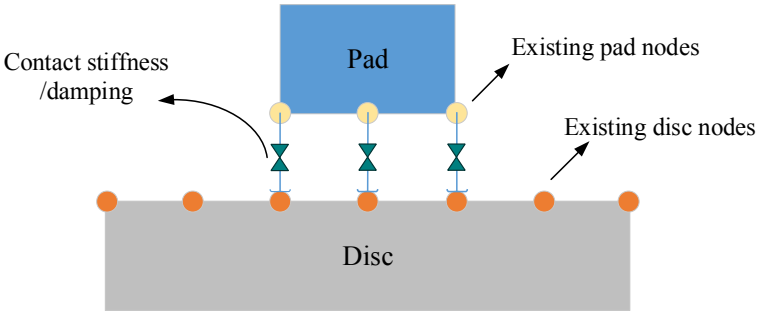

Fig. 6.1 The diagram of a pad-disc system

The physical displacements of the upper pad system and lower disc system are defined as vectors $\mathbf{x}_\mathrm{p}$ and $\mathbf{x}_\mathrm{d}$, which are in the following form:

$$\mathbf{x}_\mathrm{p} = \begin{bmatrix} \mathbf{x}_\mathrm{p}^{o} \\ \mathbf{x}_\mathrm{p}^{u} \\ \mathbf{x}_\mathrm{p}^{w} \end{bmatrix}, \quad \mathbf{x}_\mathrm{d} = \begin{bmatrix} \mathbf{x}_\mathrm{d}^{u} \\ \mathbf{x}_\mathrm{d}^{w} \\ \mathbf{x}_\mathrm{d}^{o} \end{bmatrix} \tag{6.1}$$

in which superscript *u* denotes the tangential DoFs on the interface; *w* denotes the normal DoFs on the interface; *o* denotes all the OTHER degrees of freedom (DoFs); Thus $\mathbf{x}_{\mathrm{p}}^{o}$, $\mathbf{x}_{\mathrm{p}}^{u}$ and $\mathbf{x}_{\mathrm{p}}^{w}$ are the physical displacements of the pad in *o*, *u* and *w* DoFs; $\mathbf{x}_{\mathrm{d}}^{u}$, $\mathbf{x}_{\mathrm{d}}^{w}$ and $\mathbf{x}_{\mathrm{d}}^{o}$ are the physical displacements of the disc in the corresponding DoFs. If the pad is an *n*-degree-of-freedom system and the disc is an *m*-degree-of-freedom system，then $\mathbf{x}_{\mathrm{p}}$ is an $n\times1$ vector and $\mathbf{x}_{\mathrm{d}}$ is an $m\times1$ vector.

Physical coordinates $\mathbf{x}_{\mathrm{p}}$ and $\mathbf{x}_{\mathrm{d}}$ can be expressed in the mode expansion form：

$$\mathbf{x}_{\mathrm{p}}=\boldsymbol{\Phi}_{\mathrm{p}}\mathbf{q}_{\mathrm{p}} \quad \text{and} \quad \mathbf{x}_{\mathrm{d}}=\boldsymbol{\Phi}_{\mathrm{d}}\mathbf{q}_{\mathrm{d}} \tag{6.2}$$

in which $\mathbf{q}_{\mathrm{p}}$ and $\mathbf{q}_{\mathrm{d}}$ are the modal coordinate vector of the pad and disc, $\boldsymbol{\Phi}_{\mathrm{p}}$ and $\boldsymbol{\Phi}_{\mathrm{d}}$ are the mass-normalised mode shape matrices of the pad and the disc as separate systems. If *i* modes of pad and *j* modes of the disc are used, The size of $\boldsymbol{\Phi}_{\mathrm{p}}$ and $\boldsymbol{\Phi}_{\mathrm{d}}$ is $n\times i$ and a $m\times j$; $\mathbf{q}_{\mathrm{p}}$ and $\mathbf{q}_{\mathrm{d}}$ are a $i\times1$ and a $j\times1$ vector respectively.

The mode shape matrix $\boldsymbol{\Phi}_{\mathrm{p}}$ and $\boldsymbol{\Phi}_{\mathrm{d}}$ can be partition into three submatrices, expressed as Eq. (6.3)

$$\boldsymbol{\Phi}_{\mathrm{p}}=\begin{bmatrix}\boldsymbol{\Phi}_{\mathrm{p}}^{o}\\ \boldsymbol{\Phi}_{\mathrm{p}}^{u}\\ \boldsymbol{\Phi}_{\mathrm{p}}^{w}\end{bmatrix},\quad \boldsymbol{\Phi}_{\mathrm{d}}=\begin{bmatrix}\boldsymbol{\Phi}_{\mathrm{d}}^{u}\\ \boldsymbol{\Phi}_{\mathrm{d}}^{w}\\ \boldsymbol{\Phi}_{\mathrm{d}}^{o}\end{bmatrix} \tag{6.3}$$

in which $\boldsymbol{\Phi}_{\mathrm{p}}^{o}$, $\boldsymbol{\Phi}_{\mathrm{p}}^{u}$ and $\boldsymbol{\Phi}_{\mathrm{p}}^{w}$ are the components of the mode shape vector of the pad in the *o*-， *u*- and *w*-DoF. Similarly, $\boldsymbol{\Phi}_{\mathrm{d}}^{o}$, $\boldsymbol{\Phi}_{\mathrm{d}}^{u}$ and $\boldsymbol{\Phi}_{\mathrm{d}}^{w}$ are the submatrices containing the mode shape components in the corresponding DoFs of the disc.

The mass-normalised mode shape matrix of the pad and disc satisfies the following orthogonal conditions:

$$\boldsymbol{\Phi}_{\mathrm{p}}{}^{\mathrm{T}}\mathbf{M}_{\mathrm{p}}\boldsymbol{\Phi}_{\mathrm{p}}=\mathbf{I},\quad \boldsymbol{\Phi}_{\mathrm{p}}{}^{\mathrm{T}}\mathbf{C}_{\mathrm{p}}\boldsymbol{\Phi}_{\mathrm{p}}=\widehat{\mathbf{C}}_{\mathrm{p}}=\mathrm{diag}\left(2\xi_{\mathrm{p}}\omega_{\mathrm{p}}\right),\quad \boldsymbol{\Phi}_{\mathrm{p}}{}^{\mathrm{T}}\mathbf{K}_{\mathrm{p}}\boldsymbol{\Phi}_{\mathrm{p}}=\widehat{\mathbf{K}}_{\mathrm{p}}=\mathrm{diag}\left(\omega_{\mathrm{p}}{}^{2}\right) \tag{6.4}$$

$$\boldsymbol{\Phi}_{\mathrm{d}}{}^{\mathrm{T}}\mathbf{M}_{\mathrm{d}}\boldsymbol{\Phi}_{\mathrm{d}}=\mathbf{I},\quad \boldsymbol{\Phi}_{\mathrm{d}}{}^{\mathrm{T}}\mathbf{C}_{\mathrm{d}}\boldsymbol{\Phi}_{\mathrm{d}}=\widehat{\mathbf{C}}_{\mathrm{d}}=\mathrm{diag}\left(2\xi_{\mathrm{d}}\omega_{\mathrm{d}}\right),\quad \boldsymbol{\Phi}_{\mathrm{d}}{}^{\mathrm{T}}\mathbf{K}_{\mathrm{d}}\boldsymbol{\Phi}_{\mathrm{d}}=\widehat{\mathbf{K}}_{\mathrm{d}}=\mathrm{diag}\left(\omega_{\mathrm{d}}{}^{2}\right) \tag{6.5}$$

where ω_{p} and ω_{d} are the nature frequencies of the pad and disc respectively.

6.2.1 Definitions of the contact force and the friction force

In this method, artificial linear springs and dampers are introduced to model the contact between the pad and disc. Then the contact force can be obtained by Eq. (6.6):

$$\mathbf{p}=\mathbf{n}+\mathbf{C}_{\mathrm{c}}\left(\dot{\mathbf{x}}_{\mathrm{d}}^{w}-\dot{\mathbf{x}}_{\mathrm{p}}^{w}\right)+\mathbf{K}_{\mathrm{c}}\left(\mathbf{x}_{\mathrm{d}}^{w}-\mathbf{x}_{\mathrm{p}}^{w}\right)=\mathbf{n}+\mathbf{C}_{\mathrm{c}}\left(\boldsymbol{\Phi}_{\mathrm{d}}^{w}\dot{\mathbf{q}}_{\mathrm{d}}-\boldsymbol{\Phi}_{\mathrm{p}}^{w}\dot{\mathbf{q}}_{\mathrm{p}}\right)+\mathbf{K}_{\mathrm{c}}\left(\boldsymbol{\Phi}_{\mathrm{d}}^{w}\mathbf{q}_{\mathrm{d}}-\boldsymbol{\Phi}_{\mathrm{p}}^{w}\mathbf{q}_{\mathrm{p}}\right) \tag{6.6}$$

in which $\mathbf{n}$ is the pre-load vector, $\mathbf{C}_{\mathrm{c}}$ is the contact damping matrix， $\mathbf{K}_{\mathrm{c}}$ is the contact stiffness matrix, which are in the following form:

$$\mathbf{C}_{\mathrm{c}}=\mathrm{diag}\left(c_{\mathrm{c}}{}^{i}\right),\ i=1,2,\ldots n\ ,\quad \mathbf{K}_{\mathrm{c}}=\mathrm{diag}\left(k_{\mathrm{c}}{}^{i}\right),\ i=1,2,\ldots n \tag{6.7}$$

where $k_{\mathrm{c}}{}^{i}$ and $c_{\mathrm{c}}{}^{i}$ is the stiffness and damping of the *i*th contact node.

Then, the friction force can be expressed as Eq. (6.8) , if the friction coefficient takes a constant value μ.

$$\mathbf{f}_{\mathrm{r}}=\mu\left[\mathbf{n}+\mathbf{C}_{\mathrm{c}}\left(\boldsymbol{\Phi}_{\mathrm{d}}^{w}\dot{\mathbf{q}}_{\mathrm{d}}-\boldsymbol{\Phi}_{\mathrm{p}}^{w}\dot{\mathbf{q}}_{\mathrm{p}}\right)+\mathbf{K}_{\mathrm{c}}\left(\boldsymbol{\Phi}_{\mathrm{d}}^{w}\mathbf{q}_{\mathrm{d}}-\boldsymbol{\Phi}_{\mathrm{p}}^{w}\mathbf{q}_{\mathrm{p}}\right)\right] \tag{6.8}$$

6.2.2 Mode synthesis strategy

The equation of motion of the pad and the disc in matrix can be written as：

$$\mathbf{M}_{\mathrm{p}}\ddot{\mathbf{x}}_{\mathrm{p}}+\mathbf{C}_{\mathrm{p}}\dot{\mathbf{x}}_{\mathrm{p}}+\mathbf{K}_{\mathrm{p}}\mathbf{x}_{\mathrm{p}}=\begin{bmatrix}\mathbf{0}\\ \mu\mathbf{p}\\ \mathbf{p}\end{bmatrix} \tag{6.9}$$

$$\mathbf{M}_{\mathrm{d}}\ddot{\mathbf{x}}_{\mathrm{d}}+\mathbf{C}_{\mathrm{d}}\dot{\mathbf{x}}_{\mathrm{d}}+\mathbf{K}_{\mathrm{d}}\mathbf{x}_{\mathrm{d}}=\underbrace{\begin{bmatrix}\mathbf{T}^{uu} & \mathbf{T}^{uw} & \mathbf{T}^{uo}\\ \mathbf{T}^{wu} & \mathbf{T}^{ww} & \mathbf{T}^{wo}\\ \mathbf{T}^{ou} & \mathbf{T}^{ow} & \mathbf{T}^{oo}\end{bmatrix}}_{\mathbf{T}}\begin{bmatrix}-\mu\mathbf{p}\\ -\mathbf{p}\\ \mathbf{0}\end{bmatrix} \tag{6.10}$$

in which $\mathbf{M}_{\mathrm{p}}$, $\mathbf{C}_{\mathrm{p}}$ and $\mathbf{K}_{\mathrm{p}}$ are the mass, damping and stiffness matrix of the pad; $\mathbf{M}_{\mathrm{d}}$, $\mathbf{C}_{\mathrm{d}}$ and $\mathbf{K}_{\mathrm{d}}$ are the mass, damping and stiffness matrix of the disc. A transfer matrix

T is introduced which allows the dimension of the force vector acting on the pad to be correctly matched with the force vector on the disc's interface even if the degrees of freedom of the interface of the pad and disc are different; sometimes **T**=**I** when the DoFs of the pad are identical to those of the disc's. $\mathbf{T}^{rs}$ (r, s=o, u, w) means the transfer relations between the r kind of DoF on the pad to the j kind of DoF on the disc.

By pre-multiplying $\mathbf{\Phi}_{\mathrm{p}}^{\mathrm{T}}$ on both sides of Eq. (6.9), and according to the orthogonal conditions Eq. (6.4), the equation of motion of the pad in modal coordinates is expressed as Eq. (6.11):

$$\ddot{\mathbf{q}}_{\mathrm{p}} + \widehat{\mathbf{C}}_{\mathrm{p}}\dot{\mathbf{q}}_{\mathrm{p}} + \widehat{\mathbf{K}}_{\mathrm{p}}\mathbf{q}_{\mathrm{p}} = \left(\mu\mathbf{\Phi}_{\mathrm{p}}^{u\mathrm{T}} + \mathbf{\Phi}_{\mathrm{p}}^{w\mathrm{T}}\right)\mathbf{p} \tag{6.11}$$

When substituting the expression of the contact force $\mathbf{p}$ in Eq. (6.6) into Eq. (6.11), one gets:

$$\begin{aligned}&\ddot{\mathbf{q}}_{\mathrm{p}} + \left(\widehat{\mathbf{C}}_{\mathrm{p}} + \left(\mu\mathbf{\Phi}_{\mathrm{p}}^{u\mathrm{T}} + \mathbf{\Phi}_{\mathrm{p}}^{w\mathrm{T}}\right)\mathbf{C}_{\mathrm{c}}\mathbf{\Phi}_{\mathrm{p}}^{w}\right)\dot{\mathbf{q}}_{\mathrm{p}} - \left(\mu\mathbf{\Phi}_{\mathrm{p}}^{u\mathrm{T}} + \mathbf{\Phi}_{\mathrm{p}}^{w\mathrm{T}}\right)\mathbf{C}_{\mathrm{c}}\mathbf{\Phi}_{\mathrm{d}}^{w}\dot{\mathbf{q}}_{\mathrm{d}} + \left(\widehat{\mathbf{K}}_{\mathrm{p}} + \left(\mu\mathbf{\Phi}_{\mathrm{p}}^{u\mathrm{T}} + \mathbf{\Phi}_{\mathrm{p}}^{w\mathrm{T}}\right)\mathbf{K}_{\mathrm{c}}\mathbf{\Phi}_{\mathrm{p}}^{w}\right)\mathbf{q}_{\mathrm{p}} \\ &-\left(\mu\mathbf{\Phi}_{\mathrm{p}}^{u\mathrm{T}} + \mathbf{\Phi}_{\mathrm{p}}^{w\mathrm{T}}\right)\mathbf{K}_{\mathrm{c}}\mathbf{\Phi}_{\mathrm{d}}^{w}\mathbf{q}_{\mathrm{d}} = \left(\mu\mathbf{\Phi}_{\mathrm{p}}^{u\mathrm{T}} + \mathbf{\Phi}_{\mathrm{p}}^{w\mathrm{T}}\right)\mathbf{n}\end{aligned} \tag{6.12}$$

Similarly, the equation of motion of the disc in modal coordinates can be expressed as Eq. (6.13)

$$\ddot{\mathbf{q}}_{\mathrm{d}} + \left(\widehat{\mathbf{C}}_{\mathrm{d}} + \mathbf{A}\mathbf{C}_{\mathrm{c}}\mathbf{\Phi}_{\mathrm{d}}^{w}\right)\dot{\mathbf{q}}_{\mathrm{d}} + \left(\widehat{\mathbf{K}}_{\mathrm{d}} + \mathbf{A}\mathbf{K}_{\mathrm{c}}\mathbf{\Phi}_{\mathrm{d}}^{w}\right)\mathbf{q}_{\mathrm{d}} + \mathbf{A}\mathbf{K}_{\mathrm{c}}\mathbf{\Phi}_{\mathrm{p}}^{w}\dot{\mathbf{q}}_{\mathrm{p}} - \mathbf{A}\mathbf{K}_{\mathrm{c}}\mathbf{\Phi}_{\mathrm{p}}^{w}\mathbf{q}_{\mathrm{p}} = -\mathbf{A}\mathbf{n} \tag{6.13}$$

where

$$\mathbf{A} = \mathbf{\Phi}_{\mathrm{d}}^{u\mathrm{T}}\left(\mu\mathbf{T}^{uu} + \mathbf{T}^{uw}\right) + \mathbf{\Phi}_{\mathrm{d}}^{w\mathrm{T}}\left(\mu\mathbf{T}^{wu} + \mathbf{T}^{ww}\right) + \mathbf{\Phi}_{\mathrm{d}}^{o\mathrm{T}}\left(\mu\mathbf{T}^{ou} + \mathbf{T}^{ow}\right)$$

Then by collecting the equation of motion of the pad and disc in modal coordinates, which are given in Eqs. (6.12) and (6.13), the equation of motion of the whole system in matrix form with respect to the modal coordinates can be expressed as:

$$\ddot{\mathbf{q}} + \mathbf{C}\dot{\mathbf{q}} + \mathbf{K}\mathbf{q} = \mathbf{f}_{\mathrm{n}} \tag{6.14}$$

in which

$$\mathbf{q}=\begin{bmatrix}\mathbf{q}_{\mathrm{p}}\\ \mathbf{q}_{\mathrm{d}}\end{bmatrix},\quad \mathbf{C}=\begin{bmatrix}\widehat{\mathbf{C}}_{\mathrm{p}}+\left(\mu\boldsymbol{\Phi}_{\mathrm{p}}^{u\mathrm{T}}+\boldsymbol{\Phi}_{\mathrm{p}}^{w\mathrm{T}}\right)\mathbf{C}_{\mathrm{c}}\boldsymbol{\Phi}_{\mathrm{p}}^{w} & -\left(\mu\boldsymbol{\Phi}_{\mathrm{p}}^{u\mathrm{T}}+\boldsymbol{\Phi}_{\mathrm{p}}^{w\mathrm{T}}\right)\mathbf{C}_{\mathrm{c}}\boldsymbol{\Phi}_{\mathrm{d}}^{w}\\ -\mathbf{A}\mathbf{C}_{\mathrm{c}}\boldsymbol{\Phi}_{\mathrm{p}}^{w} & \widehat{\mathbf{C}}_{\mathrm{d}}+\mathbf{A}\mathbf{C}_{\mathrm{c}}\boldsymbol{\Phi}_{\mathrm{d}}^{w}\end{bmatrix}$$

$$\mathbf{K}=\begin{bmatrix}\widehat{\mathbf{K}}_{\mathrm{p}}+\left(\mu\boldsymbol{\Phi}_{\mathrm{p}}^{u\mathrm{T}}+\boldsymbol{\Phi}_{\mathrm{p}}^{w\mathrm{T}}\right)\mathbf{K}_{\mathrm{c}}\boldsymbol{\Phi}_{\mathrm{p}}^{w} & -\left(\mu\boldsymbol{\Phi}_{\mathrm{p}}^{u\mathrm{T}}+\boldsymbol{\Phi}_{\mathrm{p}}^{w\mathrm{T}}\right)\mathbf{K}_{\mathrm{c}}\boldsymbol{\Phi}_{\mathrm{d}}^{w}\\ -\mathbf{A}\mathbf{K}_{\mathrm{c}}\boldsymbol{\Phi}_{\mathrm{p}}^{w} & \widehat{\mathbf{K}}_{\mathrm{d}}+\mathbf{A}\mathbf{K}_{\mathrm{c}}\boldsymbol{\Phi}_{\mathrm{d}}^{w}\end{bmatrix},\quad \mathbf{f}_{\mathrm{n}}=\begin{bmatrix}\mu\boldsymbol{\Phi}_{\mathrm{p}}^{u\mathrm{T}}+\boldsymbol{\Phi}_{\mathrm{p}}^{w\mathrm{T}}\\ -\mathbf{A}\end{bmatrix}\mathbf{n}$$

As the reduced model is a linear system, $\mathbf{f}_{\mathrm{n}}$ does not affect the eigenvalues of the system. The stability or the natural frequency of the reduced system can be investigated by implementing a conventional complex eigenvalue analysis of Eq. (6.14). The eigenvalues λ of the system can be calculated by Eq. (6.15)

$$\left|\lambda^{2}\mathbf{I}+\lambda\mathbf{C}+\mathbf{K}\right|=\mathbf{0} \tag{6.15}$$

The general process of conducting the stability analysis of a frictional reduced system is illustrated in Fig. 6.2.

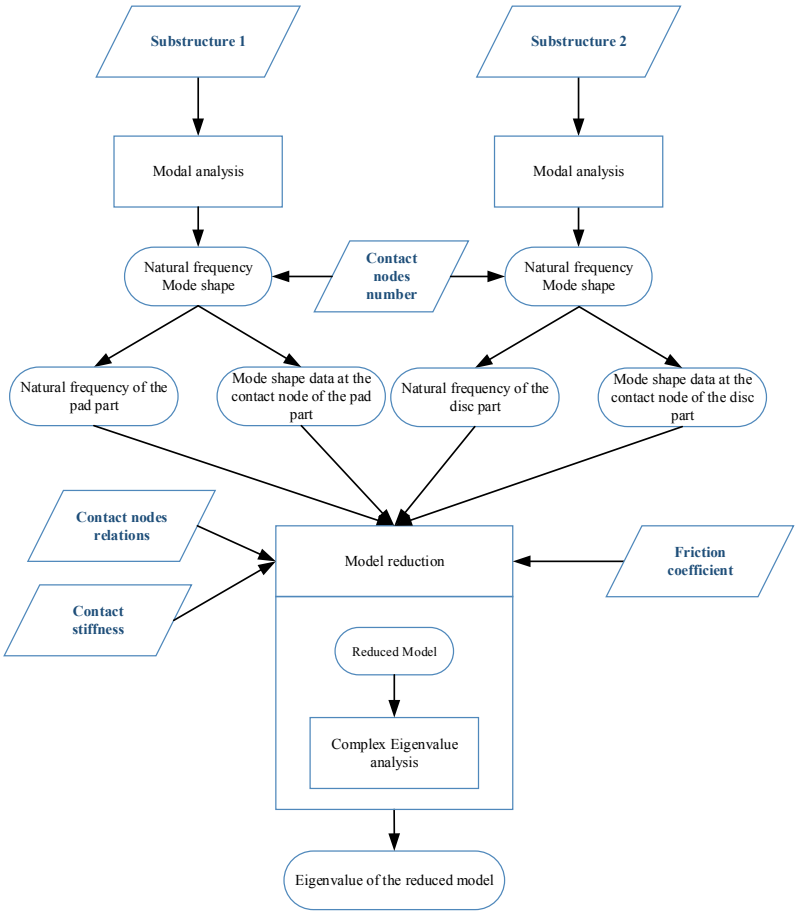

Fig. 6.2 The flow chart of the stability analysis process of the reduced model

The advantage of this strategy is that the natural frequencies and the stability of the whole system with friction can be investigated with the information of the friction coefficient and only a few modal data of the substructures: (1) the mode shape components in the DoFs on the potential contact interface and natural frequencies of the substructures, when the potential contact interfaces of the substructures are set to be free; (2) the relations between the DoFs on the interfaces of the substructures. Please note that what is being presented in this section is a general approach applicable to linear systems with multiple contact interfaces.

6.3 Applications to a 9-degree-of-freedom model

In this section, a 9-degree-of-freedom model is used to verify the applicability and accuracy of the preceding reduction strategy in the reduction of the multi-degree-of-freedom system.

6.3.1 Introduction of the 9-degree-of-freedom model

Fig. 6.3 shows the 9-degree-of-freedom undamped system with friction contact, which is comprised of two substructures (the upper slider part ('pad') and lower belt part ('disc')).

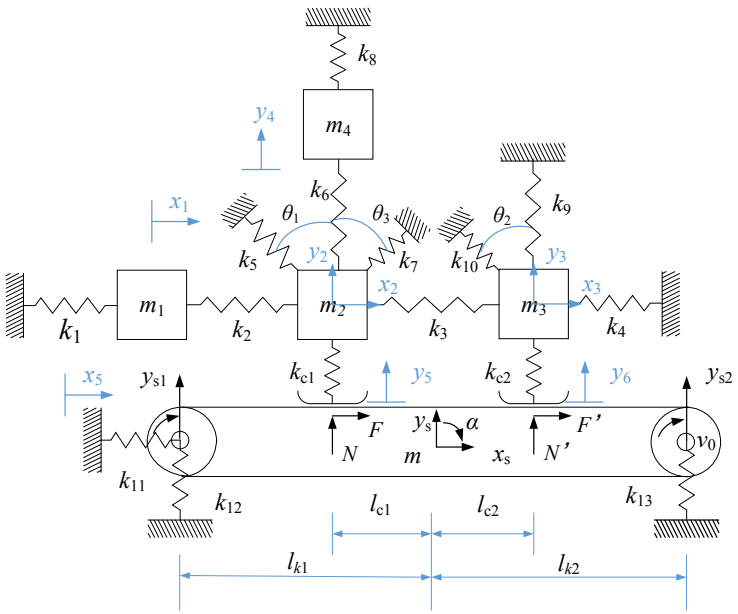

Fig. 6.3 The 9-degree-of-freedom model

The upper part is a 6-degree-of-freedom mass-spring system with four point masses m_1, m_2, m_3 and m_4, and linear springs. Among the springs, k_5, k_7 and k_{10} are three inclined springs, and the angles of them with respect to the vertical direction are θ_1, θ_2 and θ_3 respectively. The lower part is a belt modelled as a rigid body denoted by m. The length of m to the left end of the belt is l_{k1} and to the right end is l_{k2}. m_2 and m_3 are in sliding contact, which is modelled as linear springs k_{c1} and k_{c2}, with the rigid moving belt. The two contact points are massless sliders. The distances of the contact points of m_2 and m_3 to the mass centre of the belt are l_{c1} and l_{c2} respectively. Coulomb friction with a constant friction coefficient μ is considered. The definitions of the coordinates system are shown in Fig. 6.3.

6.3.2 Equations of motion of the substructures

According to the definitions of the coordinate system of the pad and the disc, the upper part is a 6-degree-of-freedom system described by x_1, x_2, y_2, x_3, y_3, y_4, and the lower belt is a 3-degree-of-freedom system described by x_5, y_5 and y_6, which also can be described by the auxiliary coordinates x_s, y_s and α, which are the horizontal and vertical displacement of the centre of the belt and the rotation of the belt at its centre.

Following the definition (Eq. (6.1)) of the displacement vector, the sub-displacement vectors of the horizontal and vertical DoFs, and the OTHER DoFs (o-DoF)can be written as:

$$\mathbf{x}_{\mathrm{p}}^{o}=\begin{bmatrix} x_1 \\ y_4 \end{bmatrix},\quad \mathbf{x}_{\mathrm{p}}^{u}=\begin{bmatrix} x_2 \\ x_3 \end{bmatrix},\quad \mathbf{x}_{\mathrm{p}}^{w}=\begin{bmatrix} y_2 \\ y_3 \end{bmatrix} \tag{6.16}$$

As the lower part does not have the o-DoF, the sub-displacement vectors in the horizontal and vertical degrees of the freedom of the contact points are written as:

$$\mathbf{x}_{\mathrm{d}}^{u}=\begin{bmatrix} x_5 \end{bmatrix},\ \mathbf{x}_{\mathrm{d}}^{w}=\begin{bmatrix} y_5 \\ y_6 \end{bmatrix} \tag{6.17}$$

Thus, the displacement vector of the slider and the belt are given in Eq. (6.18):

$$\mathbf{x}_{\mathrm{p}}=\begin{bmatrix} x_1 & y_4 & x_2 & x_3 & y_2 & y_3 \end{bmatrix}^{\mathrm{T}},\ \mathbf{x}_{\mathrm{d}}=\begin{bmatrix} x_5 & y_5 & y_6 \end{bmatrix}^{\mathrm{T}} \tag{6.18}$$

6.3.2.1 *The equation of motion of the upper slider*

The kinetic and the potential energy of the upper part are given in Eqs. (6.19) and (6.20):

$$T_{\mathrm{p}} = \frac{1}{2}m_1\dot{x}_1^2 + \frac{1}{2}m_2\dot{x}_2^2 + \frac{1}{2}m_3\dot{x}_3^2 + \frac{1}{2}m_2\dot{y}_2^2 + \frac{1}{2}m_3\dot{y}_3^2 + \frac{1}{2}m_4\dot{y}_4^2 \tag{6.19}$$

$$\begin{aligned} V_{\mathrm{p}} = \frac{1}{2}\Big[& k_1x_1^2 + k_2\left(x_2 - x_1\right)^2 + k_3\left(x_3 - x_2\right)^2 + k_4x_3^2 + k_8y_4^2 + k_6\left(y_4 - y_2\right)^2 + k_9y_3^2 \\ & + k_5\left(y_2\cos\theta_1 - x_2\sin\theta_1\right)^2 + k_7\left(x_2\sin\theta_3 + y_2\cos\theta_3\right)^2 + k_{10}\left(y_3\cos\theta_2 - x_3\sin\theta_2\right)^2\Big] \end{aligned} \tag{6.20}$$

The Lagrange equation of motion of the pad is expressed as:

$$\frac{\partial}{\partial t}\frac{\partial T_{\mathrm{p}}}{\partial \dot{x}_{\mathrm{p}i}} + \frac{\partial V_{\mathrm{p}}}{\partial x_{\mathrm{p}i}} = Q_{\mathrm{p}i},\ i = 1 \sim 6 \tag{6.21}$$

in which $x_{\mathrm{p}i}$ is the ith element in $\mathbf{x}_{\mathrm{p}}$, $Q_{\mathrm{p}i}$ is the nonconservative force.

If the contact forces between m_2 and the belt, and between m_3 and the belt are defined as N and N', and the horizontal friction forces are denoted by F and F'. Then $Q_{\mathrm{p}i}$ are given in Eq. (6.22):

$$Q_{\mathrm{p}1} = Q_{\mathrm{p}2} = 0,\ Q_{\mathrm{p}3} = F,\ Q_{\mathrm{p}4} = F',\ Q_{\mathrm{p}5} = N,\ Q_{\mathrm{p}3} = N' \tag{6.22}$$

Then the equation of the slider system is expressed as:

$$\mathbf{M}_{\mathrm{p}}\ddot{\mathbf{x}}_{\mathrm{p}} + \mathbf{K}_{\mathrm{p}}\mathbf{x}_{\mathrm{p}} = \mathbf{F}_{\mathrm{p}} \tag{6.23}$$

in which

$$\mathbf{M}_{\mathrm{p}} = \begin{bmatrix} m_1 & & & & & \\ & m_4 & & & & \\ & & m_2 & & & \\ & & & m_3 & & \\ & & & & m_2 & \\ & & & & & m_3 \end{bmatrix},\quad \mathbf{K}_{\mathrm{p}} = \begin{bmatrix} k_{\mathrm{p}}^{11} & 0 & -k_2 & 0 & 0 & 0 \\ 0 & k_{\mathrm{p}}^{22} & 0 & 0 & -k_6 & 0 \\ -k_2 & 0 & k_{\mathrm{p}}^{33} & -k_3 & -k_{\mathrm{p}}^{35} & 0 \\ 0 & 0 & -k_3 & k_{\mathrm{p}}^{44} & 0 & -k_{\mathrm{p}}^{64} \\ 0 & -k_6 & -k_{\mathrm{p}}^{35} & 0 & k_{\mathrm{p}}^{55} & 0 \\ 0 & 0 & 0 & -k_{\mathrm{p}}^{64} & 0 & k_{\mathrm{p}}^{66} \end{bmatrix}$$

where

$$\begin{cases} k_{\mathrm{p}}{}^{11} = k_1 + k_2 \\ k_{\mathrm{p}}{}^{22} = k_8 + k_6 \\ k_{\mathrm{p}}{}^{33} = k_2 + k_3 + k_5 \sin\theta_1{}^2 + k_7 \sin\theta_3{}^2 \\ k_{\mathrm{p}}{}^{44} = k_3 + k_4 + k_{10} \sin\theta_2{}^2 \\ k_{\mathrm{p}}{}^{55} = k_6 + k_5 \cos\theta_1{}^2 + k_7 \cos\theta_3{}^2 \\ k_{\mathrm{p}}{}^{66} = k_9 + k_{10} \cos\theta_2{}^2 \\ k_{\mathrm{p}}{}^{64} = k_{10} \sin\theta_2 \cos\theta_2 \\ k_{\mathrm{p}}{}^{35} = k_5 \sin\theta_1 \cos\theta_1 - k_7 \sin\theta_3 \cos\theta_3 \end{cases} \tag{6.24}$$

and

$$\mathbf{F}_{\mathrm{p}} = \begin{bmatrix} 0 & 0 & F & F' & N & N' \end{bmatrix}^{\mathrm{T}} \tag{6.25}$$

As the friction coefficient is assumed as constant value μ, the friction forces are expressed as $F = \mu N$ and $F' = \mu N'$, so the above force vector $\mathbf{F}_{\mathrm{p}}$ can also be written as:

$$\mathbf{F}_{\mathrm{p}} = \begin{bmatrix} \mathbf{0} \\ \mu\mathbf{p} \\ \mathbf{p} \end{bmatrix} = \begin{bmatrix} 0 & 0 & \mu N & \mu N' & N & N' \end{bmatrix}^{\mathrm{T}} \tag{6.26}$$

6.3.2.2 *The equation of the motion of the lower belt system*

The kinetic energy of the belt with respect to the auxiliary coordinates x_s, y_s and α is expressed as (6.27):

$$T_{\mathrm{d}} = \frac{1}{2} m \dot{x}_s^2 + \frac{1}{2} m \dot{y}_s^2 + \frac{1}{2} J \dot{\alpha}^2 \tag{6.27}$$

in which J is the moment of inertia, given in Eq. (6.28)

$$J = \frac{1}{12} m \left(l_{k1} + l_{k2} \right)^2 \tag{6.28}$$

The potential energy of the belt with respect to coordinates x_s, y_{s1} and y_{s2} is expressed as Eq. (6.29)

$$V_{\mathrm{d}} = \frac{1}{2}\left[k_{11}x_s^2 + k_{12}y_{s1}^2 + k_{13}{y_{s2}}^2\right] \tag{6.29}$$

The relations between $x_5,\ y_5,\ y_6, x_s,\ y_s,\ \alpha,\ y_{s1}$ and y_{s2} are given in Eq. (6.30)

$$\begin{cases} x_s = x_5 \\ \alpha = \dfrac{y_5 - y_6}{l_{\mathrm{c1}} + l_{\mathrm{c2}}} \\ y_s = y_5 - l_{\mathrm{c1}}\alpha = \dfrac{l_{c2}}{l_{c1} + l_{c2}} y_5 + \dfrac{l_{c1}}{l_{c1} + l_{c2}} y_6 \\ y_{s1} = y_s + l_{k1}\alpha = \dfrac{l_{k1} + l_{\mathrm{c2}}}{l_{\mathrm{c1}} + l_{\mathrm{c2}}} y_5 - \dfrac{l_{k1} - l_{\mathrm{c1}}}{l_{\mathrm{c1}} + l_{\mathrm{c2}}} y_6 \\ y_{s2} = y_s + l_{k1}\alpha = \dfrac{l_{\mathrm{c2}} - l_{k2}}{l_{\mathrm{c1}} + l_{\mathrm{c2}}} y_5 + \dfrac{l_{k2} + l_{\mathrm{c1}}}{l_{\mathrm{c1}} + l_{\mathrm{c2}}} y_6 \end{cases} \tag{6.30}$$

The Lagrange equation of the lower part is written as:

$$\frac{\partial}{\partial t}\frac{\partial T_{\mathrm{d}}}{\partial \dot{x}_{\mathrm{d}i}} + \frac{\partial V_{\mathrm{d}}}{\partial x_{\mathrm{d}i}} = Q_{\mathrm{d}i},\ i = 1 \sim 3 \tag{6.31}$$

in which $x_{\mathrm{d}i}$ is the ith element of $\mathbf{x}_{\mathrm{d}}$, and $Q_{\mathrm{d}i}$ in the non-conservative force on the disc interface, which is given in Eq. (6.32):

$$Q_{\mathrm{d1}} = 0\ ,\ \ Q_{\mathrm{d2}} = -N\ ,\ \ Q_{\mathrm{d3}} = -N' \tag{6.32}$$

According to the Lagrange equations, the equation of motion of the belt is written as

$$\mathbf{M}_{\mathrm{d}}\ddot{\mathbf{x}}_{\mathrm{d}} + \mathbf{K}_{\mathrm{d}}\mathbf{x}_{\mathrm{d}} = \mathbf{F}_{\mathrm{d}} \tag{6.33}$$

in which

$$\mathbf{M}_{\mathrm{d}} = \begin{bmatrix} m & 0 & 0 \\ 0 & m\left(\dfrac{l_{\mathrm{c2}}}{l_{\mathrm{c1}} + l_{\mathrm{c2}}}\right)^2 + \dfrac{J}{\left(l_{\mathrm{c1}} + l_{\mathrm{c2}}\right)^2} & 0 \\ 0 & 0 & m\left(\dfrac{l_{\mathrm{c1}}}{l_{\mathrm{c1}} + l_{\mathrm{c2}}}\right)^2 + \dfrac{J}{\left(l_{\mathrm{c1}} + l_{\mathrm{c2}}\right)^2} \end{bmatrix}$$

$$\mathbf{K}_{\mathrm{d}}=\begin{bmatrix} k_{11} & 0 & 0 \\ 0 & k_{\mathrm{d}}{}^{22} & -k_{\mathrm{d}}{}^{23} \\ 0 & -k_{\mathrm{d}}{}^{23} & k_{\mathrm{d}}{}^{33} \end{bmatrix} \text{ and } \mathbf{F}_{\mathrm{d}}=\begin{bmatrix} -\mu N-\mu N' \\ -N \\ -N \end{bmatrix} \tag{6.34}$$

where

$$\begin{cases} k_{\mathrm{d}}{}^{22}=k_{12}\left(\dfrac{l_{k1}+l_{\mathrm{c}2}}{l_{\mathrm{c}1}+l_{\mathrm{c}2}}\right)^2+k_{13}\left(\dfrac{l_{k2}-l_{c2}}{l_{c1}+l_{c2}}\right)^2 \\ k_{\mathrm{d}}{}^{33}=k_{12}\left(\dfrac{l_{k1}-l_{\mathrm{c}1}}{l_{\mathrm{c}1}+l_{\mathrm{c}2}}\right)^2+k_{13}\left(\dfrac{l_{k2}+l_{\mathrm{c}1}}{l_{\mathrm{c}1}+l_{\mathrm{c}2}}\right)^2 \\ k_{\mathrm{d}}{}^{23}=k_{12}\dfrac{\left(l_{k1}+l_{\mathrm{c}2}\right)\left(l_{k1}-l_{\mathrm{c}1}\right)}{\left(l_{\mathrm{c}1}+l_{\mathrm{c}2}\right)^2}+k_{13}\dfrac{\left(l_{k2}+l_{\mathrm{c}1}\right)\left(l_{k2}-l_{\mathrm{c}2}\right)}{\left(l_{\mathrm{c}1}+l_{\mathrm{c}2}\right)^2} \end{cases} \tag{6.35}$$

6.3.2.3 *The contact matrix and the transformation matrix*

As there is no external force acting on this 9-degree-of-freedom model, the contact force is expressed as Eq. (6.36), according to its definition in Section 6.2.1.

$$\mathbf{p}=\mathbf{K}_{\mathrm{c}}\left(\mathbf{x}_{\mathrm{d}}^{w}-\mathbf{x}_{\mathrm{p}}^{w}\right) \tag{6.36}$$

in which

$$\mathbf{K}_{\mathrm{c}}=\begin{bmatrix} k_{\mathrm{c}1} & 0 \\ 0 & k_{\mathrm{c}2} \end{bmatrix} \tag{6.37}$$

As the degrees of freedom of the contact points of upper part at the contact surface do not match with those of the lower belt system, then on the base of the definitions of $\mathbf{F}_{\mathrm{p}}$ (Eq.(6.25)) and $\mathbf{F}_{\mathrm{d}}$ (Eq. (6.34)), the transformation matrix of this problem is:

$$\mathbf{T}=\begin{bmatrix} 1 & 1 & 0 & 0 & 0 & 0 \\ 0 & 0 & 1 & 0 & 0 & 0 \\ 0 & 0 & 0 & 1 & 0 & 0 \end{bmatrix} \tag{6.38}$$

in which

$$\begin{gathered} \begin{bmatrix} 1 & 1 \end{bmatrix}=\mathbf{T}^{uu},\ \begin{bmatrix} 0 & 0 \end{bmatrix}=\mathbf{T}^{uw},\ \begin{bmatrix} 0 & 0 \end{bmatrix}=\mathbf{T}^{uo} \\ \begin{bmatrix} 0 & 0 \\ 0 & 0 \end{bmatrix}=\mathbf{T}^{wu},\ \begin{bmatrix} 1 & 0 \\ 0 & 1 \end{bmatrix}=\mathbf{T}^{ww},\ \begin{bmatrix} 0 & 0 \\ 0 & 0 \end{bmatrix}=\mathbf{T}^{wo} \end{gathered} \tag{6.39}$$

As there are no damping and the external force, and furthermore $\mathbf{T}^{ou}$、$\mathbf{T}^{ou}$ and $\mathbf{T}^{ou}$ in the transformation matrix are non-existent, thus the assembled equation of motion through the idea of the preceding section is simplified as：

$$\begin{bmatrix} \ddot{\mathbf{q}}_{\mathrm{p}} \\ \ddot{\mathbf{q}}_{\mathrm{d}} \end{bmatrix} + \begin{bmatrix} \widehat{\mathbf{K}}_{\mathrm{p}} + \left(\mu\boldsymbol{\Phi}_{\mathrm{p}}^{uT} + \boldsymbol{\Phi}_{\mathrm{p}}^{wT}\right)\mathbf{K}_{\mathrm{c}}\boldsymbol{\Phi}_{\mathrm{p}}^{w} & -\left(\mu\boldsymbol{\Phi}_{\mathrm{p}}^{uT} + \boldsymbol{\Phi}_{\mathrm{p}}^{wT}\right)\mathbf{K}_{\mathrm{c}}\boldsymbol{\Phi}_{\mathrm{d}}^{w} \\ -\mathbf{A}\mathbf{K}_{\mathrm{c}}\boldsymbol{\Phi}_{\mathrm{p}}^{w} & \widehat{\mathbf{K}}_{\mathrm{d}} + \mathbf{A}\mathbf{K}_{\mathrm{c}}\boldsymbol{\Phi}_{\mathrm{d}}^{w} \end{bmatrix} \begin{bmatrix} \mathbf{q}_{\mathrm{p}} \\ \mathbf{q}_{\mathrm{d}} \end{bmatrix} = \mathbf{0} \tag{6.40}$$

in which

$$\mathbf{A} = \boldsymbol{\Phi}_{\mathrm{d}}^{u\mathrm{T}}\left(\mu\mathbf{T}^{uu} + \mathbf{T}^{uw}\right) + \boldsymbol{\Phi}_{\mathrm{d}}^{w\mathrm{T}}\left(\mu\mathbf{T}^{wu} + \mathbf{T}^{ww}\right)$$

6.3.3 The equation of motion of the whole system

Generally, the equation of motion of a system is obtained through the force analysis or the Lagrange equation of the whole system, which is called the direct method here in order to distinguish this method from the model reduction method proposed in the preceding subsection.

Here, the displacement vector of the whole slider-belt model is defined as:

$$\mathbf{z} = \begin{bmatrix} x_1 & y_4 & x_2 & x_3 & y_2 & y_3 & x_5 & y_5 & y_6 \end{bmatrix}^{\mathrm{T}}$$

The kinetic and potential energy of the whole system are given in Eq. (6.41):

$$\begin{cases} T = \dfrac{1}{2}m_1\dot{x}_1^2 + \dfrac{1}{2}m_2\dot{x}_2^2 + \dfrac{1}{2}m_3\dot{x}_3^2 + \dfrac{1}{2}m_2\dot{y}_2^2 + \dfrac{1}{2}m_3\dot{y}_3^2 \\ \quad + \dfrac{1}{2}m_4\dot{y}_4^2 + \dfrac{1}{2}m\dot{x}_s^2 + \dfrac{1}{2}m\dot{y}_s^2 + \dfrac{1}{2}J\dot{\alpha}^2 \\ V = \dfrac{1}{2}\Big[k_1x_1^2 + k_2\left(x_2 - x_1\right)^2 + k_3\left(x_3 - x_2\right)^2 + k_4x_3^2 \\ \quad + k_8y_4^2 + k_6\left(y_4 - y_2\right)^2 + k_5\left(y_2\cos\theta_1 - x_2\sin\theta_1\right)^2 \\ \quad + k_7\left(x_2\sin\theta_3 + y_2\cos\theta_3\right)^2 + k_{10}\left(y_3\cos\theta_2 - x_3\sin\theta_2\right)^2 \\ \quad + k_9y_3^2 + k_{11}x_s^2 + k_{12}y_{s1}^2 + k_{13}{y_{s2}}^2\Big] \end{cases} \tag{6.41}$$

The Lagrange equation of the slider-belt system is expressed as:

$$\frac{\partial}{\partial t}\frac{\partial T}{\partial \dot{z}_i} + \frac{\partial V}{\partial z_i} = 0 \tag{6.42}$$

Then the equation of motion of the whole slider-belt model can be obtained by substituting Eq.(6.41) into (6.42):

$$\mathbf{M}\ddot{\mathbf{z}} + \mathbf{K}\mathbf{z} = \mathbf{0} \tag{6.43}$$

in which

$$\mathbf{M} = \begin{bmatrix} m_1 & 0 & 0 & 0 & 0 & 0 & 0 & 0 & 0 \\ 0 & m_4 & 0 & 0 & 0 & 0 & 0 & 0 & 0 \\ 0 & 0 & m_2 & 0 & 0 & 0 & 0 & 0 & 0 \\ 0 & 0 & 0 & m_3 & 0 & 0 & 0 & 0 & 0 \\ 0 & 0 & 0 & 0 & m_2 & 0 & 0 & 0 & 0 \\ 0 & 0 & 0 & 0 & 0 & m_3 & 0 & 0 & 0 \\ 0 & 0 & 0 & 0 & 0 & 0 & m & 0 & 0 \\ 0 & 0 & 0 & 0 & 0 & 0 & 0 & m\left(\frac{l_{c2}}{l_{c1}+l_{c2}}\right)^2 + \frac{J}{(l_{c1}+l_{c2})^2} & m\frac{l_{c1}l_{c2}}{(l_{c1}+l_{c2})^2} - \frac{J}{(l_{c1}+l_{c2})^2} \\ 0 & 0 & 0 & 0 & 0 & 0 & 0 & m\frac{l_{c1}l_{c2}}{(l_{c1}+l_{c2})^2} - \frac{J}{(l_{c1}+l_{c2})^2} & m\left(\frac{l_{c1}}{l_{c1}+l_{c2}}\right)^2 + \frac{J}{(l_{c1}+l_{c2})^2} \end{bmatrix}$$

$$\mathbf{K} = \begin{bmatrix} k_p^{11} & 0 & -k_2 & 0 & 0 & 0 & 0 & 0 & 0 \\ 0 & k_p^{22} & 0 & 0 & -k_6 & 0 & 0 & 0 & 0 \\ -k_2 & 0 & k_p^{33} & -k_3 & \mu k_{c1} - k_p^{35} & 0 & 0 & -\mu k_{c1} & 0 \\ 0 & 0 & -k_3 & k_p^{44} & 0 & \mu k_{c2} - k_p^{64} & 0 & 0 & -\mu k_{c2} \\ 0 & -k_6 & -k_p^{35} & 0 & k_{c1} + k_p^{55} & 0 & 0 & -k_{c1} & 0 \\ 0 & 0 & 0 & -k_p^{64} & 0 & k_{c2} + k_p^{66} & 0 & 0 & -k_{c2} \\ 0 & 0 & 0 & 0 & -\mu k_{c1} & -\mu k_{c2} & k_{11} & \mu k_{c1} & \mu k_{c2} \\ 0 & 0 & 0 & 0 & -k_{c1} & 0 & 0 & k_{c1} + k_d^{22} & -k_d^{23} \\ 0 & 0 & 0 & 0 & 0 & -k_{c2} & 0 & -k_d^{23} & k_{c2} + k_d^{33} \end{bmatrix}$$

where the expression of k_p^{11}, k_p^{22}, k_p^{33}, k_p^{44}, k_p^{55}, k_p^{66}, k_p^{35}, k_p^{64}, k_d^{22}, k_d^{33} and k_d^{23} are given in Eqs. (6.24) and (6.35). Apparently, the stiffness matrix of the system $\mathbf{K}$ is asymmetric.

6.3.4 Numerical analysis: Case 1

The theoretical formulations of the model reduction strategy and the direct method of the 9-degree-of freedom model are presented in the preceding sections. In this section, numerical simulations are carried out: firstly to calculate the natural frequencies and

the mode shapes of the substructures; then to implement the model reduction strategy using all the modes of the substructures and compute the natural frequencies of the system; then to compare the these frequencies with those calculated by the direct method to verify the correctness of the model reduction strategy; finally, to generate different reduced models and compare them with the full model.

The parameter values used in this subsection are: $m_1=m_2=m_3=m_4=m=1$, $\theta_1=\theta_2=\theta_3=45^\circ$, $k_1=k_2=k_3=k_4=k_5=k_6=k_7=k_8=k_9=k_{10}=k_{11}=k_{12}=k_{13}=k_{c1}=k_{c2}=1$, $l_{k1}=l_{k2}=1$, $l_{c1}=l_{c2}=0.5$.

6.3.4.1 *Modal analysis of the substructures*

Firstly, the natural frequencies and the mode shapes of the substructures are calculated. The natural frequencies of the upper slider system are shown in Table 6.1.

Table 6.1 The natural frequencies of the upper slider system (rad/s)

ω_{p1}	ω_{p2}	ω_{p3}	ω_{p4}	ω_{p5}	ω_{p6}
1	1	1.2036	1.5578	1.7321	2.0309

The mode shapes can also be obtained through modal analysis, thus the component matrices $\mathbf{\Phi}_p^o$, $\mathbf{\Phi}_p^u$, $\mathbf{\Phi}_p^w$ are:

$$\mathbf{\Phi}_p^o=\begin{bmatrix}-0.5 & 0 & -0.5501 & 0.5606 & 0 & -0.3648\\ 0 & -0.7071 & 0 & 0 & 0.7071 & 0\end{bmatrix}$$

$$\mathbf{\Phi}_p^u=\begin{bmatrix}-0.5 & 0 & -0.3033 & -0.2393 & 0 & 0.7751\\ -0.5 & 0 & 0.0795 & -0.6977 & 0 & -0.5068\end{bmatrix}$$

$$\mathbf{\Phi}_p^w=\begin{bmatrix}0 & -0.7071 & 0 & 0 & -0.7071 & 0\\ -0.5 & 0 & 0.7739 & 0.3764 & 0 & 0.0966\end{bmatrix}$$

According to the equations of motion of the belt, Eq. (6.33), natural frequencies of the lower belt system can also be calculated numerically by MATLAB, shown in Table 6.2:

Table 6.2 The natural frequencies of the belt system (rad/s)

ω_{d1}	ω_{d2}	ω_{d3}
1	1.4142	4.8990

The mode component matrices in the horizontal and vertical degrees of freedom are:

$$\boldsymbol{\Phi}_{\mathrm{d}}^{u}=\begin{bmatrix}1 & 0 & 0\end{bmatrix},\ \boldsymbol{\Phi}_{\mathrm{d}}^{w}=\begin{bmatrix}0 & -1 & -1.7321\\ 0 & -1 & 1.7321\end{bmatrix}$$

6.3.4.2 *Eigenvalue analysis of the full model*

After obtaining the modal information of the two substructures, the natural frequencies of the full system can by calculated by solving the eigenvalue problem of the equation of motion of the assembled system Eq. (6.40) with full modes of the substructures. The comparisons between the natural frequencies calculated by the substructure method with full modes and those calculated by the direct method, when the friction coefficient μ=1, are shown in Table 6.3.

Table 6.3 Comparisons of the nature frequencies (rad/s)

Mode	Substructure strategy	Direct method
1	1	1
2	1.07204803582823	1.07204803582823
3	1.07204803582823	1.07204803582823
4	1.38085112867760	1.38085112867760
5	1.56976814436112	1.56976814436112
6	1.77178792995748	1.77178792995748
7	1.99913346517545	1.99913346517545
8	2.23128655025242	2.23128655025242
9	5.49695781610159	5.49695781610159

From Table 6.3, it can be seen that the natural frequencies calculated by the substructure strategy with all the modes of the pad and the disc are completely the same with those calculated by the direct method, which indicates that the substructure strategy proposed in the current work is correct.

Moreover, evolution of the eigenvalues of the system with the friction coefficient, calculated by both methods, is also examined. It turns out that the bifurcation results by substructure strategy and the direct method are identical as well. Thus, only one set of results is illustrated in Fig. 6.4, which shows the changes of the real part and imaginary part of the eigenvalues with the friction coefficient. Because the system is a hypothetical model, the friction coefficient range under investigation is mathematical and thus may not reflect that of a real system.

It can be noticed that, while the friction coefficient is growing, some frequencies of the corresponding mode become closer and two of them coalesce at μ=0.9, where the first bifurcation happens (the 2nd and the 3rd modes); then with the further increase of the friction coefficient, the other two modes merge together and the second bifurcation takes place (the 5th and the 6th modes). Then the third bifurcation takes place at μ=14.6 (the 6th and the 7th modes), shown in Fig. 6.4 (a), at the same time one of the unstable mode (the 5th mode) become stable. Thus, there are still 4 unstable modes (the 2nd, the 3rd, the 6th and 7th modes) in total.

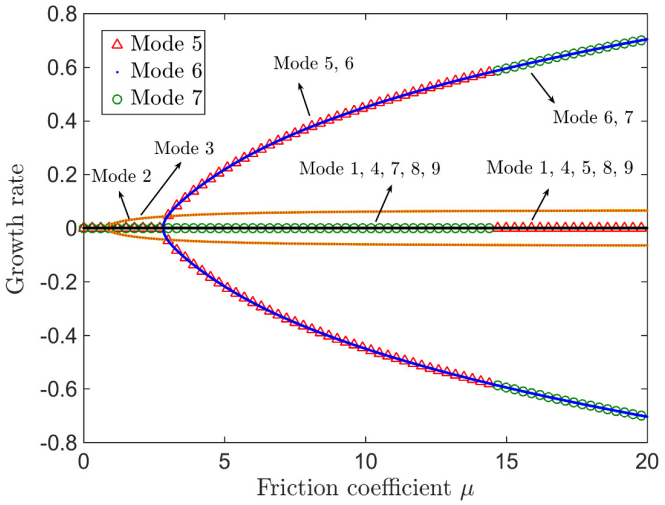

(a)

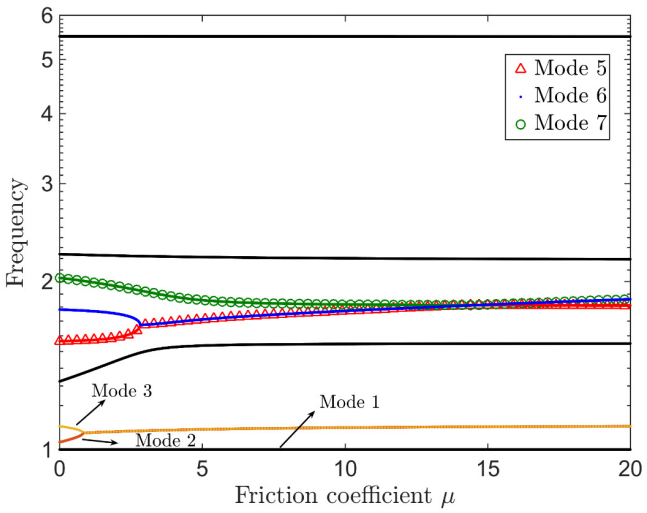

(b)

Fig. 6.4 The evolution of the real (Growth rate) and imaginary (Frequency) part of the eigenvalues with the friction coefficient. (a) The change of the real part; (b) The change of the imaginary part

From the above analysis, it can be seen that the substructure strategy not only can be realised in specific systems, but also offers the exact solutions if all the modes of the substructures are used.

6.3.4.3 *Model reduction*

In the following, the reductions on the 9-degree-of-freedom model are carried out, and the characteristics of the eigenvalues of the reduced models are analysed and compared with the results of the full model. The first reduced model (reduced model 1) is obtained by using the first three modes of the upper slider system and 2 modes of the lower belt system. The natural frequencies of reduced model 1 with μ=1 are listed in Table 6.4.

Table 6.4 Natural frequencies of reduced model 1 (rad/s)

Mode number	1	2	3	4	5
Frequency	1	1.0795	1.0795	1.4529	2.1606

Apparently, reduced model 1 only has 5 modes. By comparing with the results of the full model in Table 6.3, it can be clearly identified that the first three natural frequencies of reduced model 1 are very close to the corresponding results of the full model. However, the correlations of the 4th and 5th modes to the modes of the full model are poor. In the following, the change of the eigenvalues of reduced model 1 with the friction coefficient is examined, illustrated in Fig. 6.5. The black dots represent the results of the full model (original model), and the coloured lines are for the results of reduced model 1.

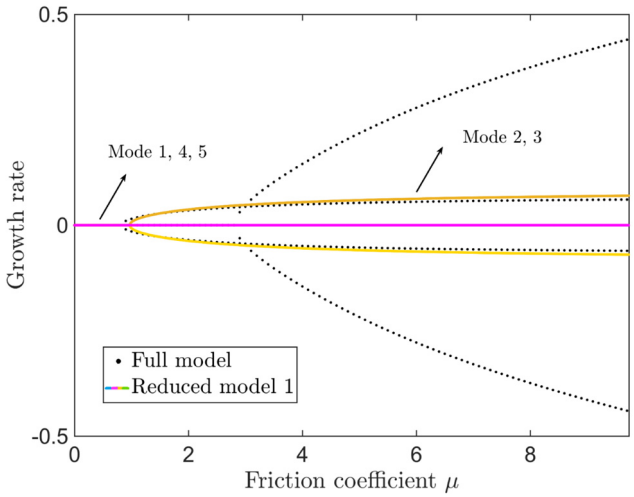

(a)

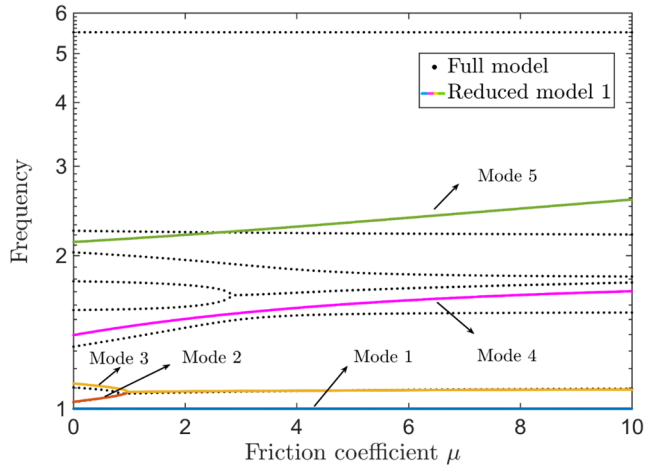

(b)

Fig. 6.5 The evolution of the real (Growth rate) and imaginary (Frequency) part of the eigenvalues with the friction coefficient. (a) The change of the real part; (b) The change of the imaginary part

It can be seen that, reduced model 1 is able to simulate the first stability bifurcation of the system (mode coupling between the 2nd and 3rd mode), and the critical friction coefficient at the bifurcation point is very close to the value of the full model. The comparison plot of the changes of the frequencies, in Fig. 6.5 (b), show that the values and also the variation trend of natural frequencies with μ of the first three modes of reduced model 1 are nearly identical to the results of the full model. Furthermore, it can be known that the 4th mode of reduced model 1 (pink line) actually corresponds to the 4th mode of the original system, but the correlation of the fifth mode of it to the full system has not very clearly been shown.

Furthermore, the eigenvalues of another reduced model (reduced model 2) with 4 slider modes and 2 belt modes are examined. The natural frequencies of reduced model 2 with μ=1 are listed in Table 6.5, which have a better accuracy than the reduced model 1 as it is expected to be.

Table 6.5 Natural frequencies of the reduced model 2 (rad/s)

Mode number	1	2	3	4	5	6
Frequency	1	1.0796	1.0796	1.4624	1.5596	2.1245

The bifurcation plot of the eigenvalues of reduced model 2 against the friction coefficient is shown in Fig. 6.6. Reduced model 2 is able to predict all the bifurcations of the full model, of which the first mode coupling is nearly the same as that of the full model, and the tendency of the second (4th and 5th mode) and the third (5th and 6th mode) mode couplings are similar to those of the full model. Moreover, the critical friction coefficients of the second and third mode couplings of the reduced model are smaller than the critical values of the full model, which over-estimate the instability, but tend to be safe.

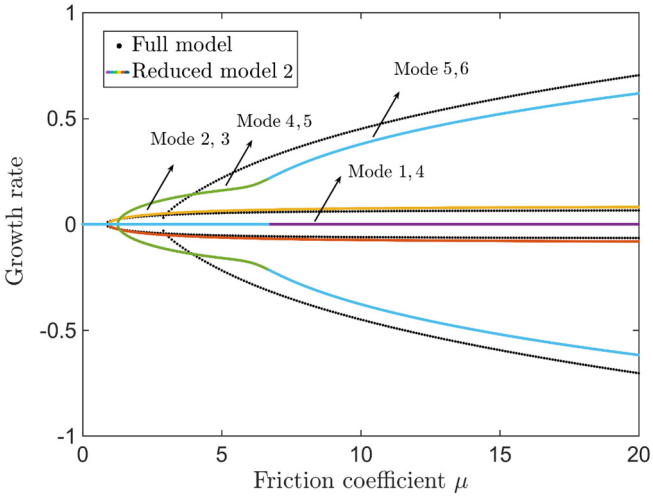

(a)

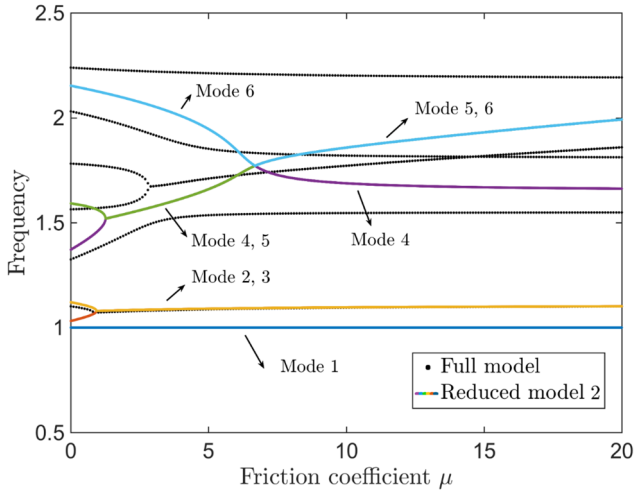

(b)

Fig. 6.6 The evolution of the real (Growth rate) and imaginary (Frequency) part of the eigenvalues with the friction coefficient. (a) The change of the real part (b) The change of the imaginary part

6.3.5 Numerical analysis: Case 2

By considering the fact that the mass of the belt is larger than the mass of the slider, constraints in the belt system are stiffer than the ones in the slider system and the contact stiffness should be also larger than the elastic constraints in the system in real applications, some of the parameter values in the preceding numerical analysis are adjusted, which change to: m=2, k_{12}=k_{13}=2, k_{c1}=k_{c2}=5.

There are several combinations of the modes of the slider and belt system that can be used in the reduced model. In the following, the analysis of two reduced models is carried out: reduced model 1 consists of 3 slider modes and 2 belt modes; reduced model 2 is assembled by 4 slider modes and 2 belt modes. Table 6.6 shows the natural frequencies of the reduced models and the full model when friction coefficient μ=1. Apparently, the results of the model with full modes calculated by the substructure strategy are identical to what are calculated by the direct method, in addition the difference between the lower frequencies of the reduced models and the full model is very small, which is coincident with the finding in previous subsection 6.3.4.

Table 6.6 comparisons between the reduced models and full model (rad/s)

Mode	Direct method	Substructure strategy		
	Full model	Full model (6+3)	Reduced model 1 (3+2)	Reduced model 2 (4+2)
1	1.0896	1.0896	1.0867	1.0893
2	1.1459	1.1459	1.1770	1.176
3	1.2247	1.2247	1.2247	1.2247
4	1.5088	1.5088	2.217	1.5715
5	1.5883	1.5883	3.357	2.2335
6	2.0938	2.0938	×	3.2473
7	2.0938	2.0938	×	×
8	3.4352	3.4352	×	×
9	6.4159	6.4159	×	×

The performance of reduced models 1 and 2 on simulating the changes of the eigenvalues of the system with the friction coefficient is investigated, which are shown in Figs. 6.7 and 6.8 respectively. With the increase of the friction coefficient, the first coalescence of the frequencies is between the 5th and the 6th mode at μ=0.4, and then the second one is between the 1st and the 2nd mode at μ=1.35. Fig. 6.7 (b) shows that reduced model 1 is only capable of predicting the second coalescence between the 1st

and 2nd modes and with a quite accurate unstable frequency, but the critical friction coefficient for the coalescence is larger than the exact value. Except the natural frequencies of the first two modes, frequencies of the other modes of the recued model are not very accurate.

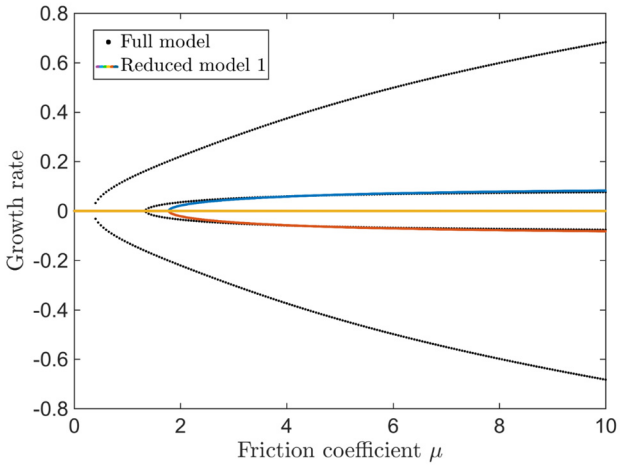

(a)

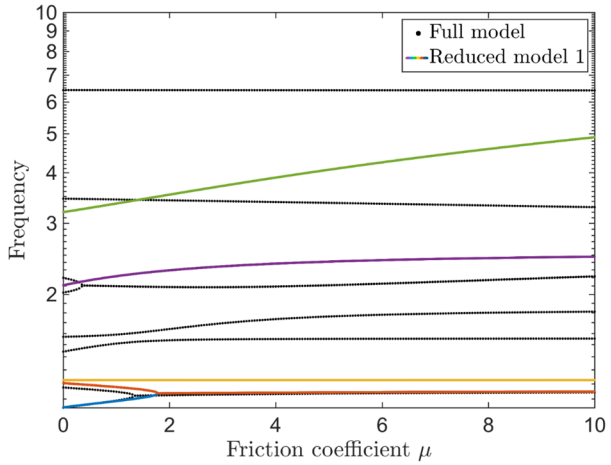

(b)

Fig. 6.7 The evolution of the real (Growth rate) and imaginary (Frequency) part of the eigenvalues with the friction coefficient. (a) the change of the real part; (b) the change of the imaginary part

As to reduced model 2 which contains 4 slider modes and 2 belt modes, shown in Fig. 6.8, it can simulate all the mode coupling instabilities of the original system (full model). The frequencies of the first three modes of reduced model 2 are very close to

the corresponding frequencies of the full model. However, the first mode coupling predicted by reduced model 2 is still about the 1st and 2nd modes, and the second mode coupling is not very accurate in terms of the critical friction coefficient and the unstable frequency value. As a whole, reduced model 2 maintains the instability characteristics of the full model and can predict the quite accurate frequencies of the lower modes. Moreover, for this 9-degree-of-freedom system, the smallest reduced model that can predict all the bifurcations of the full system should contain at least 4 slider modes and 2 belt modes.

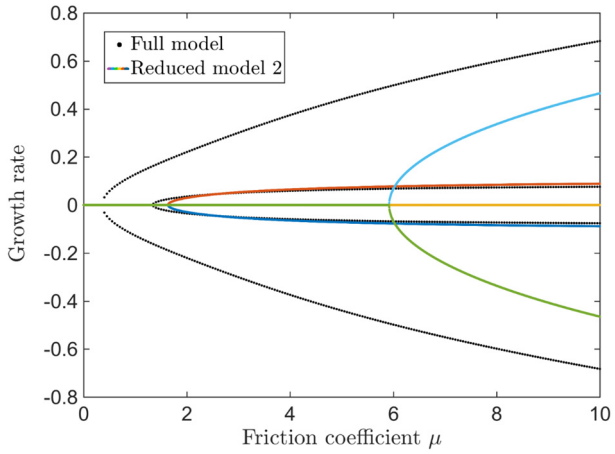

(a)

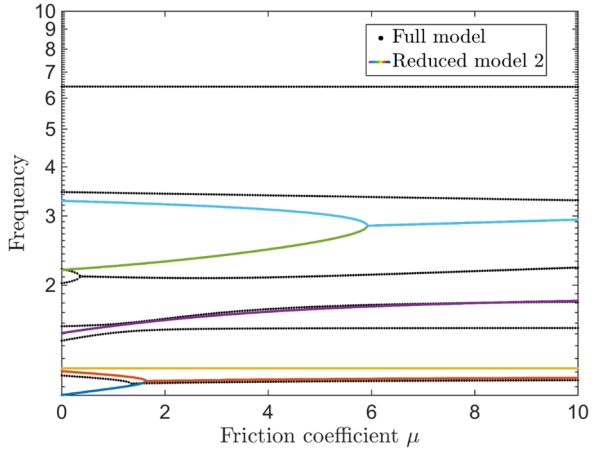

(b)

Fig. 6.8 The evolution of the real (Growth rate) and imaginary (Frequency) part of the eigenvalues with the friction coefficient. (a) the change of the real part; (b) the change of the imaginary part

6.4 Application to the system with rigid motion in the substructure

As in some of the systems like car brakes, the slider part may allow rigid motion. For example, brake pads are pushed into contact with the disc via hydraulic pressure in a car disc brake. If only the pads and the disc are included in a simplified theoretical model, the pads must be allowed to have rigid motion. The main purpose of this section is to verify the feasibility of the proposed strategy on the system with rigid-body motion in the substructures. The system used is similar to the 9-degree-of-freedom system but without spring k_9 and k_{10}, so mass m_3 of the slider is free in the vertical direction. In the numerical calculations $k_9 = k_{10} = 0$, and other parameter values are the same as the ones used in Section 6.3.4. The natural frequencies of the upper slider part are shown in Table 6.7, which has a rigid body mode whose natural frequency is zero. The frequencies of the lower belt part are the same as the belt model in Section 6.3.4.

Table 6.7 The natural frequency of the 6-degree-of-freedom slider part

ω_{p1}	ω_{p2}	ω_{p3}	ω_{p4}	ω_{p5}	ω_{p5}
0	1	1	1.4142	1.7321	2

Based on the modal analysis results of the substructures, the substructure strategy described in Section 6.2 is implemented. The results of different reduced models and the results calculated by the direct method are shown in Table 6.8.

Table 6.8 Comparisons of the natural frequency ($\mu = 1$)

Mode	Direct method	Substructure strategy			
	Full model	Full model (6+3)	Reduced model 1 (3+2)	Reduced model 2 (4+2)	Reduced model 3 (3+3)
1	0.7605	0.7605	0.8001	0.8001	0.7619
2	1	1	1	1	1
3	1	1	1	1	1

4	1.1243	1.1243	1.1839	1.1839	1.1434
5	1.1243	1.1243	2.1114	1.4142	2.1111
6	1.748	1.748	×	2.1114	5.4913
7	2	2	×	×	×
8	2.2111	2.2111	×	×	×
9	5.4966	5.4966	×	×	×

From Table 6.8, it can be seen that the model with all the modes of the slider and belt have identical natural frequency results of the direct method. Moreover, the reduced models can provide good enough lower mode frequencies. It is hard to tell the correspondence between the higher mode of the reduced model with that of the full model. To summarise, it can be proved that the reduction strategy can be directly applied in the eigenvalue analysis of the frictional systems which involves rigid-body motion in the substructure.

6.5 Applications to a pad-on-disc system with experimental results

In this section, a laboratory test rig with a pad sliding on a rotating disc and the corresponding complicated finite element model built in Abaqus are introduced. Such a test structure is a typical testing machine configuration in tribology research. The experimental and Abaqus results are provided by collaborators (Miss Xiaocui Wang and Mr Qi Zhang in Southwest Jiaotong University (SWJTU)) and the permission is given to use them in this research work by their supervisors Prof Mo Jiliang. The student (Zilin Li) also participated in part of the experiments and Abaqus simulations.

There are two goals in this section: (1) Model reduction of this real complicated pad-disc system is carried out using the reduction strategy proposed in Section 6.2 and comparison between the CEA results of the reduced model and the full FE model is made to further validate the model reduction strategy; (2) The theoretical CEA results are validated with experimental results of vibration frequencies of the test rig.

Because the test system and its FE model belong to that SWJTU research group and their research work is still going on, only a limited amount of experimental results and

numerical results are made available to be used in this PhD project. Nonetheless it is believed that these results provided by SWJTU are sufficient to show the model reduction method presented in this chapter is correct and efficient.

6.5.1 Description of the test rig of the pad-on-disc system

Fig. 6.9 shows the schematic of the experimental set-up for testing the friction-induced vibration of the pad-on-disc system, which contains two parts (an upper pad part and a lower disc part).

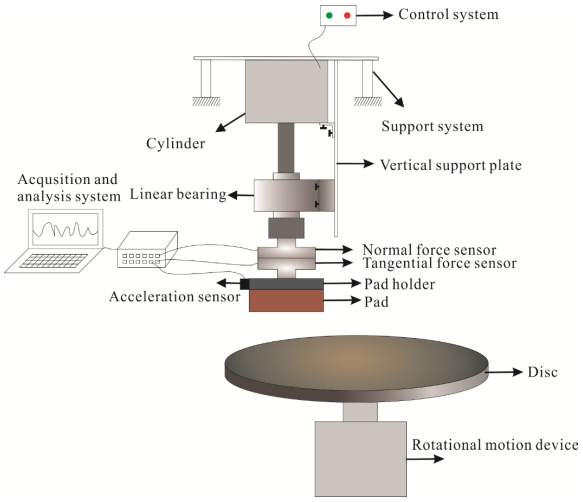

Fig. 6.9 The schematic of the experimental set-up

The pad is a friction material specimen and fixed to the upper holder. The upper holder consists of several components. An acceleration sensor is attached to the pad support, and a tangential force sensor and a normal force sensor are integrated in the holder. The horizontal motion of the upper hold machine is constrained by a linear bearing. The top of the holder is a vertical hydraulic cylinder which can generate the vertical compression force to the pad. For the disc part, the central area of the disc is held by two holders on both sides of the disc by bolts and fixed to a shaft. The upper part can move in the vertical direction controlled by hydraulic pressure in the cylinder and the disc can rotate at a constant speed.

An impact hammer modal test was carried out on the upper part and the lower part of the test rig separately, and on the whole test rig in stationary conditions (the disc is at rest). The test results are shown in Fig. 6.10 (a)-(c).

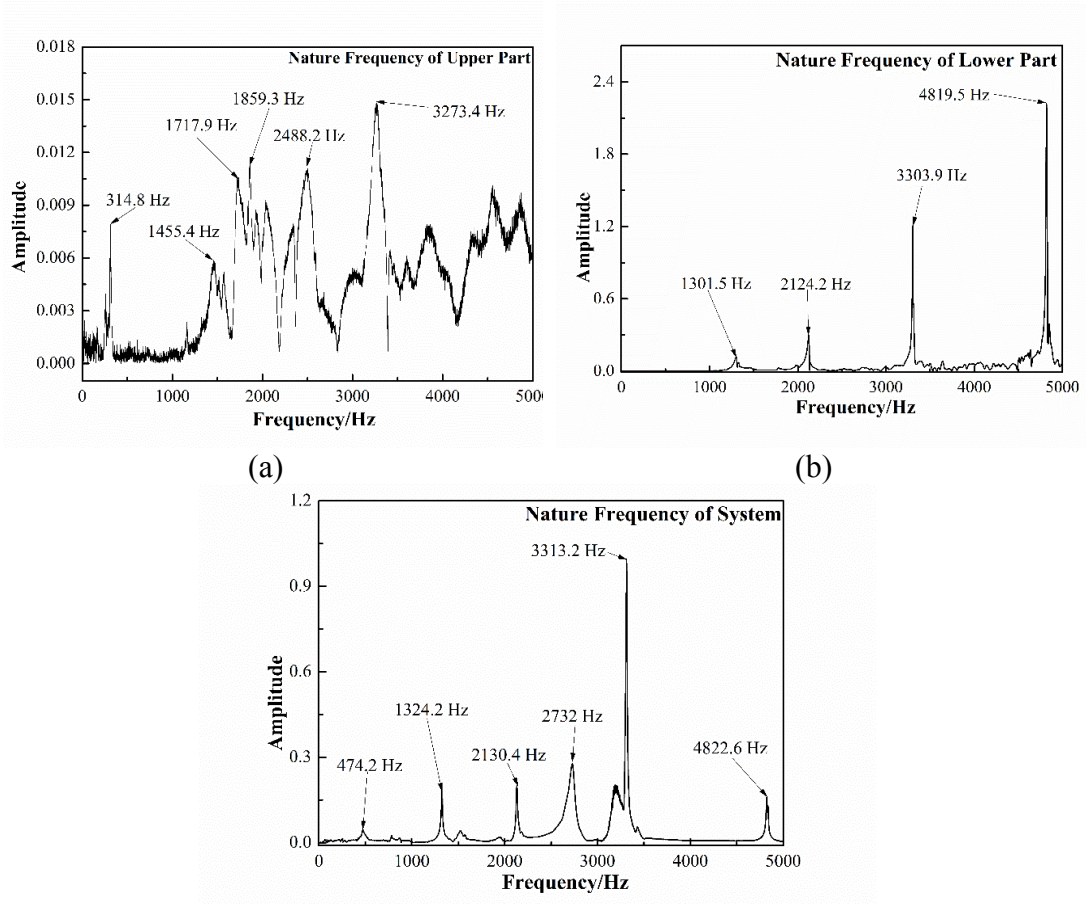

Fig. 6.10 Test results of the acceleration PSD in dB scale (the unit is $(m/s^2)^2/Hz$) of the test rig. (a) The upper part; (b) The lower part; (c) The whole machine

Furthermore, the vibration signals of the test rig from the above-mentioned three sensors, when the pad was under compression force of 500 N and the rotating speed of the disc was at 13 rad/s, were recorded. During the sliding motion, the horizontal vibration of the pad is excited, and the measured vibration frequency at the low frequency range is 492 Hz and the vibration frequency at the high frequency range is 1705Hz. The measured friction coefficient of the pad is in the range of 0.3 to 0.4.

6.5.2 Description of the finite element model

Fig. 6.11 shows the finite element model of the pad-on-disc system which is referred to as the original system with respect to the reduced model in the next few sub-sections. It includes the key components of the real test rig. In this model, the surface of pad is directly in contact with the surface of the disc, and there are 274 identical numbers of the contact node on both interface of the pad and disc. The whole model is built in a rectangular coordinate system. The boundary conditions of the upper part are: the upper surface of the spring holder is fixed in x and z direction and free in vertical y direction, and the surface of the holes of the bearing bracket plate is fixed in the y direction and elastically constrained in the x and z directions; the boundary condition of the lower part are: the inner surfaces of the disc holder and the disc are clamped in three perpendicular directions. The element type is 3-dimensional solid element and the total element number of the system is 121,864 (the degrees of freedom in total are 904,968).

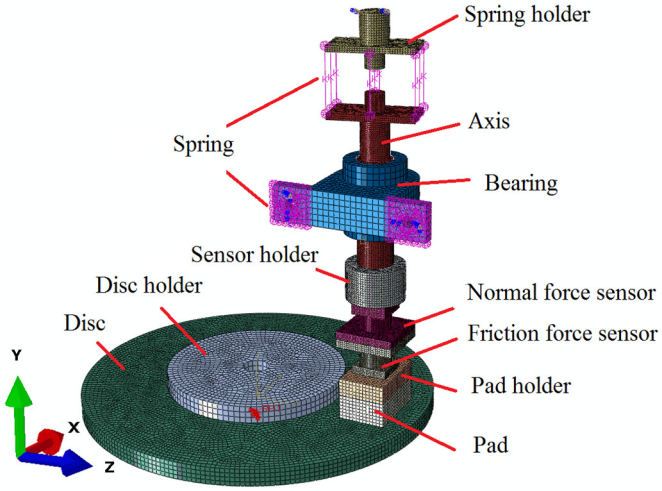

Fig. 6.11 Finite element model of the test machine

As model reduction is carried out on the base of this finite element model, verifying the correlation between the finite element model and the test rig is very important. To do this, both of the natural frequencies of each substructure (the upper part and the lower part) having the same boundary conditions but being free at the interface, and

the natural frequencies of the full model are computed by Abaqus. They are compared with measured frequencies, which indicates that there is a good correlation of the finite element model with the testing machine, shown in Table 6.9.

Table 6.9 The fundamental frequencies (Hz) by Abaqus and the modal test

	Test	Abaqus	Error
Upper part	314.8	331.44	5.02%
Lower part	1301.5	1300.6	0.07%
Whole system	474.2	510.91	7.58%

6.5.3 Reduction of the pad-on-disc system and stability analysis

To implement the model reduction on this pad-on-disc system, three kinds of information are required from Abaqus:

(1) Natural frequencies of the upper part and the lower part, denoted by ω_{p} and ω_{d} in Eqs. (6.4) and (6.5), when their contact interfaces are free.
(2) The mode shape components in the interface DoFs of the pad and disc, which are $\boldsymbol{\Phi}_{\mathrm{p}}^{u}$, $\boldsymbol{\Phi}_{\mathrm{p}}^{w}$, $\boldsymbol{\Phi}_{\mathrm{p}}^{o}$, $\boldsymbol{\Phi}_{\mathrm{d}}^{u}$, $\boldsymbol{\Phi}_{\mathrm{d}}^{w}$ and $\boldsymbol{\Phi}_{\mathrm{d}}^{o}$ in Eq. (6.14).
(3) The coordinates of the nodes on the contact interface between the pad and the disc.

6.5.3.1 *Contact stiffness in the reduced model*

As the contact in the model reduction method is described as linear springs/dampers between the nodes on the interface of the pad and disc, which cannot be identified directly from the finite element model, the surface properties must be determined by means of correlation between the reduced model and the full FE model. As the individual upper part has rigid motion in the vertical direction, there is a rigid body mode with zero natural frequency of the upper substructure. The applicability of the reduction method to systems with rigid body mode has been verified in Section 6.4. Thus, the reduction strategy is directly used here.

Firstly, a proper contact stiffness is identified by adjusting the contact stiffness value in the model reduction method to obtain a reduced model whose natural frequencies are very close to those of the full FE model computed by Abaqus, when the system is stationary. The natural frequencies of the stationary full FE model are calculated without considering friction, so the friction coefficient in the reduction process of a stationary system is zero. The specific procedure is illustrated in Fig. 6.12.

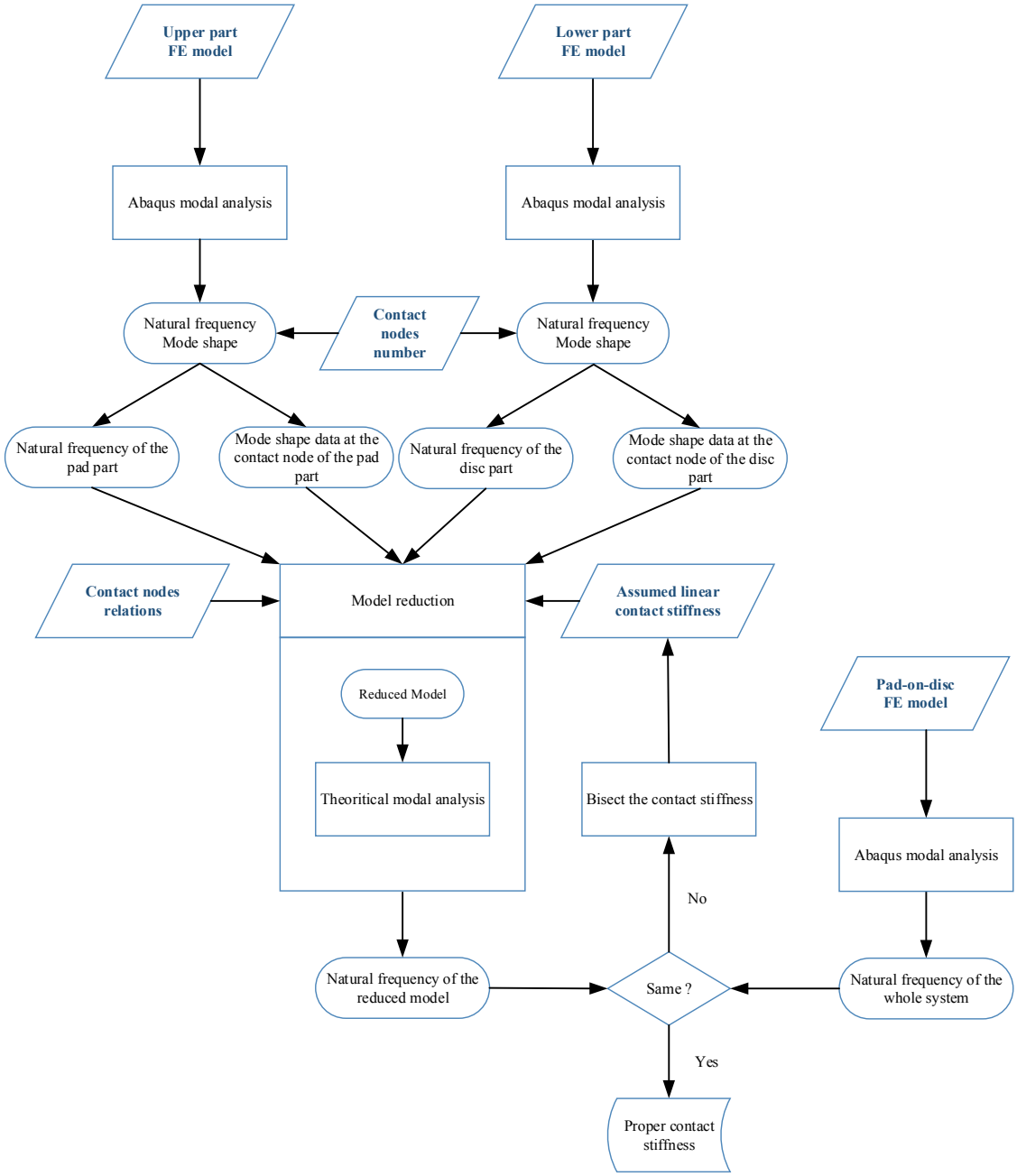

Fig. 6.12 The flow chart of calculating the contact stiffness

Natural frequencies of the four reduced models in stationary (without friction) state with linear contact springs are investigated, in which reduced model 1 (RM 1), reduced model 2 (RM 2), reduced model 3 (RM 3) and reduced model 4 (RM 4) are composed of 10 modes , 40 modes, 80 modes and 245 modes of each of the substructures (the upper part and lower part), respectively. Fig. 6.13 shows the influence of the contact stiffness on the natural frequencies of RM 2 (40 pad modes + 40 disc modes). The vertical coordinate is the error between the natural frequencies of the reduced model and the full FE model, and zero means the results of the two models are identical. It shows that when the value of the contact stiffness is in a proper level, natural frequencies of the system are not very sensitive to the change of the contact stiffness. The results of RM 1, 3 and 4 are similar to these of RM 2 and thus are not shown here for the sake of simplicity.

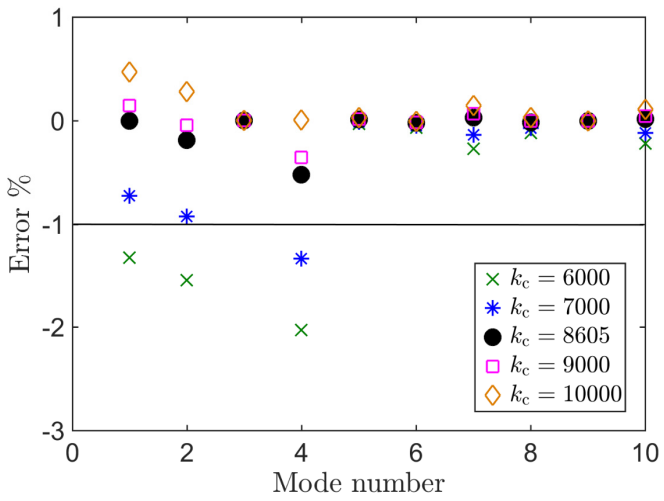

Fig. 6.13 The errors of the natural frequencies of the reduced model with different contact stiffness with respect to the full FE model

It is found that when the system is reduced, the contact stiffness for different reduced models is different. The proper contact stiffness for RM 1, 2, 3 and 4, which makes the natural frequencies of the corresponding reduced model very close to the ones of the full FE model, are 3684, 8605 (black round mark in Fig. 6.13), 10970 and 12510 N/m respectively. Table 6.10 shows the first 18 natural frequencies of the four reduced models and those calculated by Abaqus modal analysis. The error between the reduced

model and the full model of a real structure can be very small which indicates that the reduction strategy with the assumption of linear contact springs works well on predicting the natural frequencies of the real structure when it is stationary even when only 10+10 substructure modes are used.

Table 6.10 Comparisons between the natural frequencies (Hz) of the FE model and reduced models

Mode	FE model	RM 1 (error%)	RM 2 (error%)	RM 3 (error%)	RM 4 (error%)
1	510.91	510.88 (-0.003)	510.9 (-0.0005)	510.89 (-0.002)	510.908 (0.001)
2	550.79	544.86 (-1.08)	549.74 (-0.19)	553.48 (0.49)	552.01 (0.22)
3	759.54	759.54 (0)	759.54 (0)	759.54 (0)	759.54 (0)
4	1027.5	1033.42 (0.57)	1022.2 (-0.52)	1028.7 (0.12)	1026.8 (-0.07)
5	1306.7	1305.97 (-0.05)	1306.9 (0.01)	1307.2 (0.04)	1306.8 (0.008)
6	1383.8	1384.5 (0.05)	1383.5 (-0.02)	1383.7 (-0.006)	1383.7 (-0.009)
7	1469.8	1468.8 (-0.06)	1470.2 (0.03)	1470.7 (0.06)	1470 (0.01)
8	1517.1	1516.1 (-0.06)	1516.9 (-0.01)	1517.9 (0.05)	1518 (0.06)
9	1593.4	1593.5 ($-3*10^{-5}$)	1593.5 ($-3*10^{-5}$)	1593.5 ($-3*10^{-5}$)	1593.4 (0)
10	1643.1	1642.1 (-0.06)	1643.4 (0.01)	1644.7 (0.1)	1643.4 (0.02)

11	1687	1686.5 (-0.03)	1686.8 (-0.01)	1687.2 (0.007)	1687.1 (0.0005)
12	1837.7	1837.6 (-0.006)	1837.6 (-0.008)	1838.1 (0.02)	1837.9 (0.009)
13	2163.3	2162.1 (-0.05)	2161.9 (-0.06)	2165.8 (0.12)	2166.1 (0.13)
14	2256.6	2248.7 (-0.35)	2259 (0.1)	2262.6 (0.26)	2257.7 (0.04)
15	2466.1	2472.5 (0.26)	2465.8 (-0.01)	2466.4 (0.01)	2466.3 (0.006)
16	2975.4	3061.2 (2.88)	2961.9 (-0.45)	3004.3 (0.96)	2988.3 (0.43)
17	3161.2	3222.6 (1.93)	3156.1 (-0.16)	3166.9 (0.18)	3167.2 (0.19)
18	3255.8	3255.6 (-0.009)	3259.9 (0.12)	3264.1 (0.25)	3257.8 (0.06)

6.5.3.2 *Stability analysis of the reduced model*

After obtaining the appropriate contact stiffness value, the friction force can be introduced in the theoretical reduction of the FE pad-on-disc model. In the following, the stability analysis of the reduced model with friction is carried out following the flow chart shown in Fig. 6.2. Specifically, the bifurcation of the eigenvalues of the reduced model with the change of the friction coefficient is examined, followed by comparing those results calculated by the Abaqus complex eigenvalue analysis of the full FE model.

Fig. 6.14 shows the changes of the real and imaginary parts of the eigenvalues of the reduced models with the friction coefficient. Firstly, it can be seen that with the increase of the friction coefficient, some of the real part of reduced models become positive, consequently mode-coupling kind of instability can happen in the system.

The first mode coupling is between the 1st and the 2nd modes and the second one is between the 6th and the 7th modes. Secondly, the results of the four reduced models (RM1, RM2, RM3 and RM4) are very similar, although the number of modes used in the model reduction are quite different (10+10, 40+40, 80+80, 245+245). It should be noted here that damping is not included in the CEA analyses of the reduced models and the full FE model.

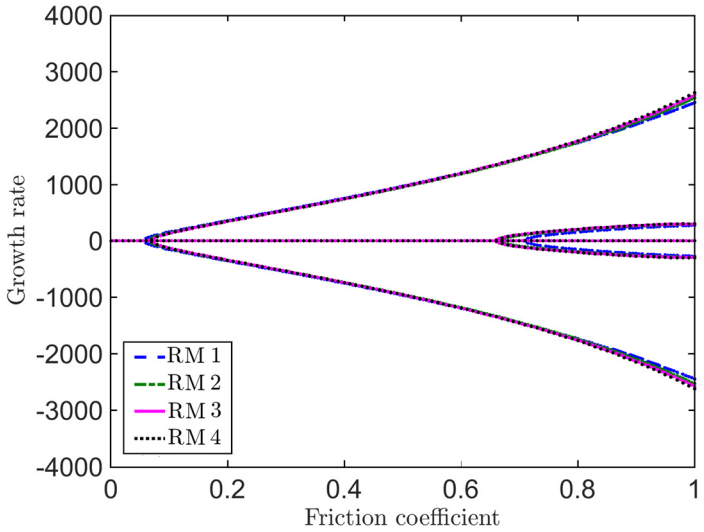

(a)

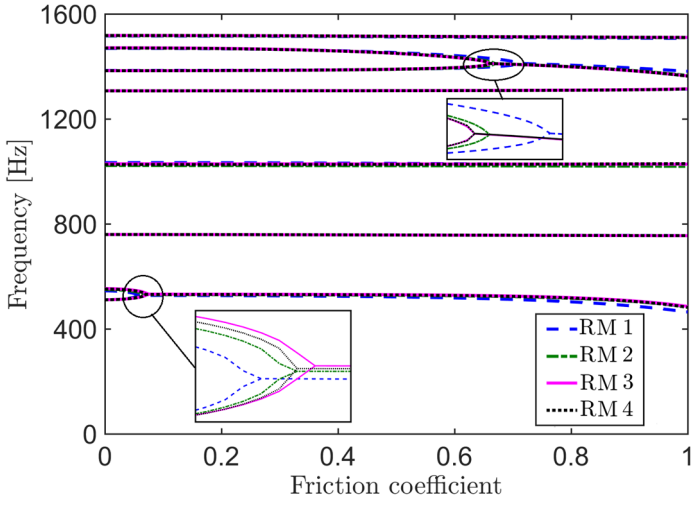

(b)

Fig. 6.14 The evolution of the real (Growth rate) and imaginary (Frequency) part of the eigenvalues of different reduced model with the friction coefficient. (a) The change of the real part (b) The change of the imaginary part

Moreover, Abaqus CEA of the full model is carried out for the real operation condition of the experiment, which is the normal compression force of 500N and the rotating speed at 13 rad/s. Fig. 6.15 illustrates the Abaqus CEA results of the full model. By comparing the results of the reduced models (Fig. 6.14(b)) with those in Fig. 6.15, it can found that the reduced models can capture the main mode-coupling instability phenomena of the whole system, which include: (1) the first coupling between the 1st and the 2nd modes and the second one between the 6th and the 7th modes, (2) the critical friction coefficient for the mode coupling in an acceptable error range, (3) a good enough unstable frequency range. Furthermore, as noise frequencies tested in the experiment are at 492 Hz (dominant) and 1705Hz, as reported in Section 6.5.1, and the unstable vibration frequencies of the reduced model are 531Hz and 1411.1 Hz (at the coalescing point of the frequency). The correlation between the reduced models and the experimental results is satisfactory.

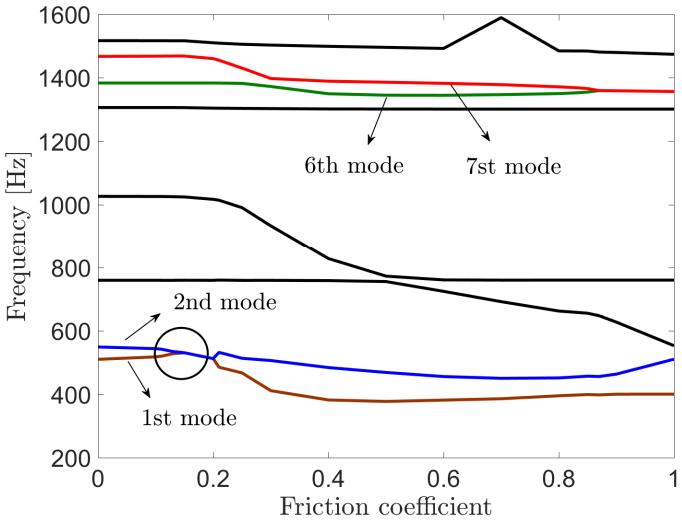

Fig. 6.15 Abaqus CEA results of the full model

On the other hand, it can be seen that some of the features of the bifurcation plot of the full model are not captured by the reduced model, such as the unlocking phenomenon of the coupling of the 1st and the 2nd mode, the decrease of the 3rd and the 4th mode with the friction coefficient, this may be due to several reasons. Two apparent reasons are that Abaqus CEA is a complex process which considers the disc-pad contact area which is influenced by the compression force and uses a particular surface-to-surface

contact algorithm, which are different from the conventional theoretical complex eigenvalue analysis implemented in the model reduction method presented in this chapter. However, the important unstable features of the real complex frictional system are reproduced at low cost.

The preceding results show that the reduction strategy of this chapter is applicable for the reduction of the complex real system with friction and the stability of the real frictional system can be implemented by the reduced model. Moreover, the reduced model is able to predict the key unstable features of the real structure, even when relatively very few modes of the substructures are used, which is verified by the CEA results of full EF model and the experimental results. With the validation, the advantages of the reduced model, in terms of the computational efficiency and applicability, are demonstrated and this model reduction method is very useful in the dynamic study of the friction-induced vibration of real structures. A further application of this method is in the dynamic transient analysis of nonlinear friction-induced vibration, which will not be covered within this project.

6.6 Conclusions

A model reduction strategy especially for the reduction of multi-degree-of-freedom system with substructures in friction contact is established. Its application to a 9-degree-of-freedom system as well as a real pad-on-disc structure is carried out. The 9-degree-of-freedom model are composed of a slider and belt substructures with linear contact springs. The real pad-on-disc test rig and the corresponding finite element model (FE model) are build up at a partner institution, and the correlation between them is established, which offers a trustworthy full FE model for the subsequent model reduction and ensures the dependability of the validation. The reduction strategy is shown to work well in the modal and stability analysis of the full model and agree well with the experiment.

The conclusions of the model reduction work are:

1. For the 9-degree-of-freedom model, the eigenvalues of the whole system with sliding friction calculated by the substructure method, when full modes are used, are exactly the same as the results calculated by using the mass and stiffness matrices of the whole model. Importantly, the mode-coupling properties of the frictional system can be kept in the reduced model if a proper number of substructure modes are used. A properly reduced model can reproduce frequencies of the lower modes at good accuracy. Moreover, depending on the parameter values, the reduced models may overestimate or underestimate the critical friction coefficient of the system, especially the critical friction coefficient of high modes.

2. The model reduction strategy can be directly applied to the frictional system in which the substructure has rigid-body motion.

3. A more specific strategy for the reduction of the real pad-on-disc structure of which the pad and disc are directly in contact is proposed. Reduction can be implemented by introducing imaginary linear contact springs between the contact nodes. Results show that the reduced model with a proper contact stiffness value, gives nearly the same natural frequencies of the full finite element model. Moreover, the stability analysis results of the reduced models have good agreement with the Abaqus CEA results of the full FE model, in terms of correctly predicting the mode-coupling of the system, even when relatively only a small number of modes of the substructures are used in model reduction. Furthermore, the unstable frequencies of the reduced models can be related to the noise frequencies measured in the experiment. Therefore, the reduction strategy is feasible, and the reduced models can be implemented in the analysis of the real structures with friction, with its own advantages at the computational efficiency and low demand of modal information of the substructures.

The current work is a preliminary step for subsequent study of the friction-induced vibration of complicated systems with stick-slip, separation or complex dynamic friction forces, and the results are promising. Further work to introduce complicated friction characteristics in dynamic analysis of frictional systems is one future task beyond this PhD project.

7 Conclusions and Outlooks

Friction is everywhere in our daily life as well as in engineering. It dissipates energy as a stabilising factor in many cases, but can also energise a system and thus become destabilizing, which cause a lot of engineering problems with unstable vibration and uncomfortable noises. To comprehensively understand friction-induced vibration problem has been a challenging target. In this PhD project, the mechanisms of friction-induced vibration in the dynamic point of view are studied in new mechanical models. Nonlinear/non-smooth vibration of both discrete and continuous frictional systems are analysed in detail. Moreover, the strategy for numerically simulating the non-smooth friction-induced vibration is proposed, which is implemented in MATLAB algorithms coded by the student. Furthermore, an idea on studying the friction-induced vibration of complicated friction systems rather than the idealised mechanical systems using model reduction is implemented in the final stage of the PhD project.

7.1 Conclusions

This research mainly focuses on the theoretical study of the complex nonlinear friction-induced vibration of a low-degree-of-freedom system and a continuous system, considering nonlinear/non-smooth phenomena such as stick-slip, separation and impact, which provides many interesting findings and gives insights to the non-smooth friction-induced vibration. Moreover, a preliminary study of complicated frictional structures, starting with the model reduction of the frictional system and followed by experimental validation, is carried out, which is essential to the future investigations of the friction-induced vibration or mechanisms of complicated frictional systems with non-smoothness/nonlinearities.

The main conclusions are as follows:

1. The mode-coupling instability of a nonlinear coupled system with dry friction is not only influenced by the friction coefficient but also highly depends on the nonlinear contact stiffness and the pre-compression force on the system. Adding certain combinations of the nonlinear contact stiffness and the pre-compression force can

stabilise an unstable linear system, which can be taken advantage of in the control of friction-induced vibration. On the transient vibration side, separation can happen during the unstable vibration, and it turns out that the pre-compression force and the nonlinear contact stiffness actually appear as destabilising factors. Ignoring the effect of separation is found to be unsafe and potentially predicts incorrect roles of the system parameters. Importantly, separation should be taken into account in nonlinear friction-induced vibration.

2. The vibration of a nonlinear system with both the mode-coupling instability, stick-slip and separation can be very complicated. The critical friction coefficient is not only an important indicator for the stability bifurcation, but also determines the dynamic behaviour in cooperation with the static and kinetic friction coefficients when stick-slip is considered.

3. Both the vertical unstable vibration of the disc and separation can be generated by the excitations from the horizontal stick-slip motion of a rotating slider system on the disc, even in a low rotating speed range. The dynamic behaviour of the system considering separation is completely different from the case that contact is assumed to be maintained during the vibration. Coulomb friction can result in stable vibration, periodic vibration and quasi-periodic vibration which is a route to chaos. Furthermore, the vibration frequencies of the unstable system with stick-slip and separation are time varying. Especially, high frequencies can arise due to separation.

4. Model reduction of complicated systems with dry friction which cover a theoretical multi-degree-of-freedom system with linear contact stiffness and a real pad-on-disc structure with a direct contact interface is carried out based on a mode synthesis method put forward by the student. Through comparison with predicted results of the full model and with the experimental results, the reduced-order model, even though a small number of modes of the corresponding substructures are used, is shown to be capable of predicting the friction-induced mode-coupling instability, accurate natural frequencies of the first several modes of the original systems, and importantly the unstable frequencies of the full model and the vibration frequencies measured in the

test, all at acceptable accuracy. These findings provide a promising foundation for nonlinear dynamic analysis of complicated frictional systems at low cost in the future.

7.2 Original contributions

1. A nonlinear 2-degree-of-freedom slider-on-moving-belt frictional model is proposed based on the linear 2-degree-of-freedom model put forward by Hoffmann in which a cubic nonlinear contact spring is introduced, loss of contact (separation) at the slider-belt interface is allowed and importantly reattachment of the slider to the belt after separation is also considered. Through complex eigenvalue analysis, the complex effects of the nonlinear contact stiffness and the pre-load on the stability of the system are identified which can be exploited in control of friction-induced vibration. The roles of separation, the nonlinear contact stiffness and the pre-load in the unstable friction-induced vibration are revealed through transient dynamic analysis. It is found that ignoring separation may underestimate the vibration magnitude, and produce incorrect vibration frequencies and importantly incorrect contributions of other parameters to the system, and thus considering separation is very important in the study of friction induced vibration. By introducing the non-smooth Coulomb's law of friction at the frictional interface of the nonlinear system, the combined effects of two kinds of non-smoothness (stick-slip, and separation and reattachment) and a cubic nonlinear contact stiffness in the dynamic behaviour of the 2-DoF system are examined, in which both the mode-coupling instability and stick-slip instability may occur. The complexity of the nonlinear/non-smooth friction-induced vibration is revealed.

2. Separation, reattachment and the subsequent impact that may occur due to nonstationary friction-induced vibration are taken into account in a rotating elastic slider-on-disc model. Theoretical formulations of the model considering stick-slip, and separation and reattachment, and an algorithm for calculating the non-smooth and discontinuous vibration of the frictional system are developed. Numerical simulations show that unstable transverse vibration of the disc can be excited by the horizontal stick-slip of the slider at a very low rotating speed, which is accompanied by intermittent separation between the disc and slider for very short time durations. By

comparing the Poincare maps of the cases of considering and ignoring separation, the important role of separation and the roles of the key parameters of the system on the nonlinear vibration considering separation are demonstrated. Moreover, the time-varying nature of the vibration frequencies of the disc-slider model with non-smooth dry friction is revealed by the time-frequency analysis. It is found that separation between the slider and the disc is responsible for high-frequency vibration of the system.

3. A model reduction strategy for complicated frictional systems are put forward, which is particularly useful in cases when the mass and stiffness matrices of the components (substructures) are not available or only a small amount of modal information of the substructures are provided. Firstly, the correctness of the reduction method and the feasibility of the reduced model in the stability analysis is verified on a theoretical multi-degree-of-freedom frictional system. Moreover, the reduction of a real pad-on-disc structure is carried out with experiment validation. It is found that the reduced model with 80 modes of each substructure can already correctly predict the mode-coupling instability of the full FE model (having over 900000 DoFs) of the real structure, and predict fairly well unstable frequencies that correspond to the unstable frequencies calculated by Abaqus CEA and the vibration frequencies measured in the test, which demonstrates that the work load can be largely reduced by the reduced model with a good enough accuracy. This work indicates that the proposed model reduction method can be promisingly applied to the study of nonlinear/non-smooth friction-induced vibration of complicated frictional systems or real structures.

7.3 Outlook

Six lines of work may be interesting and worth implementing for some scopes of future work:

1. To consider the follower force characteristic of the friction force in the work of the elastic plate excited by a moving slider system considering separation to carry out further explorations in terms of the complicated effects of friction on the friction-induced vibration. The frictional follower force changes direction while the disc is bent,

which results in a transverse component [129], and the contact force on the surface of the disc and slider, which is P when the follower force effect is not considered, becomes:

$$F_{\text{contact}} = P - F_{\text{r}} \frac{\partial w}{r_0 \partial \theta}$$

in which $F_{\text{r}} \frac{\partial w}{r_0 \partial \theta}$ the transverse component of the friction follower force. Then, with the new formulations, this work can be implemented.

2. To use a more complex and realistic friction law, for example the rate/state-dependent friction models, which has been reviewed in Section 2.4.2.

3. To implement the model reduction idea that has been validated on the FE model of a real structure (Chapter 6) involving nonlinear factors such as stick-slip, separation and contact nonlinearities. The improvements on the current reduction strategy to achieve higher precision would be explored. For considering non-smooth effects like stick-slip with Coulomb's law of friction, the friction forces on the contact points of the substructures are written as the following form during the corresponding motion state.

$$\mathbf{f}_{\text{r}} = \begin{cases} \mu_{\text{s}} \left[\mathbf{n} + \mathbf{C}_{\text{c}} \left(\boldsymbol{\Phi}_{\text{d}}^{w} \dot{\mathbf{q}}_{\text{d}} - \boldsymbol{\Phi}_{\text{p}}^{w} \dot{\mathbf{q}}_{\text{p}} \right) + \mathbf{K}_{\text{c}} \left(\boldsymbol{\Phi}_{\text{d}}^{w} \mathbf{q}_{\text{d}} - \boldsymbol{\Phi}_{\text{p}}^{w} \mathbf{q}_{\text{p}} \right) \right] & \text{stick motion} \\ \mu_{\text{d}} \left[\mathbf{n} + \mathbf{C}_{\text{c}} \left(\boldsymbol{\Phi}_{\text{d}}^{w} \dot{\mathbf{q}}_{\text{d}} - \boldsymbol{\Phi}_{\text{p}}^{w} \dot{\mathbf{q}}_{\text{p}} \right) + \mathbf{K}_{\text{c}} \left(\boldsymbol{\Phi}_{\text{d}}^{w} \mathbf{q}_{\text{d}} - \boldsymbol{\Phi}_{\text{p}}^{w} \mathbf{q}_{\text{p}} \right) \right] & \text{slip motion} \end{cases}$$

in which the specific definitions of the symbols can refer to Chapter 6.

Then with considering loss of contact in the system with multiple contacts, the contact state of the system is very complex. Therefore, the aim of this work is to reduce the computational work load of the dynamic analysis of the complicated system, and then to reveal nonlinear/non-smooth effects in the friction-induced vibration of a real structure.

4. To carry out the reduction of a complicated finite element model of a real test structure with an improved reduction technique. A laboratory test-rig and a

corresponding finite element model have been build up. The testing results will provide supports for future model reduction work on a real frictional structure. This new work is a collaboration with some colleagues in the Tribology Research Institute of Southwest Jiaotong University, China. Tests are still going on at the partners' site. A joint paper will be written later.

In Chapter 5, a slider is dragged around a stationary disc and its dynamic behaviour is studied. There are similar applications in engineering in which a disc is spinning past a stationary structure. One example is computer hard disc drives. For a spinning disc, the centrifugal force need to be involved in the theoretical formulations of the system [266]. Thus the gyroscopic effect can be examined [267]. So one future research topic is the study of the friction-induced vibration of a spinning disc with the action of a stationary slider considering gyroscopic effect, stick-slip and loss of contact.

6. Friction is well known to possess uncertain properties. Uncertainty analysis of friction-induced vibration is a well concerned and challenging research topic. Some work has been in the student’s research group, for example [268]. Introducing uncertainties and carrying out stochastic simulations on the base of the frictional system in the thesis with stochastic parameters [106] like friction coefficients or the rotating speed, are one of the future research topics.

References

[1] Bowden, F.P. and Leben, L., The nature of sliding and analysis of friction. Proceedings of Royal Society of London, 1939. A169: 371-391.

[2] Krim, J., Surface science and the atomic-scale origins of friction: What once was old is new again. Surface Science, 2002. 500(1): 741-758.

[3] Sinaer, I.L., Friction and energy dissipation at the atomic scale: A review. Journal of Vacuum Science and Technology A: Vacuum, Surfaces and Films, 1994. 12(5): 2605-2616.

[4] Festjens, H., Chevallier, G., and Dion, J.L. A numerical quasi-static method for the identification of frictional dissipation in bolted joints. in ASME International Design Engineering Technical Conferences and Computers and Information in Engineering Conference. 2012. Chicago.

[5] Sannino, A.P. and Rack, H.J., Dry sliding wear of discontinuously reinforced aluminum composites: Review and discussion. Wear, 1995. 189(1): 1-19.

[6] Cui, L., Geng, H., Wang, W., Chen, L., and Gao, J., Functionalization of multi-wall carbon nanotubes to reduce the coefficient of the friction and improve the wear resistance of multi-wall carbon nanotube/epoxy composites. Carbon, 2013. 54: 277-282.

[7] Flores, P., Ambrósio, J., Claro, J.C.P., Lankarani, H.M., and Koshy, C.S., A study on dynamics of mechanical systems including joints with clearance and lubrication. Mechanism and Machine Theory, 2006. 41(3): 247-261.

[8] Berger, E.J., Friction modeling for dynamic system simulation. Applied Mechanics Reviews, 2002. 55(6): 535-577.

[9] Ding, Q. and Zhai, H., The advance in researches of friction dynamics in mechanics system. Advances in Mechanics, 2013, 43(1): 112-131 (in Chinese).

[10] Akay, A., Acoustics of friction. The Journal of the Acoustical Society of America, 2002. 111(4): 1525-1548.

[11] Ibrahim, R.A., Friction-induced vibration, chatter, squeal, and chaos—part i: Mechanics of contact and friction. Applied Mechanics Reviews, 1994. 47(7): 209-226.

[12] Ibrahim, R.A., Friction-induced vibration, chatter, squeal, and chaos—part ii: Dynamics and modeling. Applied Mechanics Reviews, 1994. 47(7): 227-253.

[13] Wei, Y., Ma, C., and Feng, X., Mechanics in automotive engineering. Mechanics in Engineering, 2012, 34(4): 1-7 (in Chinese).

[14] Mills, H.R., *Brake squeak*, in *Technical report 9000 B*. 1938, Institution of Automobile Engineers.

[15] Fosberry, R.A.C. and Holubecki, Z., *Disc brake squeal : Its mechanism and suppression*. 1961, Lindley: Motor Industry Research Association.

[16] Sinclair, D. and Manville, N., Frictional vibrations. Journal of Applied Mechanics, Transactions of the ASME 1955. 22: 13-207.

[17] Oden, J.T. and Martins, J.A.C., Models and computational methods for dynamic friction phenomena. Computer Methods in Applied Mechanics and Engineering, 1985. 52(1): 527-634.

[18] Yuan, Y. A study of the effects of negative friction-speed slope on brake squeal. in Proceedings of the ASME Design Engineering Technical Conference. 1995. Boston.

[19] Ouyang, H., Mottershead, J.E., Cartmell, M.P., and Friswell, M.I., Friction-induced parametric resonances in discs: Effect of a negative friction-velocity relationship. Journal of Sound and Vibration, 1998. 209(2): 251-263.

[20] Chen, G. and Zhou, Z., Correlation of a negative friction–velocity slope with squeal generation under reciprocating sliding conditions. Wear, 2003. 255(1–6): 376-384.

[21] Ouyang, H., Mottershead, J.E., Cartmell, M.P., and Friswell, M.I., Friction-induced parametric resonances in discs: Effect of a negtive friction–velocity relationship. Journal of Sound and Vibration, 1998. 209(2): 251-264.

[22] Eriksson, M., & Jacobson, S., Friction behaviour and squeal generation of disc brakes at low speeds. Proceedings of the Institution of Mechanical Engineers, 2001. 215(12): 1245.

[23] Kinkaid, N.M., O'Reilly, O.M., and Papadopoulos, P., Automotive disc brake squeal. Journal of Sound and Vibration, 2003. 267(1): 105-166.

[24] Brecht, J., Hoffrichter, W., and Dohle, A., Mechanisms of brake creep groan. SAE Technical Paper 973026, 1997.

[25] Abdelhamid, M.K., Creep-groan of disc brakes. SAE Paper 951282, 1995.

[26] Leine, R.I., van Campen, D.H., and Keultjes, W.J.G., Stick-slip whirl interaction in drillstring dynamics. Journal of Vibration and Acoustics, 2002. 124(2): 209-220.

[27] Divenyi, S., Savi, M.A., Wiercigroch, M., and Pavlovskaia, E., Drill-string vibration analysis using non-smooth dynamics approach. Nonlinear Dynamics, 2012. 70(2): 1017-1035.

[28] Brace, W.F., Laboratory studies of stick-slip and their application to earthquakes. Tectonophysics, 1972. 14(3): 189-200.

[29] Byerlee, J.D., The mechanics of stick-slip. Tectonophysics, 1970. 9(5): 475-486.

[30] Tonazzi, D., Massi, F., Culla, A., Baillet, L., Fregolent, A., and Berthier, Y., Instability scenarios between elastic media under frictional contact. Mechanical Systems and Signal Processing, 2013. 40(2): 754-766.

[31] Morgan, F., Musjat, M., and Reed, D.W., Friction phenomena and the stick-slip process. Journal of Applied Physics, 1941. 12(10): 743-752.

[32] Brockley, C.A., Cameron, R., and Potter, A.F., Friction-induced vibration. Journal of Lubrication Technology, 1967. 89(2): 101-107.

[33] Martins, J.A.C., Oden, J.T., and Simões, F.M.F., A study of static and kinetic friction. International Journal of Engineering Science, 1990. 28(1): 29-92.

[34] Gao, C., Kuhlmann-Wilsdorf, D., and Makel, D.D., The dynamic analysis of stick-slip motion. Wear, 1994. 173(1): 1-12.

[35] Gao, C. and Kuhlmann-Wilsdorf, D., On stick-slip and the velocity dependence of friction at low speeds. Journal of Tribology, 1990. 112(2): 354-360.

[36] Brockley, C.A. and Ko, P.L., Quasi-harmonic friction-induced vibration. Journal of Lubrication Technology, 1970. 92(4): 550-556.

[37] Anderson, J.R. and Ferri, A.A., Behavior of a single-degree-of-freedom system with a generalized friction law. Journal of Sound and Vibration, 1990. 140(2): 287-304.

[38] Rabinowicz, E., The intrinsic variables affecting the stick-slip process. Proceedings of the Physical Society, 1958. 71(4): 668.

[39] Pontes, B.R., Oliveira, V.A., and Balthazar, J.M., On friction-driven vibrations in a mass block–belt–motor system with a limited power supply. Journal of Sound and Vibration, 2000. 234(4): 713-723.

[40] Berman, A.D., Ducker, W.A., and Israelachvili, J.N., Origin and characterization of different stick−slip friction mechanisms. Langmuir, 1996. 12(19): 4559-4563.

[41] Thomsen, J.J. and Fidlin, A., Analytical approximations for stick–slip vibration amplitudes. International Journal of Non-Linear Mechanics, 2003. 38(3): 389-403.

[42] Elmer, F.J., Nonlinear dynamics of dry friction. Journal of Physics A, 1997. **30**: 6057-6063.

[43] Hetzler, H., Schwarzer, D., and Seemann, W., Analytical investigation of steady-state stability and hopf-bifurcations occurring in sliding friction oscillators with application to low-frequency disc brake noise. Communications in Nonlinear Science and Numerical Simulation, 2007. 12(1): 83-99.

[44] Kang, J., Krousgrill, C.M., and Sadeghi, F., Oscillation pattern of stick–slip vibrations. International Journal of Non-Linear Mechanics, 2009. 44: 820-828.

[45] Pascal, M., Sticking and nonsticking orbits for a two-degree-of-freedom oscillator excited by dry friction and harmonic loading. Nonlinear Dynamics, 2014. 77(1-2): 267-276.

[46] Popp, K. and Stelter, P., Stick-slip vibrations and chaos. Philosophical Transactions of the Royal Society A: Mathematical, Physical and Engineering Sciences, 1990. 332(1624): 89-105.

[47] Galvanetto, U., Some discontinuous in a two-block stick-slip system. Journal of Sound and Vibration, 2001. 248(4): 653-669.

[48] Leine, R.I. and van Campen, D.H., Bifurcation phenomena in non-smooth dynamical systems. European Journal of Mechanics - A/Solids, 2006. 25(4): 595-616.

[49] Dankowicz, H. and Nordmark, A.B., On the origin and bifurcations of stick-slip oscillations. Physica D: Nonlinear Phenomena, 2000. 136(3): 280-302.

[50] Oestreich, M., Hinrichs, N., and Popp, K., Bifurcation and stability analysis for a non-smooth friction oscillator. Archive of Applied Mechanics, 1996. 66(5): 301-314.

[51] Yang, F., Zhang, W., and Wang, J., Sliding bifurcations and chaos induced by dry friction in a braking system. Chaos, Solitons & Fractals, 2009. 40(3): 1060-1075.

[52] Li, Q., Yan, Y., Wei, L., and Qin, Z., Complex bifurcations in a nonlinear system of moving belt. Acta Physica Sinica, 2013, 62(12): 120505 (in Chinese).

[53] North, N.R., Disc brake squeal. Proceedings of the Institution of Mechanical Engineers, 1976. C38/76: pp.169–176.

[54] Duffour, P. and Woodhouse, J., Instability of systems with a frictional point contact. Part 1: Basic modelling. Journal of Sound and Vibration, 2004. 271: 365-390.

[55] Tuchinda, A., Hoffmann, N., Ewins, D., and Keiper, W. Mode lock-in characteristics and instability study of the pin-on-disc system. in IMAC-XIX: A Conference on Structural Dynamics. 2001.

[56] Ostermeyer, G.P. and Graf, M., Mode coupling instabilities induced by a periodic coefficient of friction. SAE Int. J. Passeng. Cars – Mech. Syst., 2010. 3(2): 31-37.

[57] Hoffmann, N. and Gaul, L., Effects of damping on mode-coupling instability in friction induced oscillations. Zamm, 2003. 83(8): 524-534.

[58] Hoffmann, N., Fischer, M., Allgaier, R., and Gaul, L., A minimal model for studying properties of the mode-coupling type instability in friction induced oscillations. Mechanics Research Communications, 2002. 29(4): 197-205.

[59] Chen, F., Chern, J., and Swayze, J., Modal coupling and its effect on brake squeal. SAE Technical Paper 2002-01-0922, 2002.

[60] Flint, J. and Hultén, J., Lining-deformation-induced modal coupling as squeal generator in a distributed parameter disc brake model. Journal of Sound and Vibration, 2002. 254(1): 1-21.

[61] Sinou, J.J. and Jézéquel, L., Mode coupling instability in friction-induced vibrations and its dependency on system parameters including damping. European Journal of Mechanics - A/Solids, 2007. 26(1): 106-122.

[62] Meziane, A., Baillet, L., and Laulagnet, B., Experimental and numerical investigation of friction-induced vibration of a beam-on-beam in contact with friction. Applied Acoustics, 2010.

71(9): 843-853.

[63] Brunetti, J., Massi, F., Saulot, A., Renouf, M., and D'Ambrogio, W., System dynamic instabilities induced by sliding contact: A numerical analysis with experimental validation. Mechanical Systems and Signal Processing, 2015. 58: 70-86.

[64] Seo, Y., Yabuno, H., and Kono, G., Mode coupling-type instability of a beam subjected to coulomb friction. Journal of Vibration and Acoustics, 2013. 135(6): 064502-064502.

[65] Zhang, L., Miao, W., and Yu, Z., Experimental investigation into friction-vibration coupling characteristics of vehicle disc brake. Tribology, 2008, 28(5): 480-484 (in Chinese).

[66] Hultén, J. Drum brake squeal - a self-exciting mechanism with constant friction. in ASME Design Engineering Technical Conferences. 1993. Sacrameto,CA: ASME Paper DETC97/VIB-4161.

[67] Hultén, J. Friction phenomena related to drum brake squeal instabilities. in In: SAE Truck and Bus Meeting. 1997. Detroit, Mi, USA.

[68] Magnier, V., Brunel, J.-F., Duboc, M., and Dufrenoy, P. Influence of heterogeneous contact between disc and pad on the brake squeal noise. 2011. SAE International.

[69] Spurr, R.T., A theory of brake squeal. ARCHIVE: Proceedings of the Institution of Mechanical Engineers, Automobile Division 1947-1970, 1961. 1961(1961): 33-52.

[70] Sinou, J.J., Thouverez, F., and Jezequel, L., Analysis of friction and instability by the centre manifold theory for a non-linear sprag-slip model. Journal of Sound and Vibration, 2003. 265(3): 527-559.

[71] Jellett, J.H., *A treatise on the theory of friction*. 1872: Dublin : Hodges, Foster.

[72] Génot, F. and Brogliato, B., New results on painlevé paradoxes. European Journal of Mechanics - A/Solids, 1999. 18(4): 653-677.

[73] Stewart, D.E., Rigid-body dynamics with friction and impact. Society for Industrial and Applied Mathematics Review, 2000. 42(1): 3-39.

[74] Ballard, P. and Basseville, S., Existence and uniqueness for dynamical unilateral contact with coulomb friction: A model problem. ESAIM: Mathematical Modelling and Numerical Analysis, 2005. 39(1): 59-77.

[75] Charles, A. and Ballard, P., Existence and uniqueness of solutions to dynamical unilateral contact problems with coulomb friction: The case of a collection of points. ESAIM: Mathematical Modelling and Numerical Analysis, 2014. 48(1): 1-25.

[76] Leine, R.I., Brogliato, B., and Nijmeijer, H., Periodic motion and bifurcations induced by the painlevé paradox. European Journal of Mechanics - A/Solids, 2002. 21(5): 869-896.

[77] Champneys, A.R. and VÁRkonyi, P.L., The painlevé paradox in contact mechanics. IMA Journal of Applied Mathematics, 2016. 81(3): 538-588.

[78] Hoffmann, N. and Gaul, L., A sufficient criterion for the onset of sprag-slip oscillations. Archive of Applied Mechanics (Ingenieur Archiv), 2004. 73(9-10): 650-660.

[79] Keitzel, H. and Hoffmann, N., Influence of the contact model on the onset of sprag - slip. Proceedings in Applied Mathematics and Mechanics, 2006. 6(1): 311-312.

[80] Kang, J. and Krousgrill, C.M., The onset of friction-induced vibration and spragging. Journal of Sound and Vibration, 2010. 329(17): 3537-3549.

[81] Pilipchuk, V.N. and Tan, C.A., Creep—slip capture as a possible source of squeal during decelerated sliding. Nonlinear Dynamics, 2004. 35(3): 259-285.

[82] Chan, S.N., Mottershead, J.E., and Cartmell, M.P., Parametric resonances at subcritical speeds in discs with rotating frictional loads. Proceedings of the Institution of Mechanical Engineers, Part C: Journal of Mechanical Engineering Science, 1994. 208(6): 417-425.

[83] Ouyang, H., Mottershead, J., Brookfield, D., James, S. et al., Dynamic instabilities in a simple model of a car disc brake. SAE Technical Paper 1999-01-3409, 1999.

[84] Tseng, J.G. and Wickert, J.A., Nonconservative stability of a friction loaded disk. Journal of Vibration and Acoustics, 1998. 120(4): 922-929.

[85] Ono, K., Chen, J.S., and Bogy, D.B., Stability analysis for the head-disk interface in a flexible disk drive. Journal of Applied Mechanics, 1991. 58(4): 1005-1014.

[86] Mottershead, J.E., Vibration and friction-induced instability in disks. The Shock and vibration digest, 1998. 30(1): 14-31.

[87] Chan, S.N., Mottershead, J.E., and Cartmell, M.P., Instabilities at subcritical speeds in discs with rotating frictional follower loads. Journal of Vibration and Acoustics, Transactions of the ASME, 1995. 117(2): 240-242.

[88] Mottershead, J.E. and Chan, S.N., Flutter instability of circular discs with frictional follower loads. Journal of Vibration and Acoustics, 1995. 117(1): 161-163.

[89] Ouyang, H., Mottershead, J.E., and Li, W., A moving-load model for disc-brake stability analysis. Journal of Vibration and Acoustics, Transactions of the ASME, 2003. 125(1): 53-58.

[90] Jarvis, R.P. and Mills, B., Vibrations induced by dry friction. Proceedings of the Institution of Mechanical Engineers, 1963. 178(1): 847-857.

[91] Ouyang, H. and Mottershead, J.E., Dynamic instability of an elastic disk under the action of a rotating friction couple. Journal of Applied Mechanics, 2005. 71(6): 753-758.

[92] Kinkaid, N.M., O'Reilly, O.M., and Papadopoulos, P., On the transient dynamics of a multi-degree-of-freedom friction oscillator: A new mechanism for disc brake noise. Journal of Sound and Vibration, 2005. 287(4–5): 901-917.

[93] Chen, G., Zhou, Z., Philippe, K., and Leo, V., Effect of surface topography on formation of squeal under reciprocating sliding. Wear, 2002. 253: 411-423.

[94] Chen, G. and Zhou, Z., A self-excited vibration model based on special elastic vibration modes of friction systems and time delays between the normal and friction forces: A new mechanism for squealing noise. Wear, 2007. 262(9–10): 1123-1139.

[95] Chen, G., Liu, Q., Jin, X., and Zhou, Z., Stability analysis of a squealing vibration model with time delay. Journal of Sound and Vibration, 2008. 311(1–2): 516-536.

[96] Millner, N., An analysis of disc brake squeal. SAE Technical Paper 780332, 1978.

[97] Nishiwaki, M., Generalized theory of brake noise. Proceedings of the Institution of Mechanical Engineers, 1993. D 207: 195-202.

[98] Andreaus, U. and Casini, P., Dynamics of friction oscillators excited by a moving base and/or driving force. Journal of Sound and Vibration, 2001. 245(4): 685-699.

[99] Shin, K., Brennan, M.J., Oh, J.E., and Harris, C.J., Analysis of disc brake noise using a two-degree-of-freedom model. Journal of Sound and Vibration, 2002. 254(5): 837-848.

[100] Andreaus, U. and Casini, P., Friction oscillator excited by moving base and colliding with a rigid or deformable obstacle. International Journal of Non-Linear Mechanics, 2002. 37(1): 117-133.

[101] Hoffmann, N. and Gaul, L., Effects of damping on mode-coupling instability in friction induced oscillations. ZAMM - Journal of Applied Mathematics and Mechanics / Zeitschrift für Angewandte Mathematik und Mechanik, 2003. 83(8): 524-534.

[102] Li, Y. and Feng, Z., Bifurcation and chaos in friction-induced vibration. Communications in Nonlinear Science and Numerical Simulation, 2004. 9(6): 633-647.

[103] Luo, A.C.J. and Thapa, S., Periodic motions in a simplified brake system with a periodic excitation. Communications in Nonlinear Science and Numerical Simulation, 2009. 14(5):

2389-2414.

[104] Meng, D., Zhang, L., and Yu, Z., Analysis of disc brake judder using multipoint contact dynamic model. Journal of Vibration, Measurement & Diagnosis, 2010, 30(3): 304-309 (in Chinese).

[105] Lima, R. and Sampaio, R., Construction of a statistical model for the dynamics of a base-driven stick-slip oscillator. Mechanical Systems and Signal Processing, 2017. 91: 157-166.

[106] Kang, W.S., Choi, C.K., and Yoo, H.H., Stochastic modeling of friction force and vibration analysis of a mechanical system using the model. Journal of Mechanical Science and Technology, 2015. 29(9): 3645-3652.

[107] Kim, W.J. and Perkins, N.C., Harmonic balance/galerkin method for non-smooth dynamic systems. Journal of Sound and Vibration, 2003. 261(2): 213-224.

[108] Giné, J., On the determination of the limit cycles using the harmonic balance method. Journal of Mathematical Physics, 2013. 54(10): -.

[109] Yang, S. and Guo, S., Two-stop-two-slip motions of a dry friction oscillator. Science China Technological Sciences, 2010. 53(3): 623.

[110] Luo, A.C.J., A theory for non-smooth dynamic systems on the connectable domains. Communications in Nonlinear Science and Numerical Simulation, 2005. 10(1): 1-55.

[111] Luo, A.C.J. and Gegg, B.C., Stick and non-stick periodic motions in periodically forced oscillators with dry friction. Journal of Sound and Vibration, 2006. 291(1–2): 132-168.

[112] Luo, A.C.J. and Gegg, B.C., On the mechanism of stick and nonstick, periodic motions in a periodically forced, linear oscillator with dry friction. Journal of Vibration and Acoustics, Transactions of the ASME, 2006. 128(1): 97-105.

[113] Brunetti, J., Massi, F., D'Ambrogio, W., and Berthier, Y., Dynamic and energy analysis of frictional contact instabilities on a lumped system. Meccanica, 2015. 50(3): 633-647.

[114] Li, Z., Cao, Q., and Léger, A., The complicated bifurcation of an archetypal self-excited sd oscillator with dry friction. Nonlinear Dynamics, 2017. 89(1): 91-106.

[115] Earles, S.W.E. and Lee, C.K., Instabilities arising from the frictional interaction of a pin-disk system resulting in noise generation. Journal of Engineering for Industry, 1976. 98(1): 81-86.

[116] Earles, S.W.E. and Badi, M.N.M., Oscillatory instabilities generated in a double-pin and disc undamped system: A mechanism of disc-cbrake squeal. Proceedings of the Institution of Mechanical Engineers, Part C: Journal of Mechanical Engineering Science, 1984. 198: 143-50.

[117] Earles, S.W.E. and Chambers, P.W., Disc brake squeal noise generation: Predicting its dependency on system papameters including damping. International Journal of Vehicle Design, 1987. 8(4-6): 538-552.

[118] Tworzydlo, W.W., Hamzeh, O.N., Zaton, W., and Judek, T.J., Friction-induced oscillations of a pin-on-disk slider: Analytical and experimental studies. Wear, 1999. 236(1–2): 9-23.

[119] Emira, M.N.A., Friction-induced oscillations of a slider: Parametric study of some system parameters. Journal of Sound and Vibration, 2007. 300(3–5): 916-931.

[120] Awrejcewicz, J. and Delfs, J., Dynamics of a self-excited stick-slip oscillator with two degrees of freedom. Part i. Investigation of equilibria. European Journal Mech. A/Solids. 9: 269-282.

[121] von Wagner, U., Hochlenert, D., and Hagedorn, P., Minimal models for disk brake squeal. Journal of Sound and Vibration, 2007. 302(3): 527-539.

[122] Yang, F. and Zhang, W., Nonlinear dynamical analysis for a disc braking system. Journal of Vibration and Shock, 2009, 28(6): 93-94 (in Chinese).

[123] Bengisu, M.T. and Akay, A., Stability of friction-induced vibrations in multi-degree-of-

freedom systems. Journal of Sound and Vibration, 1994. 171(4): 557-570.

[124] Rusli, M. and Okuma, M., Effect of surface topography on mode-coupling model of dry contact sliding systems. Journal of Sound and Vibration, 2007. 308(3–5): 721-734.

[125] Butlin, T. and Woodhouse, J., Friction-induced vibration: Should low-order models be believed? Journal of Sound and Vibration, 2009. 328(1-2): 92-108.

[126] Hochlenert, D., Spelsberg-Korspeter, G., and Hagedorn, P., Friction induced vibrations in moving continua and their application to brake squeal. Journal of Applied Mechanics, Transactions ASME, 2007. 74(3): 542-549.

[127] Shen, I.Y., Response of a stationary, damped, circular plate under a rotating slider bearing system. Journal of Vibration and Acoustics, 1993. 115(1): 65-69.

[128] Mottershead, J.E., Ouyang, H., Cartmell, M.P., and Friswell, M.I., Parametric resonances in an annular disc, with a rotating system of distributed mass and elasticity; and the effects of friction and damping. Proceedings of the Royal Society of London A: Mathematical, Physical and Engineering Sciences, 1997. 453(1956): 1-19.

[129] Mottershead, J.E., Vibration and friction-induced instability in discs. The Shock and vibration digest, 1998. 30(1): 14-31.

[130] Ouyang, H., Mottershead, J.E., Cartmell, M.P., and Brookfield, D.J., Friction-induced vibration of an elastic slider on a vibrating disc. International Journal of Mechanical Sciences, 1999. 41(3): 325-336.

[131] Lee, D. and Waas, A.M., Stability analysis of a rotating multi-layer annular plate with a stationary frictional follower load. International Journal of Mechanical Sciences, 1997. 39(10): 1117-1138.

[132] Giannini, O. and Sestieri, A., Predictive model of squeal noise occurring on a laboratory brake. Journal of Sound and Vibration, 2006. 296: 583-601.

[133] Spelsberg-Korspeter, G., Hochlenert, D., Kirillov, O.N., and Hagedorn, P., In- and out-of-plane vibrations of a rotating plate with frictional contact: Investigations on squeal phenomena. Journal of Applied Mechanics, 2009. 76(4): 041006-041006-15.

[134] Hochlenert, D., Nonlinear stability analysis of a disk brake model. Nonlinear Dynamics, 2009. 58(1-2): 63-73.

[135] Kang, J., Krousgrill, C.M., and Sadeghi, F., Wave pattern motion and stick–slip limit cycle oscillation of a disc brake. Journal of Sound and Vibration, 2009. 325: 552-564.

[136] Sinou, J.J., Transient non-linear dynamic analysis of automotive disc brake squeal – on the need to consider both stability and non-linear analysis. Mechanics Research Communications, 2010. 37(1): 96-105.

[137] Liles, G., Analysis of disc brake squeal using finite element methods. SAE Technical Paper 891150, 1989.

[138] Cao, Q., Ouyang, H., Mottershead, J.E., and Friswell, M.I., Linear eigenvalue analysis of the disc-brake squeal problem. International Journal for Numerical Methods in Engineering, 2004. 61(9): 1546-1563.

[139] Liu, P., Zheng, H., Cai, C., Wang, Y.Y., Lu, C., Ang, K.H., and Liu, G.R., Analysis of disc brake squeal using the complex eigenvalue method. Applied Acoustics, 2007. 68(6): 603-615.

[140] Dai, Y. and Lim, T.C., Suppression of brake squeal noise applying finite element brake and pad model enhanced by spectral-based assurance criteria. Applied Acoustics, 2008. 69(3): 196-214.

[141] Kang, J., Krousgrill, C.M., and Sadeghi, F., Comprehensive stability analysis of disc brake vibrations including gyroscopic, negative friction slope and mode-coupling mechanisms. Journal of Sound and Vibration, 2009. 324(1-2): 387-407.

[142] Kang, J., Squeal analysis of gyroscopic disc brake system based on finite element method. International Journal of Mechanical Sciences, 2009. 51: 284-294.

[143] Wei, J., Sun, Y., Wang, S., and Zhou, P., Research on brake squeal based on abaqus. Machinery Design & Manufacture, 2016(6): 151-154 (in Chinese).

[144] Blaschke, P., Tan, M., and Wang, A., On the analysis of brake squeal propensity using finite element method. SAE Technical Paper 2000-01-2765, 2000.

[145] Meziane, A., D'Errico, S., Baillet, L., and Laulagnet, B., Instabilities generated by friction in a pad–disc system during the braking process. Tribology International, 2007. 40(7): 1127-1136.

[146] Matsuzaki, M.a.I., T., Brake noise caused by longitudinal vibration of the disc rotor. SAE Technical Paper 930804, 1993.

[147] Kang, J., Finite element modelling for the investigation of in-plane modes and damping shims in disc brake squeal. Journal of Sound and Vibration, 2012. 331(9): 2190-2202.

[148] Chen, Y., Cao, D., and Wu, Z., Recent developments in nonlinear dynamics: Theory and its applications in mechanical systems. Journal of Astronautics, 2007 28(4): 794-804 (in Chinese).

[149] Cao, Q., Zhang, T., and Li, J., A study of the static and global bifurcations for duffing equation. Applied Mathematics and Mechanics, 1999, 20(12): 1309-1316 (in Chinese).

[150] Cao, Q., Wiercigroch, M., Pavlovskaia, E.E., Grebogi, C., and Thompson, J.M., Archetypal oscillator for smooth and discontinuous dynamics. Physical Review E Statistical Nonlinear & Soft Matter Physics, 2006. 74(2): 046218.

[151] Cao, Q., Tian, R., and Han, Y., Investigations of nonlinear dynamics for sd oscillator. Journal of Shijiazhuang Tiedao University (Natural Science), 2010, 23(2): 32-37 (in Chinese).

[152] Barber, J.R. and Ciavarella, M., Contact mechanics. International Journal of Solids and Structures, 2000. 37(1): 29-43.

[153] D'Souza, A.F. and Dweib, A.H., Self-excited vibrations induced by dry friction, part 2: Stability and limit-cycle analysis. Journal of Sound and Vibration, 1990. 137(2): 177-190.

[154] Ouyang, H., Baeza, L., and Hu, S., A receptance-based method for predicting latent roots and critical points in friction-induced vibration problems of asymmetric systems. Journal of Sound and Vibration, 2009. 321(3–5): 1058-1068.

[155] Sinou, J.J., Thouverez, F., and Jézéquel, L., Methods to reduce non-linear mechanical systems for instability computation. Archives of Computational Methods in Engineering, 2004. 11(3): 257-344.

[156] Soobbarayen, K., Sinou, J.J., and Besset, S., Numerical study of friction-induced instability and acoustic radiation – effect of ramp loading on the squeal propensity for a simplified brake model. Journal of Sound and Vibration, 2014. 333(21): 5475-5493.

[157] Hu, H., Advances in dynamics of piecewise-smooth mechanical systems. Journal of Vibration Engineering, 1995, 8(4): 331-341 (in Chinese).

[158] Leine, R. and Nijmeijer, H., *Dynamics and bifurcations of non-smooth mechanical systems*. 2004, Berlin Heidelberg: Springer-Verlag. 236.

[159] Li, C. and Zhang, W., Kenetic analysis of non-smooth after the synchronous straight bevel gears with clearance being locked. Journal of Dynamics and Control, 2015, 13(6): 437-442 (in.

[160] Cao, D., Chu, s., Li, Z., and Liu, R., Study on the non-smooth mechanical models and dynamics for space deployable mechanisms. Chinese Journal of Theoretical and Applied Mechanics, 45(1): 3-15 (in Chinese).

[161] Yuan, H., Wen, b., and LI, H., Bifurcation and chaos behavior of nonlinear local rubbing rotor. Journal of Northeastern University (Natural Science), 2000, 21(6): 610-613 (in Chinese).

[162] Ding, Q. and Chen, Y., Non-stationary analysis of rotor/casing rubbing. Journal of Aerospace

Power, 2000, 15(2): 191-195 (in Chinese).

[163] Chu, F., Zhang, Z., and Feng, G., Chaotic behavior of a rub rotor model. Journal of Tsinghua University, 1996, 30(7): 52-57 (in Chinese).

[164] Zhang, Y., Ding, W., and Sun, C., Bifurcation and chaos of one degree of freedom impact vibration system with clearance and dry friction. Journal of Vibration and Shock, 2008, 27(7): 102-105 (in Chinese).

[165] Zhang, S. and Lu, Q., A non-smooth analysis to the rub-impacting rotor system. ACTA Mechanica Sinica, 2000, 32(1): 59-69 (in Chinese).

[166] Jiang, J. and Chen, Y., Advances in the research on nonlinear phenomona in rotor/stator rubbing systems. Advances in Mechanics, 2013, 43(1): 132-148 (in Chinese).

[167] Ding, W. and Xie, J., Advances of research on bifurcations and chaos in vibro-impact system. Advanced in Mechanics, 2005, 35(4): 513-524 (in Chinese).

[168] Liu, C., Chen, B., and Wang, Y., The point-surface impact model considering the friction effect in flexible multi-body system. Mechanical Engineering, 2000, 11(6): 616-619 (in Chinese).

[169] Urbakh, M., Klafter, J., Gourdon, D., and Israelachvili, J., The nonlinear nature of friction. Nature, 2004. 430(6999): 525-528.

[170] Bowden, F.P. and Tabor, D., The friction and lubrication of solids. Science, 1951. 113(2938): 443-444.

[171] Sextro, W., *Contact model*, in *Dynamical contact problems with friction: Models, methods, experiments and applications*. 2007, Springer: Berlin, Heidelberg. p. 31-79.

[172] Baumberger, T. and Caroli, C., Solid friction from stick-slip down to pinning and aging. Advances in Physics, 2006. 55(3-4): 279-348.

[173] Popov, V.L., *Contact mechanics and friction: Physical principles and applications*. English ed. 2010, Heidelberg: Springer.

[174] Lee, J.H., Sheng, G., and Chang, J.Y., Micro-tribological interface model for friction-induced cold start-up running dynamics. Microsystem Technologies, 2012. 18(9): 1469-1479.

[175] Bowden, F.P. and Tabor, D., *The friction and lubrication of solids*. Vol. 113. 1951: New York: Oxford University Press.

[176] Greenwood, J.A. and Williamson, J.B.P., Contact of nominally flat surfaces. Proceedings of the Royal Society of London A: Mathematical, Physical and Engineering Sciences, 1966. 295(1442): 300-319.

[177] Bhushan, B., *Introduction to tribology*. 2nd ed. 2013, Hoboken: John Wiley & Sons Inc.

[178] Armstrong-Hélouvry, B., Dupont, P., and Canudas de Wit, C., A survey of models, analysis tools and compensation methods for the control of machines with friction. Automatica, 1994. 30(7): 1083-1138.

[179] Threlfall, D.C., The inclusion of coulomb friction in mechanisms programs with particular reference to dram au programme dram. Mechanism and Machine Theory, 1978. 13(4): 475-483.

[180] Duan, C. and Singh, R., Dynamics of a 3dof torsional system with a dry friction controlled path. Journal of Sound and Vibration, 2006. 289(4–5): 657-688.

[181] Dieterich, J.H., Time-dependent friction and the mechanics of stick-slip. Pure and Applied Geophysics, 1978. 116(4): 790-806.

[182] Ruina, A., Slip instability and state variable friction laws. Journal of Geophysical Research: Solid Earth, 1983. 88(B12): 10359-10370.

[183] Rice, J.R. and Ruina, A.L., Stability of steady frictional slipping. Journal of Applied Mechanics,

1983. 50(2): 343-349.

[184] Dupont, P.E. and Bapna, D., Stability of sliding frictional surfaces with varying normal force. Journal of Vibration and Acoustics, 1994. 116(2): 237-242.

[185] Scholz, C.H., Earthquakes and friction laws. Nature, 1998. 391(6662): 37-42.

[186] Dahl, P., *A solid friction model*. 1968, Aerospace Corp El Segundo Ca.

[187] Haessig, D.A. and Friedland, B. On the modeling and simulation of friction. in American Control Conference, 1990. 1990.

[188] Canudas de Wit, C., Olsson, H., Astrom, K.J., and Lischinsky, P., A new model for control of systems with friction. IEEE Transactions on Automatic Control, 1995. 40(3): 419-425.

[189] Armstrong-Hélouvry, B., *Control of machines with friction*. 1991, Boston: Kluwer Academic Publishers.

[190] Liu, L., Liu, H., Wu, Z., and Wang, Z., An overview of friction models in mechanical systems. Advances in Mechanics, 2008, 38(2): 201-213 (in Chinese).

[191] Bernardo, M.d., Budd, C.J., Champneys, A.R., Kowalczyk, P., Nordmark, A.B., Tost, G.O., and Piiroinen, P.T., Bifurcations in nonsmooth dynamical systems. SIAM Review, 2008. 50(4): 629-701.

[192] Shin, K., Oh, J.E., and Brennan, M.J., Nonlinear analysis of friction induced vibrations of a two-degree-of-freedom model for disc brake squeal noise. JSME International Journal Series C, 2002. 45(2): 426-432.

[193] Vielsack, P., Stick–slip instability of decelerative sliding. International Journal of Non-Linear Mechanics, 2001. 36(2): 237-247.

[194] Heilig, J. and Wauer, J., Stability of a nonlinear brake system at high operating speeds. Nonlinear Dynamics, 2003. 34(3): 235-247.

[195] Shi, w., Wei, D., Hu, M., Pan, Z., and Chen, Z., Study of dry friction induced multiple limit-cycle patterns in automotive brake groan. Chinese Journal of Automotive Engineering, 2015, 5(1): 35-42 (in Chinese).

[196] Benson, D.J. and Hallquist, J.O., A single surface contact algorithm for the post-buckling analysis of shell structures. Computer Methods in Applied Mechanics and Engineering, 1990. 78(2): 141-163.

[197] Popp, K., Hinrichs, N., and Oestreich, M., Dynamical behaviour of a friction oscillator with simultaneous self and external excitation. Sadhana, 1995. 20(2): 627-654.

[198] van de Vrande, B.L., van Campen, D.H., and de Kraker, A., An approximate analysis of dry-friction-induced stick-slip vibrations by a smoothing procedure. Nonlinear Dynamics, 1999. 19(2): 159-171.

[199] Chargin, M.L., Dunne, L.W., and Herting, D.N., Nonlinear dynamics of brake squeal. Finite Elements in Analysis and Design, 1997. 28(1): 69-82.

[200] Leine, R.I., van Campen, D.H., de Kraker, A., and van den Steen, L., Stick-slip vibrations induced by alternate friction models. Nonlinear Dynamics, 1998. 16(1): 41-54.

[201] Zeng, J. and Luo, R., Non-linear analysis of disc brake-induced vibrations for railway vehicles. Proceedings of the Institution of Mechanical Engineers, Part F: Journal of Rail and Rapid Transit, 2011. 225(1): 48-56.

[202] Hoffmann, N.P., Linear stability of steady sliding in point contacts with velocity dependent and lugre type friction. Journal of Sound and Vibration, 2007. 301(3–5): 1023-1034.

[203] Gdaniec, P., Weiß, C., and Hoffmann, N.P., On chaotic friction induced vibration due to rate dependent friction. Mechanics Research Communications, 2010. 37(1): 92-95.

[204] Jia, S. and Li, Q. Friction-induced vibration and noise on a brake system. in IEEE International Conference on Information and Automation. 2013.

[205] Li, B., Ding, Q., and Chen, Y., Numerical study on the self-excited vibration of disc brake system. Science & Technology Review, 2007, 25(23): 28-32 (in Chinese).

[206] Johnson, K., One hundred years of hertz contact. Proceedings of the Institution of Mechanical Engineers, 1982. 196(1): 363-378.

[207] Lee, T. and Wang, A., On the dynamics of intermittent motion mechanisms. ASME Paper, 1982(82-DET): 65.

[208] Mickens, R.E., Generalization of the senator-bapat method to systems having limit cycles. Journal of Sound and Vibration, 1999. 224(1): 167-171.

[209] Hu, H., A modified method of equivalent linearization that works even when the non-linearity is not small. Journal of Sound and Vibration, 2004. 276(3-5): 1145-1149.

[210] Nayfeh, A.H. and Mook, D.T., *Nonlinear oscillations*. 2004, New York: Wiley.

[211] Pierre, C., Ferri, A.A., and Dowell, E.H., Multi-harmonic analysis of dry friction damped systems using an incremental harmonic balance method. Journal of Applied Mechanics, 1985. 52(4): 958-964.

[212] Spanos, P.T.D. and Iwan, W.D., On the existence and uniqueness of solutions generated by equivalent linearization. International Journal of Non-Linear Mechanics, 1978. 13(2): 71-78.

[213] Liu, S.Y., Gordon, J.T., and Özbek, M.A., Nonlinear model for aircraft brake squeal analysis: Model description and solution methodology. Journal of Aircraft, 1998. 35(4): 623-630.

[214] Sinou, J.J., Coudeyras, N., and Nacivet, S., Study of the nonlinear stationary dynamic of single and multi-instabilities for disk brake squeal. International Journal of Vehicle Design, 2009. 51(1-2): 207-222.

[215] Coudeyras, N., Sinou, J.J., and Nacivet, S., A new treatment for predicting the self-excited vibrations of nonlinear systems with frictional interfaces: The constrained harmonic balance method, with application to disc brake squeal. Journal of Sound and Vibration, 2009. 319(3): 1175-1199.

[216] Sinou, J.J., Thouverez, F., and Jezequel, L., Application of a nonlinear modal instability approach to brake systems. Journal of Vibration and Acoustics, 2004. 126(1): 101-107.

[217] Chevillot, F., Sinou, J.J., and Hardouin, N., Nonlinear transient vibrations and coexistences of multi-instabilities induced by friction in an aircraft braking system. Journal of Sound and Vibration, 2009. 328(4–5): 555-574.

[218] Adams, G.G., Self-excited oscillations of two elastic half-spaces sliding with a constant coefficient of friction. Journal of Applied Mechanics, 1995. 62(4): 867-872.

[219] Elmaian, A., Gautier, F., Pezerat, C., and Duffal, J.M., How can automotive friction-induced noises be related to physical mechanisms? Applied Acoustics, 2014. 76: 391-401.

[220] Baillet, L., Linck, V., D'Errico, S., Laulagnet, B., and Berthier, Y., Finite element simulation of dynamic instabilities in frictional sliding contact. Journal of Tribology, 2005. 127(3): 652-657.

[221] Baillet, L., D'Errico, S., and Berthier, Y., Influence of sliding contact local dynamics on macroscopic friction coefficient variation. Revue Européenne des Éléments Finis, 2005. 14(2-3): 305-321.

[222] Massi, F., Baillet, L., Giannini, O., and Sestieri, A., Brake squeal: Linear and nonlinear numerical approaches. Mechanical Systems and Signal Processing, 2007. 21(6): 2374-2393.

[223] Baillet, L., D'Errico, S., and Laulagnet, B., Understanding the occurrence of squealing noise using the temporal finite element method. Journal of Sound and Vibration, 2006. 292(3–5):

443-460.

[224] Wang, H., Liu, X., Shan, Y., and He, T., Nonlinear behavior evolution and squeal analysis of disc brake based on different friction models. Journal of Vibroengineering, 2014. 16(5): 2593-2609.

[225] Rusli, M. and Okuma, M., Squeal noise prediction in dry contact sliding systems by means of experimental spatial matrix identification. Journal of System Design and Dynamics, 2008. 2(2): 585-595.

[226] Akay, A., Giannini, O., Massi, F., and Sestieri, A., Disc brake squeal characterization through simplified test rigs. Mechanical Systems and Signal Processing, 2009. 23: 2590-2607.

[227] Tonazzi, D., Massi, F., Baillet, L., Culla, A., Di Bartolomeo, M., and Berthier, Y., Experimental and numerical analysis of frictional contact scenarios: From macro stick–slip to continuous sliding. Meccanica, 2014. 50(3): 649-664.

[228] Mai, Y., Dong, B., and Wang, S., Experimental study on the relation between sliding speed and friction-induced high-frequency noise. Lubrication Engineering, 2016, 41(4): 53-56 (in Chinese).

[229] Ouyang, H., Nack, W., Yuan, Y., and Chen, F., Numerical analysis of automotive disc brake squeal: A review. International Journal of Vehicle Noise and Vibration, 2005. 1(3-4): 207-231.

[230] Kang, J., Krousgrill, C.M., and Sadeghi, F., Comprehensive stability analysis of disc brake vibrations including gyroscopic, negative friction slope and mode-coupling mechanisms. Journal of Sound and Vibration, 2009. 324: 387-407.

[231] Kang, J., Analytical approach for modal instability of a rigid brake pad. Proceedings of the Institution of Mechanical Engineers, Part D: Journal of Automobile Engineering, 2014. 229(6): 719-727.

[232] Hochlenert, D. and Von Wagner, U. How do nonlinearities influence brake squeal? 2011. SAE International.

[233] Bajer, A., Belsky, V., and Zeng, L.J. Combining a nonlinear static analysis and complex eigenvalue extraction in brake squeal simulation. 2003. SAE International.

[234] Chevallier, G., Renaud, F., and Dion, J.L. Viscoelastic damping effect on brake squeal noise. in ASME International Design Engineering Technical Conferences and Computers and Information in Engineering Conference. 2009.

[235] Wang, D., Mo, J., Wang, Z., Chen, G., Ouyang, H., and Zhou, Z., Numerical study of friction-induced vibration and noise on groove-textured surface. Tribology International, 2013. 64: 1-7.

[236] Mahajan, S.K., Hu, Y.K., and Zhang, K. Vehicle disc brake squeal simulations and experiences. 1999. SAE International.

[237] AbuBakar, A.R. and Ouyang, H., Complex eigenvalue analysis and dynamic transient analysis in predicting disc brake squeal. International Journal of Vehicle Noise and Vibration, 2006. 2(2): 143-155.

[238] Besselink, B., Tabak, U., Lutowska, A., van de Wouw, N., Nijmeijer, H., Rixen, D.J., Hochstenbach, M.E., and Schilders, W.H.A., A comparison of model reduction techniques from structural dynamics, numerical mathematics and systems and control. Journal of Sound and Vibration, 2013. 332(19): 4403-4422.

[239] Craig, J., A review of time-domain and frequency-domain component mode synthesis methods. International Journal of Analytical and Experimental Modal Analysis, 1987. 2(2): 59-72.

[240] Real, F.F., Fontanela, F., Ritto, T.G., Batou, A., and Desceliers, C., A probabilistic model of uncertainties in the substructures and interfaces of a dynamical system: Application to the torsional vibration of a drill-string. Archive of Applied Mechanics, 2017. 87(4): 685-698.

[241] Lü, H. and Yu, D., Brake squeal reduction of vehicle disc brake system with interval parameters by uncertain optimization. Journal of Sound and Vibration, 2014. 333(26): 7313-7325.

[242] Do, H.Q., Massa, F., Tison, T., and Lallemand, B., A global strategy for the stability analysis of friction induced vibration problem with parameter variations. Mechanical Systems and Signal Processing, 2017. 84, Part A: 346-364.

[243] Brizard, D., Chiello, O., Sinou, J.J., and Lorang, X., Performances of some reduced bases for the stability analysis of a disc/pads system in sliding contact. Journal of Sound and Vibration, 2011. 330(4): 703-720.

[244] Fazio, O., Nacivet, S., and Sinou, J.J., Reduction strategy for a brake system with local frictional non-linearities – application for the prediction of unstable vibration modes. Applied Acoustics, 2015. 91: 12-24.

[245] Kappagantu, R. and Feeny, B.F., An "optimal" modal reduction of a system with frictional excitation. Journal of Sound and Vibration, 1999. 224(5): 863-877.

[246] Kappagantu, R.V. and Feeny, B.F., Part 2: Proper orthogonal modal modeling of a frictionally excited beam. Nonlinear Dynamics, 2000. 23(1): 1-11.

[247] Kappagantu, R.V. and Feeny, B.F., Part 1: Dynamical characterization of a frictionally excited beam. Nonlinear Dynamics, 2000. 22(4): 317-333.

[248] Loyer, A., Sinou, J.J., Chiello, O., and Lorang, X., Study of nonlinear behaviors and modal reductions for friction destabilized systems. Application to an elastic layer. Journal of Sound and Vibration, 2012. 331(5): 1011-1041.

[249] Rao, S.S., *Vibration of continuous systems*. 2007, Hoboken, New York: Wiley.

[250] Rao, S.S. and Yap, F.F., *Mechanical vibrations*. 5th ed. 2011, Singapore: Prentice Hall.

[251] James, M.L., *Vibration of mechanical and structural systems: With microcomputer applications*. 1989: Harper & Row, Publishers.

[252] Nack, W.V. and Joshi, A.M. Friction induced vibration: Brake moan. 1995. SAE International.

[253] McFarland, D. and Smith, B.L., *Analysis of plates*. 1972, New York: Spartan Books.

[254] Bowman, F., *Introduction to bessel functions*. 1938: London: Longmans.

[255] Pollard, H. and Tenenbaum, M., *Ordinary differential equations*. 1964, New York: Harper & Row.

[256] Fu, L., Wang, Q., and Wang, S., Time-stepping for multibody dynamics with friction-affected bilateral constraints. Progress in Natural Science, 2009. 19(12): 1799-1804.

[257] Zhao, Z. and Liu, C., Contact constraints and dynamical equations in lagrangian systems. Multibody System Dynamics, 2016. 38(1): 77-99.

[258] Yao, W., Chen, B., and Xu, J., Frictional collision of multi-rigid-body systems based on energetic coefficient of restitution. Acia Scientiarum Naturalium Universitatis Pekinensis, 2007, 43(5): 585-591 (in Chinese).

[259] Fu, L. and Wang, Q., Method for estimating largest lyapunov exponent in non-smooth multibody systems. Journal of Beijing University of Aeronautics and Astronautics, 2011, 37(1): 45-48 (in Chinese).

[260] Jin, L. and Lu, Q., A method for calculating the spectrum of lyapunov exponents of non-smooth dynamical systems. ACTA Mechanica Sinica, 2005, 37(1): 40-47 (in Chinese).

[261] Meirovitch, L., *Dynamics and control of structures*. 1990: John Wiley & Sons.

[262] Medio, A. and Lines, M., Nonlinear dynamics. Cambridge Books, 2001.

[263] Gong, S. and Zhang, W., Experimental study on nonlinear vibration of flat-belt system. Journal of Dynamics and Control, 2014(4): 368-372 (in Chinese).

[264] Ouyang, H., Moving-load dynamic problems: A tutorial (with a brief overview). Mechanical Systems and Signal Processing, 2011. 25(6): 2039-2060.

[265] Stăncioiu, D., Ouyang, H., and Mottershead, J.E., Vibration of a beam excited by a moving oscillator considering separation and reattachment. Journal of Sound and Vibration, 2008. 310(4-5): 1128-1140.

[266] Deng, H. and Ouyang, H., Vibration of spinning discs and powder formation in centrifugal atomization. Proceedings of the Royal Society A: Mathematical, Physical and Engineering Science, 2010. 467(2126): 361.

[267] Hervé, B., Sinou, J.J., Mahé, H., and Jézéquel, L., Analysis of squeal noise and mode coupling instabilities including damping and gyroscopic effects. European Journal of Mechanics - A/Solids, 2008. 27(2): 141-160.

[268] Nobari, A., Ouyang, H., and Bannister, P., Uncertainty quantification of squeal instability via surrogate modelling. Mechanical Systems and Signal Processing, 2015. 60: 887-908.